



HAL
open science

Nitrogen incorporation and polytype stability of SiC single crystal growth from the vapor phase

Nikolaos Tsavdaris

► **To cite this version:**

Nikolaos Tsavdaris. Nitrogen incorporation and polytype stability of SiC single crystal growth from the vapor phase. Materials. Université Grenoble Alpes, 2015. English. NNT : 2015GREAI011 . tel-01249570

HAL Id: tel-01249570

<https://theses.hal.science/tel-01249570>

Submitted on 4 Jan 2016

HAL is a multi-disciplinary open access archive for the deposit and dissemination of scientific research documents, whether they are published or not. The documents may come from teaching and research institutions in France or abroad, or from public or private research centers.

L'archive ouverte pluridisciplinaire **HAL**, est destinée au dépôt et à la diffusion de documents scientifiques de niveau recherche, publiés ou non, émanant des établissements d'enseignement et de recherche français ou étrangers, des laboratoires publics ou privés.

THÈSE

Pour obtenir le grade de

DOCTEUR DE L'UNIVERSITÉ DE GRENOBLE

Spécialité : **Matériaux, Mécanique, Génie civil, Electrochimie**

Arrêté ministériel : 7 août 2006

Présentée par

Nikolaos Tsavdaris

Thèse dirigée par **Didier Chaussende** et
codirigée par **Eirini Sarigiannidou**

préparée au sein du **Laboratoire des Matériaux et du Génie
Physique**
dans l'**IMEP-2**

Incorporation d'azote et stabilité des polytypes lors de la croissance en phase gazeuse de monocristaux de SiC

Thèse soutenue publiquement le **6 Janvier 2015**,
devant le jury composé de :

Dr. Michel Pons

Directeur de Recherche CNRS, Univ. Grenoble Alpes, Président

Dr. Gabriel Ferro

Directeur de Recherche CNRS, UCBL Lyon, Rapporteur

Dr. Toru Ujihara

Professeur, Université de Nagoya, Rapporteur

Dr. Nathalie Valle

Luxembourg Institut of Science and Technology, Examineur

Dr. Alexandre Tallaire

Chargé de Recherche CNRS, Université Paris 13, Examineur

Dr. Eirini Sarigiannidou

Maitre de Conférence, Grenoble INP, co-directeur de thèse

Dr. Didier Chaussende

Directeur de Recherche CNRS, Univ. Grenoble Alpes, directeur de thèse



General information

The current thesis was elaborated in Laboratoire des Matériaux et du Génie Physique (LMGP) of Grenoble INP and it was financially supported by the European Marie Curie Training network on Functional Interfaces for Silicon Carbide “*NetFISiC*” (FP7/2007-2013). The main scientific objective of the NetFISiC program is to provide Silicon carbide material (of various polytypes) with improved and adequate functional interfaces for getting a step forward in electronic devices performance. Research efforts are dedicated to solve the problems faced by important devices like MOSFET and Schottky diodes. Besides, some fundamental research is performed both on the growth aspect and on new and innovating devices. Applications in high temperature, high power and harsh environment are targeted.

NetFISiC consortium is composed of 12 partners, including 3 companies. 13 early stage researchers (ESR) and 4 experienced researchers (ER) were recruited and trained within this network. The consortium is divided in 3 technical work-packages:

- WP1 (Material growth and related aspects) is dedicated to the development of less mature polytypes than 4H (3C and 15R).
- WP2 (Characterization of material and functional interfaces) is in charge of studying the properties of the materials surface and interfaces.
- WP3 (Devices and demonstrators) is in charge of the electrical testing and fabrication of the targeted devices.

For each of these young researchers, the individual training at the host institution is enriched by specific shared training in other partner's institution and joint training activities (2 workshops, 3 training schools, 3 tutorial days and other training events) organized by the network.

The work of the current thesis is performed within WP1. Collaborations were mainly achieved with 4 partners of the network. A two-week shared training took place in the “Applied Physics department” of “Friedrich-Alexander-Universität Erlangen” in Germany. Hall electrical measurements were performed in nitrogen doped SiC crystals (the results are presented in Chapter 5). A secondment of one week was performed in “Laboratory Charles Coulomb” at the “University of Montpellier 2” in France. Raman spectroscopy analysis was carried out in nitrogen doped samples (the results are given in

Chapter 5) and a conference proceeding was written. 15R-SiC bulk crystals were optically characterized in “Institute of Applied Sciences, Division of Optical Diagnostics” of “Vilnius University” in Lithuania. Three conference proceedings were written, including an oral presentation. Structural analysis of polytype interfaces was performed using a TEM at the “Department of Physics” of “Aristotle University of Thessaloniki” in Greece. Results of the analysis are presented in Chapter 4. Last, a close collaboration took place with the second ESR of the network at the “Laboratoire des Matériaux et du Génie Physique” of “Grenoble INP” in France. A combined work of experiments and numerical simulation was made, for a better understanding of the phenomena related to the growth process. Some of the topics that were studied are: development of the process, foreign polytype nucleation and nitrogen doping. Numerical simulation results and thermodynamic analysis results are given in Chapters 2, 3 and 4. In total, four conference proceedings, including two oral presentations and one journal paper were written.

Besides NetFiSiC network, collaborations were made with the “Nanophysics and Semiconductors” departments of “NEEL Institute” of Grenoble, for the cathodoluminescence analysis of SiC crystals (results are given in Chapter 3) and the “Institut Laue – Langevin” of Grenoble for X-ray analysis of the grown crystals. The nitrogen concentration of SiC crystals was determined using SIMS at “Centre de Recherche Public-Gabriel Lippmann” at Luxembourg (results given at Chapter 5).

Acknowledgements

The present PhD thesis came as a result of the combined effort and support of people, whom I had the pleasure to meet, and I would like to acknowledge.

I would like to express my deepest gratitude to my supervisor Dr. Didier Chaussende and co-supervisor Dr. Eirini Sarigiannidou, for giving me the opportunity to collaborate with them. They encouraged me from the very first, till the last moments of my PhD, showing me the way to become a research scientist. Words are not enough to describe their support in all situations (from common everyday issues, up to the preparation for oral conference talks and writing papers), helpful scientific discussions and advices. I will always remember the discussions with Didier, early in the morning in the experimental room, accompanied with coffee and croissant and the *long “Greek way” discussions* with Eirini. Also, I would like to thank them for being patient and supportive, in order to correct and help me complete the present dissertation. I will carry with me all of their advices, mentality and experience as a priceless gift that was given to me.

I should also thank all current and former members of the Cristallogénèse group, Odette Chaix, Jean-Marc Dedulle, Roland Madar, Thierry Ouisse, Pierre Bouvier, Joseph La Manna, Lucile Parent-Bert, Julien Lefebure, Yun Ji Shin, Sven Tengeler, Lu Shi, Hoang-Long LE-TRAN, Martin Seiss, Le Thi Mai Hoa and Dimitrios Zevgitis for all their help, support, advices, moments that we share in and out of the laboratory and most important for their friendship. They have been all like a family to me. I should give some special thanks to my colleague and PhD student Kanaparin Ariyawong. Beside the daily scientific discussions and his contribution to many of the results presented in this thesis, oral presentations and papers, he was also a very good friend. I would like to thank him for sharing all those moments in our trips, all the moments of anxiety and happiness. I am glad that I was able to collaborate with such a good colleague and make such a good friend.

I would like also to thank, all the non-permanent and permanent members (especially Beatrice Doisneau, Maria Carmen Jimenez Arevalo, Laetitia Rapenne-Homand, Herve Roussel and Arnaud Robin), PhD and post-doctoral students, as well as the former director Dr. Bernard Chenevier and current director Dr. Franz Bruckert of Laboratoire

des Matériaux et du Génie Physique, for their hospitality, fruitful discussions, help characterizing and analyzing my samples and support during my stay in the laboratory. Also, I should give my acknowledgement to Dr. Dominique De Barros, for his great help building and developing the experimental apparatus, sharing his knowledge and experience with me as well as for being a good friend.

All the consortium of the NetFiSiC European program (young fellows, researchers and their supervisors) gave me a great help. Through the common shared training events and conferences, I gained valuable experience for the future and managed to create strong friendships. Some special recognition should be given to Tomasz Sledziwski, Pawel Kwasnicki and their supervisors, for hosting me in their institutions for 1 month in total, in order to characterize my samples. Also Dr. Gediminas Liaugaudas contribution was significant, in both characterization and submission of scientific papers.

I should thank Dr. Pierre Courtois from ILL institute and Dr. Fabrice Donatini from Neel institute for X-ray and cathodoluminescence characterization. As well as, Dr. Nathalie Valle of Centre de recherche public Gabriel Lippmann, for providing the SIMS analysis of our samples.

Without all of my close friends in Grenoble and Greece, I wouldn't be able to complete this work. Their advices and encouragement were important during all this period. Last, I would like to thank my parents and my sister, for all of their support not only during my PhD and all the years of my studies, but for being next to me, in all of my life. My parents taught me all the important things and set me up for life. I owe them everything.

Contents

Introduction	1
1 SiC Background, History and Growth	5
1.1 SiC Background	6
1.1.1 SiC History	6
1.1.2 SiC Electronic Applications	7
1.1.3 Polytypism in SiC	9
1.1.4 Polarity of SiC	14
1.1.5 Doping of SiC	15
1.2 Growth of SiC	17
1.2.1 Growth techniques for SiC	18
1.2.2 Modified Lely method	19
1.3 Purpose and main contribution of the current thesis	24
2 Process development	27
2.1 Experimental apparatus	28
2.1.1 PVT set-up	28
2.1.2 Crucible	32
2.1.3 Growth procedure	42
2.2 Process development	44
2.2.1 Contactless growth	44
2.2.2 Crystal shape	47
2.3 Conclusions of Chapter 2	59
3 Nucleation and propagation of foreign polytypes	63
3.1 Introduction	64
3.2 Experimental details and theoretical calculations	65
3.3 Observation of foreign polytype formation and propagation	69
3.4 Nucleation mechanism of a foreign polytype	76
3.5 Discussion	77
3.5.1 Discussion on nucleation of foreign polytypes	77
3.5.2 Discussion on propagation of foreign polytypes	80
3.6 Conclusions of Chapter 3	93

4	Towards the bulk crystal growth of 15R-SiC	97
4.1	Introduction	98
4.2	Experimental details	101
4.3	15R-SiC crystals	103
4.3.1	Effect of polarity	103
4.3.2	Effect of Nitrogen	108
4.3.3	Effect of Si/C ratio in the gas phase	114
4.4	Conclusions of chapter 4	117
5	Nitrogen doping of SiC bulk crystals	119
5.1	Introduction	120
5.2	Experimental details	122
5.3	Temperature dependence	123
5.3.1	Hall Electrical measurements	124
5.3.2	Raman spectroscopy measurements	131
5.3.3	Surface Morphology	132
5.4	Nitrogen incorporation as a function of nitrogen partial pressure	144
5.5	Discussion	139
5.6	Conclusions of chapter 5	145
	General Conclusions and future studies	149
	Résumé de la thèse en français	153

Introduction

Electronics is one of the most attractive and rapidly growing technological field, due to the importance in economical, industrial and social life of people. Electronics can be separated in different categories based either on their characteristics or the applications they serve. Semiconductor electronics exploit the electronic properties of semiconductor materials like Silicon, Germanium, Gallium Arsenide and Silicon Carbide (SiC). Regardless the semiconductor used, some of the requirements that all electronic applications need are high efficiency, low production cost and adaptability to the various needs. Silicon is the most widely used semiconductor. That arises from the properties of the material itself, the fact that it can be grown in large size crystals and form easily an oxide (Silicon dioxide) with exceptional properties that are important for electronic devices. However, due to the demands for further improvement in efficiency and energy saving, Silicon technology, in power electronics, is reaching its limits. Thus, researchers are exploring other semiconductor materials to substitute Silicon. Silicon Carbide is one of the most promising competitors and SiC devices have already replaced silicon devices in some specific electronic systems.

A great effort was given by industrial and university researchers in the last decades, in order to increase the size and quality of the grown SiC crystals, improve the epilayers characteristics, study the interfaces of SiC and SiC oxides and the implantation of various dopants, solve the problems faced in MOSFET and Schottky diodes, develop the packaging of SiC devices and implement SiC modulus in electronic circuits.

This thesis will bring some new insight into the field of SiC bulk growth from the vapor phase. The topics that were studied are i) development of the process: the aim is to propose and evaluate some strategies in order to enlarge SiC crystals of a few millimeters in diameter. This requires a thorough study of heat and mass transfers in the growth cell, ii) polytype stability: the purpose is to highlight the governing parameters for the destabilization of SiC polytypes and study the propagation of foreign polytype inclusions. Such polytype instabilities lead to the degradation of the grown material and continuously of the produced devices, iii) bulk crystal growth of 15R-SiC. Indeed a possible candidate to replace 4H-SiC polytype in MOSFET devices, effort is given to find the key parameters for 15R-SiC stabilization, iv) nitrogen incorporation: With

nitrogen being the most commonly used n-type dopant in SiC, a better description of the dependence of nitrogen concentration in the grown crystals with respect to the various growth parameters is needed.

According to the presented topics, the structure of the present thesis is as following. The first chapter is an introduction to SiC technology followed by the presentation of its main structural characteristics and properties. An introduction to the growth technique that was used in the present work follows. At the end, the main contribution of the current thesis in the field is mentioned.

In the second chapter, we present details of the growth process. The growth apparatus that was used is displayed, as well as the effect of the various crucible characteristics in the temperature distribution, the growth rate and other important parameters for growth. Effort was given towards the development of the process, in order to grow SiC crystals of sufficient size and structural quality. Initially, a contactless growth configuration was developed and continuously numerous components of the growth crucible were modified, to allow the control of crystals' characteristics.

In the third chapter, we investigate the nucleation and propagation of foreign polytypes during the bulk growth of SiC crystals. This is a combined work of experimentally obtained transitions and a thermodynamic analysis coupled with full computational simulation of the process. Two specific criteria must be fulfilled for a foreign polytype to be nucleated. Once the nucleation point is located, the propagation of the foreign polytype in the volume of the grown crystal can be comprehended. That is depending on the evolution of crystal's shape and the competition of the various growth mechanisms.

Once the stabilization or destabilization of the SiC polytypes are better perceived, an attempt is made to stabilize the growth of the 15R-SiC polytype. In the fourth chapter, the effect of various growth parameters in the stabilization of the specific polytype are explored. As a final objective, the growth parameters that could preferentially enhance the growth of the 15R-SiC are highlighted.

The fifth and last chapter is dedicated to the nitrogen incorporation during bulk growth by the Physical Vapor Transport method. Indeed as the most commonly used dopant, no

full description exist for the incorporation of nitrogen in SiC. We contribute to this effort by exploring the nitrogen concentration in the grown crystals as a function of various growth parameters. Considering the adsorption/desorption mechanisms at the growing surface, effort is given to explain the experimentally obtained trends.

At the end general conclusions, open issues and propositions for future studies close the current study.

Chapter 1

Silicon Carbide Background, History and Growth

This chapter is an introduction to Silicon Carbide and its growth techniques. In the first part, a brief overview of SiC history and electronic applications is given, followed by the analysis of its characteristics, like polytypism, polarity and doping. The second part is dedicated to the growth of SiC, focusing on seeded sublimation growth, which is the technique used at this work. The contribution of the present thesis to the bulk crystal growth of SiC from the vapor phase will close this chapter.

1.1 SiC Background

1.1.1 SiC History

The history of Silicon Carbide begins back in 1824 when Jöns Jakob Berzelius (Swedish chemist) suggested the idea that a Silicon-Carbon chemical bond could exist. A few decades later the American inventor Edward G. Acheson after quitting from Thomas A. Edison's laboratories, began his own experiments on methods for producing artificial diamonds in an electric furnace. In 1891, he heated a mixture of clay and powdered coke in an iron bowl, with the bowl and an ordinary carbon arc-light serving as the electrodes. He found bright green crystals attached to the carbon electrode and thought that he had prepared some new compound of carbon and alumina from the clay. He called the new compound Carborundum because the natural mineral form of alumina is called corundum. This idea gave birth to the commercial Acheson process, named by its founder, for making large quantities of SiC for the abrasive industry, since SiC is second in hardness after diamond [1]. SiC can also form naturally, however it is an extremely rare mineral that is even older than our solar system. Produced as supernova remnants or ejected from carbon rich red giant stars, these pre-solar SiC grains are trapped as micron size particles in meteorites. Moissanite is the name given to naturally formed SiC, in honor of the French chemist Henri Moissan who first discovered moissanite after examining rock samples from a meteor crater located in Canyon Diablo, Arizona in 1905 [2]. The world record for natural Moissanite is a crystal found by Shefa Yamim, an Israeli exploration and mining company along the Kishon River, near Haifa in northern Israel. The length of the crystal is about 4.1 mm [3].

Almost a century later and in 1907, H.J. Round produced the first Light Emitting Diode (LED) by applying 10V to contacts placed on a SiC crystal, observing yellow, green & orange luminescence at the cathode [4]. In 1912, H. Baumhauer used the word "polytypie" to describe the ability of SiC to crystallize into different forms varying only in their stacking sequence in one direction [5] and in 1950 Frank [6] developed the screw dislocation theory. Subsequent growth spiral observations on the (0001) face of SiC crystals by Amelinkx [7] & Verma [8] seemed to confirm the idea. The possible use of SiC in the semiconductor

industry, created the need of high quality crystals. The beginning was made in 1955 by Lely, who developed a method of producing SiC crystals from the vapor phase [9]. It took not too long for the first SiC conference to be held in Boston, USA in 1959. The growth of high quality SiC crystals produced by the Lely method attracted the interest of many researchers and many pioneering works were published after that. However a couple of decades later, SiC technology started to fade. The way towards industrially available SiC electronics was blocked by the small size of the Lely crystals (~10 mm in length). At that critical point, Tairov and Tsvetkov in 1978, introduced a modification of the Lely method that opened the way towards controlled growth of bulk SiC crystals [10]. The modified Lely method is the only process used today in the industry to produce SiC wafers for electronic applications. The first wafers were commercialized by Cree research Inc., in 1991. The later year's efforts were mainly focused towards the increase of size and improvement of quality of SiC wafers and epilayers. Significant was the contribution of Matsunami et al. in the development and establishment of step-controlled epitaxy [11]. Today 6 inch SiC wafers are available, free of micropipe defects while further efforts are made to reduce basal plane dislocations density in order to improve the characteristics of the produced electronic devices.

1.1.2 SiC Electronic Applications

Our modern society is based on the availability of electrical energy, which is produced by various means like nuclear power, oil, water, sun and wind. This energy has to be converted and transferred to the consumers either in an AC form through networks or in a DC form with batteries. This transfer is achieved by using electrical energy management and conversion circuits, consisted of the so-called power electronics. These high frequency and high voltage applications require semiconductor materials with high electron velocity and high critical field. The transfer of the electrical energy has to be achieved with the lowest cost, meaning that the losses of power should be minimized.

Si is the most widely used semiconductor for power device applications. It is now reaching its theoretical limits due to its small band gap and small breakdown field. Having as criteria the large band gap, strong chemical bond, thermal stability and high thermal

conductivity, Silicon Carbide, gallium nitride (GaN), diamond and Zinc oxide (ZnO) are some of the possible candidates for power electronics (see Table 1.1). Although they share similar properties SiC has the largest area of interest as it can be seen in Figure 1.1 compared to Si and GaN. That fact, combined with its mature technological status, makes SiC the preferred candidate for power electronics.

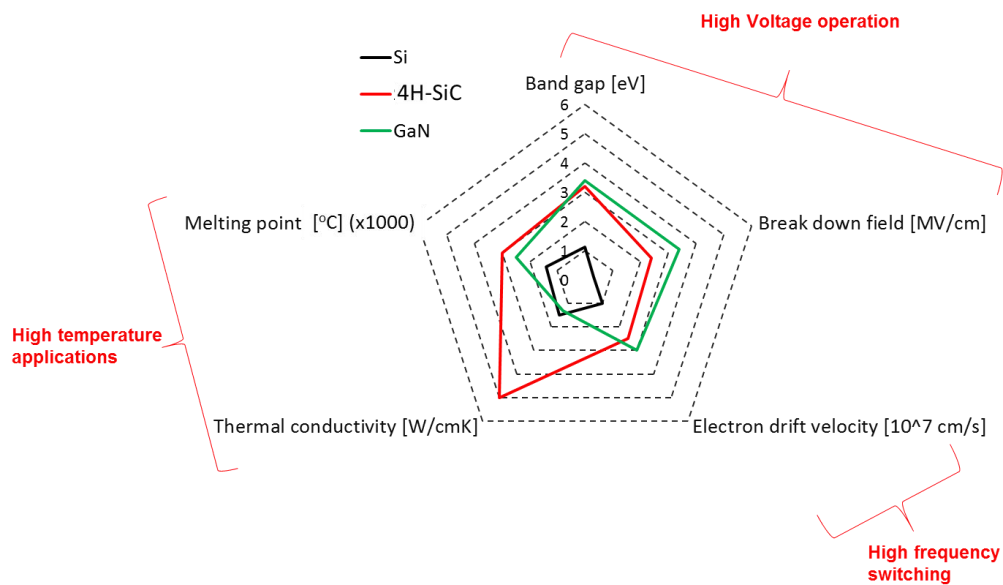


Figure 1.1. Diagram of the most important physical properties for power electronics for Silicon, Gallium Nitride and Silicon Carbide.

Compared to Si, the breakdown field of SiC is an order of magnitude higher, its saturation velocity two times higher and its thermal conductivity three times higher. Practically this means that ten times higher voltage and frequency applications can be held with SiC devices, while the losses can be much smaller and the operational temperature three times higher. Based on the properties of SiC the on-state resistance of a SiC Schottky Diode is around 300 times smaller compared to Si and a MOSFET device operating at 3kV can practically be 10 times smaller. The ability to create smaller power electronic devices compared to Si gives a

big advantage in terms of manufacturing cost, but also heat management. The higher thermal conductivity combined with the lower thermal losses of SiC systems, simplify the cooling systems and thus the total operational and manufacturing cost.

Table 1.1: Electrical properties of semiconductor materials [12, 13]

	Si	4H-SiC	GaN	Diamond (C)
Band gap at 300 k [eV]	1.11	3.2	3.4	5.4
Break down field [MVcm ⁻¹]	0.3	2.4	3.4	10
Electron mobility [cm ² V ⁻¹ s ⁻¹]	1500	980	1250	2200
Hole mobility [cm ² V ⁻¹ s ⁻¹]	450	120	30	2000
Thermal conductivity [Wcm ⁻¹ K ⁻¹]	1.5	5	1.3	20
T _{max} [°C]	125	500	650	700

1.1.3 Polytypism in SiC.

Silicon Carbide (SiC) exists in more than one crystal structures, a phenomenon that is called polymorphism. Specifically in the case of SiC, polymorphism appears along one crystallographic direction, a phenomenon called polytypism. The different crystallographic forms are called polytypes and in the case of SiC more than 200 polytypes can form [14, 15]. However, only 4 polytypes are mainly studied, with only one of them being an industrial product for power devices.

Two different approaches can be assumed in order to understand polytypism in SiC. In the first one, we consider a crystallographic plane with the highest density of atoms (74%) that is called close-packing plane which corresponds to the (0001) crystallographic plane (Figure 1.2). Atoms added above the initial plane (atoms in position A) could occupy either the available positions B or C. The atoms placed in a third plane could occupy the empty available positions A, so the cubic Zinc Blende structure is formed, or the position C (or B)

and the hexagonal Wurtzite structure is created. In the cubic structure the stacking sequence of the atoms along the [0001] direction will be ...ABCABC... while in the hexagonal structure it will be ...ABAB... If the spheres of the presented model are replaced by a Silicon-Carbon pair, the 100% cubic polytype and hexagonal polytype of SiC will be formed. A longer scale stacking sequence along the c-axis direction can give rise to a vast number of different structures.

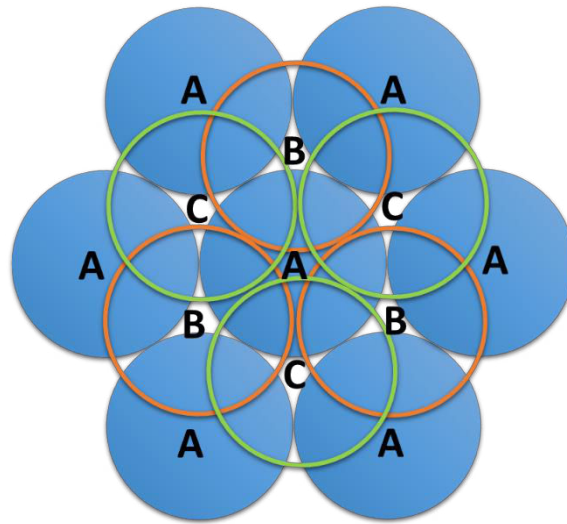


Figure 1.2. Closed packed structure plane. Additional atoms can be added above that plane (consisted of atoms A) either in position B or C.

Another way to describe the structure of the SiC polytypes is as following. A tetrahedron consisting of 4 silicon (carbon) and 1 carbon (silicon) atoms (CSi_4 or SiC_4), can be considered as the basic structural unit of SiC, see Figure 1.3. A 180° rotation of the tetrahedron along the c-axis direction will shift the position of the central atom, when the structure is observed through the [11-20] direction (Figure 1.4). The atoms at the edges of the tetrahedron are shared between neighboring tetrahedrons. The different stacking of A, B, C layers as described before can now be simulated from the 180° rotation or not of the basic unit tetrahedron. The stacking sequence of the basic SiC polytypes, the cubic 3C-SiC, the hexagonal 2H-SiC, 4H-SiC, 6H-SiC and the rhombohedral 15R-SiC are shown in Figure

1.5. The number refers to the number of Si-C bilayers or tetrahedron planes necessary to form a unit cell and the letters H, C and R to the hexagonal, cubic and rhombohedral structure. A larger settlement of tetrahedrons will result in the reproduction of all the SiC polytypes.

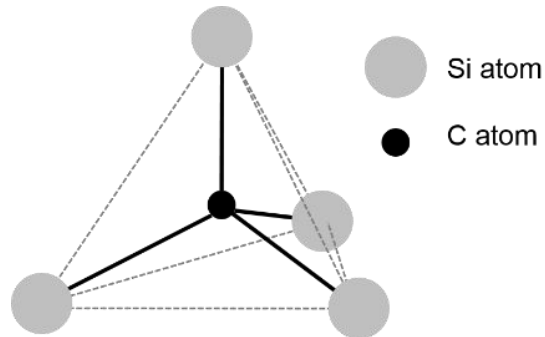


Figure 1.3. Basic structural tetrahedron unit of SiC. It consists of four atoms and those on the apex are shared between neighboring tetrahedrons.

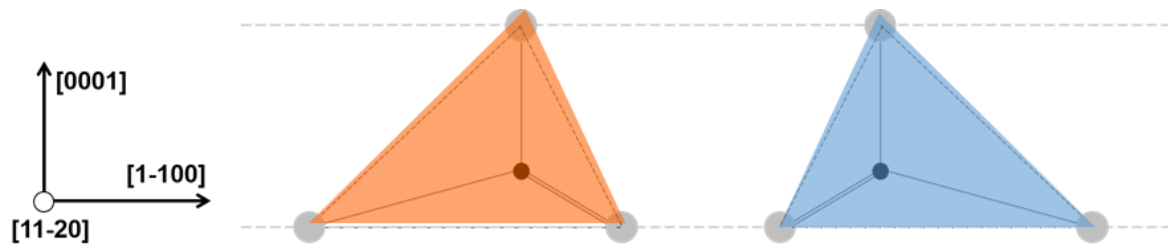


Figure 1.4. SiC tetrahedron as seen along the $[11-20]$ direction. A rotation of 180° will shift the position of the central atom.

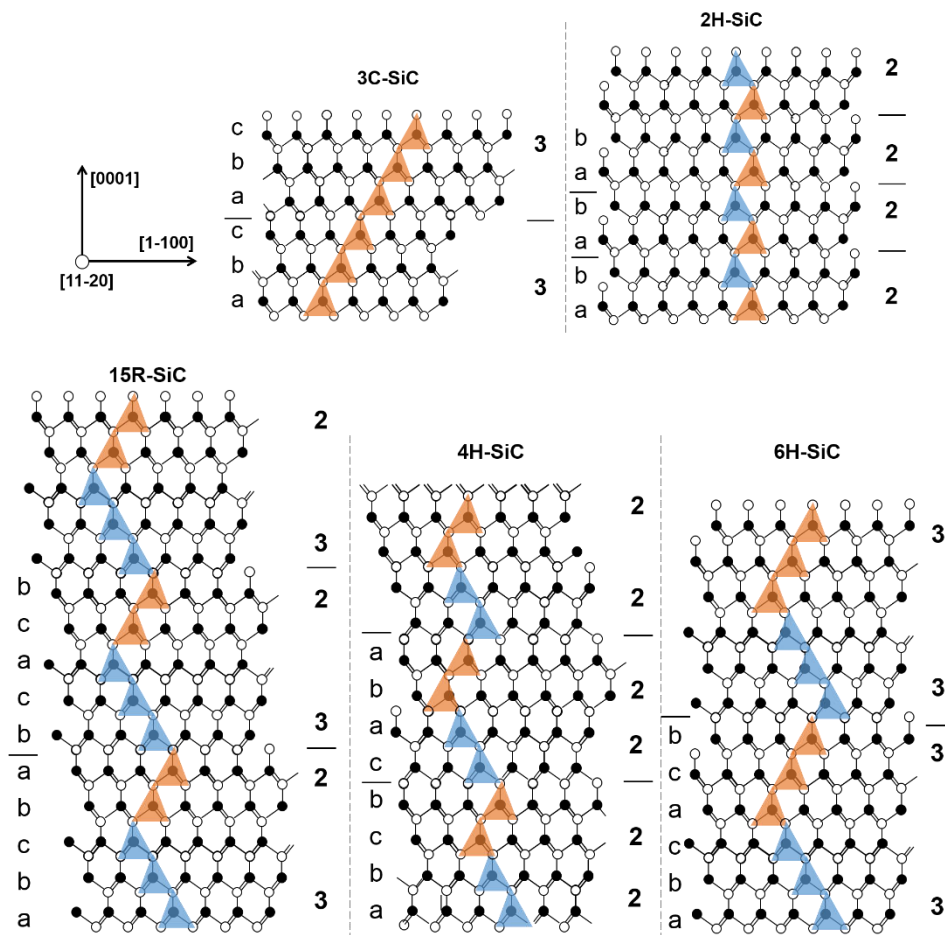


Figure 1.5. Crystallographic structure of the basic SiC polytypes as seen along the [11-20] direction.

Based on the surrounding layer stacking sequence hexagonal and cubic sites are formed. Sites with hexagonal-structured surrounding are denoted hexagonal sites and those with cubic stacking are denoted cubic sites. Hexagonal and cubic sites differ in the location of the next-nearest neighbor. Cubic 3C-SiC consists of only cubic sites, while 2H-SiC of only hexagonal sites. Hexagonality is the number of hexagonal sites to the total number of hexagonal and cubic sites. The hexagonality of 3C-SiC is zero while the one of 2H-SiC is 100%. The hexagonality of the most important SiC polytypes is given in Table 1.2. The electrical properties of SiC polytypes depend on their hexagonality. The bandgap takes a

minimum value of 2.3 eV for 3C-SiC and a maximum of 3.3 eV for the case of 4H-SiC (Figure 1.6).

Table 1.2. Structural characteristics of SiC polytypes

Polytype	Space group	a (Å)	c (Å)	Indirect Bandgap (eV)	Hexagonality (%)
3C	T ² _d -F43m	4.36	4.36	2.3	0
2H	C ⁴ _{6v} -P6 ₃ mc	3.073	5.048	3.3	100
4H	C ⁴ _{6v} -P6 ₃ mc	3.073	10.05	3.2	50
6H	C ⁴ _{6v} -P6 ₃ mc	3.073	15.11	3	33.3
8H	C ⁴ _{6v} -P6 ₃ mc	3.073	20.15	2.86	25
10H	P3m1	3.073	25.18	2.8	20
15R	C ⁵ _{3v} -R3m	3.073	37.7	3	40
21R	C ⁵ _{3v} -R3m	3.073	52.89	2.85	28.5
24R	C ⁵ _{3v} -R3m	3.073	60.49	2.73	25
27R	C ⁵ _{3v} -R3m	3.073	68	2.73	44
33R	C ⁵ _{3v} -R3m			3.01	36

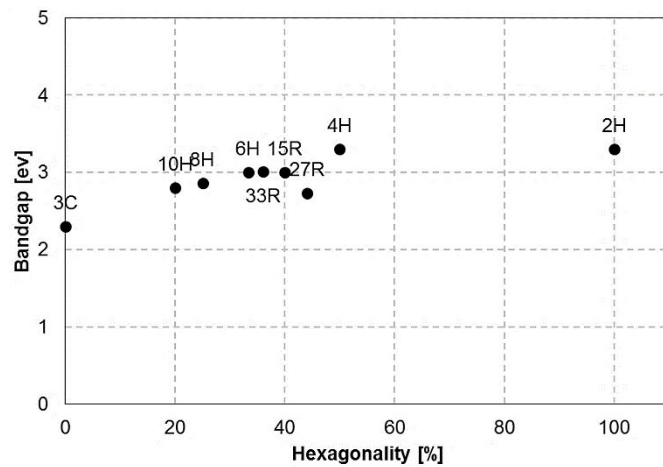


Figure 1.6. Indirect bandgap of various SiC polytypes as a function of their hexagonality.

1.1.4 Polarity of SiC.

Electronegativity of Silicon and Carbon is not the same, thus the bond between Si and C is 88% covalent and 12% ionic. A difference in polarity appears along the bond and continuously along the c-axis direction. It is energetically favorable to cleave one bond between Si and C, rather than three bonds at the bottom of the tetrahedron. As a result, Si and C terminated (0001) and (000-1) planes will be formed with the opposite polarity (Figure 1.7). Pearson et al. calculated the surface energy of Si and C terminated planes and found it to be 2.2 J/m^2 and 0.3 J/m^2 respectively [16].

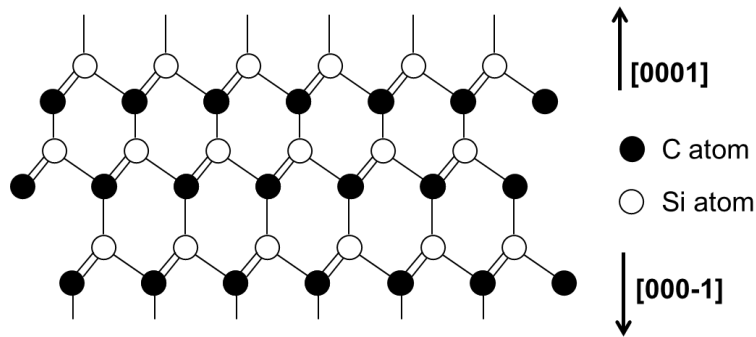


Figure 1.7. Silicon and Carbon terminated planes with opposite polarity formed in SiC.

In more recent studies, the surface energy of the different polytypes was reconsidered using ab initio calculations [17]. While small differences in the bulk energy of the different polytypes were calculated, the surface energy is found to strongly depend on the hexagonal or cubic character of the polytype. The Si-face cubic surface termination has a lower energy compared to the hexagonal one, while for the C-face the opposite occurs. Also, the surface energy is linearly dependent of the hexagonality of the polytypes, as shown in Figure 1.8. The trend is more intense for the case of Si-face, while on C-face no particular evolution is obtained. The above findings have a major importance in a number of experimentally obtained trends, like the step bunching on the Si-face and the preferable nucleation of specific polytypes on silicon and carbon faces.

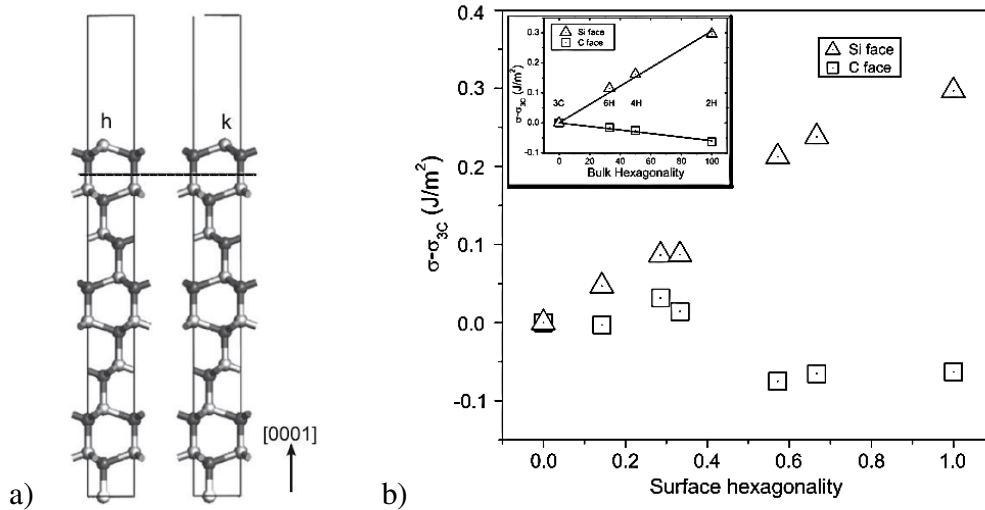


Figure 1.8. a) Cubic and hexagonal surface termination (k and h respectively) for the case of 6H-SiC. b) Surface energy relative to the 3C polytype versus surface hexagonality. In the inset, the relative surface energy is plotted versus the bulk hexagonality [17].

1.1.5 Doping of SiC

In order to ensure reproducible and reliable semiconducting properties, SiC crystals or epitaxial layers should be doped in a controlled way. For the n or p-type doping of SiC, elements of the VA or IIIA group of the periodic table are used respectively. Aluminum and Boron are the most commonly used p-type dopants, while for n-type doping Nitrogen and Phosphorous are the usual choice. Each dopant will create a different ionization energy state depending on the cubic or hexagonal sites (N_{2k} and N_{2h} respectively) that the dopant will occupy and also on the dopant concentration in the material [18-20]. The ionization energy of the main dopants is given in Table 1.3. The size of the dopants in comparison with the ones of the Si and C, will define in which position of the SiC lattice they will be incorporated. Si atoms of the SiC lattice will be substituted by Al and P atoms, while C atoms by N. Boron is reported to occupy both the Si-site and the C-site, however other reports support that it is incorporated only in Si-sites [21].

Table 1.3. Ionization energy (in [meV]) of main dopants in SiC polytypes.

SiC polytype	Dopant				
	n-type doping			p-type doping	
	N _{2h}	N _{2k}	P	Al	B
4H-SiC	50	90	80	220	330
6H-SiC	80	140	80	220	330
3C-SiC	50			270	

Substitution of Si or C atoms by dopants could induce variations in the SiC lattice parameters along the a- and c-axis. Both First-Principles Calculations and experimental measurements verify the above statement [22-24]. In Figure 1.9 the calculated c/na ratio of doped 4H-SiC is plotted as a function of the impurity concentration [23], where a, c and n are the a-lattice constant, c-lattice constant and n the number of bilayers constituting the elementary stacking sequence, e.g. $n=4$ for the case of 4H-SiC. The obtained trend is opposite for the case of nitrogen and aluminum doping. Above 10^{20} cm^{-3} the ratio is increasing for the case of Al doping while it decreases when nitrogen is incorporated into the SiC lattice. The variations of the a- and c-lattice constants as a function of the incorporated nitrogen, boron and aluminum in bulk 6H-SiC crystals were reported by Stockmeier et al. [24]. In Figure 1.10 the two lattice constants and the lattice volume of 6H-SiC are plotted as a function of the doping concentration. Aluminum will increase both the a- and c-lattice parameters while boron has the opposite effect. An increase of nitrogen will increase the 6H-SiC lattice along the c-axis direction but will decrease the size of it along the a-axis. The lattice deformation caused by the presence of dopants can be responsible for the appearance of stress during the growth and the formation of defects [25]. The effect is more pronounced during the first steps of bulk growth of SiC, due to the presence of residual dopants in the source material.

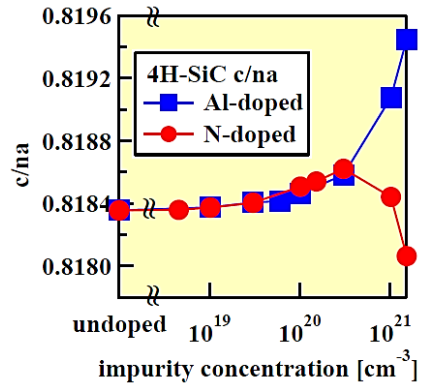


Figure 1.9. Change of c/na of nitrogen and aluminum doped 4H-SiC as a function of dopant concentration [23].

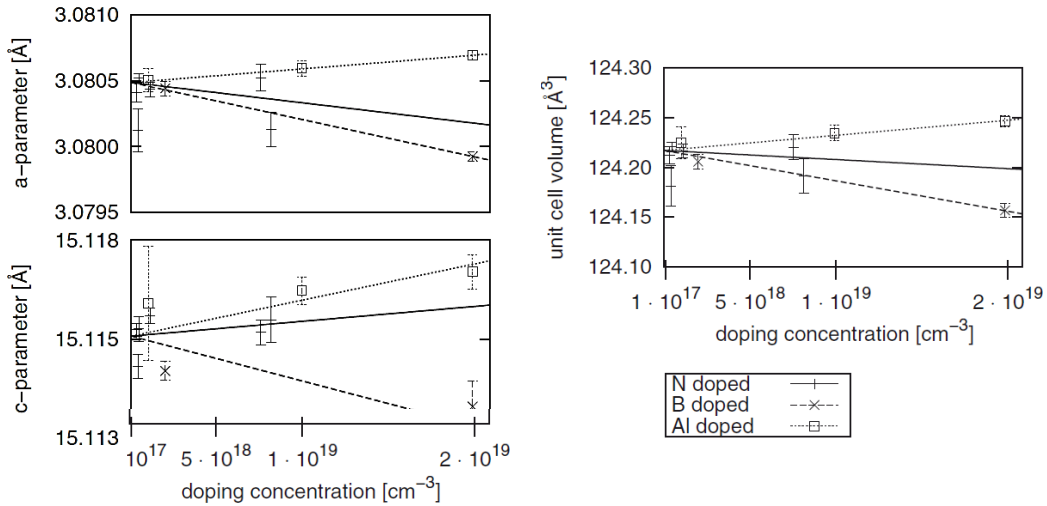


Figure 1.10. a and c lattice parameters and unit cell volume measured by XRD in dependence of doping concentration for nitrogen, boron and aluminum doped 6H-SiC [24].

1.2 Growth of SiC

The only condensed phases that occur in the Si and C phase diagram are Si, SiC and graphite, Figure 1.11. Unlike most semiconductor materials, growth from the melt cannot be applied in the case of SiC. The calculated values show that stoichiometric SiC would melt only above 100000 atm and 3200°C [26]. SiC can also dissolve in certain melts e.g. silicon, but the solubility of carbon in silicon is very low. Thus, growth from the vapor phase is the

mainly used method taking advantage of the sublimation of SiC at 2800°C (P=1atm) and it is called sublimation growth. An artificial way to grow SiC from a vapor phase is by bringing Si and C-bearing vapors together at high temperatures, through growth by gaseous cracking called Chemical Vapor Deposition. Last, the growth from solution can be used with Si or Si alloys melts due to their ability to dissolve carbon.

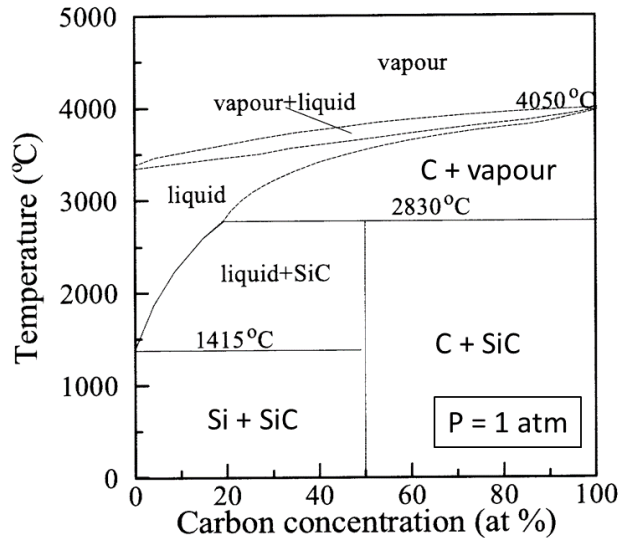


Figure 1.11. Phase diagram of Si – C system [27].

1.2.1 Growth techniques for SiC

Growth from the vapor phase is the preferable technique for growing SiC crystals according to its phase diagram. Lely method was the first to grow SiC crystals of different polytypes of sufficient quality for electronic applications. The modified Lely method or physical vapor transport method (PVT) opened the way to industrialization of SiC and today it is the only method producing SiC wafers. The need for further improvement of quality and control of growth led to additional improvement of the PVT process or exploring other viable options. The principle of gaseous cracking for the supply of Si and C was further developed in order to achieve growth rate comparable to the PVT method and produce industrial wafers. The technique developed is called high temperature chemical vapor deposition (HT-CVD) [28, 29]. Further concepts were presented such as the Halide CVD (H-CVD) [30], Modified

PVT (M-PVT) [31] and a combination of HT-CVD and PVT reactor called Continuous Feed PVT (CF-PVT) [32]. However the latter techniques are far from producing SiC wafers and are currently used at an academic level. In the last years, growth from solution has gained interest from many researchers as the potential to grow SiC wafers of large size and of high quality has emerged.

1.2.2 Modified Lely method

SiC crystals grown by the Lely method are self-nucleated and their size and shape cannot be controlled as they are depending on the local supersaturation close to the growing crystal. The main achievement of the PVT technique compared to the Lely method was the control of the process in general and the crystallization of SiC in particular. The idea lies in the controlled crystallization point on a SiC seed. The resulting geometry for that idea is shown in Figure 1.12. A graphite crucible is used for the growth, as in the case of the Lely method, because it can withstand the temperature ($>2000^{\circ}\text{C}$) necessary for the sublimation of SiC. The source material consist of a SiC powder, which is placed in the bottom of the crucible. At the top of the crucible, a SiC single crystal is placed as seeding material. The crucible is surrounded by insulating graphite foam and induction (the most common case) or resistive heating are used for operating the necessary high temperature.

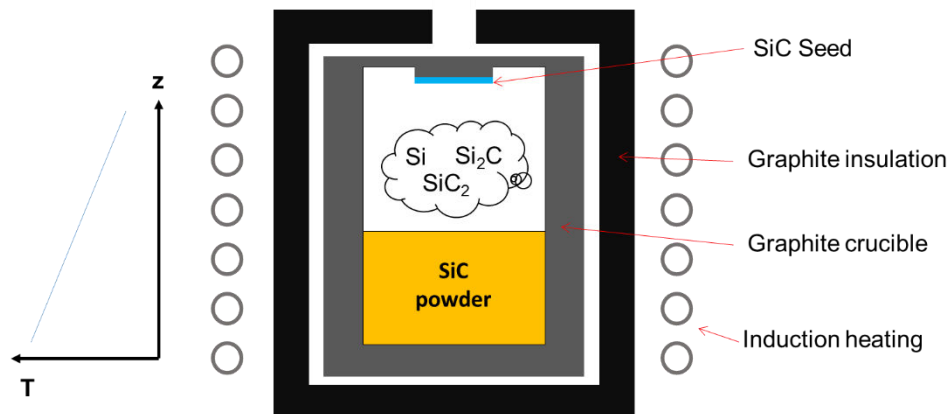


Figure 1.12. Schematic representation of the seeded sublimation process. The temperature profile is shown on the left hand side.

The 3 main elementary steps of the growth are:

- 1) Dissociative sublimation of the SiC source.
- 2) Mass transfer of the gaseous species.
- 3) Crystallization or condensation onto the seed SiC crystal.

At temperatures above 1800°C the SiC source material will sublime through the decomposition of SiC into Si- and C-containing species, with the more important to be Si, Si₂C and SiC₂. The non-congruent sublimation of SiC leads to a Si-rich vapor phase and carbon remains after the SiC is consumed. The species formed from the sublimation of the powder are then transferred to the SiC seed crystal. The driving force is a temperature gradient applied along the graphite symmetry axis. Typical values of the temperature gradient between the source and the seed crystal are 5-15 K/cm. Crystallization takes place at the SiC seed, through condensation processes that take place at the growing surface. The sublimation and condensation rate depends on the difference in equilibrium partial pressure and actual partial pressure of the SiC species near the source and the seed respectively. The equilibrium partial pressure is depending on the temperature while the actual pressure of the species depends on mass transfer phenomena. The difference among the equilibrium and the actual partial pressure is also used to express supersaturation. The higher the difference between these two quantities (the higher the supersaturation is) the higher the crystallization rate will be.

For a better understanding of the process, the heat and mass transport mechanisms will be analyzed.

Heat transfer. The heat transfer mechanisms in the PVT system are i) conduction, ii) convection and iii) radiation.

- i) Conduction takes place in the solids due to the difference in temperature. In the case of PVT process for SiC, the solids are the graphite parts, the solid SiC and the insulation.

The energy flux density (W/m^2) is proportional to the temperature gradient dT/dx , (equation 1.1).

$$Q/A = -k \frac{dT}{dx} \quad \text{Eq.1.1}$$

Q is the energy per unit time [W], A the surface [m^2], k the thermal conductivity of the material [$\text{Wm}^{-1}\text{K}^{-1}$], dT/dx the temperature gradient.

- ii) Convection is the transfer of energy between an object and its environment, due to fluid motion. As before, flux density Q/A , is proportional to the fluid/solid temperature difference, (equation 1.2).

$$Q/A = h(T_2 - T_1) \quad \text{Eq.1.2}$$

h is the convective heat transfer coefficient.

- iii) Radiation. Radiative heat transfer is energy transport due to emission of electromagnetic waves from a surface. The radiation does not require a heat transfer medium, and can occur in vacuum. The heat transfer by radiation is proportional to the fourth power of the absolute material temperature, (equation 1.3).

$$Q/A = \varepsilon \sigma T^4 \quad \text{Eq.1.3}$$

The proportionality constant σ is the Stefan-Boltzmann constant equal to $5.67 \times 10^{-8} \text{Wm}^{-2}\text{K}^{-4}$ and ε is the surface's emissivity.

Heat transfer through radiation in open cavities is the most significant heat transfer mechanism because of the high temperatures involved in SiC growth. The design of the growth crucible is of major importance for the efficiency of heating and proper temperature profile for growth, as will be analyzed in chapter 2.

Mass transfer. The mass transfer of silicon and carbon containing vapor species from the source to the seed is mainly driven by convection and diffusion. Convection arises from the pressure difference due to the chemical reactions and temperature differences and diffusion

arises from the concentration or temperature gradients. The total flux of the species J^{total} is the contribution of the two phenomena and it can be written,

$$J^{\text{total}} = J^{\text{D}} + J^{\text{C}} \quad \text{Eq.1.4}$$

J^{D} is the total diffusion flux and J^{C} the total convection flux.

Diffusion flux is created due to the contribution of the concentration and temperature gradient, thus it can be written,

$$J^{\text{D}} = -\sum_{\text{l}} D_{\text{kl}} \nabla n_{\text{l}} - D_{\text{k}}^{\text{T}} \frac{\nabla T}{T}, \quad k = 1, \dots, N \quad \text{Eq. 1.5}$$

where D and D^{T} are the diffusion coefficients and n the molar density. Thermal diffusion is a second order phenomenon and it is usually significantly weaker than concentration diffusion.

Convection flux is caused due to Stefan and buoyancy flow. Buoyancy is a temperature difference and gravitational induced phenomenon. Stefan flow is a pressure gradient transport phenomenon induced by the production or removal of the species at an interface. Such processes in the PVT system are the sublimation at the SiC source and the condensation at the SiC seed. The lower the pressure of the inert gas (usually argon) is, the more important the convection due to the pressure gradient (Stefan flow) will be. If the pressure of the inert gas is comparable to the partial pressure of the SiC species the interaction of argon species cannot be neglected. The distribution of argon gas inside the growth cavity was calculated by Gao et al. [33]. The difference in argon pressure between the source and seed areas indicate that a flow of argon opposed to the upward movement of species (Figure1.13). Therefore, the interaction between argon and species will reduce the growth rate.

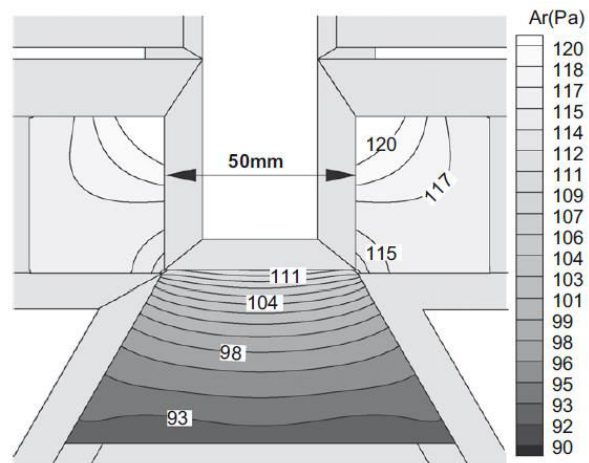


Figure 1.13. Pressure distribution of argon inside the growth cavity [33].

The contribution of each of the transfer mechanisms in the total growth rate is a complex problem to study. For that, the full computational modelling of the process is required. Various models that include or not the spatial and temporal evolution of the process as well as different chemical reactions, boundaries conditions and mass transfer mechanisms have been proposed [34].

1.3 Purpose and main contribution of the current thesis.

The present work is focused on the bulk growth of SiC by the top seeded sublimation process. The main contribution to the field is in two main topics. The first one include the problem of polytype stabilization or destabilization during bulk growth of SiC crystals and the second the nitrogen incorporation in the PVT process.

We will try to answer the following questions: why SiC polytypes destabilize during PVT bulk growth? Where and when a foreign polytype inclusion is formed? How a foreign polytype will propagate in the crystal's volume once formed? What is the way to stabilize 15R-SiC? How can we describe the incorporation of nitrogen during PVT growth of SiC? Is the incorporation of nitrogen independent of the polytype of the grown crystal? What are the physical laws that describe the incorporation of nitrogen with respect to various growth parameters in the PVT process and what are the most contributing incorporation mechanisms of nitrogen in SiC?

In an effort to answer these questions the following “strategy” consisting of four steps was followed: i) development of the process: the aim was to propose and evaluate some strategies in order to enlarge SiC crystals from a few millimeters to 15-20 mm in diameter. This required a thorough study of heat and mass transfers in the growth cell, ii) polytype stability: the purpose is to highlight the governing parameters for the destabilization of SiC polytypes and study the propagation of foreign polytype inclusions, iii) bulk crystal growth of 15R-SiC: various growth conditions were applied in an effort to find the key parameters for 15R-SiC stabilization and iv) nitrogen incorporation: nitrogen concentration in the grown crystals was determined as a function of various growth parameters.

References

1. E.G.Acheson. 1893.
2. H.Moissan, C.R. Acad. Sci. Paris, 1905(140): p. 450.
3. E.Fritsch, V.T., A.Matlins, Record-Size Natural Moissanite Crystals Discovered in Israel. 2014: Gems & Gemology.
4. H.J.Round, Electr. World, 1907. **19**: p. 309.
5. H.Baumhauer, Uber die Kristalle des Carborundums. Z.Kristallogr., 1912. **50**.
6. Frank, F.C., The influence of dislocations on crystal growth. Discussions of the Faraday Society, 1949. **5(0)**: p. 48-54.
7. Amelinckx, S., Spiral Growth on Carborundum Crystal Faces. Nature, 1951. **167(4258)**: p. 939-940.
8. Verma, A.R., Spiral Growth on Carborundum Crystal Faces. Nature, 1951. **167(4258)**: p. 939-939.
9. A.Lely, Ber. Dtsch. Keram. Ges., 1955. **32**: p. 229-236.
10. Tairov, Y.M. and V.F. Tsvetkov, Investigation of growth processes of ingots of silicon carbide single crystals. Journal of Crystal Growth, 1978. **43(2)**: p. 209-212.
11. Matsunami, H. and T. Kimoto, Step-controlled epitaxial growth of SiC: High quality homoepitaxy. Materials Science and Engineering: R: Reports, 1997. **20(3)**: p. 125-166.
12. Camassel, J., S. Contreras, and J.-L. Robert, SiC materials: a semiconductor family for the next century. Comptes Rendus de l'Académie des Sciences - Series IV - Physics, 2000. **1(1)**: p. 5-21.
13. G.Dhanaraj, X.R.H., M.Dudley, V.Prasad, and R.-H. Ma, Crystal Growth Technology, ed. K.B.a. T.Ohachi. 2003: Springer-Verlag Berlin Heidelberg New York.
14. Cheung, R., Silicon Carbide Microelectromechanical Systems for Harsh Environments. 2006: Imperial College Press.
15. Mirgorodsky, A.P., et al., Molecular approach to the modeling of elasticity and piezoelectricity of SiC polytypes. Physical Review B, 1995. **52(6)**: p. 3993-4000.
16. Pearson, E., et al., Computer modeling of Si and SiC surfaces and surface processes relevant to crystal growth from the vapor. Journal of Crystal Growth, 1984. **70(1-2)**: p. 33-40.
17. Mercier, F. and S.-i. Nishizawa, Role of surface effects on silicon carbide polytype stability. Journal of Crystal Growth, 2012. **360**: p. 189-192.
18. Chang, H.C., Le May, Ch.Z., Wallace, L.F., Silicon carbide - a high temperature semiconductor J.R. O'Connor, Smiltens, Editor. 1960, Oxford, London, New York, Paris: Pergamon Press.

19. Ikeda, M., H. Matsunami, and T. Tanaka, Site effect on the impurity levels in SiC. *Physical Review B*, 1980. **22**(6): p. 2842-2854.
20. Pensl, G. and W.J. Choyke, Electrical and optical characterization of SiC. *Physica B: Condensed Matter*, 1993. **185**(1-4): p. 264-283.
21. Larkin, D.J., SiC Dopant Incorporation Control Using Site-Competition CVD. *physica status solidi (b)*, 1997. **202**(1): p. 305-320.
22. Jin, H.-b., et al., Microwave synthesis of Al-doped SiC powders and study of their dielectric properties. *Materials Research Bulletin*, 2010. **45**(2): p. 247-250.
23. Matsumoto, T., S. Nishizawa, and S. Yamasaki, Calculation of Lattice Constant of 4H-SiC as a Function of Impurity Concentration. *Materials Science Forum*, 2010. **645-648**: p. 247-250.
24. Stockmeier, M., et al., On the lattice parameters of silicon carbide. *Journal of Applied Physics*, 2009. **105**(3): p. -.
25. Ohshige, C., et al., Defect formation during the initial stage of physical vapor transport growth of 4H-SiC in the direction. *Journal of Crystal Growth*, 2014. **408**(0): p. 1-6.
26. Glass, R.C., et al., SiC-Seeded Crystal Growth. *MRS Bulletin*, 1997. **22**(03): p. 30-35.
27. Tairov, Y.M., V.F. Tsvetkov, Handbook on Electrotechnical Materials, in "Semiconductor Compounds AIVBIV", Y.V. Koritskii, V.V. Pasyukov, B.M. Tareev, Editor. 1988.
28. Ellison, A., et al., SiC Crystal Growth by HTCVD. *Materials Science Forum*, 2004. **457-460**: p. 9-14.
29. Kordina, O., et al., *Growth of SiC by "Hot-Wall" CVD and HTCVD*. *physica status solidi (b)*, 1997. **202**(1): p. 321-334.
30. Fanton, M., et al., Growth of nitrogen-doped SiC boules by halide chemical vapor deposition. *Journal of Crystal Growth*, 2006. **287**(2): p. 359-362.
31. Wellmann, P., et al., SiC single crystal growth by a modified physical vapor transport technique. *Journal of Crystal Growth*, 2005. **275**(1-2): p. e555-e560.
32. Chaussende, D., et al., *Control of the Supersaturation in the CF-PVT Process for the Growth of Silicon Carbide Crystals: Research and Applications*. *Crystal Growth & Design*, 2005. **5**(4): p. 1539-1544.
33. Gao, B., et al., Analysis of SiC crystal sublimation growth by fully coupled compressible multi-phase flow simulation. *Journal of Crystal Growth*, 2010. **312**(22): p. 3349-3355.
34. K.Ariyawong. 2015, Ph.D Thesis, Universite de Grenoble.

Chapter 2

Process development

In the present work, SiC crystals were grown from the vapor phase, using the modified Lely or PVT method. The high temperature growth apparatus that was used and the various parts of the growth furnace are presented in the first part of this chapter. The development of the growth process in order to control the shape and the evolution of the grown SiC crystals is analyzed in the second part. All these modifications allowed the growth of reproducible SiC single crystals of a few millimeters in thickness and in length.

2.1 Experimental apparatus

Temperatures above 2000 °C are necessary for the growth of SiC crystals from the vapor phase. This introduces limitations in the control and/or monitoring of the growth process and the materials that can be used for the growth furnace. The different units of the PVT reactor (section 2.1.1) and the crucible used for growth (section 2.1.2) are described below.

2.1.1 PVT set-up

The growth apparatus used consists of the following units: the power generator, the capacitor box, the electronic controller, the safety sensors, the temperature and pressure measurement devices and the reactor itself, as shown in Figure 2.1.

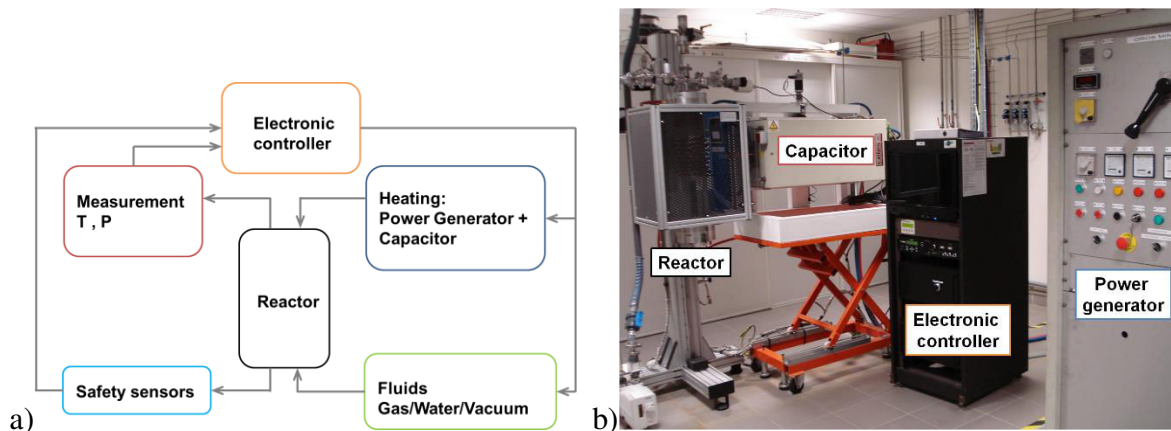


Figure 2.1. (a) Illustration of the different units that consist a PVT growth apparatus. (b) Photo of the growth apparatus that was used for the growth of bulk SiC crystals.

AC power circuit. The SiC growth reactor is heated by induction. For that, an AC circuit consisted of a generator, a capacitor and an inductor is created, as shown in Figure 2.2a. The generator provides an AC signal to the circuit. The sinusoidal nature of the voltage and current of the AC circuit are in phase and the electrical power that is voltage times current

($P = V \cdot I$) is maximized when the voltage and current are “lined up” with each other. The use of a resistor in an AC circuit will not cause a phase shift and the power consumed is called “active” or “real” power and is measured in Watts [W]. It corresponds to the power consumed by the system to produce a real work and it is the desired outcome of an electrical system.

The use of a capacitor or an inductor will cause a 90 degree phase shift between voltage and current. The resulting power will have a value of zero every time the voltage or current has a zero value since the two quantities are multiplied to get power. This is not a desirable model because although the source is generating power, no work is being done at the load. This type of power is known as “reactive” power because it counteracts the effects of “real” power and it is measured in reactive volt-amps [VA]. The inductor will “lead” and the capacitor will “lag” the voltage waveform by 90 degrees compared to the current. So it is said that the inductor consumes while the capacitor generates “reactive” power. Since we need an inductor in our circuit, a capacitor is connected in parallel, in order to provide the “reactive” power.

Due to the use of resistive, capacitive and inductive elements in our system the phase angle between voltage and current will vary. The desired outcome is to maximize the “real” or “active” power and reduce the reactive one. A power triangle is created (Figure 2.2b), showing the interrelation between the different in feature power losses. The power that we have to supply in order to obtain the power needed by our system (the real power) is called “complex” power and is measured in volt-amps [VA]. It is the vector sum of the “real” and “reactive” power,

$$S = \sqrt{P^2 + Q^2} \quad \text{Equation 2.1}$$

where S is the complex power, P the active power and Q the reactive power.

Depending on the characteristics of the coil, the dimensions of the crucible placed inside the coil, the operational frequency, the appropriate capacitance and the power of the generator are well defined.

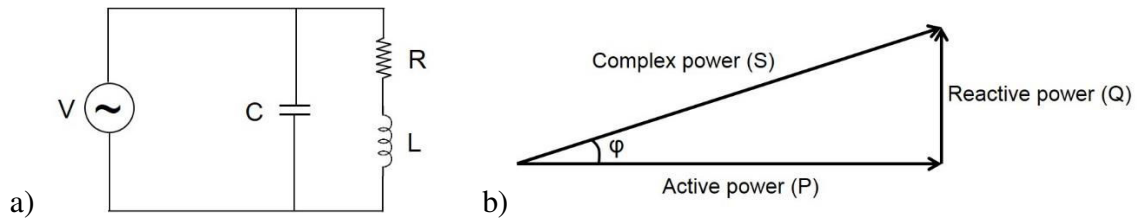


Figure 2.2. a) Electronic circuit used in the experimental apparatus. Inductive, resistive and capacitance elements are used in the AC system. b) Power triangle formed after the use of the mentioned elements.

Electronic controller. It consists of a homemade electronic unit (automation) that controls all the peripheral electronic systems: a gas system (pressure controllers, mass flow controllers and pneumatic valves), a heating system (capacitor and generator), a CPU unit with the necessary software and a screen.

The reactor. The chamber is composed of a water cooled quartz jacket, mounted on specially designed aluminum flanges at the top and the bottom. The graphite crucible is placed inside the quartz tube. The crucible is supported by a cylindrical graphite tube and its position on the vertical axis is fixed. Outside the quartz tube, a water cooled copper coil is placed, as shown in Figure 2.3. The coil can move in the vertical direction. As a result, the relative position of the coil and the crucible can be adjusted. At the top of the reactor, a dichromatic optical pyrometer [1] is placed for the measurement of the temperature inside the crucible. For that, a quartz window is located in the top aluminum cover. The whole system of the PVT reactor is supported on a specially designed aluminum chassis, able to sustain the gas panel of the reactor and the wiring necessary for all the controllers and sensors. The chamber is perfectly sealed and no leakage can be detected using a secondary vacuum He tester.

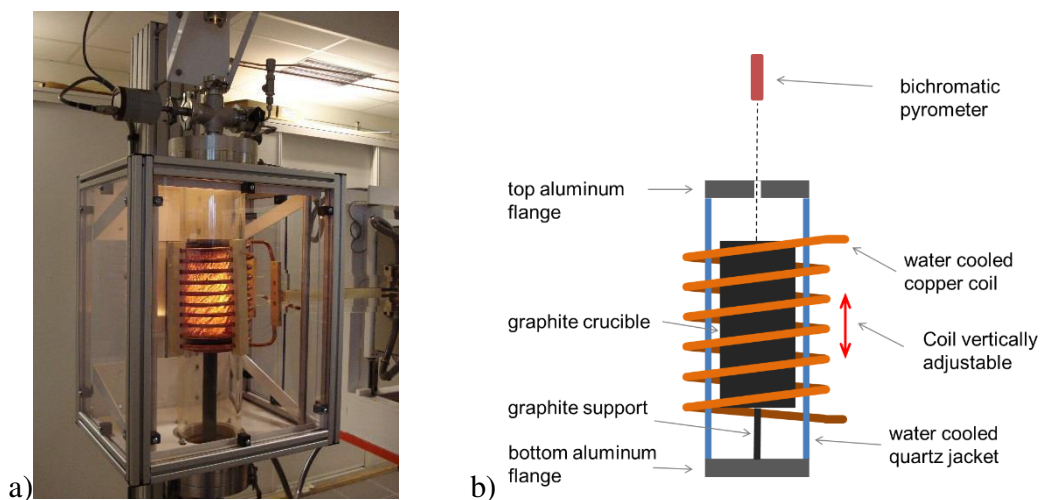


Figure 2.3. a) Photo and b) schematic representation of the PVT reactor. The graphite crucible is placed inside a double water cooled quartz tube. The induction coil is surrounding the quartz crucible and is water cooled. On the top, a pyrometer is placed for the measurement of the temperature through a quartz window. The crucible is supported by a graphite support attached to the bottom aluminum flange of the reactor.

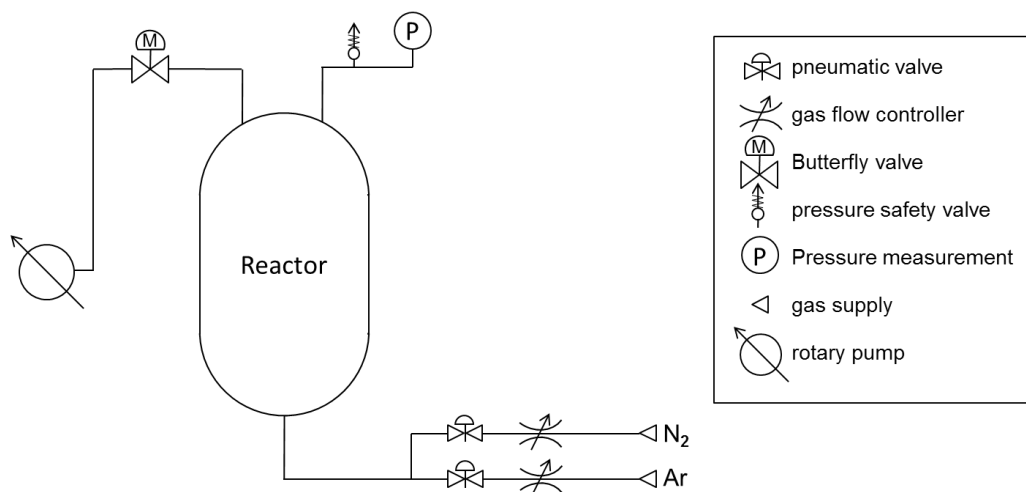


Figure 2.4. Gas panel of the PVT reactor used. At the input, argon and nitrogen gas supplies are connected through a system of mass flow controllers and pneumatic valves. At the output, a butterfly valve for pressure control is connected to a rotary pump. All the necessary equipment for pressure measurement is connected to the body of the reactor.

Gas panel. For the needs of our experiments, the gas panel of the reactor was customized, as shown in Figure 2.4. Argon and nitrogen gases are used. For both gases a set of mass flow controllers, pneumatic valves and micro-valves ensure a large flexibility of gas injections under controlled total pressure. That allows to perform nitrogen marking during growth and to have a precise control of the two gases ratio during nitrogen doping. The input of the gases is at the bottom part of the reactor. At the top, the pressure measurement, a pressure safety valve and a butterfly valve are located. The flow of argon and nitrogen during an experiment has an upward direction. A rotary pump able to create a vacuum of 10^{-3} mbar is used for pressure control.

2.1.2 Crucible

Due to the need of high temperature processing for SiC growth (above 2000°C), the building materials of the growth crucible must have the following characteristics: i) it should be a refractory material, in order to withstand the high temperature growth, ii) chemical stability with the chemical system of Si-C studied, must be ensured, iii) the cost of the material must be reasonable and iv) the material itself should allow easy handling (ex. mechanical machining). Graphite is the best solution, fulfilling all the requirements and it is used for the fabrication of the crucible in our experiments. A schematic representation of the crucible and photos of the main parts used are given in Figure 2.5 and Figure 2.6. Two different types of graphite materials are combined, high density graphite parts (called crucible) and porous graphite felt with a “fiber like” structure (called insulation). As shown in Figure 2.5 the crucible is surrounded totally by insulation.

The crucible can be separated in two parts. First, the inner graphite crucible, where growth takes place that consists of the “support of crucible”, the “container of the source material”, the “reaction chamber” and the “seed holder” and second, the outer graphite crucible called the “susceptor”, as shown in Figure 2.5.

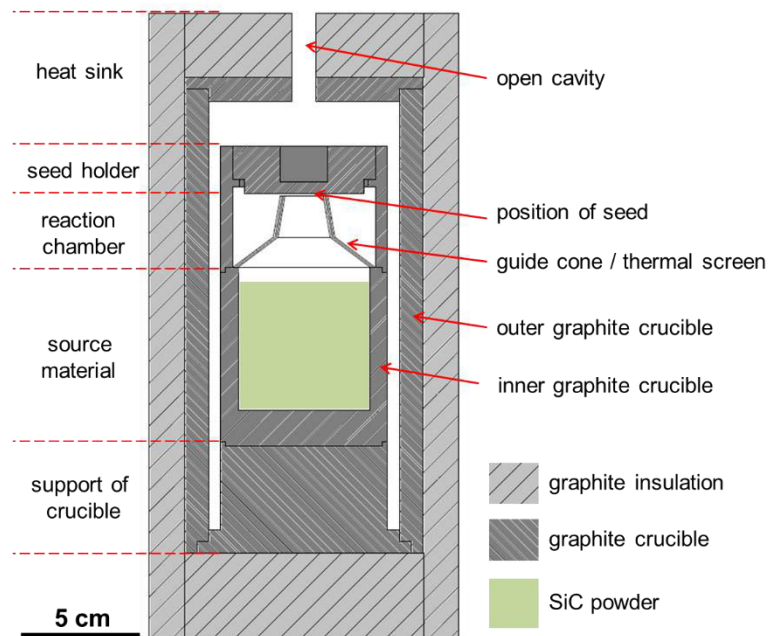


Figure 2.5. Schematic representation of the experimental apparatus used for the growth. Two different types of graphite materials were used, bulk graphite (crucible) and porous graphite felt with a fiber-like structure (insulation). The main parts of the crucible are displayed.

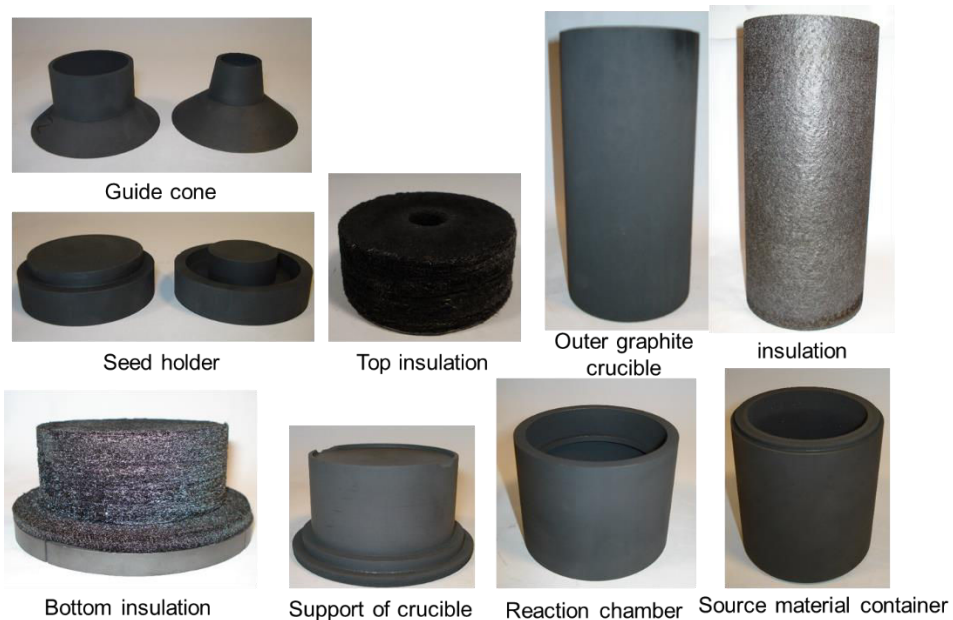


Figure 2.6. Main parts of the graphite crucible used for the growth of bulk SiC crystals.

Indirect heating. Due to the presence of the electromagnetic field (EM), caused by a high-frequency alternating current AC in the induction coil, the electrically conductive graphite susceptor is heated due to Eddy or Foucault currents. The resistance of the graphite material will lead to its Joule heating. The intensity of the electromagnetic field inside a conductive material is reducing exponentially from its surface. The depth at which the intensity of the radiation inside the material falls to $1/e$ (about 37%) of its original value at the surface is called penetration or skin depth δ . In the limit where $\sigma \gg \omega\epsilon$, δ equals to

$$\delta = \sqrt{2 / \sigma \mu \omega} \quad [\text{m}] \quad \text{Eq. 2.2}$$

where ω is the angular frequency of the electromagnetic wave [s^{-1}], σ the conductivity of the material [Sm^{-1}] and μ the magnetic permeability [$\text{H} \cdot \text{m}^{-1}$]. The lower the frequency is, the higher the penetration depth will be.

Two different cases can be distinguished based on the frequency of the EM. When high frequency (~ 100 kHz) is applied, a susceptor is used. The susceptor is the only graphite part heated due to the EM, because of the small penetration depth. Thus, the inner graphite crucible is heated by radiation in open cavities, conduction when there is contact between two or more parts and convection. The outer crucible (susceptor) works as a heating furnace. Like this, more homogeneous heating can be achieved, and the temperature profile is less sensitive to possible fluctuations of the coil's current and degradation of insulating materials. This is called indirect way of heating. In the second case, when a low frequency EM is applied (~ 10 - 20 kHz), no susceptor is used. The inner crucible will be heated because of the EM, due to the higher penetration depth. As a result, precise control of the temperature distribution in the crucible and a selective heating of graphite parts can be achieved. This is called direct way of heating. In our experiments, indirect heating was applied due to the high operational frequency (100 kHz).

Top heat sink. The modified Lely method is based on the sublimation and continuously condensation of SiC and this implies that both source and seed have different temperatures. The implementation of an axial temperature gradient is thus necessary in the crucible. In order to achieve and control that, an open hole is created at the top of the crucible and

insulation acting as a heat sink (Figure 2.5). The same hole also allows the temperature measurement close to the back side of the crystal. The influence of the heat sink diameter on the calculated temperature distribution in the crucible has been examined by many authors [2-4]. Two different cases can be mentioned:

i) A fixed power supply is considered. Results from simulation (Figure 2.7) show that the temperature in the different parts of crucible is reduced when increasing the diameter of the heat sink, as the radiative heat losses are increased [2]. The temperature drop is higher if closer to the heat sink. As a result, the temperature gradient will increase by increasing the diameter of the heat sink (Figure 2.7). In another study, it was shown that the radial temperature gradient will also be influenced but in a smaller extent compared to the axial temperature gradient (Figure 2.8a).

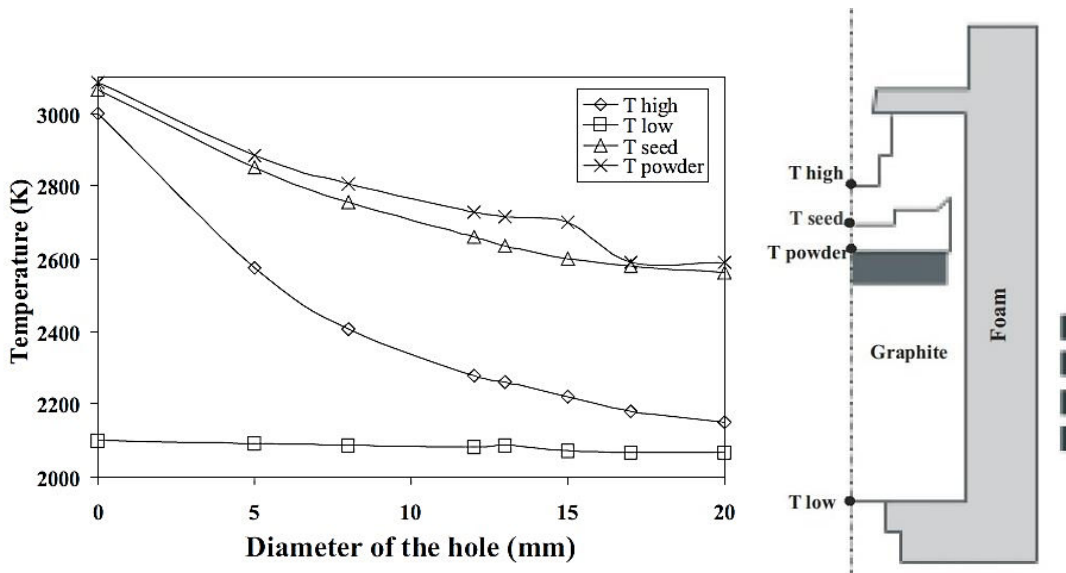


Figure 2.7. Influence of the diameter of the hole used as a heat sink on the temperature of the different part of the reactor along the symmetry axis [2]. Simulation results for a fixed input power.

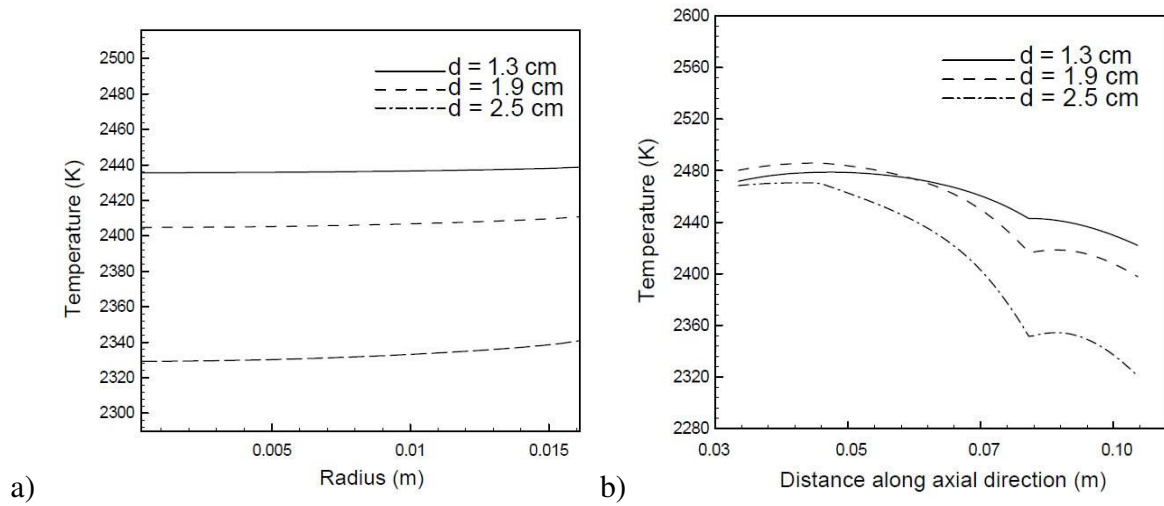


Figure 2.8. (a) Radial temperature variations across the seed surface (0 is the position of the center and 0.016 the edge of the seed), (b) axial temperature variations (0 is the position of the top of the powder and at 0.08 the seed crystal) for various top window diameters [3]

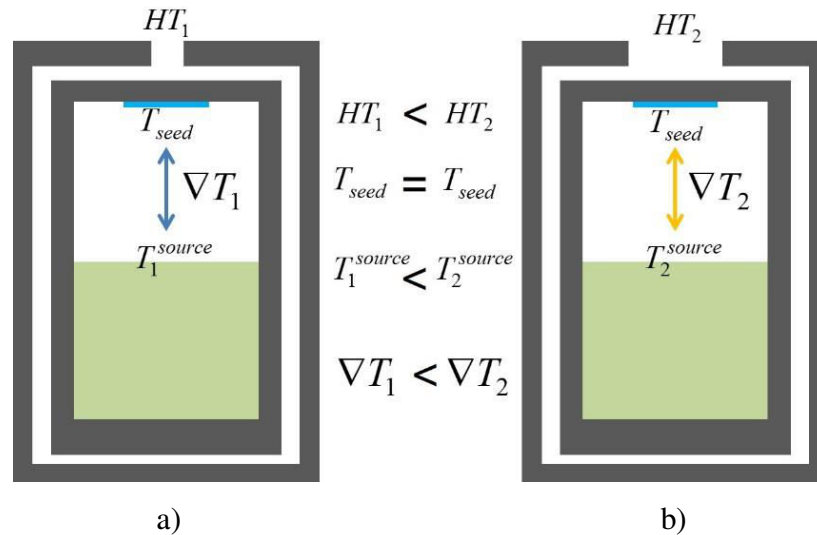


Figure 2.9. Difference in the temperature gradient (∇T) for the case of a weaker (a) and a stronger (b) heat sink (HT), for the same seed temperature. In case (b) higher power is needed due to higher losses of heat. As a result the temperature in the source will be increased. The temperature gradient will be higher for case (b).

ii) A fixed temperature in the seed is considered and the effect of the heat sink is examined. In order to reach a specific temperature more power is needed in the case of a stronger heat sink (Figure 2.9b). As a result, the temperature of the powder will be higher, resulting in a higher temperature gradient. The trend is similar as before, as an increase of the heat sink size will lead to an increased temperature gradient.

Seed holder. The top part of the inner crucible is composed of the “seed holder” that is used for the support of the seed and the grown crystal. The geometry of this part locally influences the temperature profile in the close to the seed area and the formation of parasitic polycrystal. As it was shown in previous works [5-7] by the proper design of the seed holder part, a shift in the isothermal lines can be achieved. This has a direct effect on the shape of the crystal, that can change from flat or concave to convex. As a consequence, the SiC single crystal can expand over the parasitic polycrystal SiC grown at the periphery, on the graphite crucible (Figure 2.10). As a consequence, by optimizing the seed holder, the size and the quality of the grown crystals can be improved (Figure 2.11).

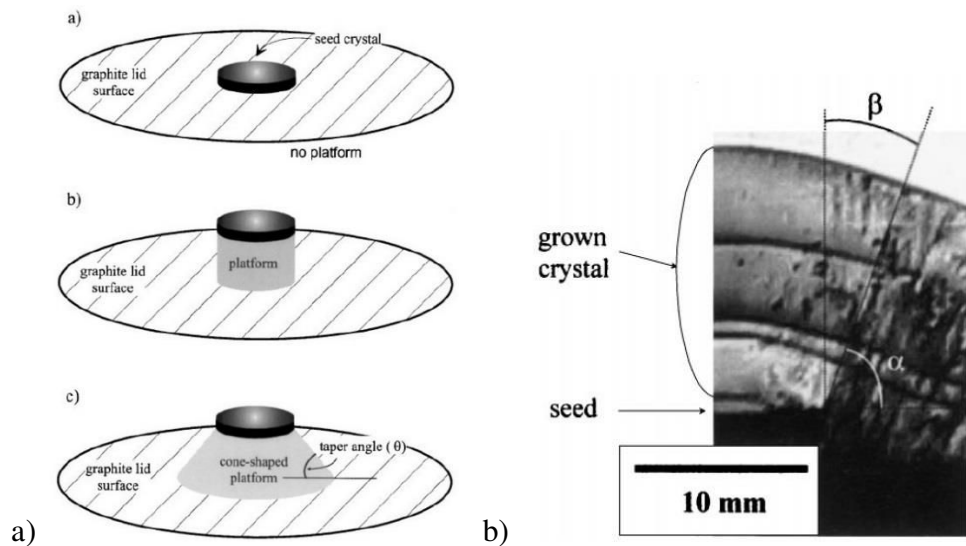


Figure 2.10. a) Three different graphite lid designs. b) Crystal grown by using the design (c) allowed the enlargement of the SiC crystal over the parasitic polycrystal SiC [7].

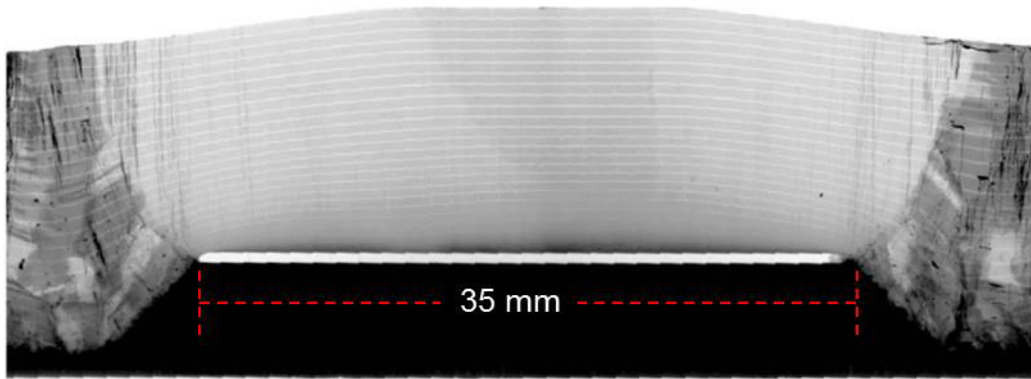


Figure 2.11. Longitudinal cut of a 6H-SiC crystal showing an increase in diameter from 35 to 45 mm over the polycrystal SiC grown on the graphite, after using a conical seed holder [6].

Thermal screen. Thermal screens are located in the reaction chamber area, between the SiC source and seed, Figure 2.5. These graphite parts serve four basic needs i) guide the SiC species of the gas phase, ii) shape the isothermal lines or the temperature profile in the reaction chamber and close to the seed area, iii) react with SiC species and iv) work as carbon source.

In order to improve the process yield and to avoid the formation of polycrystal over SiC single crystal, graphite parts have to be used in order to guide the SiC gaseous species towards the SiC substrate and not the graphite crucible. At the same time these graphite parts work as thermal screens [5, 8, 9]. The aim is to create a temperature field in the crucible with higher temperature everywhere else compared to the growth interface. As a consequence, SiC species will be preferably deposited on the substrate. The experimental and simulation results of this idea are presented in (Figure 2.12) [5]. Due to the use of a flat screen the parasitic polycrystal nucleation on the graphite lid was suppressed and the contactless growth of a single crystal SiC was achieved. From simulation results, it is shown that due to the temperature profile created by the flat screen, the carbon flux was increased in the area of the substrate, Figure 2.12.

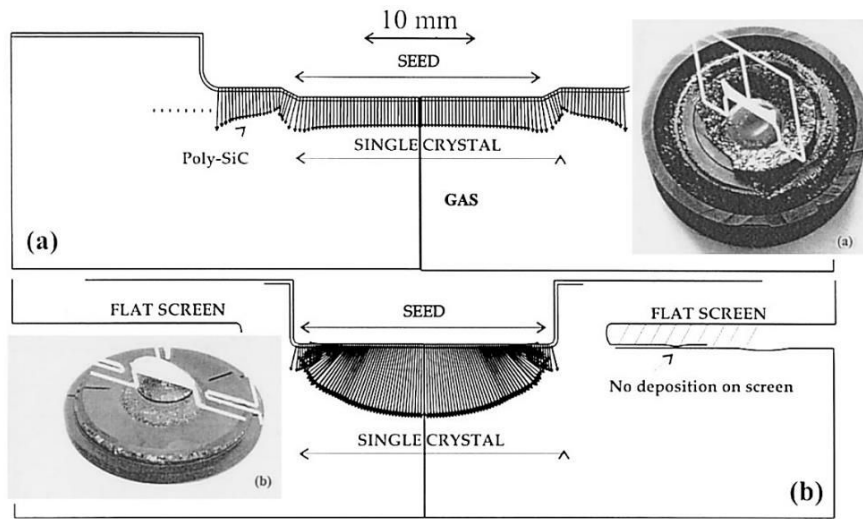


Figure 2.12. Deposited carbon flux for two different growth configurations. Direct flux to the top of crucible (a) and use of a flat screen at the periphery (b). In case (b) no parasitic polycrystalline SiC is observed [5].

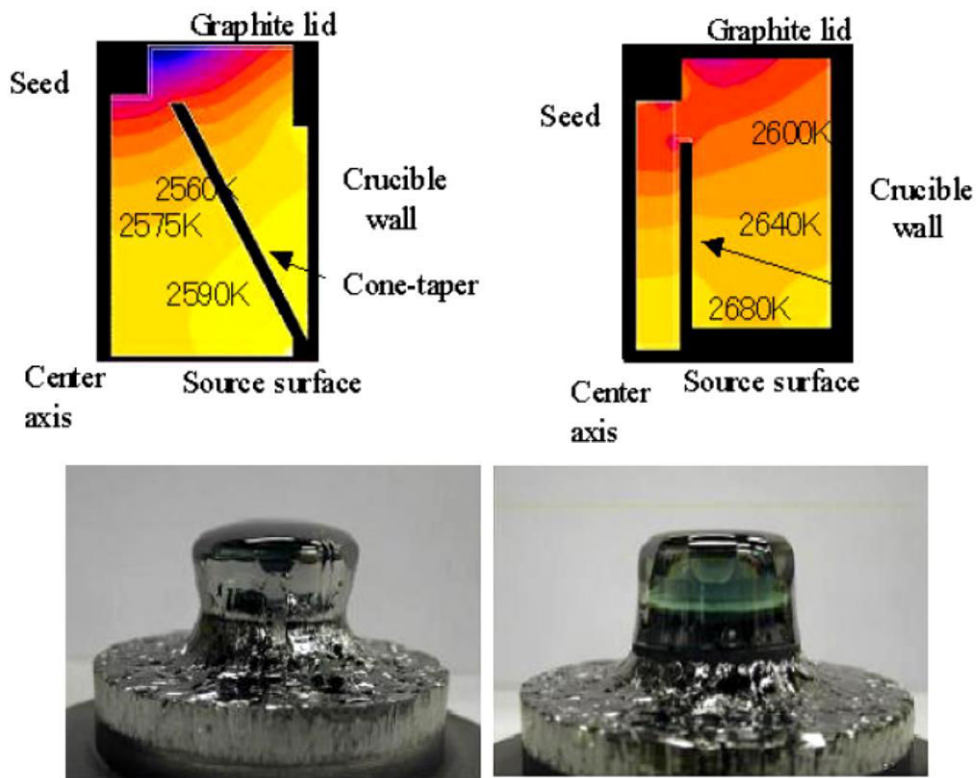


Figure 2.13. Effect of thermal screen shape on the temperature distribution inside the growth vessel and the grown crystal shape [9].

Further studies have shown that the geometry of the thermal screens can directly affect the shape of the grown crystals [9]. Two different types of thermal screens were used, Figure 2.13. The conical one allowed the enlargement of the SiC grown crystal, while a crystal with constant diameter was grown with a cylindrical guide. Simulation results show the change in the isothermal lines from convex in the first case to flat in the second one.

Powder. The SiC source material is located at the bottom of the inner crucible. Due to the fact that the SiC growth is non-congruent, carbon remains after the growth, giving rise to a graphitization from the edge to the center. The powder can be separated in three areas after growth as shown in Figure 2.14. The graphitized area, located usually at the periphery, the top part with a needle like structure and the central part with sintered SiC. The area in the growth furnace with the higher temperature is called “hot point” and is usually located in the area of the powder. The position of the hot point depends on the coil and crucible geometry but mainly upon the relative position of the two.

A higher growth temperature will increase the sublimation rate of the SiC source powder. This is shown in Figure 2.15a-b for growth temperature of 2350°C and 2200°C respectively. The bigger graphitized area and the growth rate which is 3-4 times higher at 2350°C (~1mm/h) compared to 2200°C (250-300 μm/h), is a direct indication of higher powder consumption. The change in the growth temperature has no significant effect in the position of the hot point which is located in the bottom of the powder for both cases (area in red dashed lines). For a given growth temperature (2200 °C), the coil was shifted 1 cm higher (Figure 2.15c) compared to case in Figure 2.15b. The direction of the diffusion paths of the gaseous SiC species (white arrows) changes towards the top and bottom of the crucible, according to the temperature distribution. The shift in coil’s position has shifted the position of the hot point to the middle of SiC powder’s volume.

Even if many studies have been made on source powder consumption and the different features formed [10, 11] up to the lately 3D depiction of the PVT growth [12], the powder consumption is not yet fully described. The main difficulty arises from the fact that the system of SiC powder and graphitized areas is evolving during growth. Someone has to tackle the problem of continuously moving boundaries between the different areas and the

change in density and thermoelectrical properties, Figure 2.16. As a consequence, both the heating efficiency and the temperature profile are affected. Continuously, the temperature gradient, the growth rate and the Si/C ratio in the gas phase will change. All the above must be considered in the case of a long time experiment to ensure growth stability.

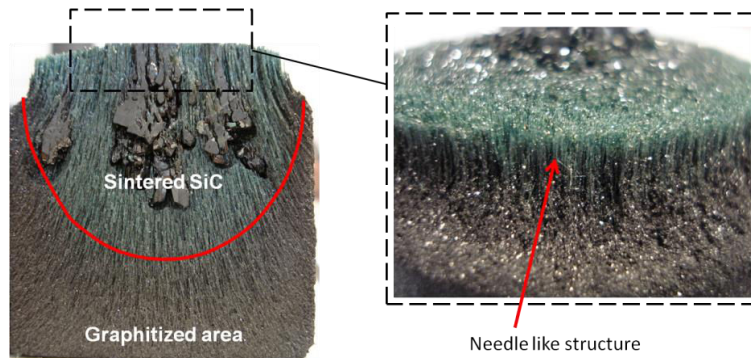


Figure 2.14. Section of the SiC source powder after 25 hours of growth. The growth temperature was 2200 °C, the temperature gradient around 10°C/cm and the pressure 12 mbar. Three different areas are found, the graphitized area at the periphery (due to the non-congruent growth of SiC), the sintered SiC area and the top part with a needle like structure.

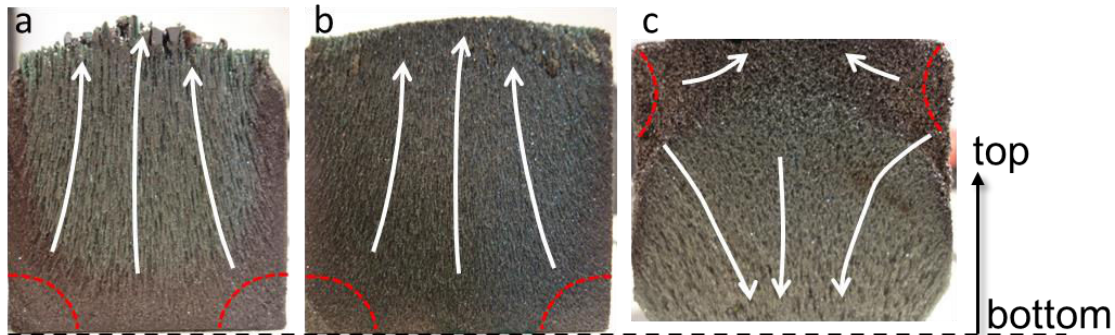


Figure 2.15. Consumption of SiC source powder for (a) $T_{\text{growth}} = 2350^{\circ}\text{C}$ and (b) $T_{\text{growth}} = 2200^{\circ}\text{C}$. The pressure was 13mbar and the duration of the growth 7 hours. (c) Shift of coil compared to case (b) by 1cm, while the growth temperature was kept constant at 2200°C. The red dashed lines indicate the hot point area, while the white arrows show the diffusion paths of the SiC species.

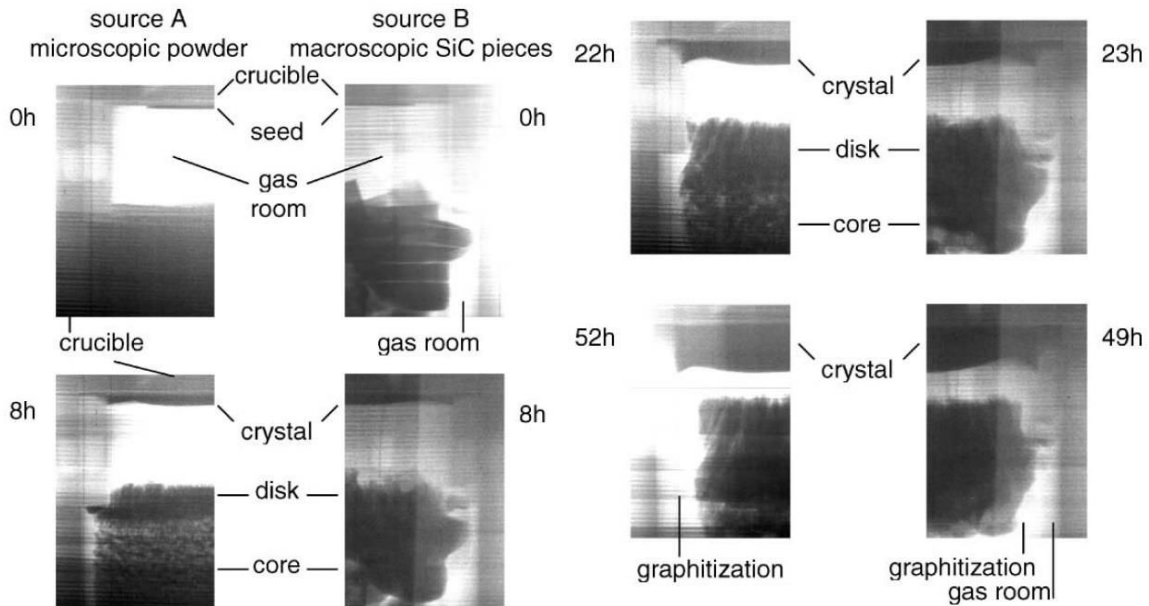


Figure 2.16. Consumption of SiC powder during a 50 hours PVT growth. Series of digital X-ray images captured online during PVT crystal growth of SiC for different SiC sources and different stages of growth. Source A(B) contained microscopic SiC powder (pieces) with a particle size of 10-50 μm (5-20 mm) [11].

2.1.3 Growth procedure

For growth of SiC single crystals, seeds of different polytypes (4H-SiC, 6H-SiC and 15R-SiC) grown in our laboratory and Lely crystals were used. The orientation of growth was on-axis and 3-4° off-axis towards [11-20] direction of both Si and C-face polarities. The dimensions of the substrate were in the range of 5 to 17 mm and it varied depending on the demands of each experiment. In all cases, the growth surface was polished by chemical mechanical polishing (CMP).

Before growth, a vacuum of 10^{-3} mbar is obtained. The different stages of growth are summarized in Figure 2.17. The crucible is manually heated up to a temperature higher than (1000 °C) that is possible to detect by the pyrometer. Above 1100°C the heating rate is

automatic and fixed at $8^{\circ}\text{C}/\text{min}$, up to the growth temperature (time period t_1 - t_2). At the same time, the pressure is set at 200 mbar in order to prevent the sublimation of SiC powder. Once the crucible is heated at the growth temperature, both temperature and pressure are constant for a time period t_2 - t_3 . Afterwards, pressure is decreased (t_3 - t_4) down to the growth pressure and it is the moment that growth actually starts. Before this step, SiC powder sublimates despite the high pressure in the reaction chamber but the growth rate is very low so it can be considered that no growth occurs. During growth, all parameters are stable (t_4 - t_5). In order to stop the growth the pressure in the reactor is increased at 250 mbar and sublimation of the SiC powder is prevented. Next a cooling rate is settled (t_5 - t_6).

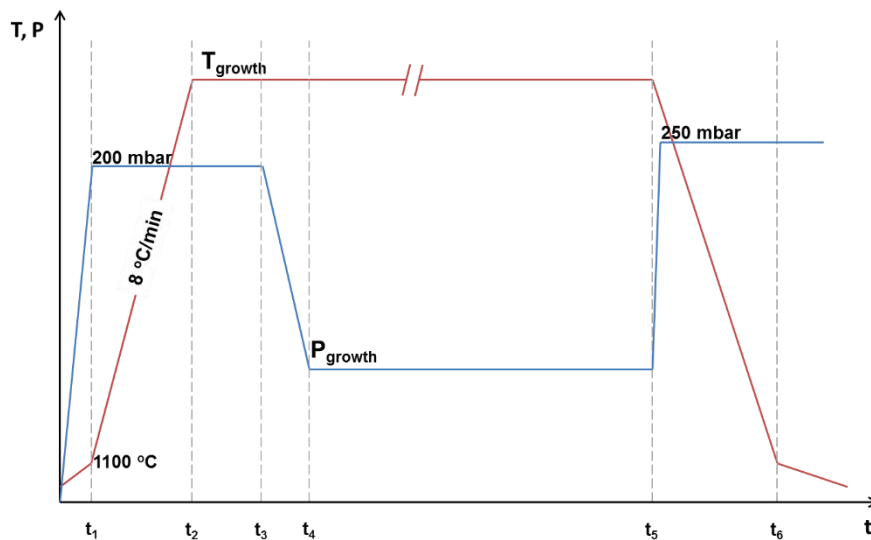


Figure 2.17. Experimental procedure followed in all the experiments mentioned in the current work. The variations of temperature (red line) and pressure (blue line) at the different steps are shown.

2.2 Process development

Effort was made to improve the quality and increase the size of the grown crystals. Contact between the grown crystal and the graphite crucible or parasitic polycrystalline SiC can lead to degradation of crystal quality through the formation of defects, low angle boundaries, foreign polytype inclusions and remaining strain during cooling down process due to different thermal expansion properties. For that, the geometry of the graphite crucible was redesigned in order to enhance a contactless growth of the single SiC crystal. Also, improvement was made in controlling the shape of the crystal and its evolution during growth, as it is related to the propagation of defects and the occurrence of foreign polytypes (see Chapter 3).

2.2.1 Contactless growth

During seeded sublimation growth of SiC, the grown crystal can be in contact with the walls of the graphite crucible on which parasitic polycrystalline SiC can nucleate. As a consequence, defects, low angle boundaries, formation of foreign polytype inclusions and remaining strain in the grown crystal due to the different thermal expansion coefficient are created [8, 13]. Studies have been made towards the control of the parasitic polycrystal SiC formation through the control of supersaturation [14], the use of thermal screens [5] or modifications of the graphite crucible [6].

In order to improve the quality and the size of the grown crystals a geometry that allows the contactless growth of crystals was developed. That was achieved mainly by modifications in the seed holder. The improvement on the grown crystals is shown in Figure 2.18. In Figure 2.18a the grown crystal is in direct contact with the parasitic polycrystal and its enlargement is blocked. By reducing the thickness of the graphite part in front of the seed (Figure 2.19a-b), the diameter and length of the crystal have been increased, see Figure 2.18b. However SiC polycrystal is still present close to the seed and the grown crystal.

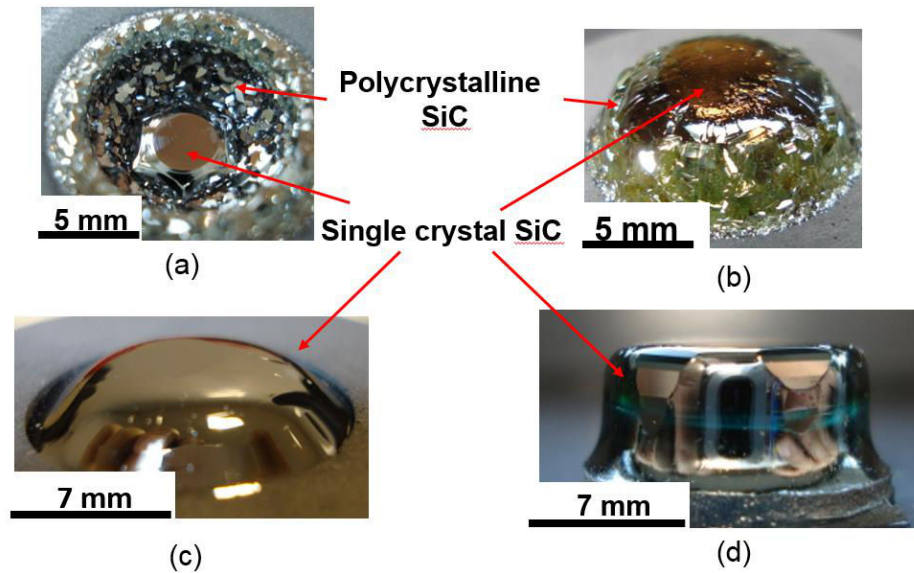


Figure 2.18. Improvement of crystal size and quality from a to d of SiC crystals grown by the PVT method. a) SiC single crystal in contact with graphite crucible and parasitic polycrystalline SiC. b) By modifying the graphite crucible (see text) the diameter and length of the grown crystal is increased. c) After further improvement of the supersaturation profile close to crystallization area, no parasitic polycrystal SiC is formed close to the grown crystal. d) A contactless geometry is finally developed where the characteristics of the crystal are improved.

Further improvement of the crucible followed, in order to prevent the formation of polycrystal SiC. The graphite seed holder was modified from the design shown in Figure 2.19a, to one of Figure 2.19b. An area of lower temperature compared to the one of the crystallization area was created at the top of the crucible. As a result, supersaturation distribution close to the seed area changed and a flux of SiC gaseous species towards the top part of the crucible (flux J_p) was created. That particular flux of species contributes to the formation of polycrystal SiC at the lower temperature area. The J_p flux is the sum of i) the flux of SiC species coming directly from the SiC source material (J_{SC}) and ii) the flux of SiC species resublimed from the SiC crystal (J_{RS}). Using such a configuration, the formation of polycrystal SiC close to the single crystal and a contact of the grown single crystal with the graphite guide cone is avoided. The crystal grown in this crucible configuration is shown in

Figure 2.18c. The single SiC crystal is free of parasitic polycrystal. The surface of the crystal is free of cracks, macrodefects and low angle boundaries, which is a direct indication of the low strain in the crystal due to contactless growth. Last, increase of crystal's length was considered. Longer growth experiments were performed and the design of the thermal screen was considered in order to allow the growth of crystals a few millimeters in thickness and length, without any contact with the graphite crucible. The grown crystal is shown in Figure 2.18d and Figure 2.20a-b.

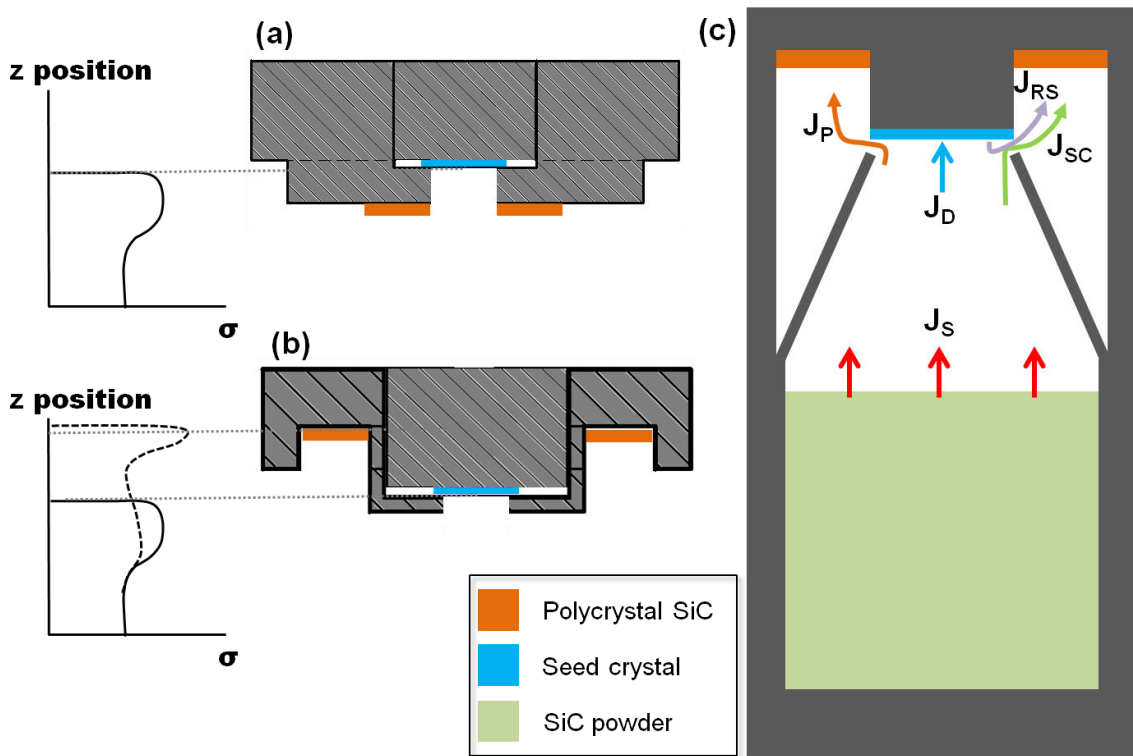


Figure 2.19. (a) Graphite seed holder that leads to the formation of parasitic polycrystal SiC close to the seed area. (b) Modified geometry that prevents the formation of polycrystal SiC close to the single crystal by changing the supersaturation (dotted line) close to the seed area. (c) Schematic representation of the main fluxes of SiC species in the growth crucible. J_S is the flux due to sublimation of SiC source powder, J_D the deposition flux ($J_D = J_S - J_{RS}$), J_P the total flux for the formation of polycrystal SiC, J_{RS} the flux of resublimated SiC species from the SiC grown crystal and J_{SC} the flux of species coming from the powder at the top part of the guide cone and $J_P = J_{RS} + J_{SC}$.

Even if the presence of the J_p flux is of major importance for contactless growth, caution should be given in order not to reduce the process yield. J_p flux is directly related to the flux of sublimed species from the SiC source powder (J_s) and the deposition flux at the growth surface (J_D). If J_p is high enough, compared to the J_s and J_D , the process yield will be low. Thus, J_p should be as low as possible (in order keep the yield of the growth high) down to the point that the formation of polycrystal SiC and the contact of the grown crystal with the graphite crucible is prevented. The optimization of the process is not a topic of this thesis, mainly because seeds of different size were used for the needs of our studies. For that, continuous adjustments on the graphite parts and the crucible were made.

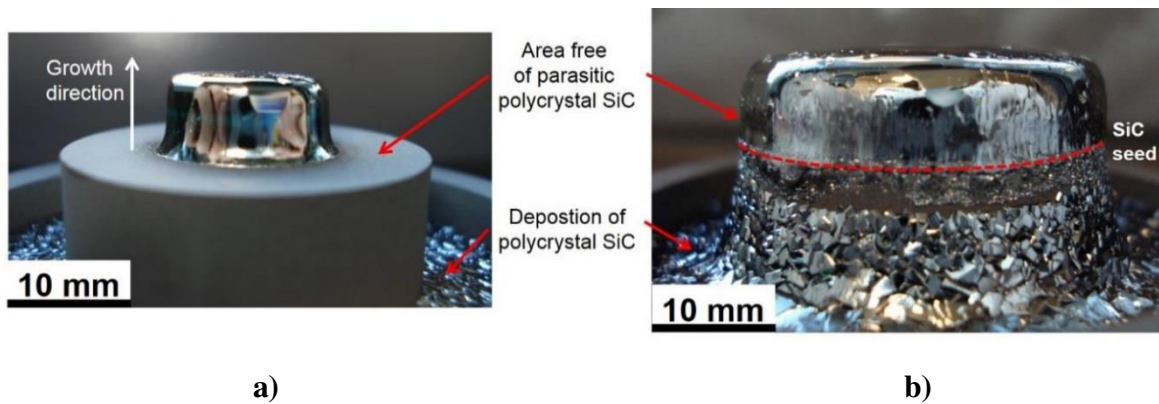


Figure 2.20. SiC single crystal of smaller (a) and bigger (b) diameter as grown in the graphite crucible. By proper design of the graphite part that supports the crystal nucleation.

2.2.2 Crystal shape

The shape of the crystal and its evolution during growth is related to the presence of stress during growth especially in large scale growth [15], propagation of threading dislocations [16] and occurrence of foreign polytypes, as will be analyzed in chapter 3. The shape is a result of mass transport, i.e. the growth rate variation along the growth interface radius. This radial variation is mainly depending on three factors:

i) The temperature profile in the crucible and mainly close to the growth front, considering the absolute value of the temperature but also the radial and axial temperature gradients.

ii) The design of the graphite crucible and more specific, the graphite part that supports the crystal. Either in a direct way since the grown crystal can follow the shape of the graphite part, or indirectly by modifying the temperature profile.

iii) The pressure of growth, as a lower growth pressure can lead to a convex crystal shape and vice versa [17].

In this chapter the first two factors were mainly examined.

Temperature profile. The temperature profile in a PVT crucible can be settled by a number of parameters like the top heat sink, the relative position of the coil and crucible, the insulation thickness and the design of the crucible. In order to differentiate and distinguish the contribution of these parameters, it was chosen to change one parameter and keep the others stable. Periodic nitrogen marking was used during growth to mark the growth interface for different periods of growth.

Modifications were made in the graphite holder design (close to the seed area) while keeping all the other growth parameters constant. The geometry shown in Figure 2.19b, will result in a flat crystal for the first 4 mm of growth that progressively changes to convex. The convex crystal shape is also enhanced by the higher crystal etching at the periphery due to an increase of the resublimation of the SiC crystal (flux J_{RS} , as mentioned in Figure 2.19). The geometry of the graphite holder was modified close to the seed area and the temperature profile is shown (Figure 2.22a). The temperature is lower at the periphery compared to the center of the growth front. This will result in a concave crystal shape for the first 3-4 mm of growth, as shown in Figure 2.21. However, progressively the curvature of the crystal is changing during growth, leading in a flat crystal.

In the last case, an open cavity in the graphite part at the back of the seed was formed, Figure 2.22b. The schematic representation of the temperature profile is shown. The

temperature is lower at the center of the growth front compared to the edge. As a result the grown crystal exhibits a convex shape, since the beginning of growth, Figure 2.21.

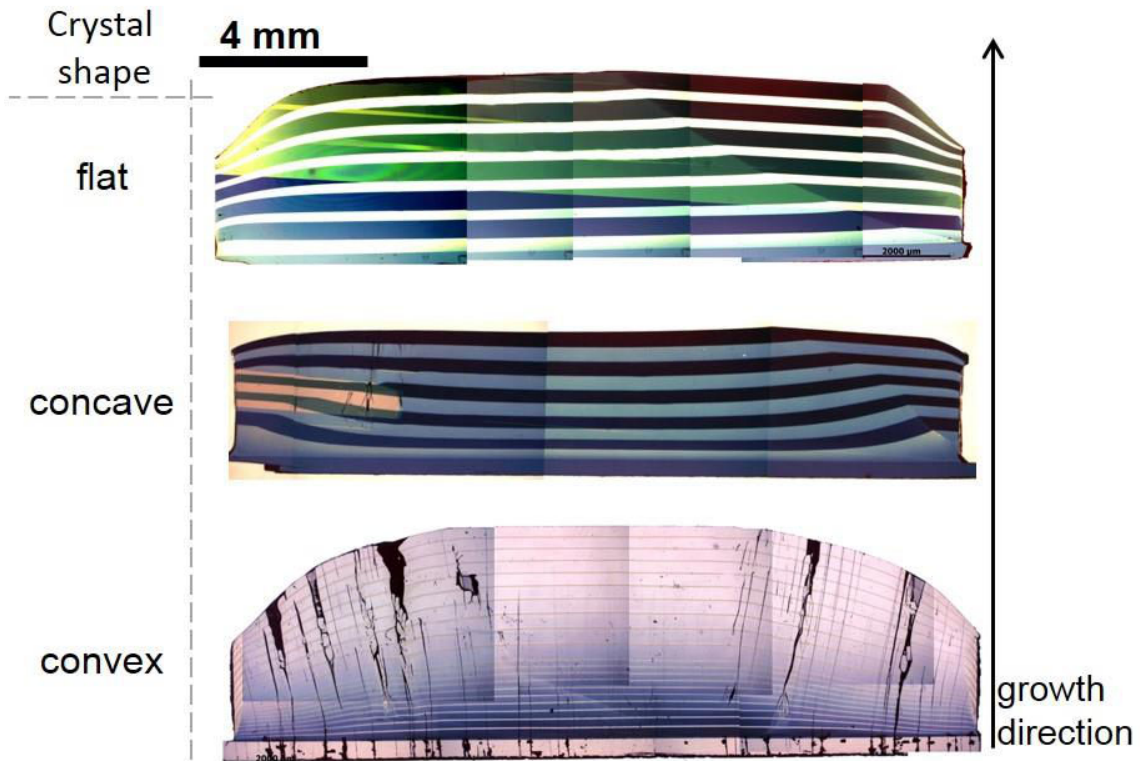
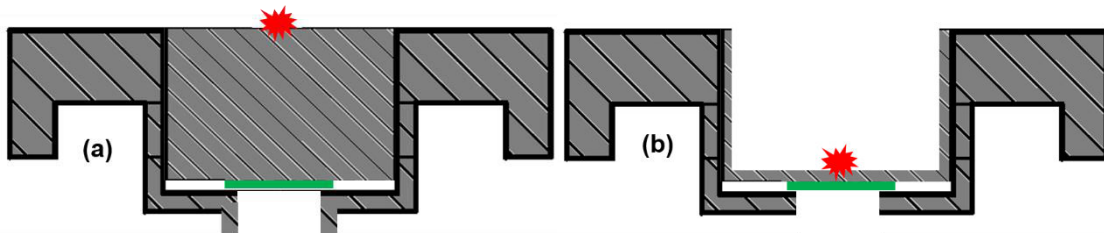


Figure 2.21. Control of crystal shape by modification of the graphite crucible. The dark and bright stripes correspond to nitrogen doped and undoped areas respectively. As it is seen by the nitrogen stripes the shape can change from concave to convex from the first stages of growth.



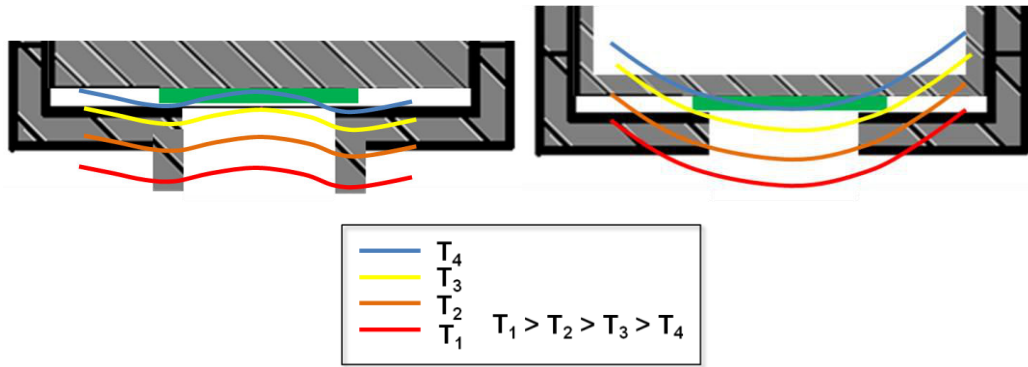
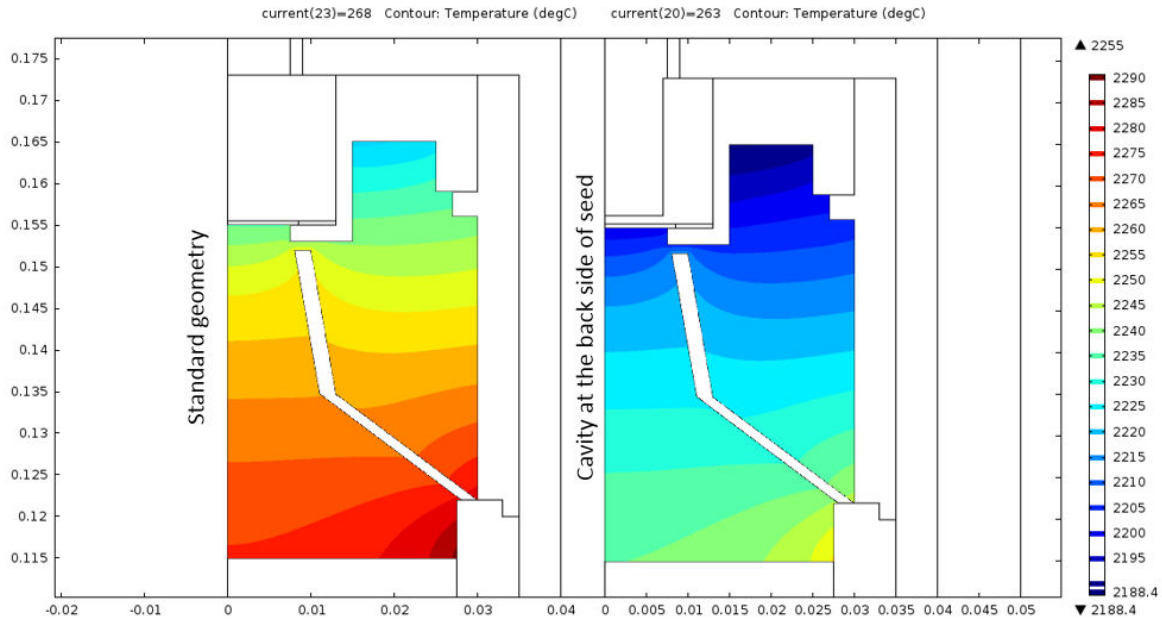


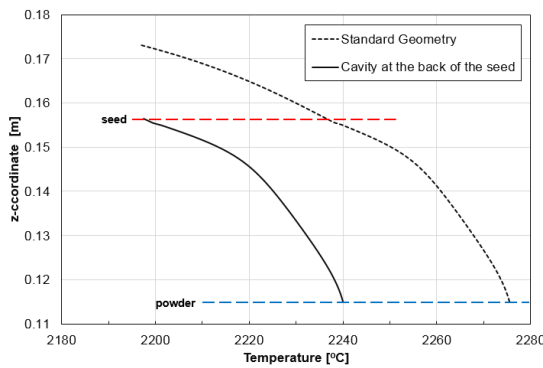
Figure 2.22. Schematic representation of the temperature profile for two different designs of the seed holder. The temperature in the middle is higher (lower) case a (b) in the middle compared to the periphery. This will lead to a concave crystal shape, while geometry (b) to a convex (Figure 2.21). The red mark indicates the point where the growth temperature is experimentally measured.

Numerical simulation was implemented in order to calculate the temperature distribution in the growth cavity for the case of the “Standard geometry” given in Figure 2.19b and the case where a cavity is formed on the back of the seed (geometry of Figure 2.22b). The shape of the grown crystal is flat in the first case and convex in the second one (Figure 2.21). The calculations of electromagnetic and the coupled heat and mass transfer problems were performed by Finite Element Method (FEM) in a two dimensional axisymmetric geometry. The temperature distribution inside the growth chamber is given in Figure 2.23a, the temperature profile along the z symmetry axis and along the growth front in Figure 2.23b,c respectively. Due to the cavity formed on the back of the seed crystal, the growth temperature is measured (experimentally) closer to the seed crystal compared to the standard geometry (red mark in Figure 2.22a,b). Simulation results show that the difference in temperature of the seed crystal is around 35°C between the two geometries (Figure 2.23b). The axial temperature gradient, defined by the temperature difference and the distance between the seed and the powder is similar between the two geometries, 10°C/cm and 11°C/cm for the case of the standard and the modified geometry respectively. More important is the change in the temperature profile along the seed radius (Figure 2.23c). The minimum temperature

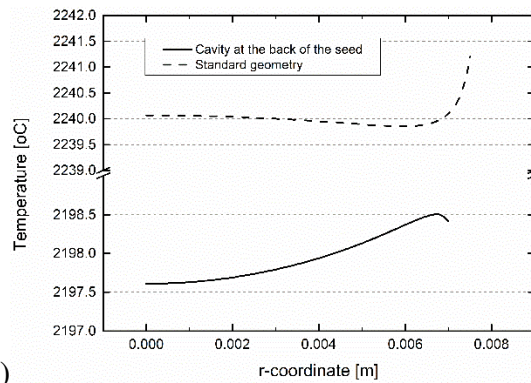
of the growth front is located at the periphery (0.075 m) in the case of the standard geometry, while it shifts to the center of the growth front (zero position in the r-coordinate scale) when a cavity on the back side of the seed is used.



a)



b)



c)

Figure 2.23. a) Simulation image of the temperature in the growth cavity for the case of the “standard geometry” and the case where a cavity is formed at the back of the seed. b) Temperature profile along the z symmetry axis. The positions of the powder and the seed crystal are indicated. c) Temperature profile along the growth front. Zero value corresponds to the center and 0.075m to the edge of the seed crystal.

Even if the presence of a cavity at the back side of the seed crystal does not introduce a significant difference in the axial temperature gradient, compared to the standard case, it affects the absolute temperature value of the seed crystal and the source powder (Figure 2.23b). The Si/C ratio along the crystal radius was computed for the two different geometries and the result is shown in Figure 2.24. It is shown that the Si/C ratio in the gas phase is increased when a strong heat sink is used. Thus, the main contribution of the growth cavity formed is i) the change in crystal shape and ii) increase the Si/C ratio in the gas phase.

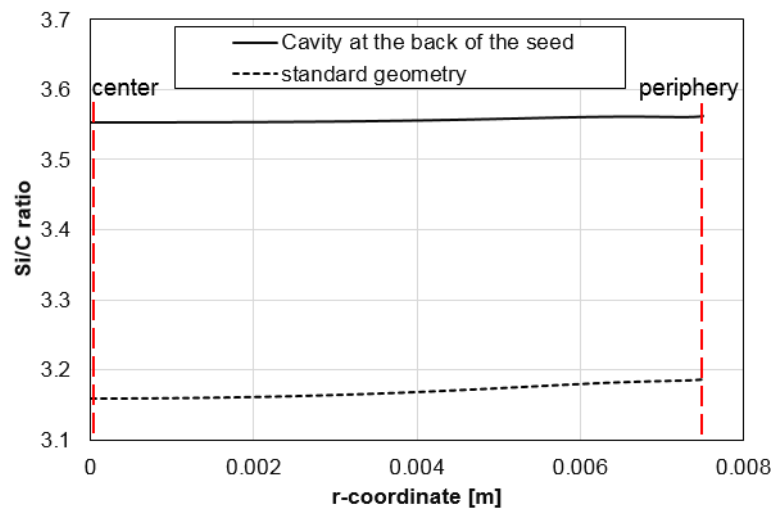


Figure 2.24. Si/C ratio distribution along the crystal radius for the case of the standard geometry and the case where a cavity at the back of the seed is formed. The positions of the center and periphery at the seed crystal are indicated.

The axial growth rate along the [000-1] direction at the center and the periphery of the convex and concave crystals demonstrated at Figure 2.21 was measured (Figure 2.25). For the case of a convex crystal, the growth rate at the center is higher compared to the edge during growth. The value of the growth rate is reducing exponentially, as reported by many authors [18, 19] and is attributed to a number of parameters like the increase of the temperature of the growth front as the length of the crystal is increasing or the decrease of Si/C ratio due to the consumption of the SiC powder. In the case of a concave crystal, the growth rate is higher at the periphery in the beginning of growth compared to the center.

However during growth (after 10 hours), the growth rate at the center is increasing and decreasing at the periphery. As a result the curvature of the crystal is changing progressively from concave to flat, Figure 2.21.

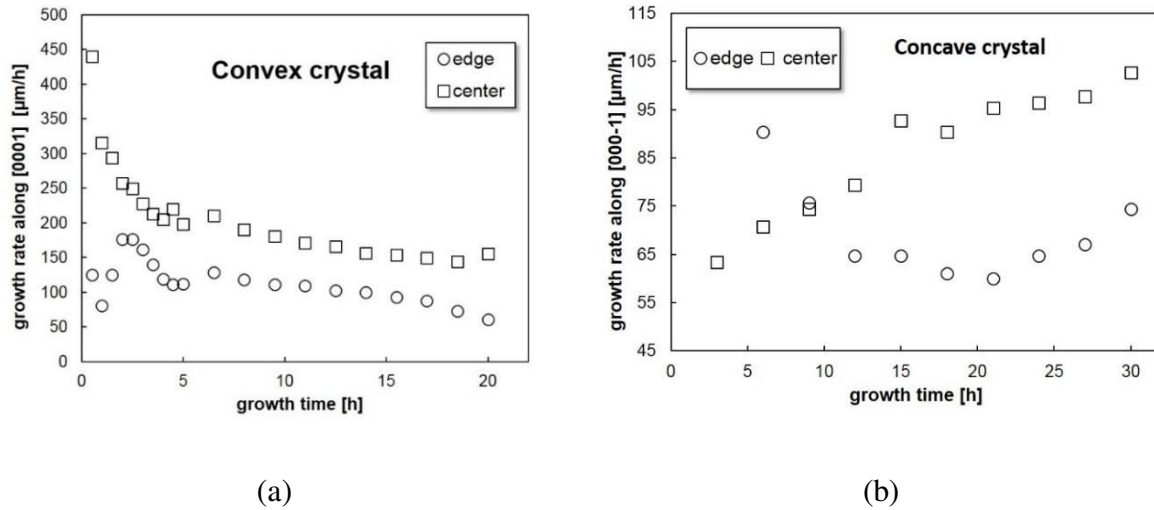
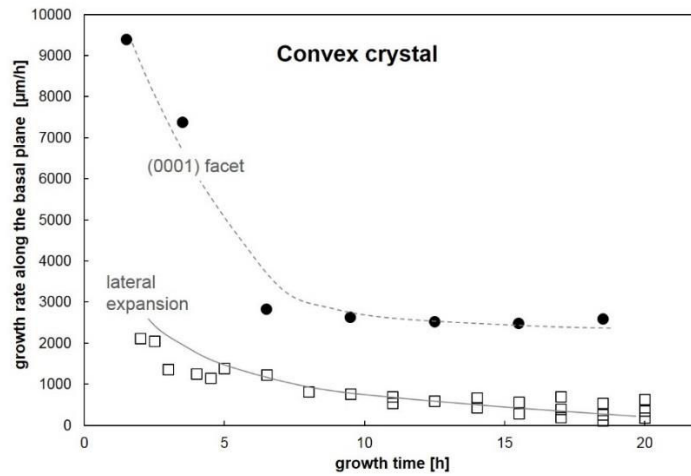
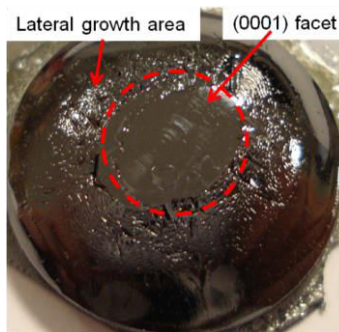


Figure 2.25. Growth rate along the [000-1] growth direction for the case of a convex (a) and concave (b) crystal shape. The growth temperature and pressure are the same in both cases.

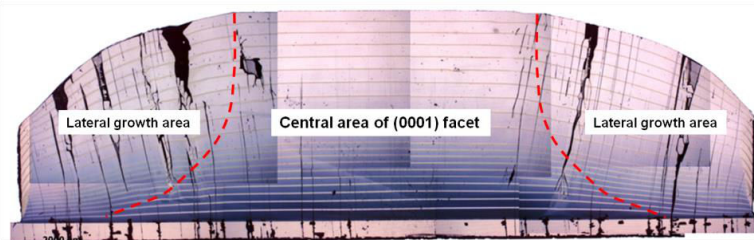
Additionally, the growth rate on the basal plane (lateral growth) was calculated for the case of a convex crystal. At the lateral growth area, the distance between two N_2 stripes was measured. Once the growth time between two stripes is known, the growth rate was determined. The lateral growth rate on the basal plane is found to be an order of magnitude higher than the axial one, as shown in Figure 2.26a. Also the lateral growth rate on the (0001) facet is higher compared to the lateral growth area. As shown by Herro et al. [6], the step density is changing when comparing the central (0001) facet and the lateral areas, due to the curvature of the crystal (Figure 2.27). This has a direct effect on the velocity of the steps, as it is shown in Figure 2.26a.



(a)



(b)



(c)

Figure 2.26. (a) Growth rate on the basal plane at the (0001) facet and the lateral growth area during growth. (b) Photo and (c) cross section as observed under a cross polarized optical microscope of a 15R-SiC grown crystal. The (0001) facet is separated from the lateral growth area by red dashed lines. Periodic nitrogen marking (lines in cross section image) was used in order to mark the evolution of the crystal.

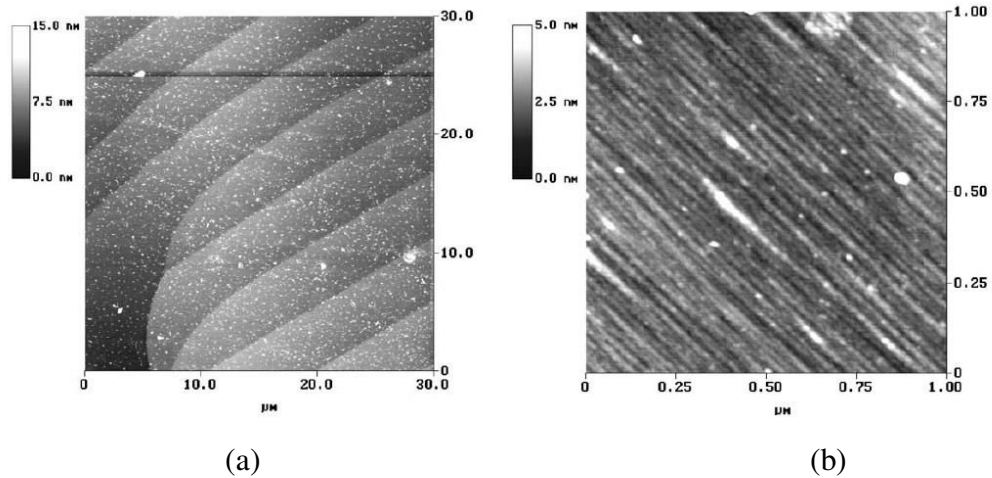
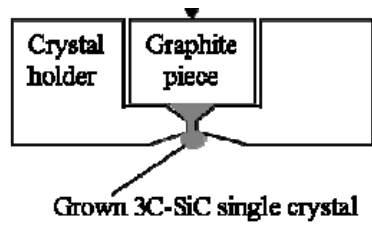
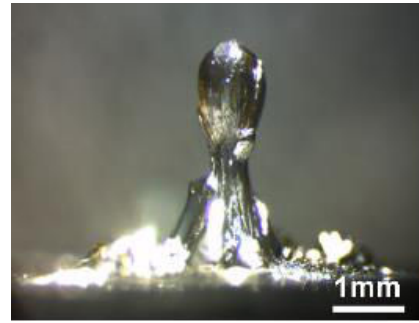


Figure 2.27. AFM performed on a 6H-SiC crystal surface at the (a) (0001) facet and (b) lateral convex grown area. In case (b) nano-scale steps are observed in contradiction to (a). The grey scale on the top left shows the variation of depth.

Design of crucible. The second parameter that was studied is the direct effect of crucible design on crystal shape. In this case, the concept of the necking technique was considered. The formation of neck is used in crystal growth from the melt, in order to reduce the density of defects and increase the crystal quality [20]. The basic principle is to increase the diameter of the crystal, starting from a small growth area. The area of the enlarged crystal will be free of threading structural defects and the quality of the crystal will be improved. In growth from the vapor phase, it was proposed by Galben-Sandulache et al. [21] using the continuous feed PVT (CF-PVT) method, as a possible technique for bulk 3C-SiC growth Figure 2.28. Effort was given to study and improve the proposed idea in the PVT system for the growth of 15R-SiC bulk crystals. Due to the lack of 15R-SiC substrates of good quality and size of a few centimeters it is necessary to grow from small substrates of 15R-SiC. However, at this point, only the development of necking technique and the effect of the crucible design on crystal shape will be analyzed.



(a)



(b)

Figure 2.28. The necking technique used in the CF-PVT system for the growth of 3C-SiC. (a) Schematic representation of the graphite holder and (b) as grown 3C-SiC crystal [21].

The graphite holder was designed as shown in Figure 2.29. A cavity was created in front of the SiC substrate that allows the growth of a conical crystal. A hole whose diameter is smaller than the diameter of the seed is found at the end of the cone. Then, the crystal is free to grow in the growth cavity.

A 4H-SiC crystal grown by using this geometry is shown in Figure 2.30. The crystal follows the shape given by the graphite crucible. In the top part, polycrystal SiC is formed, however, as shown in Figure 2.30a the single crystal is free of parasitic polycrystal and no attachment with the graphite crucible exist. Typical growth conditions were used giving a growth rate of around 250 $\mu\text{m}/\text{h}$. The growth temperature was 2200°C and the pressure 15 mbar.

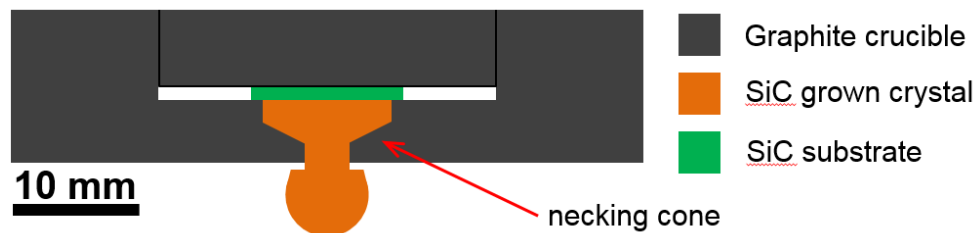


Figure 2.29. Schematic representation of the graphite lid that was used. A conical geometry was created in order to decrease the diameter of the grown crystal and subsequently allow its free expansion.

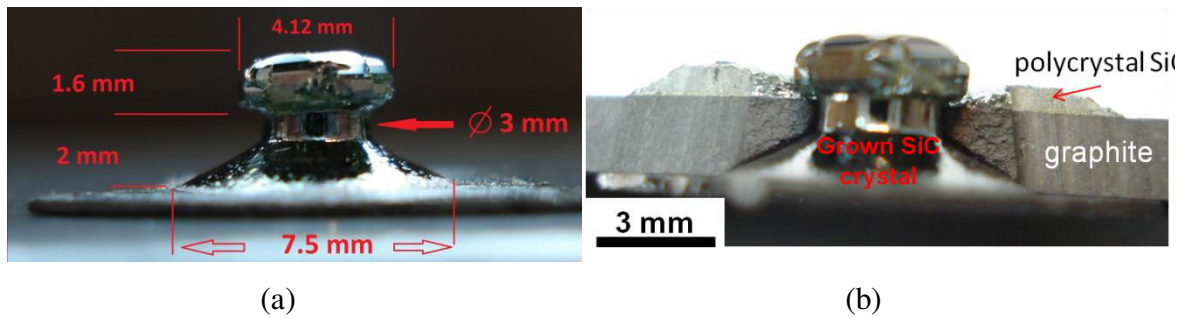


Figure 2.30. (a) SiC crystal grown by the necking technique in the PVT system. (b) SiC crystal as grown in the graphite crucible. The crystal follows the shape of the graphite holder. No strong attachment was observed between the crystal and the graphite or the polycrystal SiC.

Crystals grown by the necking technique were cut in cross section and examined under a cross polarized optical microscope. In Figure 2.31a the cross section of the crystal shown in Figure 2.30 is given. A 15R-SiC C-face 3° off-axis substrate was used and the grown crystal is a mixture of 15R-SiC and 4H-SiC as found by Raman spectroscopy. The poor quality of the 15R-SiC substrate is obvious by the presence of macrodefects that in most of the cases expand in the grown crystal. Threading defects expand along the c-direction and the propagation of those located at the periphery is terminated in the graphite sidewalls due to the conical shape of the growth cavity. In the specific example, due to polytypic transition from 15R-SiC to 4H-SiC, defects are generated at the boundary between the two polytypes that propagate along the c-direction. As a result, it is not possible to evaluate the defect density and the possible contribution of the necking technique in the improvement of crystal quality.

Substrates of C-face 4H-SiC polytype were also used, to ensure polytype stability during growth. Representative examples are given in Figure 2.31b-c. In all cases, the crystals are able to follow the shape of the graphite part in the conical or necking area. Macrodefects are usually present in the area after the neck. After a few millimeters of growth the propagation of the macrodefects is stopped and the quality of the crystal is improved.

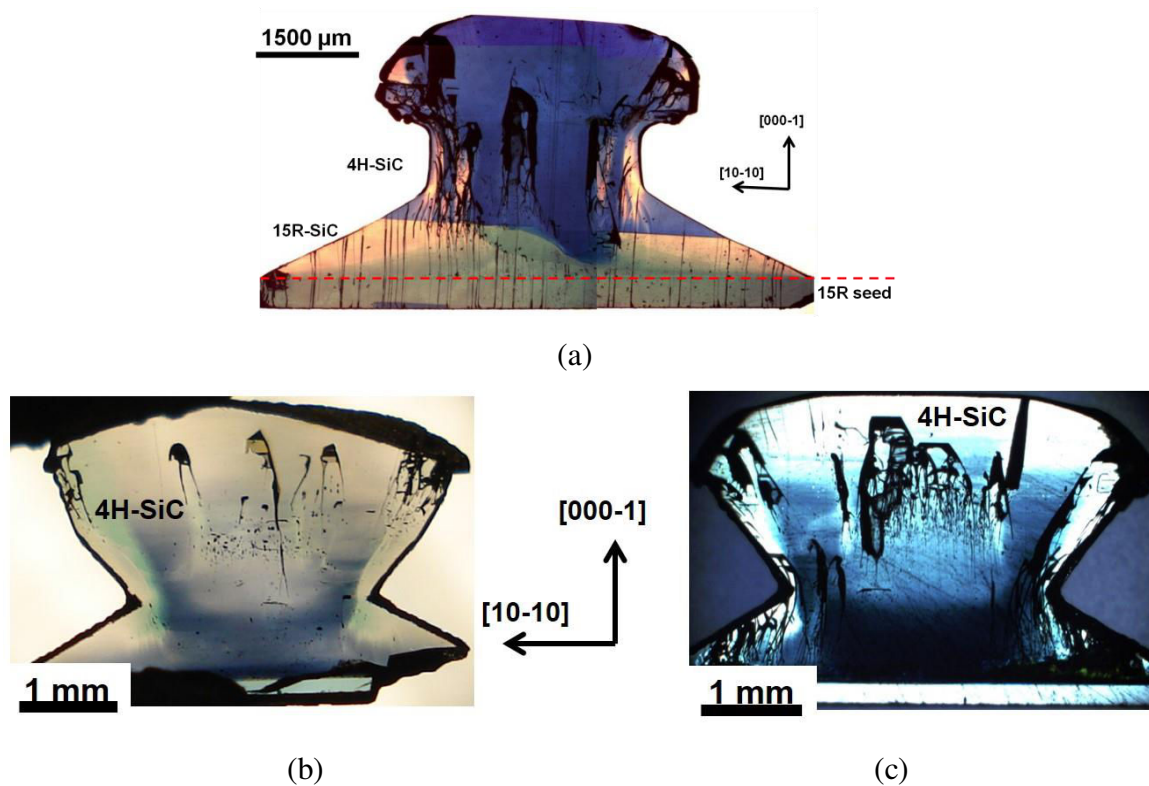


Figure 2.31. Cross section of SiC crystals grown with the necking technique observed under a cross polarized microscope. (a) A 15R-SiC C-face 4° off-axis substrate was used. The grown crystal is a mixture of 15R (yellow color) and 4H (blue color crystal). Micropipes at the periphery terminate at the graphite walls. Additional defects are created in the boundaries between the two polytypes. (b,c) 4H-SiC C-face 4° off-axis crystal homoepitaxially grown. Low growth rate $\sim 190 \mu\text{m/h}$ (b) leads to a better control of growth in the beginning avoiding the nucleation of 3C-SiC compared to a higher one $\sim 390 \mu\text{m/h}$ (c).

2.3 Conclusions of Chapter 2.

In this chapter we have proposed and evaluated some strategies in order to enlarge SiC crystals from a few millimeters to 15-20 mm in diameter. This required a thorough study of heat and mass transfers in the growth cell.

The first part of this chapter was an introduction to the experimental apparatus. The proper coupling of the frequency of the generator, the characteristics of the capacitor and the coil geometry have to be achieved in order to heat efficiently the growth furnace. Besides that, the design of the growth furnace on its own is of major importance for SiC growth. A direct or indirect way of heating can be selected, depending on the frequency of the EM field applied. The top heat sink, the design of seed holder and that of thermal screens, the relative coil – crucible position and the insulating capability of the system affect the temperature distribution in the growth cavity. The temperature distribution is directly related to the growth rate, the consumption of the SiC source material and the shape of the grown crystal. It is a matter of choice of each grower to select and define those parameters, based on the needs of the growth experiments.

In our case, a crucible geometry that allows a contactless growth of the SiC crystals was developed. Through the proper design of the top part of the crucible, a colder area compared to the crystallization area is created. As a result, an additional flux of SiC species was formed with a direction towards the colder area. That configuration allows the growth of SiC single crystals free of contact with the graphite crucible and free of parasitic polycrystalline SiC.

The shape of the crystal was controlled by two different ways. First, through the thermal field close to the seed area by modifying the design of the graphite lid. Under the presence of a cavity at the back of the seed crystal, a convex crystal shape is enhanced. With the proper design of the graphite part of the seed holder, the temperature at the periphery of the growth front is lowered compared to the center. In the latest case, the shape of the crystal is concave. Second, the control of crystal shape was achieved, using the necking technique. It was shown that the grown crystal can follow the shape of the graphite part, while no attachment between the grown crystal and the graphite crucible was observed. However, further studies are needed in order to achieve a better control of growth and to eliminate the

formation of macodefects inside the necking zone. After the necking zone, the crystal is enlarged and its quality is improved.

References

1. Fally, J., For performing successive temperature measurements. 1996, Google Patents.
2. Madar, R., et al., Numerical Simulation of SiC Boule Growth by Sublimation. *Materials Science Forum*, 2000. **338-342**: p. 25-30.
3. Ma, R.H., et al., Integrated process modeling and experimental validation of silicon carbide sublimation growth. *Journal of Crystal Growth*, 2003. **252**(4): p. 523-537.
4. Moulin, C., et al., SiC Single Crystal Growth by Sublimation: Experimental and Numerical Results. *Materials Science Forum*, 2001. **353-356**: p. 7-10.
5. Pons, M., et al., State of the art in the modelling of SiC sublimation growth. *Materials Science and Engineering: B*, 1999. **61-62**: p. 18-28.
6. Herro, Z.G., et al., Effective increase of single-crystalline yield during PVT growth of SiC by tailoring of temperature gradient. *Journal of Crystal Growth*, 2004. **262**(1-4): p. 105-112.
7. Bahng, W., et al., Rapid enlargement of SiC single crystal using a cone-shaped platform. *Journal of Crystal Growth*, 2000. **209**(4): p. 767-772.
8. Kitou, Y., et al., Flux-Controlled Sublimation Growth by an Inner Guide-Tube. *Materials Science Forum*, 2002. **389-393**: p. 83-86.
9. Nishizawa, S., et al., High-Quality SiC Bulk Single Crystal Growth Based on Simulation and Experiment. *Materials Science Forum*, 2004. **457-460**: p. 29-34.
10. Wellmann, P.J., et al., In situ visualization and analysis of silicon carbide physical vapor transport growth using digital X-ray imaging. *Journal of Crystal Growth*, 2000. **216**(1-4): p. 263-272.
11. Wellmann, P.J., et al., Impact of source material on silicon carbide vapor transport growth process. *Journal of Crystal Growth*, 2001. **225**(2-4): p. 312-316.
12. Neubauer, G., et al., Real-Time Measurement of the Evolution of Growth Facets during SiC PVT Bulk Growth Using 3-D X-Ray Computed Tomography. *Materials Science Forum*, 2014. **778-780**: p. 9-12.
13. Kato, T., S.-I. Nishizawa, and K. Arai, Dislocation constraint by etch back process of seed crystal in the SiC sublimation growth. *Journal of Crystal Growth*, 2001. **233**(1-2): p. 219-225.
14. Tairov, Y.M., Growth of bulk SiC. *Materials Science and Engineering: B*, 1995. **29**(1-3): p. 83-89.
15. Nakabayashi, M., et al., Growth of Crack-Free 100mm-Diameter 4H-SiC Crystals with Low Micropipe Densities. *Materials Science Forum*, 2009. **600-603**: p. 3-6.
16. Mokhov, E.N., et al., Growth of Faceted Free-Spreading SiC Bulk Crystals by Sublimation. *Materials Science Forum*, 2003. **433-436**: p. 29-32.

17. Pons, M., R. Madar, and T. Billon, Principles and Limitations of Numerical Simulation of SiC Boule Growth by Sublimation, in Silicon Carbide, W.J. Choyke, H. Matsunami, and G. Pensl, Editors. 2004, Springer Berlin Heidelberg. p. 121-135.
18. Selder, M., et al., Global numerical simulation of heat and mass transfer for SiC bulk crystal growth by PVT. Journal of Crystal Growth, 2000. **211**(1-4): p. 333-338.
19. Rost, H.J., et al., Influence of different growth parameters and related conditions on 6H-SiC crystals grown by the modified Lely method. Materials Science and Engineering: B, 1999. **61-62**: p. 68-72.
20. Dash, W.C., Silicon Crystals Free of Dislocations. Journal of Applied Physics, 1958. **29**(4): p. 736.
21. Galben-Sandulache, I.G., et al., Study of the Spontaneous Nucleation of 3C-SiC Single Crystals Using CF-PVT Technique. Materials Science Forum, 2010. **645-648**: p. 55-58.

Chapter 3

Nucleation and propagation of foreign polytypes.

In the present chapter, the nucleation and propagation of foreign polytypes during seeded sublimation growth of SiC is addressed on a macroscopic footing, using a coupled approach based on experiments and numerical simulations. We will demonstrate that the occurrence of a foreign polytype is linked to the combined effect of i) the presence of the natural {0001} facets and ii) the minimization of 2D nucleation energy. Areas with higher probability for a foreign polytype to nucleate, can thus be predicted. Once formed, the progress or vanishing of foreign inclusions is directly related to their interaction with the macroscopic growth interface of the crystal.

3.1 Introduction

While one of the most fascinating properties of SiC is its polytypism, it remains one of the most difficult issues to study while trying to get a single polytype, single crystalline SiC ingot [1]. During bulk growth by PVT, foreign polytype inclusions are quite commonly obtained and are usually accompanied by a host of defects (ex. threading dislocations) generated at the boundaries between the different polytypes [2-5]. Hofmann et al. attributes the generation of micropipes at the boundaries of foreign polytypes, to the stress resulting from the incoherent boundaries (Figure 3.1) [2]. A breakthrough in the understanding and the stabilization of a single SiC polytype was the development of the so-called “step controlled epitaxy” [6]. Basically, such a technique prevented the occurrence of foreign polytype by decreasing the two dimensional (2D) nucleation probability. The idea lay in the application of a misorientation to the growth surface, giving rise to a step density high enough to replicate the polytype of the substrate by a classical step flow mechanism [6]. This approach has been systematically used during epilayer growth by chemical vapor deposition and was also attempted for PVT growth of bulk crystals [7]. However, in this latter case, the off-cut angle only help stabilizing the polytype during the initial stage. As the growth proceeds, the macroscopic growth interface of the crystal drastically evolves and the step flow cannot be maintained under a stationary state.

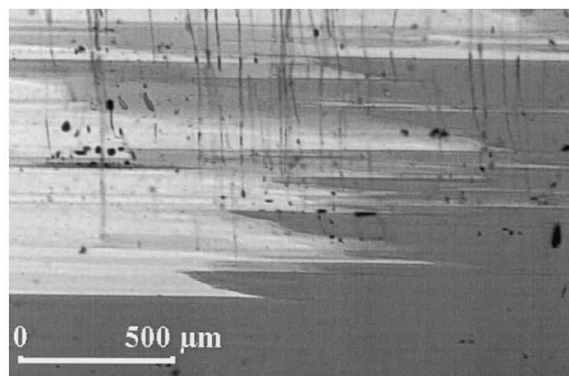


Figure 3.1. Cross section microscopy image of a 4H-SiC crystal. During growth 15R-SiC (light color polytype) is formed. Micropipes (thin dark lines) are generated at the interface of the two polytypes [2].

PVT is intrinsically a non-stationary growth process and most of the growth parameters evolve during this process [8, 9]. Physical parameters, such as Si/C ratio, temperature distribution and supersaturation vary both spatially and temporally. The impact of the system's evolution on the occurrence and propagation of foreign polytype inclusions has scarcely been mentioned. At the industrial level, the growth of 6 inch diameter single polytype 4H-SiC ingots is achieved but the mechanisms related to polytype shift and propagation of inclusions remains unclear. An interesting approach towards the clarification of this problem arose by including the classical nucleation theory in SiC growth, proposed by Fissel et al. [10] into the full PVT process simulation [11].

By combining process simulation and experiments, we aim in this chapter to bring new insight about these issues, especially on the effect of growth system evolution on the occurrence of foreign polytype inclusions. It will be demonstrated that the occurrence of a foreign polytype is linked to the combined effects of i) the presence of the natural {0001} facets and ii) the minimization of 2D nucleation energy. As a consequence, areas with high probability for a foreign polytype to nucleate can be predicted. Once formed, their progress or disappearance is directly related the interaction of the polytype inclusion with the macroscopic growth interface of the crystal.

3.2 Experimental details and theoretical calculations

Experimental details. Top seeded sublimation growth has been implemented in a fully automated homemade furnace, as presented in section 2.1. Pressure (P), temperature (T) and nitrogen partial pressure (P_{N_2}) are controlled during the process. Growth temperature is constant over the whole study, set at 2200 °C and the growth pressure was varied in the 6-12 mbar range. Growth was carried out in argon ambient, using periodic nitrogen marking to track the evolution of the growth interface shape. For the present study, crystals of about 5 mm in length and 15 mm in diameter were produced. Different substrates were used, varying the polytype (4H-SiC and 15R-SiC), the misorientation (on-axis or 4° off-axis) and the surface polarity (silicon face or carbon face). To modify the growth interface shape, i.e. to have a slightly concave or convex growth front, small

modifications in the crucible design were introduced very close to the crystallization area, as described in section 2.2.2. Such small geometrical modifications have a very local impact and do not affect the overall temperature distribution in the crucible. Consequently, growth rate was kept within the same range of 0.2 mm/hr. Grown crystals were then cut in sections parallel to the growth direction and observed with a cross-polarized optical microscope after double side polishing. The identification of polytypes was carried out using Raman spectroscopy in a backscattering geometry and cathodoluminescence (CL). A Jobin-Yvon/Horiba LabRam Raman spectrometer equipped with a N₂-cooled CCD detector was used. It employs a He-Ne laser with a wavelength $\lambda = 632.8$ nm with a total power of 11 mW as well as an Ar-Ion laser with $\lambda = 514.5$ nm with a total power of 3.2 mW. All measurements were conducted at room temperature conditions. The light has been focused to a $1 \mu\text{m}^2$ spot using a x50 long working distance objective. The Cathodoluminescence -based techniques are built around a scanning electron microscope (SEM) (FEI Quanta 200) equipped with a liquid helium cryogenic stage (Gatan) to cool down the sample from room temperature to 5K. The light generated in the sample materials by the SEM e-beam is collected by a parabolic mirror and focused on the entrance slit of a spectrometer (Jobin Yvon HR460). A nitrogen cooled silicon CCD (Jobin Yvon Spectrum One) and a single channel detector (Hamamatsu multi-alkali PMT R928) are placed at the exits of the spectrometer. They are used for the acquisition of the CL spectra and mappings (panchromatic or monochromatic), respectively. TEM experiments have been carried out in a JEOL 2010 electron microscope with a 0.19 nm point resolution.

We have used the crucible geometry for contactless growth which has been presented in section 2.2.1. The aim is to eliminate the formation of parasitic SiC polycrystal around the single crystal and to reduce the contact with the crucible as both phenomena can be the origin of polytype inclusions [12, 13]. The trends to be presented, are extracted from a set of almost 20 experiments conducted under the various experimental conditions mentioned above, see Table 3.1. The most representative results were selected to be illustrated in this chapter.

Theoretical calculations. In parallel with the experiments, numerical simulation of the process was carried out using a Finite Element Method (FEM) code. Classical nucleation theory was included to assess the probability of occurrence of different polytypes at the growth front. The simulation results were compared to the experimental results. First, the global modeling for the sublimation growth process of SiC including induction heating, heat transfer, fluid flow, and mass transport was performed in a two dimensional axisymmetric geometry [14]. The temperature and the partial pressure of the Si₂C and SiC₂ vapor species were computed along the radius of the growth front. Fissel et al. [10] introduced a way to calculate Gibbs free energy for 2D nucleation in SiC and this approach and database were used. Kakimoto et al. [15], introduced the idea presented by Fissel et al. into the PVT system. Based on Kakimoto's approach, the supersaturation (Equation 3.1) and the corresponding chemical potential difference ($\Delta\mu$, Equation 3.2) were calculated from the partial pressure of the vapor species and the temperature along the growth front. Finally, the free energy of 2D nucleation was calculated from Equation 3.3. A refined calculation of surface energy was used, compared to Fissel et al. for the surface energy of the various polytypes [16].

$$\frac{p}{p_0} = \frac{p_{\text{Si}_2\text{C}} + 2p_{\text{SiC}_2}}{p_{\text{Si}_2\text{C}}^0 + 2p_{\text{SiC}_2}^0} \quad \text{Eq. 3.1}$$

$$\Delta\mu = kT \ln \frac{p}{p_0} \quad \text{Eq. 3.2}$$

$$\Delta G_2 = \frac{b^4 \sigma_1^2}{\Delta\mu - (\sqrt{3}/2)b^2(\sigma_1 + \sigma_i - \sigma_s)} \quad \text{Eq. 3.3}$$

Where p and p_0 are the partial and equilibrium partial pressures respectively, ΔG_2 is the free energy for 2D nucleation, b is the first neighbor distance corresponding to the in-plane lattice constant, $\Delta\mu$ is the difference in the chemical potential between the gas and solid phase and σ_1 , σ_i , σ_s are the surface energy of the epitaxial layer, the epitaxial layer/substrate interface and the substrate, respectively.

Table 3.1. List of all the experiments, where polytype destabilizations were observed.

Experiment	Seed			Grown crystal		Growth parameters	
	Polytype	Orientation	Polarity	Polytype	Interface	Temperature [°C]	Pressure [mbar]
B165	15R-SiC	4° off-axis	C-face	4H-SiC	15R/4H	2200	15
B176	15R-SiC	On-axis	Si-face	15R-SiC	15R/6H	2200	20
B194	4H-SiC	4° off-axis	C-face	4H-S-C	15R/4H	2200	12
B198	15R-SiC	4° off-axis	Si-face	15R-SiC	15R/6H	2200	12
B214	15R-SiC	4° off-axis	C-face	4H-SiC	15R/4H	2200	15
B245	4H-SiC	4° off-axis	C-face	4H-SiC	4H/15R	2200	10
B251	15R-SiC	-	C-face	15R+4H	15R/4H	2200	5
B254	4H-SiC	4° off-axis	C-face	4H-SiC	4H/6H,4H/15R	2200	10
B256	4H-SiC	4° off-axis	C-face	4H-SiC	4H/6H,4H/15R	2200	12
B257	15R-SiC	4° off-axis	C-face	4H-SiC	15R/4H	2200	15
B258	15R-SiC	on-axis	Si-face	15R+6H	15R/6H	2200	6
B262	15R-SiC	On-axis	Si-face	4H+6H	15R/6H, 6H/4H	2200	8
B264	15R-SiC	on-axis	Si-face	15R	15R/6H	2200	10
B265	4H-SiC	4° off-axis	Si-face	4H-SiC	4H/15R/6H	2200	10
B266	4H-SiC	4° off-axis	Si-face	4H-SiC	4H/15R/6H	2200	10
B267	4H-SiC	4° off-axis	C-face	4H-SiC	4H/15R	2200	10
B268	4H-SiC	4° off-axis	C-face	4H-SiC	4H/15R	2200	10
B272	15R-SiC	On-axis	Si-face	15R+6H	15R/6H	2200	13
B276	4H-SiC	4° off-axis	C-face	4H-SiC	4H/15R	2200	13
B284	15R-SiC	On-axis	Si-face	6H-SiC	15R/6H	2200	13
B285	15R-SiC	On-axis	Si-face	6H-SiC	15R/6H	2150	10

3.3 Observation of foreign polytype formation and propagation

A cross section of a crystal grown on a C-face 4° off-axis 4H-SiC seed observed under a cross polarized microscope is presented in Figure 3.2a (crystal B256). To help visualizing, the (000-1) growth sector is outlined by the orange dashed lines. This area corresponds to the trajectory of the (000-1) facet during growth. This growth sector appears a little darker within the doped stripes, which is attributed to a higher incorporation of nitrogen on the C-polar facet than elsewhere [17, 18], this point will be analyzed in Chapter 5. In this cross section, three different polytype inclusions were seen. Their starting points, indicated by the red circles, are all located in the (000-1) growth sector. The first one (circle Nb#1 in Figure 3.2a) is a permanent polytype change from 4H-SiC to 6H-SiC. The other two (circles Nb#2, 3 in Figure 3.2a) are thin 15R-SiC lamellae, i.e. they do not expand axially along the [000-1] direction. Once formed on the facet, inclusions expand laterally following the steps propagation towards the [11-20] direction and spread all along the crystal diameter. A higher magnification picture of inclusion #2 is shown in Figure 3.2b.

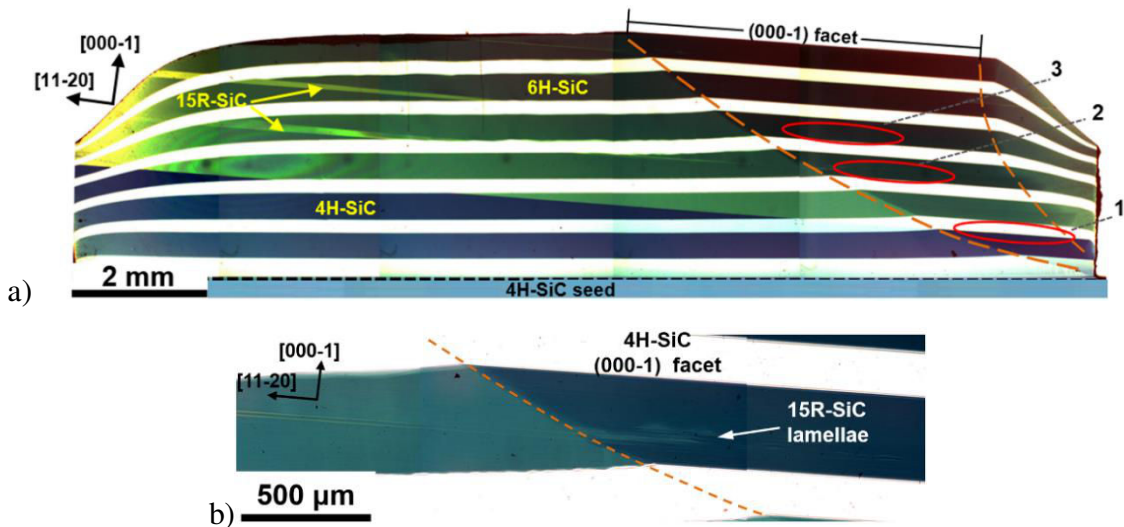


Figure 3.2. a) Cross section of a SiC crystal (crystal B256), observed under cross-polarized microscope. The seed used is a C-face 4° off-axis 4H-SiC, indicated by the black dashed line. The dark and bright stripes correspond to nitrogen doped and undoped areas, respectively. The (000-1) growth sector is delineated by the orange dashed lines. Red circles numbered 1, 2, 3 indicate the nucleation areas of one 6H-SiC (#1) and two 15R-SiC (#2-3) inclusions, respectively. b) Observation of inclusion #2 at higher magnification. The doped (undoped) stripe correspond to 3hours (1.5 hour) of growth.

In Figure 3.3, a cross section of another crystal grown on a C-face 4° off-axis 4H-SiC seed is presented (crystal B254). In this case, slight modifications of the growth cavity design have induced a more pronounced concave crystal interface, especially at the beginning of growth. The consequence, is the occurrence of two (000-1) facets at both sides of the section. On the right-hand side facet, three 6H-SiC thin lamellae nucleate – pointed with circles Nb#1, 2 and 3 (Figure 3.3a)- and expand towards the [11-20] direction. A higher magnification image of inclusions #1,2,3 at the area of the facet and the middle of the crystal, is shown in Figure 3.3b-c. On the left hand side facet, a thick 15R-SiC inclusion nucleates (left side of Figure 3.3). In contrast to the previous case (Figure 3.2), the foreign polytypes do not cross all the crystal length. Instead, their expansion on the basal plane is blocked.

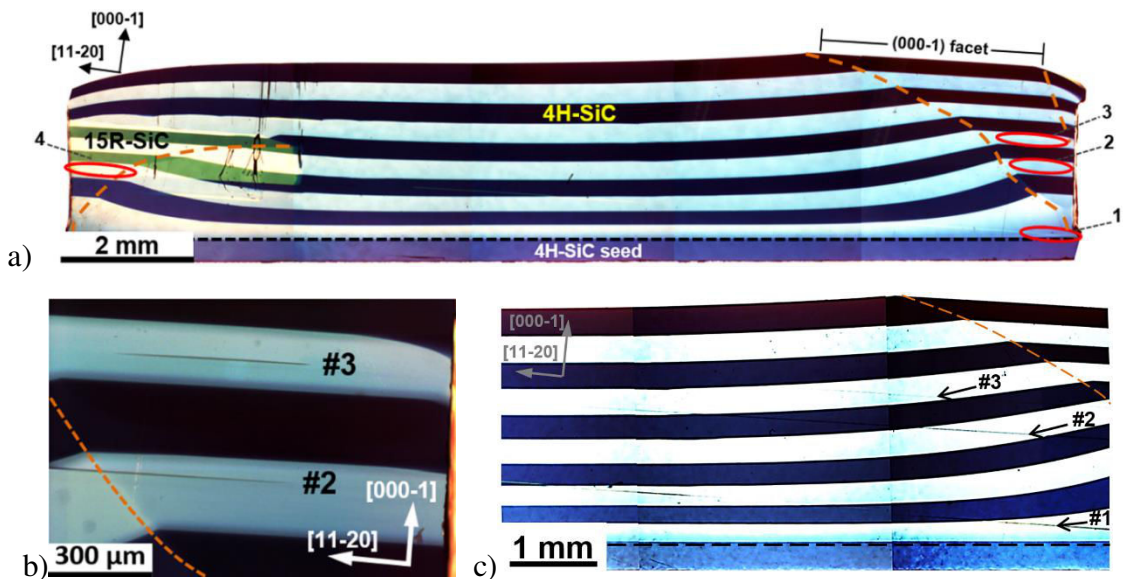


Figure 3.3. a) Cross section of a SiC crystal (crystal B254), observed with cross-polarized microscopy. The seed used is a C-face 4° off-axis 4H-SiC separated from the crystal by the black dashed line. The dark and bright stripes correspond to nitrogen doped and undoped areas, respectively. Two (000-1) growth sectors are delineated by the orange dashed lines on both sides of the crystal. Red circles indicate the nucleation point of 6H-SiC lamellae (# 1, 2, 3) and thick 15R-SiC inclusion (#4). b-c) Observation of inclusions #1, #2 and #3 at higher magnification. Each doped and undoped stripe corresponds to 3hours growth.

Cathodoluminescence (CL) technique was used for polytype identification and observation of the different polytypes, for crystal B254, additionally to Raman measurement. That was mainly done due to the higher spatial resolution of CL which is in the nanometer scale compared to the 3-5 μm of Raman and also for the possibility to perform polytype mapping. Observations were conducted in room (300K) and low (5K) temperature conditions. Due to the wide band gap of SiC the luminescence signal/background noise ratio is low at room temperature and thus no clear indication of the polytypes, neither polytype mapping could be made. In order to increase the signal/background ratio, low temperature (LTCL) measurements were performed.

Low temperature cathodoluminescence (LTCL) observation (5K). The luminescence signal was collected from inclusions #Nb2, #Nb4 and the main crystal. In parallel, a 4H-SiC commercial wafer and a 6H-SiC and 15R-SiC Lely crystals were measured as reference samples. All the spectra are compared to the ones reported in the literature.

Polytype identification. The spectra collected from the inclusions #Nb2, #Nb4 and the main crystal are given in Figure 3.4a-b and the ones of the reference samples at Figure 3.4c-d.

- Inclusion #Nb2: A peak is found at 414 nm and a broad peak at 470 nm (Figure 3.4a-b). The same peaks are obvious for the case of the 6H-SiC Lely crystal (Figure 3.4c-d). The peak of 414 nm is characteristic of the 6H-SiC [19].
- Inclusion #Nb4: A broad peak at 470 nm and a smaller side peak at 445 nm are obvious, Figure 3.4a. The same peaks are observed for the 15R-SiC Lely crystal, Figure 3.4b. An additional peak at 418 nm (Figure 3.4d), characteristic of the 15R-SiC [19] exist only for the 15R-SiC Lely crystal.
- 4H-SiC commercial wafer: The non-phonon line at ~382 nm and the one-phonon and two-phonon peaks at ~390nm and 408nm are obvious, Figure 3.4c-d. The peak at 382nm appears in higher intensity due to the high nitrogen concentration ($>10^{17}\text{cm}^{-3}$, according to supplier specifications) [20]. The broad peak at ~550nm, Figure 3.4c at green luminescence (GL) can be attributed to boron involved recombination centers [20].

- Main crystal: A broad peak at ~420 nm and a side peak at 405 nm are obvious. The broad peak at 420 nm is reported in the case of 4H-SiC and is attributed to N-Al donor-acceptors pairs [21].

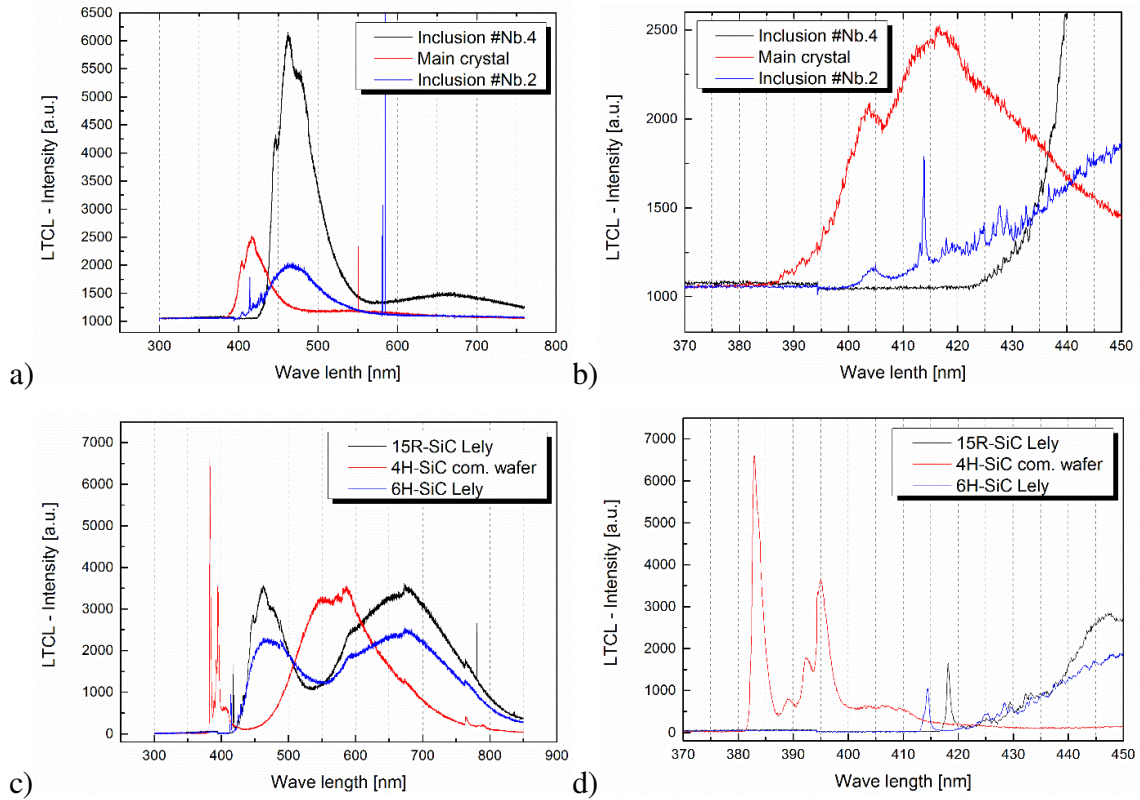


Figure 3.4. a,b) LTCL signal from inclusions #Nb. 2 and 4 and the main crystal B254. c,d) LTCL signal from 6H-SiC, 15R-SiC Lely crystals and 4H-SiC commercial wafer. The crystals were used as reference samples.

Based on the collected spectra, the identification of the various polytypes is difficult to be validated with certainty. That is mainly due to the shift and width broadening of some characteristic peaks, due to the presence of dopants. Thus, for polytype identification Raman spectroscopy is a preferable method, despite the higher spatial resolution of CL.

Polytype mapping. Monochromatic LTCL images for emission at 470 ± 2 nm (higher LTCL intensity of inclusion #Nb.2) and 385 ± 2 nm (higher LTCL intensity of the main

crystal) were obtained (Figure 3.5a and b, respectively). The starting position of inclusion #Nb.2 and a clear separation with the main crystal can be made. This verifies that indeed the foreign polytype #Nb2 forms a thin inclusion in crystal volume.

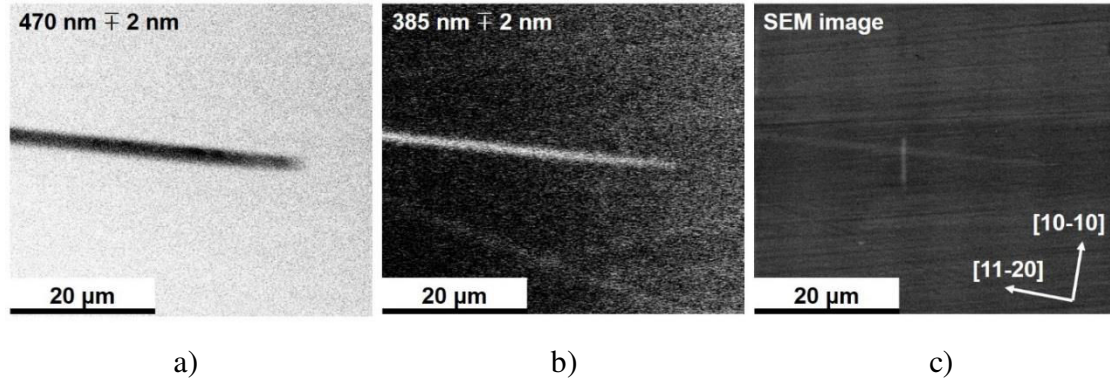


Figure 3.5. Monochromatic LTCL images for emission at a) 470 ± 2 nm and b) 385 ± 2 nm and c) SEM image of inclusion #Nb.2 of crystal B254.

To resolve the geometrical evolution of the crystal, we quantified both normal (along the [000-1] direction) and lateral (along the [11-20] direction) growth rates. Also, the lateral propagation of the polytype inclusions (A1-A3 and B1-B3 for #1-3 inclusions of crystal B256 and B254, respectively) was systematically evaluated. In particular, the lateral growth rate was calculated once the length of the inclusions was measured along [11-20] direction within each doped and undoped stripe. For the same positions, the thickness of each doped and undoped stripe was measured along [000-1] direction, thus the normal growth rate was determined. The measurements obtained from nitrogen marking are gathered in Figure 3.6. The ratio between growth rates along the [000-1] direction taken at the center (symmetry axis) and at the edge (facet location) is plotted as a function of growth time in Figure 3.6a. For crystal B256, the ratio is always slightly higher than one, except at the very beginning. The crystal surface is thus slightly convex. For crystal B254, the growth rate ratio is close to 0.5 at the beginning and progressively increases to reach 1.4 after 15 hours. The growth interface is thus concave at the beginning, then progressively flattens and turns to slightly convex at the very end of the growth. The lateral growth rate along the [11-20] direction is around one order of magnitude higher than the axial growth rate in the [000-1] direction (Figure 3.6b). Also, the lateral growth rate shows much larger variations than the axial one. The growth rate

along $[11-20]$ increases at the center of the growth front and minimizes at the periphery, while no significant difference is observed for different polytypes. The fact that the maximum is not exactly at the center of the growth front is due to the 4° miscut angle. To complete this set of measurements, we plotted the same growth rate ratio as a function of the angle between the tangent of the crystal surface and the basal plane (Figure 3.6c). As the normal growth rate (along the $[000-1]$ direction) shows only small variations, it is mainly the lateral growth rate (along the $[11-20]$ direction) that significantly varies. This lateral growth rate exhibits an exponential-like decay versus the angle between the local crystal surface and the basal plane.

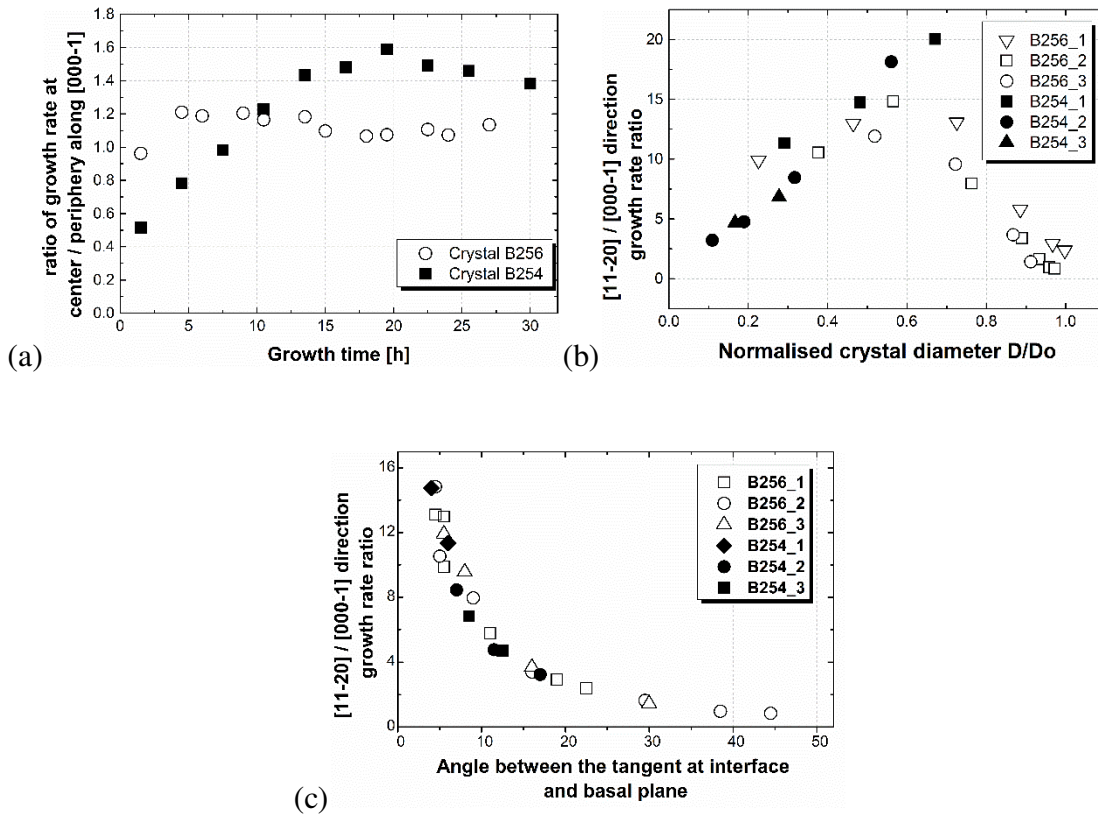


Figure 3.6. (a) Ratio between the growth rate along $[000-1]$ direction taken at the center of the crystal and at the edge (facet), with respect to growth time, for the crystals shown in Figure 3.2 and 3.3. Ratio of the growth rate along $[11-20]$ and $[000-1]$ as a function of (b) the normalized diameter (D/D_0) and (c) the angle between the tangent at the crystal interface and the basal plane of crystals B256 and B254.

To induce other kind of polytype inclusions and/or transitions, we have also used different seeds. Figure 3.7 shows a cross-section of a crystal grown on a 15R-SiC on-axis Si-face seed (crystal B258). By Raman spectroscopy, it is found that the grown crystal is a mixture of 15R-SiC and 6H-SiC. The poor quality of the 15R-SiC seed used is reflected in the grown crystal, as micropipes are present both in the seed and the crystal. Also, many micropipes and macrodefects are formed at the boundaries between the foreign polytypes. In this specific case, we significantly increased the crystal surface curvature, which rapidly shifted from concave to highly convex crystal surface during the first few hours of growth. At the beginning of the run, the growth interface is slightly concave. Similar to the case of crystal B254, two (0001) facets form at both sides of the crystal. Precisely at the location of the facets, a transition from 15R-SiC to 6H-SiC occurs giving rise to the two lateral 6H-SiC inclusions. While turning to convex, the growth interface develops another (0001) facet at the center of the crystal. After a few millimeter in thickness, a 6H-SiC inclusion appears at the center of the crystal and expand laterally.

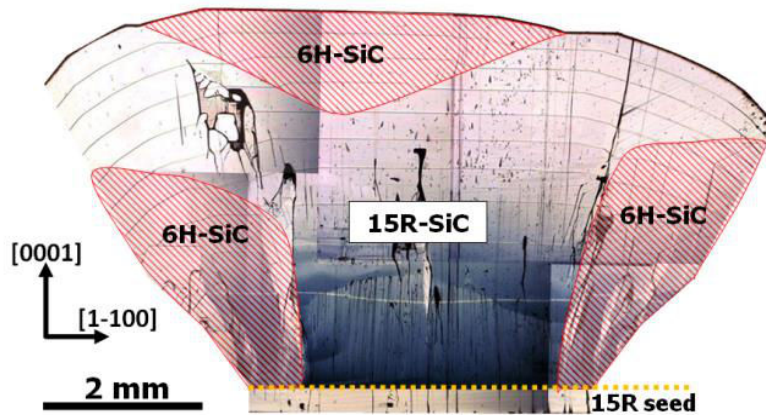


Figure 3.7. Cross section of a SiC crystal (crystal B258), observed under cross-polarized optical microscope. The seed used is Si-face on axis 15R-SiC indicated by the yellow dotted line. Periodic nitrogen marking was used in order to observe the evolution of the crystal shape. The crystal is a mixture of 15R-SiC and 6H-SiC, with the 6H-SiC areas being indicated by the red shaded regions.

3.4 Nucleation mechanism of a foreign polytype

The Gibbs free energy for the formation of a 2D nuclei was calculated for 4H-SiC, 6H-SiC and 15R-SiC on a Si-face 15R-SiC seed as a function of the crystal radius, for two different crystal thicknesses for crystal B258 (Figure 3.8). In all the conditions used, the Gibbs free energy of 6H-SiC nucleation is lower compared to the other polytypes, 15R and 4H being rather close to each other. Most interesting is the location of the minima of 2D nucleation energy along the crystal radius. At the beginning of growth, the minimum of 2D nucleation energy is located at the periphery of the growth front (Figure 3.8a). After a few mm of growth (here 3 mm), the situation becomes totally different and the minimum of 2D nucleation energy occurs on the symmetry axis of the crucible, i.e. at the center of the crystal (Figure 3.8b).

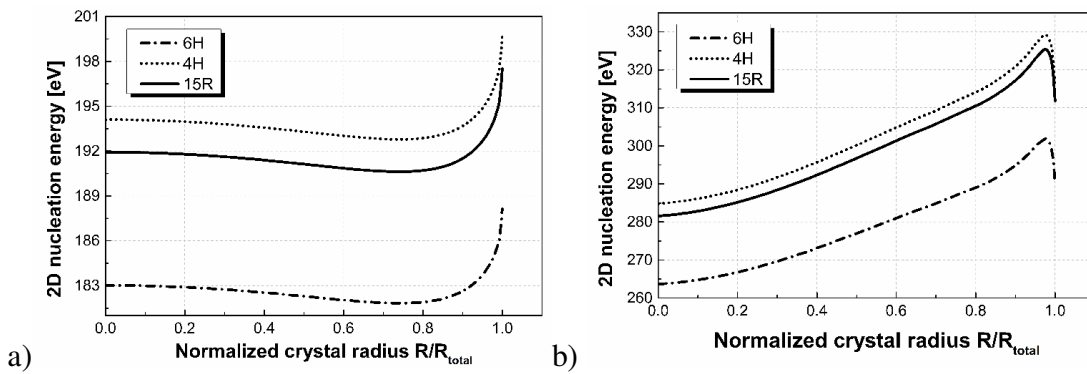


Figure 3.8. (a) 2D nucleation energy of 4H, 6H and 15R on 15R Si-face substrate at the beginning of growth of B258. The minimum is located close to the periphery of the growth front. (b) 2D nucleation energy of 4H, 6H and 15R on 15R Si-face substrate after 3 mm of growth of B258. The minimum is located at the center of the growth front.

Similar calculation was performed for crystal B254. The 2D nucleation of 4H-SiC, 6H-SiC and 15R-SiC on a 4H-SiC C-face substrate is computed as a function of crystal radius in the beginning and after 3mm of growth. Despite the larger growth area, compared to crystal B258, the minimization of 2D nucleation energy follows the same behavior as previously. It shifts from the periphery to the center of the growth front during growth (Figure 3.9).

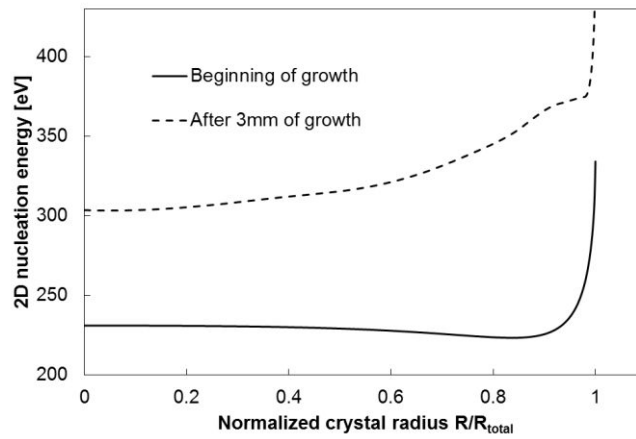


Figure 3.9. Gibbs free energy for 2D nucleation along the crystal radius, calculated for crystal B254. The calculation was performed for the beginning and after 3mm of growth. The plots are identical for all the polytypes.

3.5 Discussion

3.5.1 Discussion on nucleation of foreign polytypes.

The 2D Gibbs free energy of nucleation is a rough approach of the polytype transition problem. In the analysis undertaken, only carbon-containing species are used in the calculation of Gibbs free energy [11] and the effect of dopants on surface energy of different polytypes [22] is not considered. Such approximations are made in order to compensate for example the lack of data related to the surface energy of different polytypes [16]. Consequently, the prognosis of the preferable polytype to be nucleated cannot be taken for granted. However, we speculate that the location of the nucleation energy minima is correctly described, since it is process-dependent and not polytype dependent. Such assumption is reasonable, because we are able to compute accurately the crystal shape, meaning that the supersaturation distribution – which is the driving force for nucleation- is well described. Then, a minimum in the Gibbs free energy of nucleation does not necessarily imply a polytype transition but should be understood to signal a higher probability to form a foreign polytype nucleus.

Experimentally, we have exclusively observed the origin of foreign polytype inclusions in the growth sector corresponding to the Si-polar or C-polar {0001} facets. Terraces - covered by spirals - are found systematically at the {0001} facets (Figure 3.10a-b). It is worth noting that such observations are also an indirect proof that polytype transitions occur on the growing surface through a 2D heterogeneous nucleation mechanism, as proposed by Harada et al. during SiC solution growth [23]. The occurrence of facets is related to the crystal structure and the process itself. For on axis substrates, a convex surface will develop a facet at the center of the crystal, whereas a concave surface will exhibit an additional facet at the periphery of the crystal. For off-axis substrates, the trends are similar but an asymmetry in the crystal shape appears, corresponding to the miscut angle.

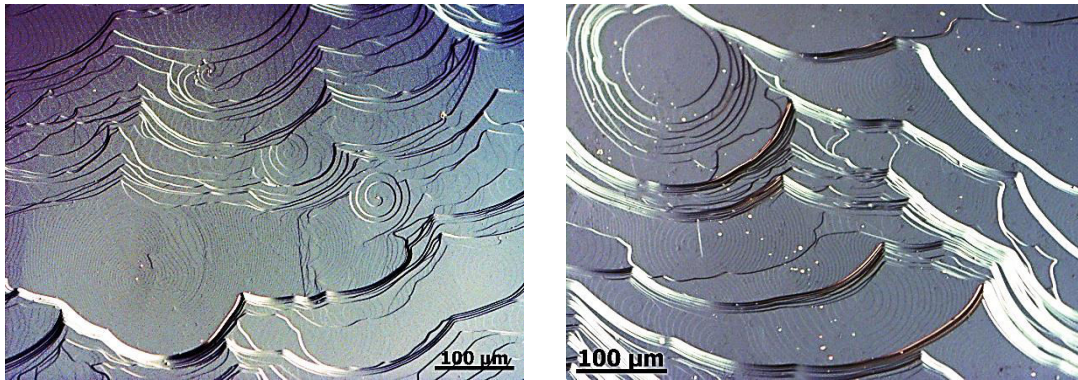


Figure 3.10. Silicon (0001) facet of a 6H-SiC crystal with nitrogen concentration of approximately $5 \times 10^{18} \text{cm}^{-3}$, observed in a Nomarski microscope. Terraces formed are covered by spirals. Crystals were grown at 2200 °C.

Calculations of the Gibbs free energy of nucleation along the crystal radius have shown that minima, corresponding to a higher 2D nucleation probability could be observed, Figures 3.8-3.9. Such minima can be precisely located, their location being dependent on the growth interface shape and on the growth time. For example, we have shown that at the beginning of growth, a slightly concave interface creates a minimum of the nucleation energy curve at the edge of the crystal. After a few millimeters of growth, the minimum is located at the center of the crystal once the interface shape has turned to slightly convex.

By combining both experimental observations and numerical calculations it is possible to draw a macroscopic model for foreign polytype occurrence. The different conditions are gathered in Figure 3.11.

- If the $\{0001\}$ facet and the minimization of 2D nucleation energy are located at the same point, then the probability to form a foreign polytype is highest on the facet.
- If the $\{0001\}$ facet and the minimization of 2D nucleation energy are not located at the same point, then the probability to nucleate a foreign polytype on the facet is much lower.
- Out of the facet, 2D nucleation probability is extremely low as the kinks density for adatoms incorporation is high enough, meaning that the replication of the substrate polytype is favorable.

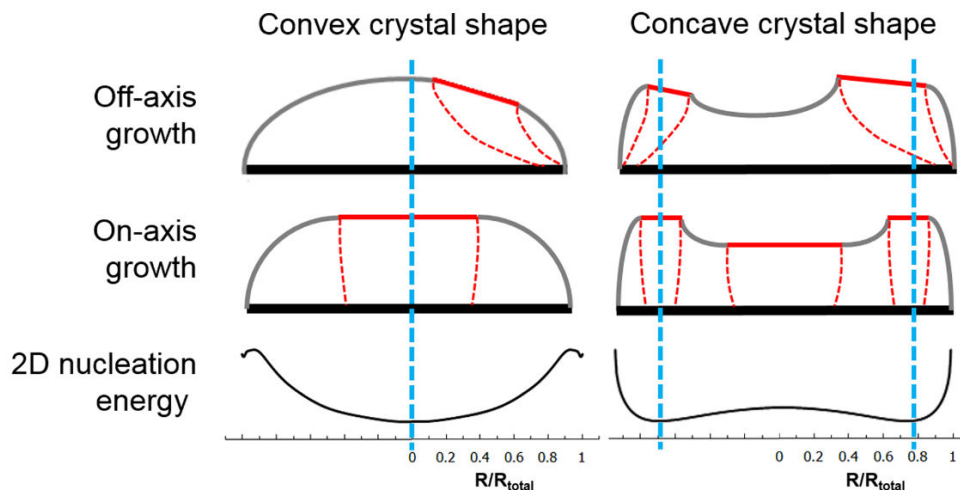


Figure 3.11. Schematic representation of the interrelation between the crystal shape, the formation of facets and the position of minimum of 2D nucleation energy. The red dashed lines describe approximately the evolution of the facets during growth. The vertical blue dashed lines indicate the position of the minimal 2D nucleation energy on the crystals.

In other words, the presence of a facet is a prerequisite for the occurrence of a foreign polytype but is not sufficient. The Gibbs free energy of nucleation must also minimize at the same location as the facet. For a convex crystal shape, the higher growth rate in the center implies a higher supersaturation and this will lead to a lower value of the 2D

nucleation energy. For a concave crystal surface, the minimum of 2D nucleation energy will appear at the periphery.

3.5.2 Discussion on propagation of foreign polytypes

Once formed, it becomes important to consider the expansion or not of a foreign polytype inclusion. To address this question, we have considered successively the lateral (on the basal plane) and the axial (perpendicular to the basal plane, along the c direction) expansions.

A. Expansion on the basal plane. Expansion along the basal plane will be separated in the $\{0001\}$ facet and the step flow area.

A1. Expansion on the $\{0001\}$ facet. If the formation of a 2D nuclei can change the polytype of the spirals found in the $\{0001\}$ facet, a model based mainly on geometrical characteristics, can be proposed. In Figure 3.12, a schematic representation of the main growth center of the $\{0001\}$ facet is illustrated, with blue color. In red color, growth centers (spirals) of a different polytype are shown, in two positions on the terrace widths of the main spiral (#A-B). The propagation of each of the foreign polytype spirals will be considered in the basal plane.

- Spiral A: It is located at a terrace formed at the main growth center of the facet. The spiral can expand in all crystallographic directions in the basal plane. Nevertheless, the propagation in the direction that will meet the advanced propagating edge of the facet's main spiral will be blocked, Figure 3.12b,d.
- Spiral B: The expansion of this spiral is not blocked by any competing adjacent spiral and a free expansion towards all directions is expected.

It must be mentioned that this is a simplified idea and it refers to an ideal case. Usually in the terraces more than one growth centers are found as seen in Figure 3.10. The expansion of a given growth center in the basal plane can be blocked in additional directions due to smaller advancing growth centers, compared to the main spiral.

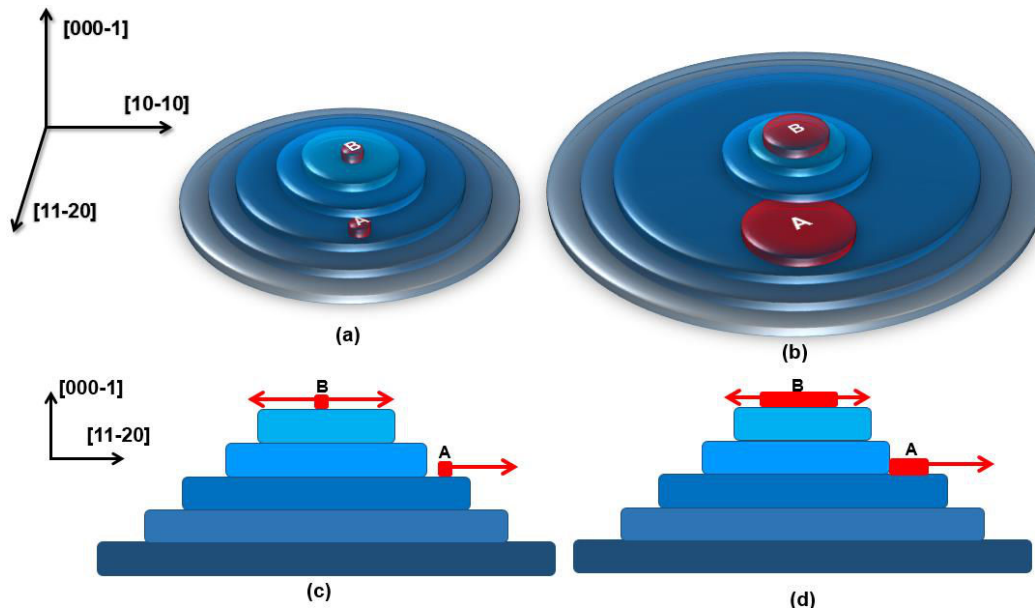


Figure 3.12. Representation of the growth centers at a $\{0001\}$ facet from top view (a,b) and side view (c,d). In blue color the main growth center of the facet and in red color foreign polytype centers are illustrated. Two positions for a foreign polytype growth center to appear are indicated A,B.

Experimentally obtained foreign polytype inclusions seems to verify the above idea. Inclusions that are similar to:

- Growth center A.
1. #Nb.2-3 of crystal B256 and #Nb.1 of crystal B254 in Figure 3.2 and Figure 3.3 respectively, can be attributed to a growth center similar to #A. They nucleate on the facet, they do not cross all the length of it and expand towards $[11-20]$ and $[10-10]$ direction (for $[10-10]$ direction it is not shown here, but it was found from cross-section samples prepared parallel to the one in Figure 3.2 and Figure 3.3). A similar example is shown in Figure 3.13 for the case of a 15R-SiC inclusion, in a 4H-SiC C-face 4° off-axis crystal B267. In this case the thickness of the inclusion is bigger compared to the previous cases ($\sim 130 \mu\text{m}$).
 2. Inclusions #Nb.2-3 of crystal B254, nucleate on the facet, they do not cross all the length of it and they expand along the $[11-20]$ direction but not $[10-10]$ direction. Inclusions #Nb.2-3 are not obvious in cross section samples parallel to the one in Figure 3.3 towards $[10-10]$ but only to the opposite of that direction, Figure 3.14.

This implies that growth centers like #A (Figure 3.12) can be attributed to these two inclusions.

3. In Figure 3.15 a 15R-SiC inclusion nucleates on the facet and expands towards the opposite of the miscut direction. No trace of this polytype were found in second half of the facet towards [11-20] direction.
 - Growth center B. For that case a total transition of the polytype in the grown crystal is expected, as there are no other blocking growth centers. That is the case of transition #Nb. 1 in crystal B256 (Figure 3.2) and inclusion #Nb.4 in crystal B254 (Figure 3.3). In the second case the expansion of the 15R-SiC inclusion is finally blocked but that was due to the change in crystal shape as will be analyzed later on in that chapter.

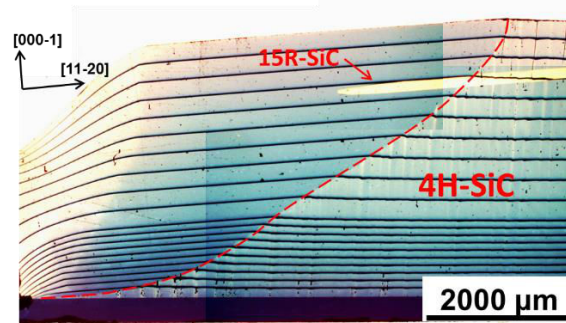


Figure 3.13. Cross-section image of a 4H-SiC C-face 4° off-axis crystal B267. A 15R-SiC inclusion nucleated at the (000-1) facet and expand towards the [11-20] direction. 15R-SiC inclusion can be attributed to a growth center similar to #A of Figure 3.12.

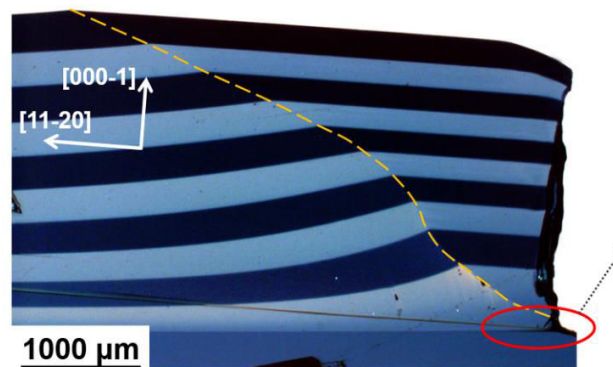


Figure 3.14. Cross section sample parallel towards [10-10] direction to cross section of crystal B254 shown in Figure 3.3. Inclusion #Nb.1 is obvious in the two cross-section samples while inclusions #Nb.2-3 do not expand towards [10-10] direction. (000-1) facet is separated from the step flow by the yellow dashed line.

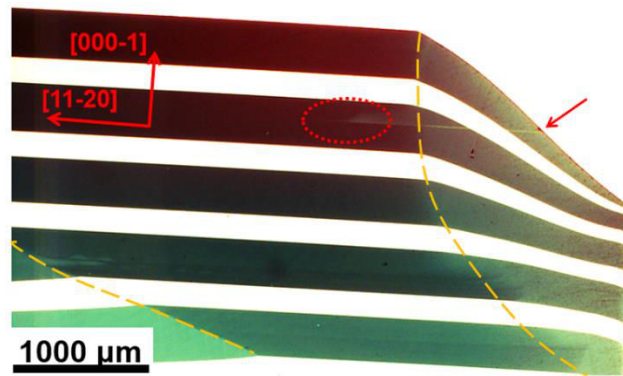


Figure 3.15. Cross section image of crystal B256. A 15R-SiC inclusion nucleates on the (000-1) facet (red dotted circle) and expands towards the opposite of the miscut angle direction (red arrow). The 15R-SiC inclusion can be attributed to a growth center similar to #A as shown in Figure 3.12.

A Transmission Electron Microscope (TEM) sample of transition #Nb.1 of crystal B256 (Figure 3.2) was prepared using a Focus Ion Beam (FIB) instrument. Sample was studied in a 200 KeV TEM and both high resolution images and diffraction pattern of the transition area #Nb.1 were obtained. Successive diffraction patterns along the transition area reveal the presence of the 4H-SiC (a) and 6H-SiC (e) polytype (Figure 3.16), as spots of the two polytypes are found (Figure 3.16 b-d). High resolution images show that in the transition area from 4H-SiC to 6H-SiC altering bands of the two polytypes exist (Figure 3.17). A direct shift of the stacking sequence from 4H-SiC to 6H-SiC (and vice versa) takes place at each of the interfaces between two polytypes. The stacking sequence is (22)(42) and (42)(22) in the case of a transition from 4H-SiC to 6H-SiC and opposite, according to Zhdanov notation. The altering bands of 4H-SiC and 6H-SiC in the transition area contain from 3 up to almost 30 unit cells of either the 4H-SiC or 6H-SiC polytypes. It is reasonable to assume that such a polytype interface can arise from the overlapping of different growth centers. However, further TEM images from exactly the transition area at the {0001} facet of various samples must be studied and compared to validate or not the proposed idea.

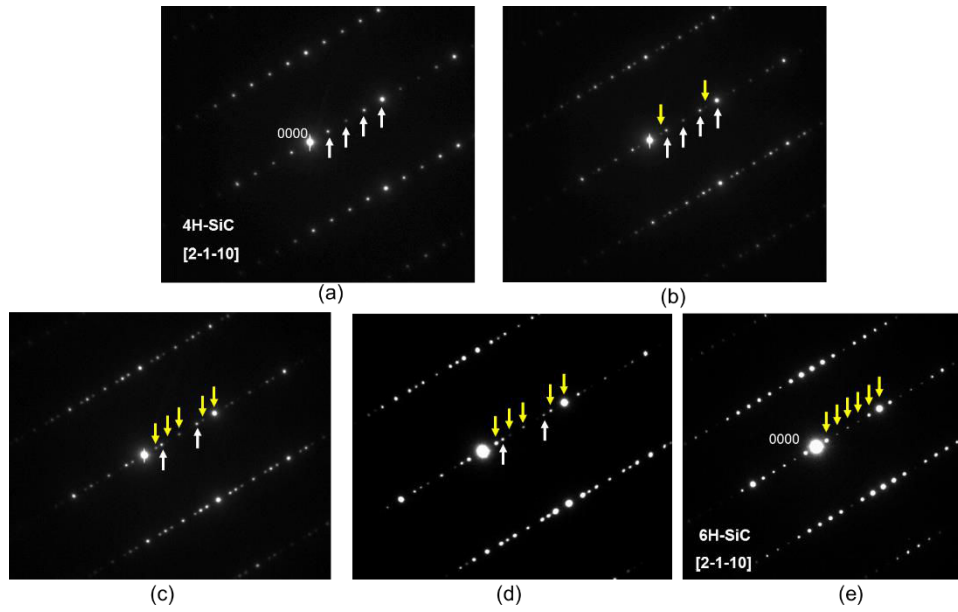


Figure 3.16. TEM diffraction patterns along transition #Nb.1 in crystal B256 from (a) to (e). 4H-SiC spots indicated by white arrows progressively disappear along the transition area. At the same time 6H-SiC spots (yellow arrows) start to appear until they remain as the main diffraction spots.

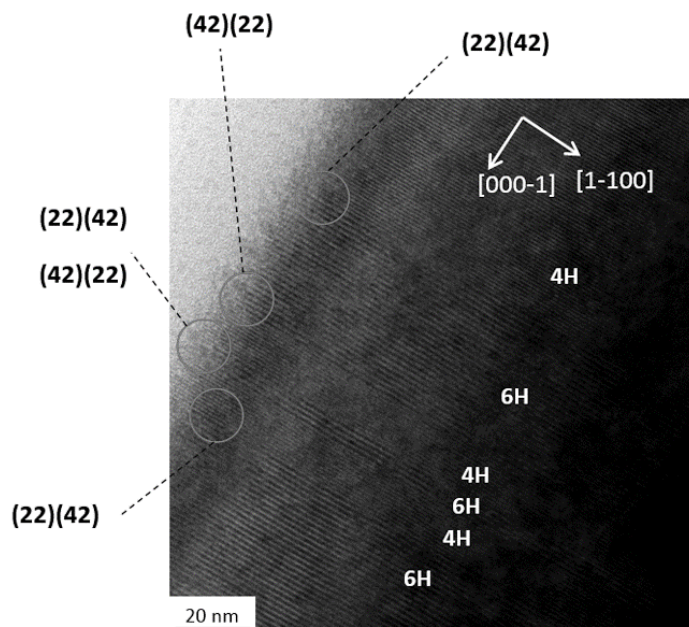


Figure 3.17. High resolution image of the transition area #Nb.1 in crystal B256. Altering bands of 4H-SiC and 6H-SiC exist between the initial 4H-SiC and final 6H-SiC polytype areas. The stacking sequence of each polytype transition interface indicate a direct polytype shift.

A2. Expansion at the step flow area. Once a foreign polytype nucleates at the {0001} facet, it can expand laterally on the basal plane beyond the so called facet area. The lateral expansion from the {0001} facet, which actually corresponds to the propagation of steps, is related to the interface curvature. Figure 3.6c demonstrates that the lateral velocity of the polytype inclusion expansion is at its maximum when the angle between the tangent to the interface and the basal plane is close to zero. As the angle increases, the lateral velocity drastically decreases. Then, convex or concave interfaces give rise to two different scenarios. A convex interface promotes the expansion of an inclusion up to the edge of the crystal, as both the interface and the inclusion have the same propagation direction. It is observed for inclusions #Nb1-3 of crystal B256 in Figure 3.2. All the inclusions initiated on one side of the crystal having a convex interface propagate over the full crystal diameter. A concave interface implies that two opposite surfaces move to meet one another. This is a blocking situation for an inclusion, as its lateral expansion will be stopped by an interface propagating from the opposite direction. This is the case for the inclusion #Nb.1-4 of crystal B254 presented in Figure 3.3.

B. Expansion in the c-axis direction. Concerning the expansion along the c-axis direction, phenomena are a little bit more complex as we do not have any direct observation to explain why some inclusions have an axial component and some have not, staying as thin lamellae. As a reasonable explanation, the following mechanism is proposed. The growth on a facet is usually characterized by the presence of a spiral as described by the standard Burton Cabrera Frank (BCF) theory of crystal growth (Figure 3.10). We can thus classify the different growth centers according to their “strength” or “efficiency”. For instance, a micropipe providing a much higher step density than a single screw dislocation will be considered as a stronger growth center. Then the question is, does the newly nucleated polytype inclusion contain its own growth center and if yes, what is the strength of this growth center compared to the surrounding ones? Mechanisms related to the creation of a spiral of another polytype has been recently reported in the literature during solution growth [23]. If the polytype inclusion has no growth center, or if its growth center is weak such as a single screw dislocation, then the axial component is too small to compete with the surrounding and will be rapidly overlapped. Once the growth center is overlapped, it is “deactivated” and the axial component of the inclusion

drops down to zero. In such case, the inclusion forms a thin lamella (inclusions # 2, 3 in Figure 3.2 and #1, 2, 3 in Figure 3.3). The schematic representation of that mechanism is shown in Figure 3.18a-b. If the inclusion contains a stronger growth center than the surrounding, then its axial component dominates and the inclusion can develop along the c direction (inclusion #1 in Figure 3.2 and #4 in Figure 3.3). In the opposite case, the expansion along the c-direction is blocked and thin inclusions are formed, Figure 3.18c-b.

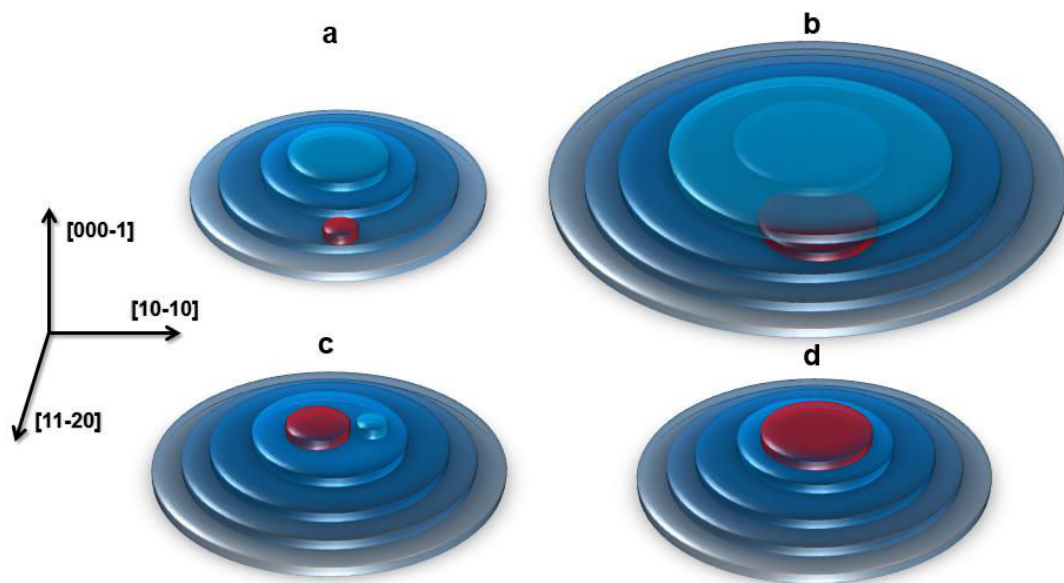


Figure 3.18. Schematic representation of the growth centers at a $\{0001\}$ facet. In blue color the main growth center of the facet and in red color foreign polytype centers are illustrated.

Once the expansion of foreign polytypes in the basal plane and c-axis direction were presented, the competition of foreign polytypes with respect to the shape of the crystal will be analyzed. Initially, for the case that a change in crystal shape takes place and continuously when the shape of the crystal is unchangeable.

Polytype overlapping due to a change in crystal shape. One example for off-axis and one for on-axis growth will be demonstrated.

- Case of off-axis growth. A magnified picture of inclusion Nb#4 of crystal B254 is presented in Figure 3.19.

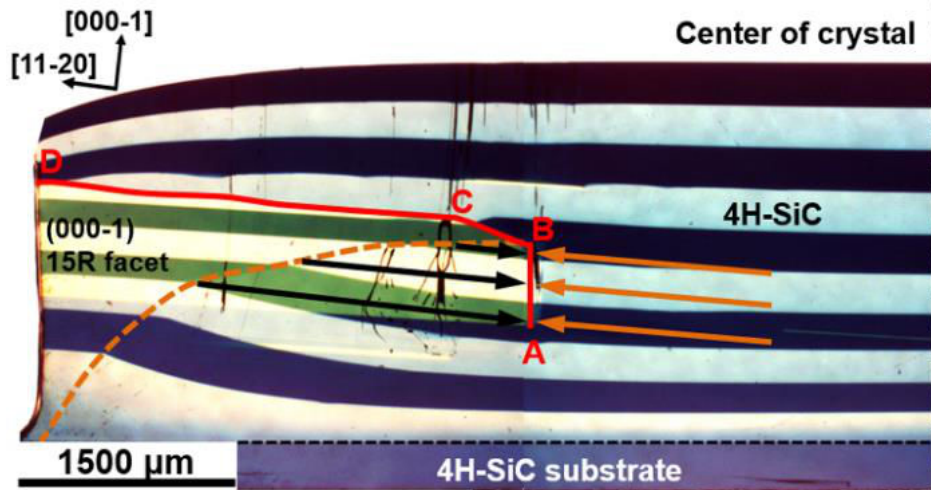


Figure 3.19. Magnified image of the 15R-SiC nucleation and propagation area of the crystal B254 shown in Figure 3.3. The orange dashed line corresponds to the boundaries of the (000-1) facet, while the black (and orange) arrows indicate the propagating direction of the 15R-SiC (and 4H-SiC) steps. The boundary between the different polytypes is indicated by the AD line.

The 15R-SiC inclusion nucleates on the (000-1) facet and expands laterally towards the center of the crystal, following the movement of the growth front (black arrows). The angle between the basal plane and the tangent at the crystal surface is less than 10° . If we refer to Figure 3.6c, such a value of angle promotes a fast lateral step velocity of the 15R-SiC inclusion towards the center of the crystal. However, due to the concave crystal shape, another interface is moving in the opposite direction from the other side of the crystal (orange arrows). The angle between this latter interface and the basal plane is also less than 10° , which ensures a high lateral velocity as well. The merging point of the two moving interfaces of competing steps, creates the hetero-polytype boundary AB. At the same time, the (000-1) 15R-SiC facet is expanding towards the center of the crystal with time, as can be seen by the orange dashed line that corresponds to the trajectory of facet's edge. At point B the (000-1) 15R-SiC facet meets the AB boundary and the competing growth modes change from step-step, to step-facet competition. At that point, 4H-SiC

starts to overlap 15R-SiC, line CD and the interface of the two polytypes change. Additionally, the growth rate along the c-direction keeps decreasing at the periphery (Figure 3.6a) and so the rate of generating new steps. Thus, the rate at which the 15R-SiC is overlapped by the 4H-SiC is increasing, line BC and CD. Finally a bulk 15R-SiC inclusion is formed once the overlapping is complete.

To help visualizing the polytype overlapping of the previous example, a photo was taken on a crystal where the same polytype overlapping mechanism appears (Figure 3.20). At the top of the image, the (000-1) facet formed because of the miscut angle of growth is indicated. In the step flow area, repeated smaller facets of the 4H-SiC and 15R-SiC polytype are located, as found by Raman. Similar to the mechanism described before steps propagating along the [11-20] direction overlap the facet they meet along this direction. The moment captured at the surface of the crystal corresponds to the BD line mentioned in the previous example.

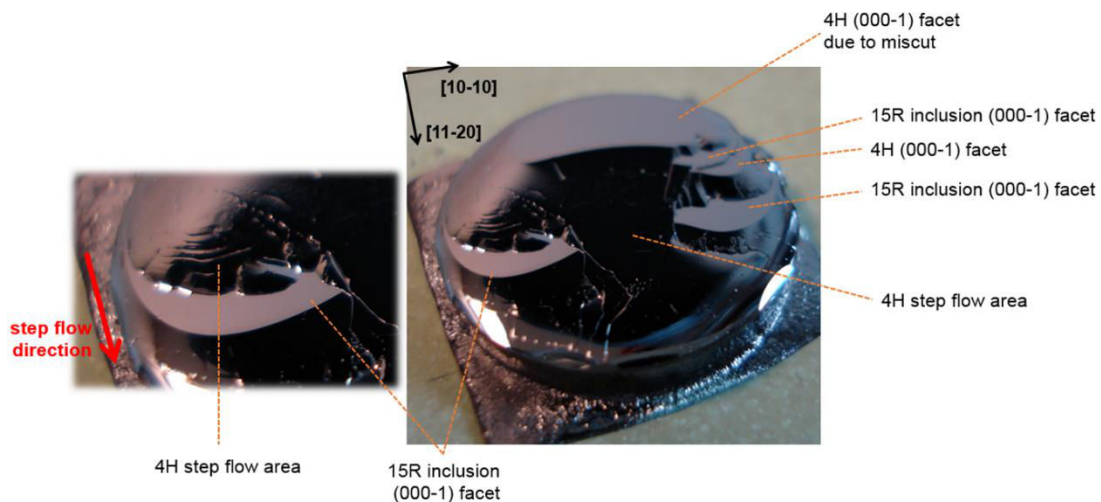


Figure 3.20. Photo of an as grown 4H-SiC C-face 4° off-axis crystal. 15R-SiC inclusions are present. The overlapping of the different (000-1) facets formed from the propagating steps is indicated.

○ Case of on-axis growth. For crystal B258, a change of the shape of the crystal takes place but for on-axis growth. At the beginning of growth the 15R-SiC grows at the center and 6H-SiC nucleated at the periphery of the growth front. The growth front of the 6H-SiC is more advanced compared to the 15R-SiC due to concave crystal shape (seen by nitrogen marking, Figure 3.7). After 1-2mm of growth, the shape of the crystal

is changing from concave to convex, similar to crystal B254. Due to the higher growth rate at the center of the crystal compared to the periphery, the 15R-SiC growth front is enhanced compared to the 6H-SiC. The axial and lateral expansion of the 15R-SiC is faster compared to the 6H-SiC and thus, that allows the 15R-SiC to progressively overlap the 6H-SiC at the periphery (Figure 3.21).

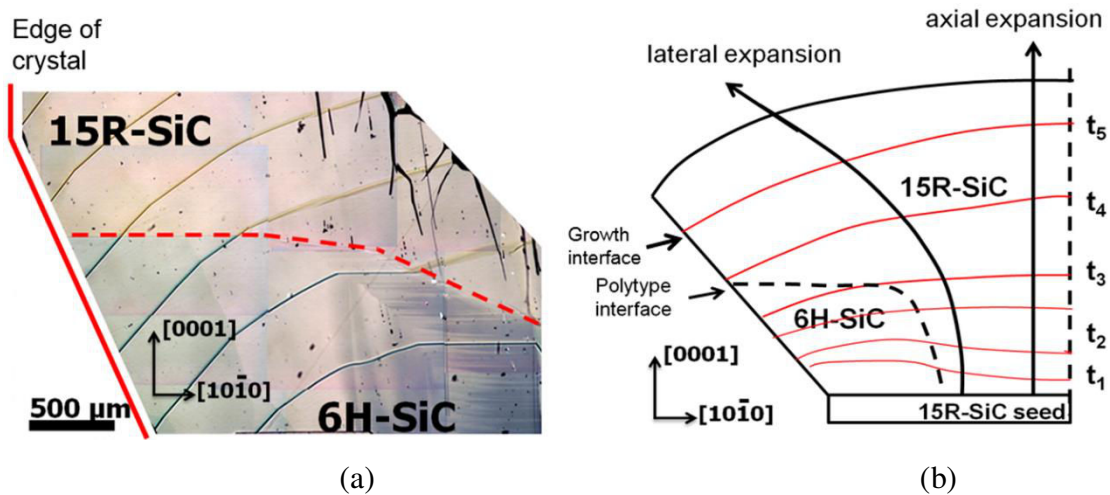


Figure 3.21. (a) Higher magnification of 15R-SiC / 6H-SiC transition area of crystal B258, shown in Figure3.7. (b) Schematic illustration of the polytype transitions in (a). The continuous red lines correspond to the growth interface at different time periods (t_1 - t_5), the black dashed line to the heteropolytype boundary and the arrows indicate the propagation of the 15R-SiC.

Polytype overlapping under a constant crystal shape.

○ Case of convex crystal shape: In the second transition of crystal B258 (Figure3.7), the 6H-SiC nucleated at the center overlaps progressively the 15R-SiC. In this case, no change in the shape of the crystal takes place in the area of the transition, as the crystal is constantly convex. The axial and lateral growth rate of the 6H-SiC (R_{g6H} and L_{g6H}) and that of the 15R-SiC (R_{g15R} and L_{g15R}) at the periphery will be considered, Figure 3.22.

The growth rate normal to a crystallographic plane, (in this case the axial growth rate R_{g15R} and R_{g6H}) depends on the velocity of the steps v and the density of the steps ρ [24]:

$$R=v\rho \quad \text{Eq. 3.4}$$

where $\rho=h/\Lambda$, with h being the height of the propagating steps and Λ the step spacing. The growth rate V normal to the slope formed by the propagating steps is given by

$$V=R\cos\theta \quad \text{Eq. 3.5}$$

The schematic representation is given in Figure 3.23. The advance of a step is determined by the net flux of atoms on the surface j_{net} :

$$v=\alpha^2 j_{net}\Lambda \quad \text{Eq. 3.6}$$

where α^2 is the area of the kink sites at the step edge [24].

The flux of atoms or the supersaturation conditions at the (0001) facet, is similar for both 6H-SiC and 15R-SiC. Thus the advancement of the 6H-SiC occurs from the difference in the crystal structure between the two polytypes. The step height of 6H-SiC growth spirals is one unit cell (6 bilayers of Si-C) compared to the step height of 5 Si-C bilayers (1/3 of the unit cell) of the 15R-SiC [25]. A higher step density ρ exists for 6H-SiC and thus a higher growth rate (Equation 3.4). Once an advanced 6H-SiC growth front is formed, a lateral expansion in the basal plane takes place. Similar to the previous example, a competition between step flow growth and spiral growth takes place, with the 6H-SiC steps overlapping the 15R-SiC facet (Figure 3.22). That is defined by the lateral growth rate L_{g6H} , which is depending on the flux of the atoms and the spacing or width of the formed steps Λ (Equation 3.6).

During the first steps of growth of crystal B258, the overlapping of the 6H-SiC comes as a result of the change in crystal shape and the advanced growth front of the 15R-SiC. At the second transition, it is the difference in step density between the two polytypes that allows the advancement of the 6H-SiC.

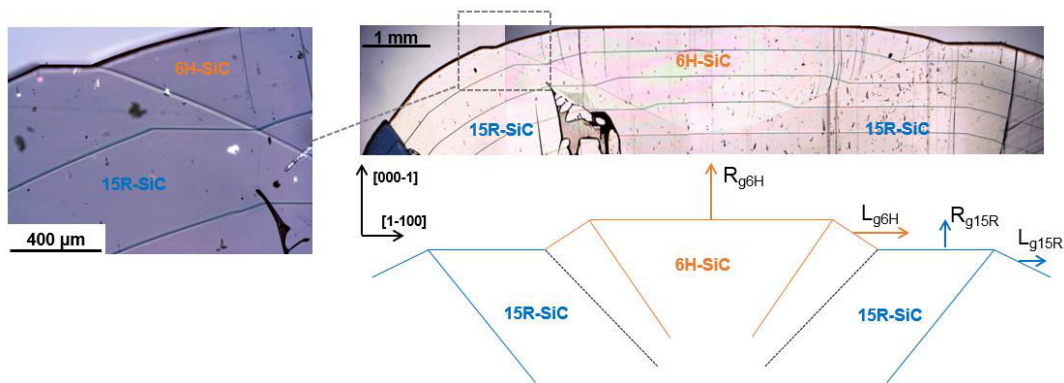


Figure 3.22: Higher magnification and schematic representation of the polytype transition in crystal B258, of Figure 3.7. The 15R-SiC and 6H-SiC areas are indicated. Rg and Lg corresponds to the growth rate along the [0001] and [1-100] direction.

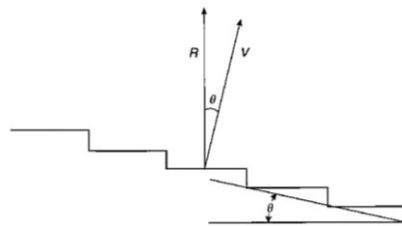


Figure 3.23. Schematic illustration of the growth rate normal to a crystallographic plane R and to the slope formed by the propagating steps V [24].

○ Case of concave crystal shape: In Figure 3.24 the cross-section of crystal B257 is shown. A 15R-SiC C-face 3° off-axis seed was used and the grown crystal is a mixture of 15R-SiC (light green color) and 4H-SiC (blue color). The contrast differences in the 4H-SiC are due to variations in doping and will be analyzed in the Chapter 5. The same crucible geometry and growth temperature to crystal B258 (Figure 3.7) were applied. However growth pressure was increased, leading to an enhanced concave crystal shape at the first steps of growth (as seen by nitrogen marking). The effect of pressure in the axial growth rate between the two crystals is shown in Figure 3.25. Especially in the first steps of growth the axial growth rate at the center at B258 is two times higher. 4H-SiC nucleates at the periphery of the growth front and 15R-SiC at the center. Due to the concave crystal shape the propagation of the growth front is enhanced towards the center of the crystal (schematic representation in Figure 3.24c). Along the [11-20] direction the

expansion of the 4H-SiC leans on the (000-1) plane over the 15R-SiC, forming a sharp interface (Figure 3.24b). Due to the continuous concave crystal shape at the area of the transition, the 4H-SiC growth front is advanced over the one of 15R-SiC. The expansion of 4H-SiC towards the opposite of the miscut direction is opposed to the propagation of 15R-SiC steps propagation from the center of the growth front. A step-like morphology is formed (Figure 3.24 b-c). In contradiction to the case of inclusion Nb#4 of B254, no change in the crystal shape takes place at the area of the transition and the foreign polytype (the 4H-SiC in case of B257) will overlap the main polytype. Also it should be noted that in crystal B257 the interface between the 15R-SiC and 4H-SiC is sharp and has a step-like shape. That is different from the “progressive or smooth” interface formed in inclusion Nb#4 of B254 (boundary BD, Figure 3.19). This is believed to be due to the competing growth modes between 4H-SiC and 15R-SiC. However, further analysis is needed to understand the shape of the interface between two polytypes, based on the competing growth mechanisms.

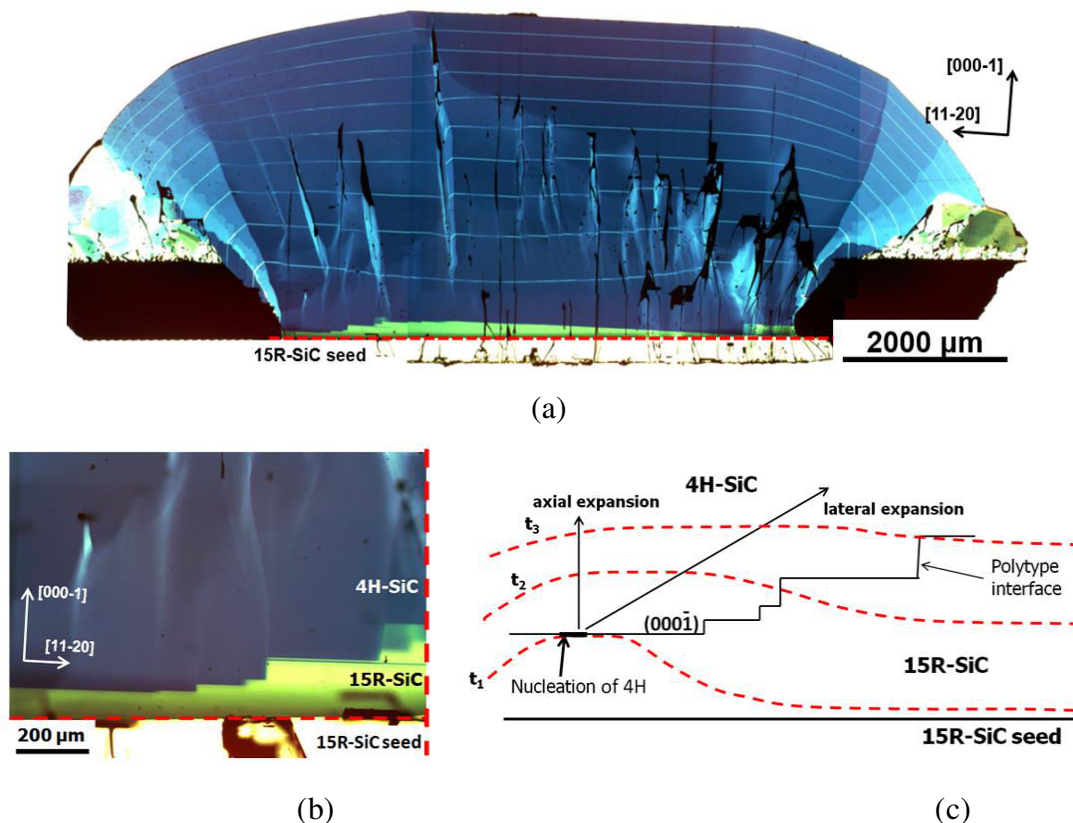


Figure 3.24. (a) Cross section image of a 4H-SiC crystal as observed by a cross-polarized optical microscope. The seed (separated by red dashed line) is a 15R-SiC C-face 3° off-axis and the crystal is a mixture of 15R-SiC (light green color) and 4H-SiC

(blue color area). The variation of contrast in the 4H-siC is due to different incorporation of nitrogen. (b) Transition area at the left side of (a) in higher magnification. (c) Schematic representation of transition area in (b). The red dashed lines represent the growth interface at three different time periods (t_1 - t_3).

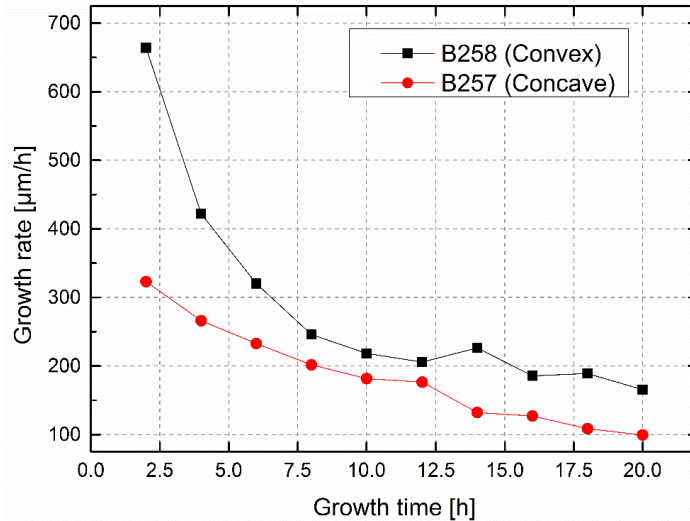


Figure 3.25. Growth rate along the c-axis (growth) direction for crystal B258 and crystal B257. Same crucible design and growth temperature (2200 °C) but different growth pressure 6 mbar and 15mbar for crystal B258 and B257 respectively, were applied.

3.6 Conclusions of chapter 3.

The occurrence and propagation of foreign polytype inclusions were systematically studied and compared with growth front topology. The nucleation of foreign polytypes has the highest probability when the presence of a $\{0001\}$ facet and the minimization of 2D nucleation energy occur at the same place and at the same time. Based on the orientation of the growth (on-axis or off-axis) and the shape of the crystal (convex or concave) areas with higher probability of a foreign polytype to nucleate appear. While the position where a foreign polytype is likely to nucleate can be spotted (through the

description of supersaturation), further improvement in the thermodynamic analysis is needed towards the “prediction” of the right polytype to nucleate.

The propagation of foreign inclusions were considered at the (0001) basal plane and the c-axis direction. In both cases, the growth center is free to expand in all the crystallographic directions, but not towards the ones where a more advanced growth center is located. Thus, the propagation can be blocked either along the c-axis, so a thin inclusion is formed, or either along the basal plane, so the inclusion do not cross all the area of the facet. Out of the facet area, the foreign polytypes propagate along the step flow direction. The expansion rate drastically increases for small angles between the local crystal surface and the basal plane. The foreign polytype expansion will be blocked if the direction of its propagation is opposed to the movement of the growth front (case of convex crystal shape).

Last, the overlapping of polytypes was considered with respect to the evolution of the crystal shape. Foreign polytypes nucleated at the periphery (due to the initial concave crystal shape) can either form a foreign polytype inclusion (inclusion #Nb4 of crystal B254) or overlap over the main polytype (4H-SiC at crystal B267). In the first case, it is the change in crystal's shape from concave to convex that will act as the driving force for the overlapping to occur. While in the second case, the advancement of the growth front from the periphery to the center (due to the constant concave shape at the area of the transition), will promote the propagation of the foreign polytype. A foreign polytype will nucleate at the center of the growth front due to a convex crystal shape for on-axis growth. The higher flux of atoms on the surface at the center of the growth front and the relative growth rate of the foreign and the main polytype growth spirals will rule the competition of the two polytypes (case of crystal B258). In all the cases, the shape of the interface between two polytypes will be defined by the competing growth mechanisms.

References

1. Tairov, Y.M. and V.F. Tsvetkov, Progress in controlling the growth of polytypic crystals. *Progress in Crystal Growth and Characterization*, 1983. **7**(1-4): p. 111-162.
2. Hofmann, D., et al., Analysis on defect generation during the SiC bulk growth process. *Materials Science and Engineering: B*, 1999. **61-62**: p. 48-53.
3. Ohtani, N., et al., Dislocation processes during SiC bulk crystal growth. *Microelectronic Engineering*, 2006. **83**(1): p. 142-145.
4. Sanchez, E.M., et al., The Nucleation of Polytype Inclusions during the Sublimation Growth of 6H and 4H Silicon Carbide. *Materials Science Forum*, 2002. **389-393**: p. 71-74.
5. Siche, D., et al., Evolution of domain walls in 6H- and 4H-SiC single crystals. *Journal of Crystal Growth*, 2002. **237-239**: p. 1187-1191.
6. Matsunami, H. and T. Kimoto, Step-controlled epitaxial growth of SiC: High quality homoepitaxy. *Materials Science and Engineering: R: Reports*, 1997. **20**(3): p. 125-166.
7. Pelissier, B., et al., Seed Surface Preparation for SiC Sublimation Growth. *Materials Science Forum*, 2000. **338-342**: p. 47-50.
8. Bogdanov, M.V., et al., Modeling Analysis of Free-Spreading Sublimation Growth of SiC Crystals. *MRS Proceedings*, 2011. **742**.
9. Madar, R., et al., Numerical Simulation of SiC Boule Growth by Sublimation. *Materials Science Forum*, 2000. **338-342**: p. 25-30.
10. Fissel, A., Thermodynamic considerations of the epitaxial growth of SiC polytypes. *Journal of Crystal Growth*, 2000. **212**(3-4): p. 438-450.
11. Shiramomo, T., et al., Thermodynamical analysis of polytype stability during PVT growth of SiC using 2D nucleation theory. *Journal of Crystal Growth*, 2012. **352**(1): p. 177-180.
12. Syväjärvi, M., et al., Morphology and polytype disturbances in sublimation growth of SiC epitaxial layers. *Journal of Crystal Growth*, 1999. **198-199**: p. 1019-1023.
13. Kitou, Y., et al., Flux-Controlled Sublimation Growth by an Inner Guide-Tube. *Materials Science Forum*, 2002. **389-393**: p. 83-86.
14. Thesis, K.A.P. 2015, Grenoble Institute of Technology
15. Kakimoto, K., et al., Thermodynamic analysis of SiC polytype growth by physical vapor transport method. *Journal of Crystal Growth*, 2011. **324**(1): p. 78-81.
16. Mercier, F. and S.-i. Nishizawa, Role of surface effects on silicon carbide polytype stability. *Journal of Crystal Growth*, 2012. **360**: p. 189-192.

17. Rost, H.J., D. Schulz, and D. Siche, High Nitrogen Doping During Bulk Growth of SiC, in Silicon Carbide, W.J. Choyke, H. Matsunami, and G. Pensl, Editors. 2004, Springer Berlin Heidelberg. p. 163-178.
18. Rost, H.J., et al., Influence of nitrogen doping on the properties of 4H-SiC single crystals grown by physical vapor transport. *Journal of Crystal Growth*, 2003. **257**(1-2): p. 75-83.
19. Siche, D., et al., Effect of Nitrogen Doping on the Formation of Planar Defects in 4H-SiC. *Materials Science Forum*, 2005. **483-485**: p. 39-42.
20. Kakanakova-Georgieva, A., et al., Cathodoluminescence identification of donor-acceptor related emissions in as-grown 4H-SiC layers. *Journal of Applied Physics*, 2002. **91**(5): p. 2890.
21. Kimoto, T., et al., Nitrogen donors and deep levels in high-quality 4H-SiC epilayers grown by chemical vapor deposition. *Applied Physics Letters*, 1995. **67**(19): p. 2833.
22. Shiramomo, T., et al., Study of the effect of doped impurities on polytype stability during PVT growth of SiC using 2D nucleation theory. *Journal of Crystal Growth*, 2014. **385**: p. 95-99.
23. Harada, S., et al., Polytype Transformation by Replication of Stacking Faults Formed by Two-Dimensional Nucleation on Spiral Steps during SiC Solution Growth. *Crystal Growth & Design*, 2012. **12**(6): p. 3209-3214.
24. Markov, I.V., *Crystal Growth for Beginners: Fundamentals of Nucleation, Crystal Growth, and Epitaxy*. 2004: Word Scientific.
25. Seiss, M., *Characterisation of the elementary growth processes of silicon carbide on-axis crystals*. 2013, Université de Grenoble.

Chapter 4

Towards the bulk crystal growth of 15R-SiC.

In this chapter, the growth of 15R-SiC bulk crystals by seeded sublimation method is studied. Possible parameters that can stabilize/destabilize 15R-SiC were examined, like: growth temperature and pressure, design of the graphite crucible, gaseous ambient of growth, shape of the crystal (convex or concave), as well as the orientation and the polarity of growth. The effect of i) surface polarity of the seed crystal, ii) the presence of nitrogen and iii) the Si/C ratio in the gas phase on the growth of bulk 15R-SiC crystals was examined.

4.1 Introduction

The 15R-SiC polytype is usually considered as a parasitic inclusion during the growth of 4H-SiC ingots by the seeded sublimation method. Though most of the works are related to its elimination, a few promising attempts to grow 15R-SiC bulk crystals have been reported [1-3]. These studies were mainly driven by the interest of using 15R-SiC in SiC MOSFET devices, because of the larger channel mobility compared to 4H-SiC and 6H-SiC [4, 5]. The stabilization of 15R-SiC was treated experimentally, in all the reported works. The influence of different growth parameters, such as the growth temperature, Si/C ratio in the gas phase, seed polytype and polarity on the stabilization of 15R-SiC during PVT have been examined.

Homoepitaxial growth of 15R-SiC is preferable to grow bulk 15R-SiC crystals, compared to growth on 4H-SiC and 6H-SiC seeds (Figure 4.1a). 15R-SiC can grow on both silicon and carbon face of a 15R-SiC seed, though more stable growth appears along the [11-20] direction. This is attributed to the fact that the stacking sequence of the 15R-SiC appears in the growth front, so it is easier to duplicate the polytype of the seed crystal [1, 2, 4]. In the case of heteroepitaxial growth, 15R-SiC can stabilize on C-face 4H-SiC and Si-face 6H-SiC seeds, but for a lower temperature and pressure range compared to homoepitaxial growth [1, 2]. The use of 15R-SiC Lely crystals as a seed is the preferable choice, but the small size and availability of the specific crystals hold back the progress in the bulk growth of 15R-SiC.

Growth temperatures in the range of 1800 to 2100 °C are reported for 15R-SiC bulk growth. These values are lower compared to the growth temperature of 4H-SiC and 6H-SiC bulk crystals (2200°C-2500°C). Growth temperature depends on the polytype of the seed and orientation of growth. Nishiguchi et al. showed that the stabilization of 15R-SiC will occur in a different growth temperature range while growing on a Si- or C-face 15R-SiC seeds (Figure 4.1b) [4]. The establishment of a low growth rate (0.1-0.5 mm/h) is essential for 15R-SiC stabilization. A low axial temperature gradient is usually applied (~5K/cm) in order to ensure a low growth rate [1, 3, 4, 6].

a)

polarity \ polytype	(0001)Si	(000 $\bar{1}$)C	(11 $\bar{2}$ 0)
15R-SiC	○	○	○
4H-SiC	×	○	×
6H-SiC	○	×	×

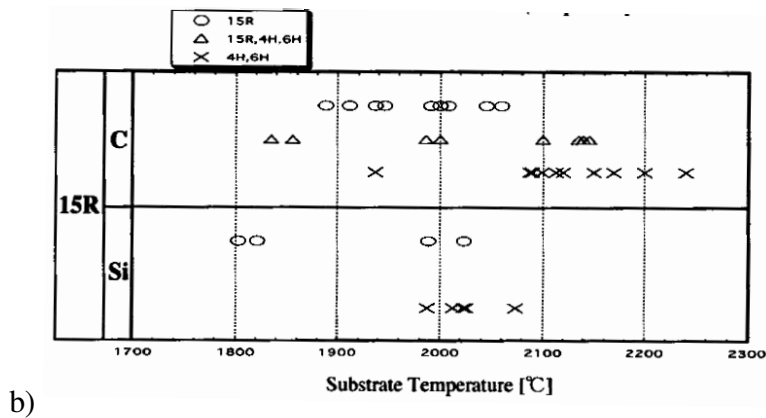


Figure 4.1. a) 15R-SiC growth versus the polytype and surface polarity of the substrate. The circle indicates a stable 15R-SiC growth, while the X and unstable 15R-SiC growth. [2]. b) Relationship between the substrate and the grown polytype. The upper line corresponds to growth on the C-face of 15R-SiC substrate, while the lower on the Si-face. Each point represents the polytype(s) that grew at the corresponding substrate temperature [4].

The presence of extra Si in the source material, in order to compensate the loss of silicon during growth was examined by Schulze et al [3]. By placing two 15R-SiC seeds of both Si- and C-face in the growth crucible, it was shown that 15R-SiC will preferentially grow on the (0001)Si-face 15R-SiC plane when no extra Si is added in the source SiC material (Figure 4.2). The authors attributed this behavior to the vapor composition in the crucible (determined by the Si content in the source material) and the hexagonality of the grown crystal.

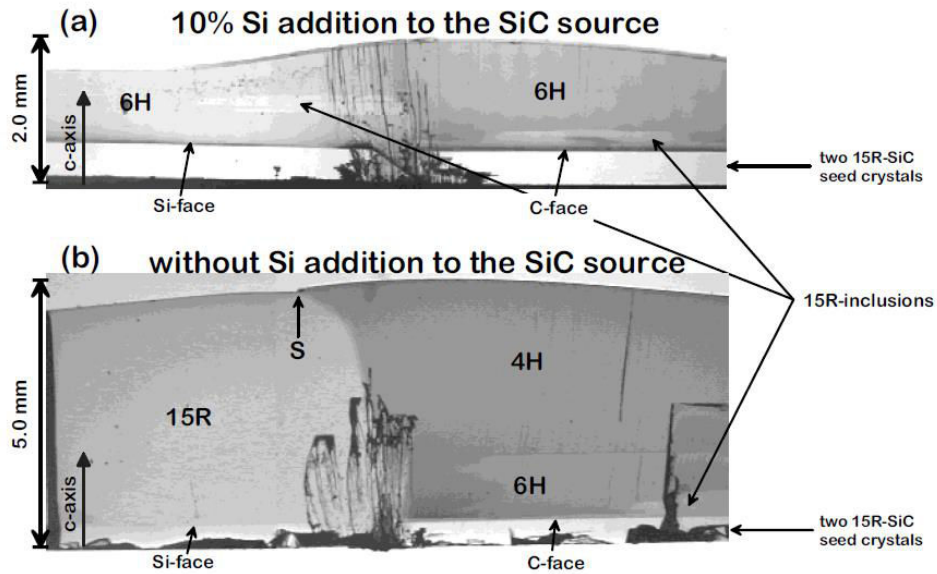


Figure 4.2. Cross section image of two crystals grown under identical growth conditions on a Si-face and C-face 15R-SiC Lely platelet a) by adding 10% Si powder b) without adding any Si in the source SiC material [3].

Despite the effort made, no optimized conditions for the growth of 15R-SiC bulk crystals were reported, nor 15R-SiC crystals of sufficient size and quality – to be used in the industry – were demonstrated. We will attempt to bring more insight into the stabilization of 15R-SiC bulk growth. Crystals were homoepitaxially grown on both 15R-SiC silicon and carbon face, while the orientation of growth was along the c-axis or 3-4° off axis. The effect of i) polarity of growth, ii) presence of nitrogen and iii) the Si/C ratio in the gas phase on the growth of bulk 15R-SiC crystals was examined.

4.2 Experimental details

Experiments were carried out in the top seeded sublimation growth graphite furnace, presented in the second chapter. 15R-SiC Lely platelets and 15R-SiC crystals extracted from parasitic inclusions formed in previous experiments were used as seeds. The growth direction was either along the c-axis or 3-4° off-axis, on both silicon and carbon faces. The graphite support of the seed was slightly modified between experiments either to adjust the size of the different seeds or to change the shape of the grown crystal. Such modifications have a very local effect in the temperature distribution close to the seed area. Argon and nitrogen gasses were used, while periodic nitrogen injections were used in some experiments to mark the evolution of crystals interface. The growth temperature and pressure were varying in the different experiments. In most experiments, the growth rate was in the range of 0.1-0.5 mm/h. A list of all the 15R-SiC growth experiments is given in Table 4.1. Grown crystals were cut either in cross section or perpendicular to the growth direction. Samples were optically polished and structural defects were observed in an optical cross polarized microscope. Raman spectroscopy was employed for the identification of the polytypes and determinations of free carrier concentration. A Jobin-Yvon/Horiba LabRam Raman spectrometer equipped with a N₂-cooled CCD detector was used. It employs a He-Ne laser with a wavelength $\lambda = 632.8$ nm with a total power of 11 mW as well as an Ar-Ion laser with $\lambda = 514.5$ nm with a total power of 3.2 mW. All measurements were conducted at room temperature, in back-scattering geometry.

Table 4.1. List of the 15R-SiC growth experiments.

Experiment	Seed			Grown parameters			Grown crystal		
	Polytype	Polarity	Orientation	Temperature [°C]	Pressure [mbar]	pN ₂	Polytype	Growth rate [μm/h]	Free carrier concentration [cm ⁻³]
B165	15R	C-face	3° off-axis	2200	15	0	4H	117	3-4x10 ¹⁷
B176	15R	Si-face	On-axis	2200	20	0	6H+15R	222	-
B198	15R	Si-face	4° off-axis	2200	12	0	15R+6H	160	-
B214	15R	C-face	4° off-axis	2200	15	0	4H	420	-
B251	15R	C-face	-	2000	5	0	15R+4H	100	-
B253	15R	Si-face	On-axis	2100	10	0	15R+6H	-	-
B255	15R	Si-face	On-axis	2200	15	0	15R+6H	237	-
B257	15R	C-face	4° off-axis	2200	15	0.05	4H	180	2-3 x10 ¹⁹
B258	15R	Si-face	On-axis	2200	6	0	15R+6H	210	-
B262	15R Lely	C-face	On-axis	2200	8	0	4H	-	-
B264	15R	Si-face	On-axis	2200	10	0	15R	215	-
B270	15R Lely	C-face	On-axis	2200	13	0.05	4H	-	2-3 x10 ¹⁹
B272	15R Lely	Si-face	On-axis	2200	13	0.024	15R+6H	-	1-2 x 10 ¹⁸
B274	15R	Si-face	3° off-axis	2200	13	0.024	6H	115	~ 1 x 10 ¹⁸
B277	15R Lely	Si-face	On-axis	2200	13	0.05	6H	400	-
B284	15R Lely	Si-face	On-axis	2200	13		6H	130	-
B285	15R Lely	Si-face	On-axis	2150	10	0.15	6H-SiC	80	-

4.3 15R-SiC crystals

The results are categorized depending on i) the polarity of the growth surface, ii) the intentional addition of nitrogen in the growth ambient and iii) the axial temperature gradient during growth.

4.3.1 Effect of polarity

Despite the variations of the growth parameters (temperature, pressure and partial pressure of nitrogen), the use of different orientation for growth (see Table 4.1) and the use of different crucible geometry, a clear trend was observed. 4H-SiC systematically forms on the (000-1) C-face and 6H-SiC on the (0001) Si-face of the 15R-SiC seed. In Figure 4.3 the occurrence of 4H-SiC and 6H-SiC as a function of the surface polarity of the seed crystal is shown for all the experimental results of Table 4.1. In most of the cases the grown crystals were a mixture of 15R-SiC with one of the two hexagonal polytypes. The simultaneous nucleation of 4H-SiC and 6H-SiC in the same crystal was never observed and in a few exceptions, stable 15R-SiC growth has been obtained.

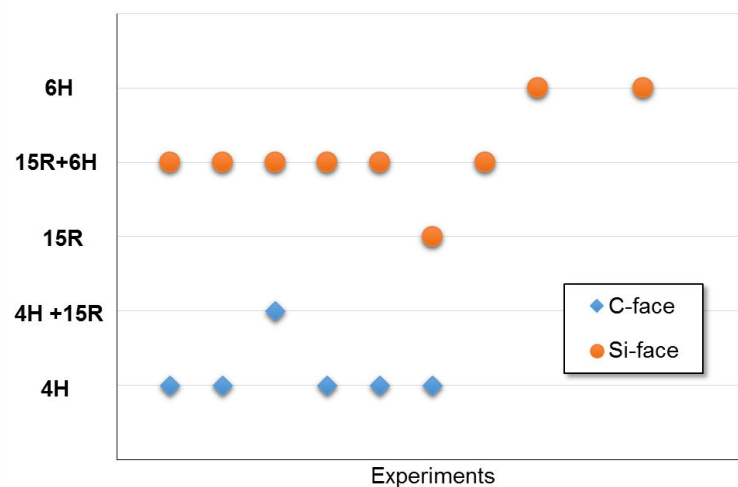


Figure 4.3. Occurrence of 6H-SiC, 15R-SiC and 4H-SiC during the growth of 15R-SiC bulk crystals based on the surface polarity of the 15R-SiC seed crystal.

Four experiments were selected to be analyzed. The first two experiments to discuss are B270 and B277. For both experiments the same growth parameters were applied, 2200°C for the growth temperature, 13mbar for the pressure and the partial pressure of nitrogen was at 0.05. Also the geometry of the growth crucible and the size of the seeds are identical in both cases, as 15R-SiC platelets were used. However, the surface polarity of the seed crystal is not the same for the two experiments. Crystal B270 is 4H-SiC and crystal B277 is 6H-SiC, while no 15R-SiC inclusions were found. Photos of the grown crystals are shown in Figure 4.4. Crystal B270 was cut perpendicular to the growth direction, however the interface with the 15R-SiC could not be located. In the case of B277, the presence of macrodefects - obvious on the surface of the crystal (Figure 4.4b) did not allow further structural analysis.

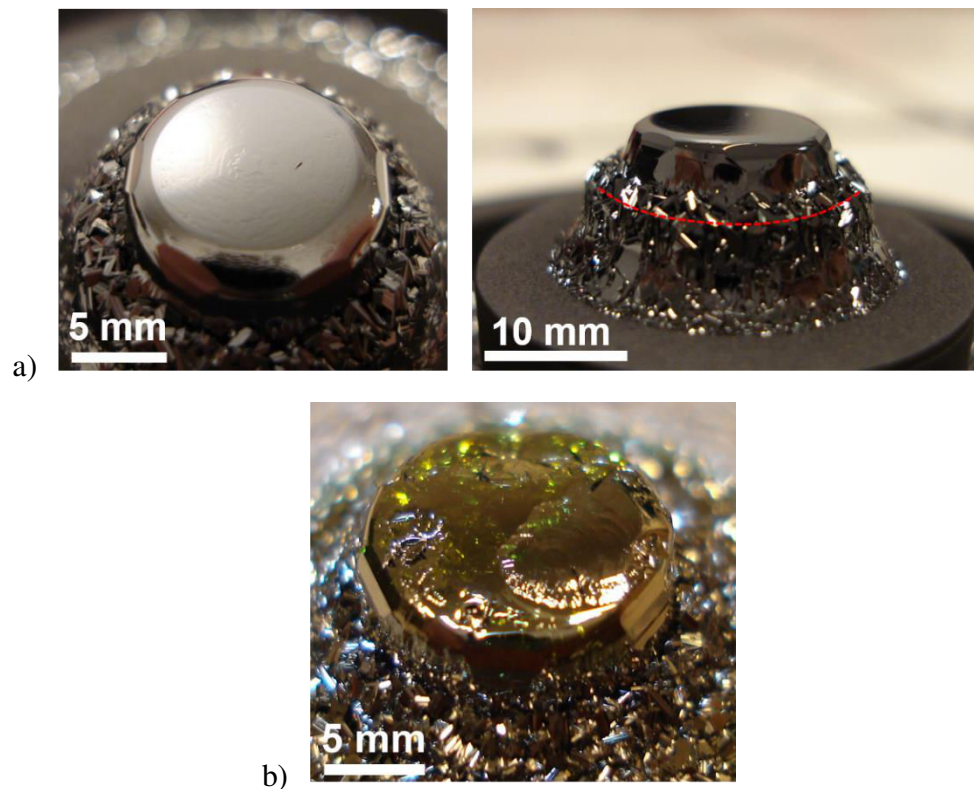


Figure 4.4. Photos of crystal a) B270, 4H-SiC, C-face growth and b) B277, 6H-SiC, Si-face growth. Crystals were grown under the same growth conditions on 15R-SiC seeds, Table 4.1.

In order to locate the point where the transition from 15R-SiC to one of the hexagonal polytypes takes place, cross section samples of the grown crystals were prepared. The cross section of crystal B214 is shown in Figure 4.5. By Raman it was found that the crystal is a mixture of 15R-SiC (green/brown color) and 4H-SiC (blue color). Due to the 3° off-axis growth, a (000-1) facet is formed and it is separated by orange dashed lines in Figure 4.5b. The starting point of 4H-SiC is on the (000-1) facet and later during growth a sharp overlapping of the 4H-SiC over the 15R-SiC takes place.

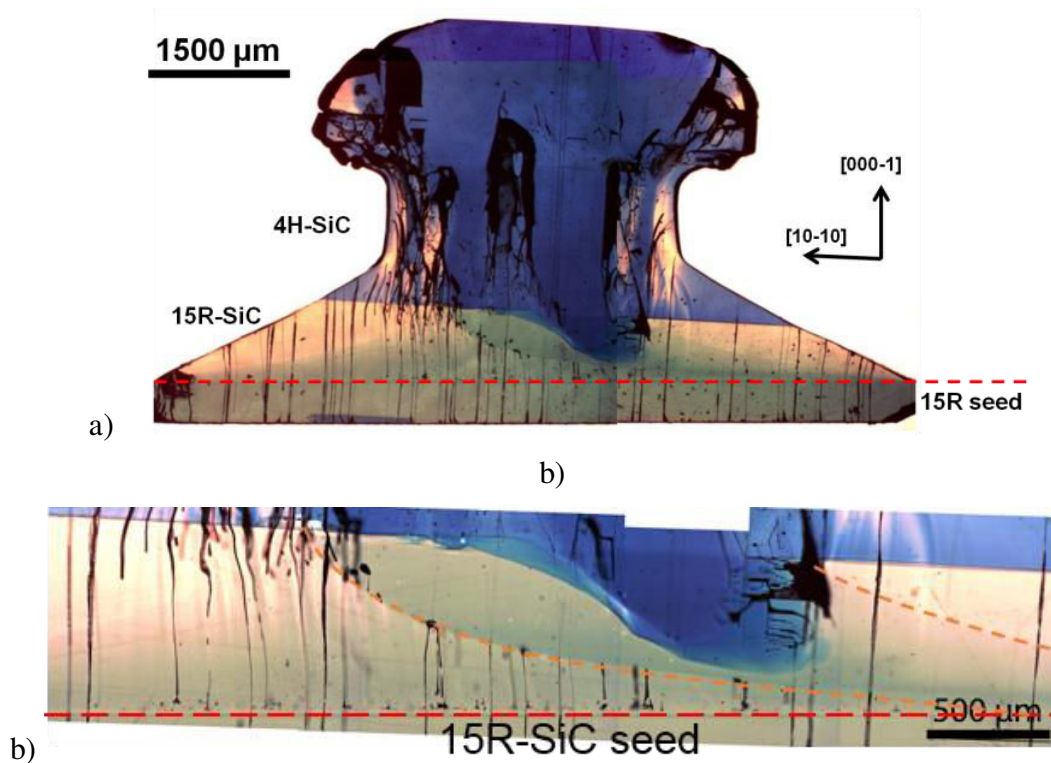


Figure 4.5. a) Cross section image of a SiC crystal B214 grown at 2000°C and 15 mbar of pressure. The seed is a 15R-SiC 3° off-axis C-face and the grown crystal is a mixture of 4H-SiC (blue color) and 15R-SiC (green color). b) Higher magnification image of the area where the transition takes place. The limits of the (000-1) facet are indicated by orange dashed lines.

The last sample to analyze is crystal B198. A photo of the grown crystal is shown in Figure 4.6. By Raman it was found that the crystal is a 15R-SiC, while on the (0001) facet a 6H-SiC growth center is located. The growth conditions were similar to B214, as seen in Table 4.1, but the design of the graphite support of the seed is different, due to the difference in the size of the seeds that were used (~6mm for B214 and ~15mm for B218). Despite the differences in the temperature profile close to the seed area introduced by the different geometry – as analyzed in the second chapter – the occurrence of the hexagonal polytypes are related to the presence of a {0001} facet.

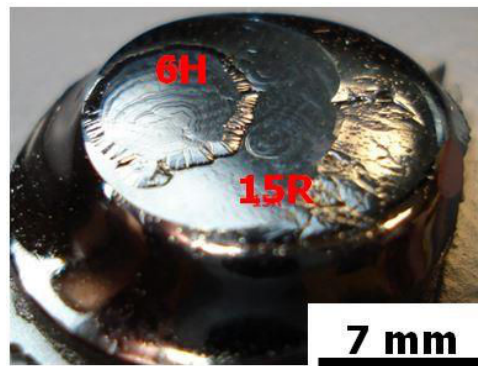


Figure 4.6. Crystal B198 grown on a 15R-SiC 3 θ off-axis Si-face seed. The crystal is of the 15R-SiC polytype and a 6H-SiC growth center is located on the (0001) facet.

Areas of 20 μm x 20 μm at the surface of the (0001) facet of B198, were scanned using an atomic force microscope (AFM). The step height of spirals found in the 6H-SiC growth center were of approximately 1.55 nm which corresponds to the height of 6 Si-C bilayer or the unit cell of 6H-SiC (Figure 4.7b). In the rest of the (0001) facet, spirals with step height of 5 bilayers of Si-C (~1.3 nm) were found. This height corresponds to 1/3 of the unit cell of 15R-SiC. The axial growth rate depends on the step density and the step height of the growth spirals, as shown in Equation 3.4 and 3.6 (Chapter 3). The bigger step height of the 6H-SiC spirals contribute to the advanced growth front of the 6H-SiC growth center over the 15R-SiC, taking into account that on the (0001) facet 15R-SiC and 6H-SiC spirals grow under similar supersaturation conditions.

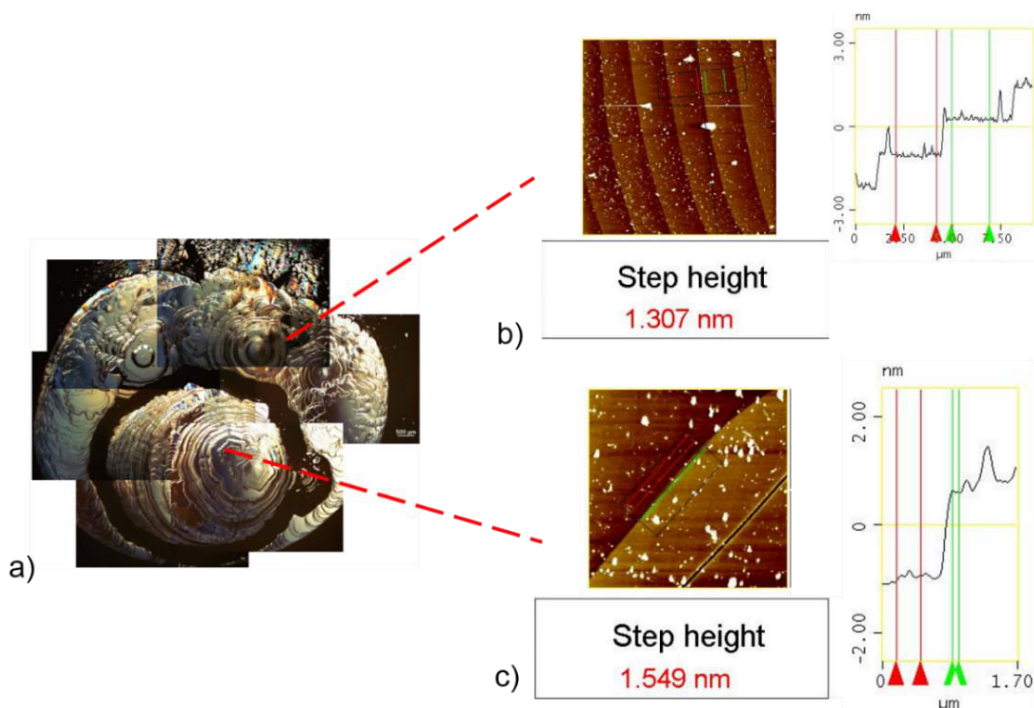


Figure 4.7. a) Nomarski image of crystal B198. Spirals at different areas were scanned by AFM. The step height of b) 5 Si-C bilayers and c) 6 Si-C bilayers correspond to 1/3 of the step height of 15R-SiC and the unit cell of 6H-SiC.

The problem of facet occurrence and the probability to nucleate a foreign polytype was already analyzed in chapter 3. The position of the transitions, the orientation of growth and the macroscopic shape of the crystals are in agreement with the model that was proposed in chapter 3. This observation implies that the occurrence of 4H-SiC or 6H-SiC during the bulk growth of 15R-SiC arise due to the formation of a 2D nuclei on the 15R-SiC spirals. An additional argument to that statement is that the occurrence of the hexagonal polytype depends on the growth polarity. It was systematically observed that 6H-SiC nucleates at the Si-face 15R-SiC (0001) facet, while 4H-SiC at C-face 15R-SiC (000-1) facet. Similar trends for Si-face 15R-SiC was reported by Schulze et al., however on C-face both 6H-SiC and 4H-SiC were obtained [6]. Nishiguchi et al. did not obtain any “polarity preferential” polytype occurrence, as grown crystals were a mixture of all the three polytypes (Figure 4.1b) [4]. The importance of polarity in the nucleation of a foreign polytype is already

described for 4H-SiC and 6H-SiC. The growth of 6H-SiC on the Si-face and 4H-SiC on the C-face of the 4H-SiC polytype is attributed to the difference in surface energy of the two polar planes [7].

4.3.2 Effect of nitrogen

The experiments are separated based on the surface polarity of the 15R-SiC seed used for the growth.

Growth on (000-1) C-face. A 15R-SiC C-face 3-4° off-axis substrate was used for both experiments B165 and B257. The growth temperature was set at 2200°C and the pressure at 15 mbar. For B165 no nitrogen gas was intentionally added in the growth ambient and any dopant incorporated in the crystal, is due to unintentional doping coming from the SiC source material. In contrast, nitrogen was added in the argon gas in the case of B257 growth, with the partial pressure of nitrogen being 0.05. The free carrier concentration at the surface of the crystals was estimated, using the LO and TA Raman mode [8], at $3-4 \times 10^{17} \text{cm}^{-3}$ and $2-3 \times 10^{19} \text{cm}^{-3}$ for B165 and B257 respectively.

The cross sections of crystals B165 and B287, observed under a cross polarized microscope are shown in Figure 4.8. The crystals are a mixture of 15R-SiC and 4H-SiC. In both cases, 4H-SiC nucleates on the (000-1) plane at the beginning of growth at the periphery of the growth front. Due to the concave crystal shape, 4H-SiC overlaps the 15R-SiC at the center (as described in Chapter 3). Macrodefects generate at the boundaries of the two polytypes, expand along the growth direction and terminate at the surface of the grown crystal.

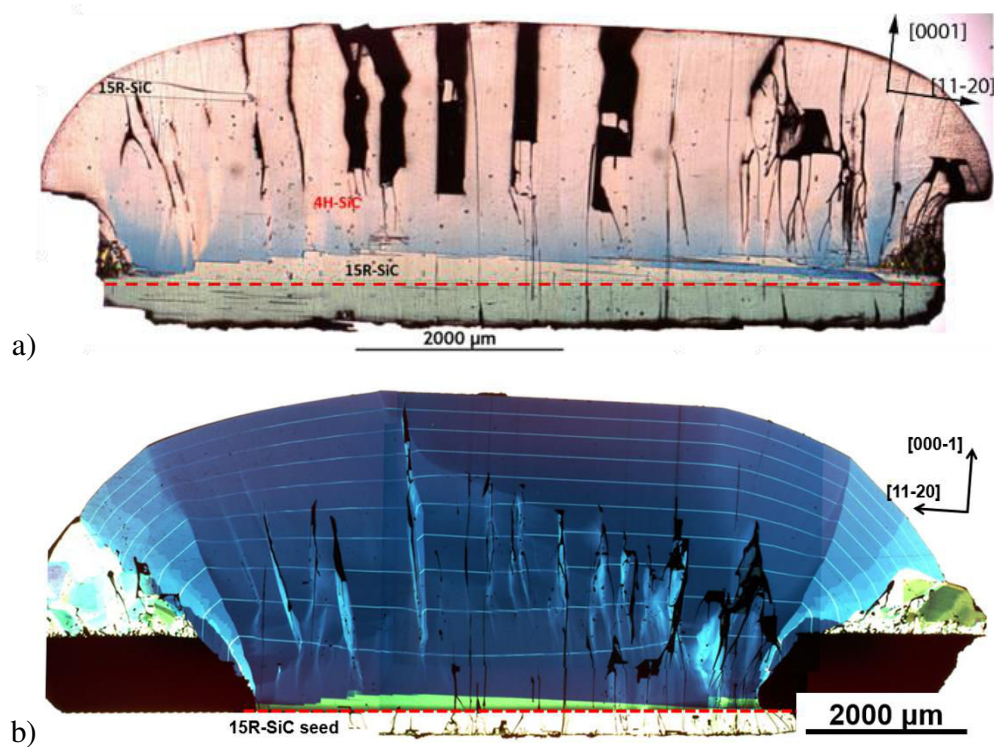


Figure 4.8. Cross-section images of 4H-SiC crystals a) B165 and b) B257 grown without and with the presence of nitrogen. The 3° off-axis 15R-SiC seed used in both cases is separated by red dashed line. Crystals are a mixture of 15R-SiC (green color polytype) and 4H-SiC (blue color polytype).

Even if the 15R/6H transition is well described, it is not the case for the 15R-SiC to 4H-SiC transition. The transition of 15R-SiC to 6H-SiC is attributed to different mechanisms [9-11]. Harada et al. proposed that during solution growth of SiC, a 15R-SiC to 6H-SiC can occur due to the formation of a 2D nuclei on the grown spirals, Figure 4.9 [9]. A Shockley type stacking fault (SF) could result in the formation of a 15R-SiC inclusion. If a spiral can replicate 6H-SiC type SFs then a transition from 15R-SiC to 6H-SiC will take place. However, the proposed model cannot explained the transition from 15R-SiC to 4H-SiC.

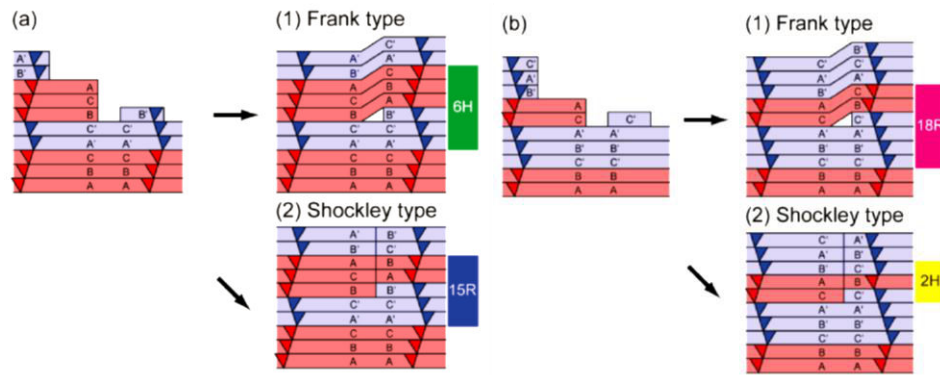


Figure 4.9. Schematic illustration of two possible configurations a and b for 2D nucleation on a 15R-SiC spiral. Frank and Shockley type SFs can lead to the formation of 6H-SiC inclusion [9].

A TEM sample was prepared from crystal B165, close to the area where the 15R-SiC to 4H-SiC transition takes place. Due to the non-availability of FIB it was not possible to locate the exact position of the transition area in the TEM sample. In the TEM image of Figure 4.10, a 15R/4H interface was spotted and no further 15R-SiC inclusions or transition were found in the 4H-SiC area. Basal plane defects exist in the 15R-SiC as seen by the conventional TEM image (left) and the high resolution TEM (HR-TEM) image revealed that these defects are mainly multiple twins. The 15R-SiC stacking changes from (23) to a twinned (32) sequence, according to Zhdanov notation. Close to the transition area, the stacking sequence of 15R-SiC (32) shifts to (22) of the 4H-SiC polytype. The schematic illustration of the transition is shown in Figure 4.11b. Despite the multiple twins in the 15R-SiC, the transition to the 4H-SiC polytype is direct, according to the HR-TEM image. The following two scenarios can be made in order to explain the obtained result:

- 1) When growth spirals of different polytypes overlap, the interface can be “sharp”, which is the case in crystal B256 (see Chapter 3). The atomically direct transition seen by the HR-TEM image corresponds to an area where different polytype growth spirals overlap and not to the area where the 4H-SiC nucleated.
- 2) The formation of a 2D nuclei of one Si-C bilayer height is not able to explain the 15R/4H transition as described in Figure 4.9 for 6H-SiC. However that corresponds to an ideal case, as usually a disturbed stacking zone is obtained between two different polytypes.

The formation of a 3D nuclei or the combined effect of multiple nucleus on the terrace of a spiral can be considered.

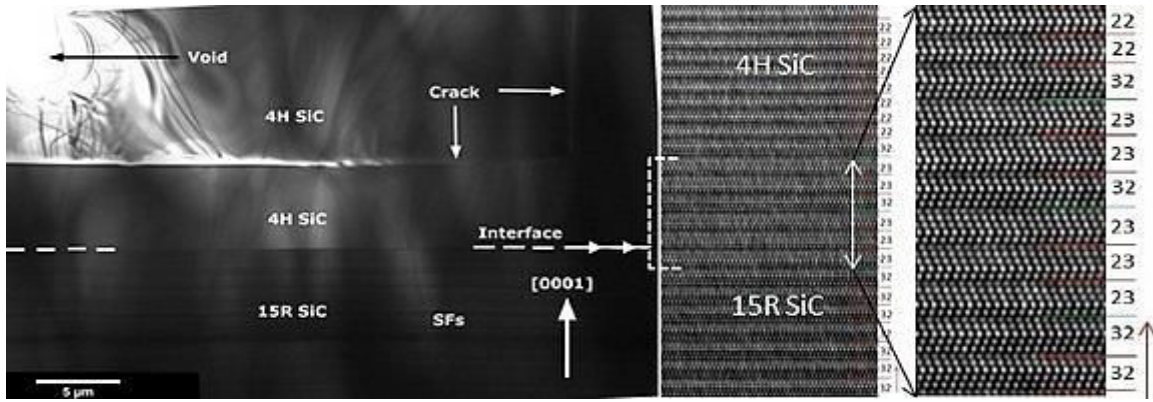


Figure 4.10. TEM image of a 15R/4H polytype transition. Planar defects are obvious in the low magnification TEM image (left side). High resolution image of the transition area reveals twins in the 15R-SiC before the 15R/4H interface.

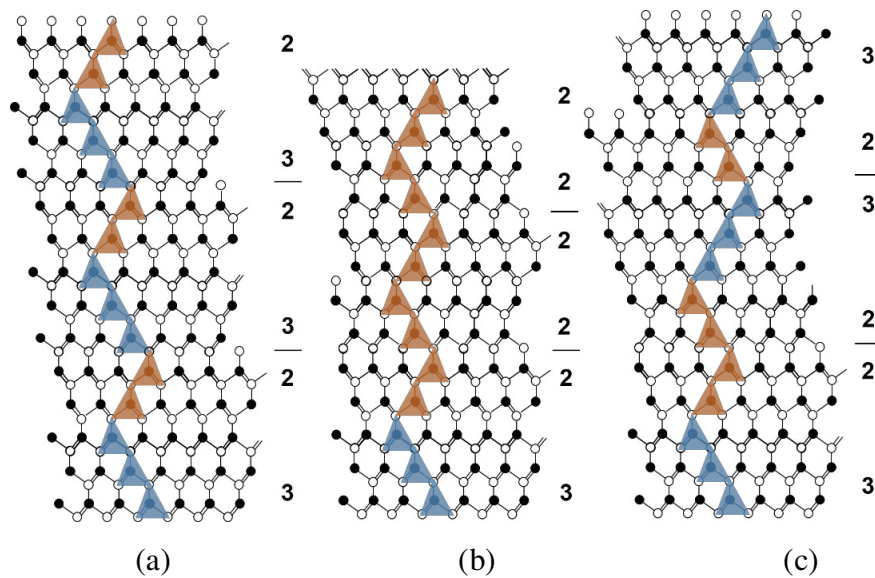


Figure 4.11. Schematic illustration using Zhdanov notation of the stacking sequence of a) the perfect (32) sequence of 15R-SiC, b) the (32)/(22) of the 15R/4H transition and c) a (32)/(23) twin in the 15R-SiC is shown.

The cross section sample of B165 was etched in molten KOH at 550°C for 5 minutes in order to reveal the structural defects. Two cross polarized images of the step-like 15R/4H interface are shown in Figure 4.12. Inside the 15R-SiC area basal plane defects are evidenced, in correspondence to the defects found from the TEM images. While the 4H-SiC is free of such kind of defects. The planar defects shown in the TEM image all located in the area of the TEM sample, but exist in all the volume of the 15R-SiC crystal and close to the interface with the 4H-SiC as well. A growth spiral of 15R-SiC consists of steps with height of 5 Si-C bilayers. Therefore 3 spiral turns are necessary to complete a 15R-SiC unit cell. If we assume that the stacking of the 5 bilayers is ABCBA, a forbidden stacking sequence would occur after one turn (ABCBA ABCBA). This is not possible and as a consequence a stacking fault must be formed in order to fix the stacking sequence [12]. Due to that, a high density of basal plane defects is expected.

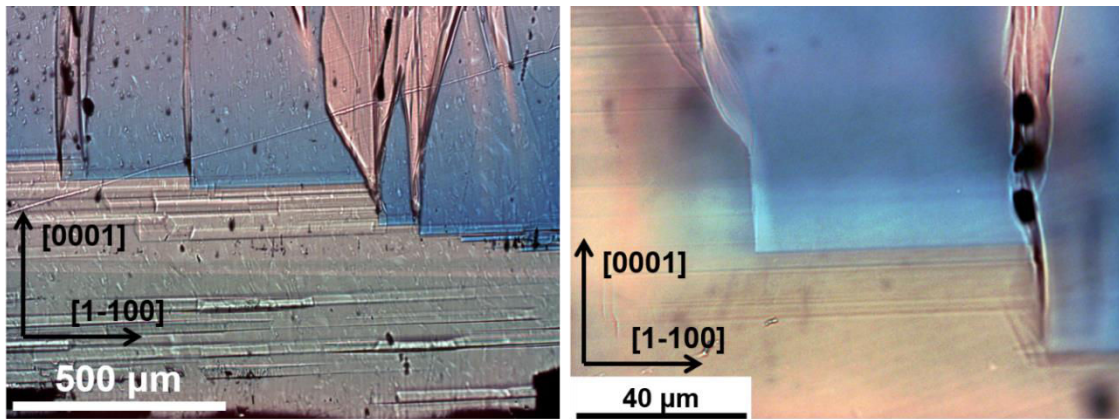


Figure 4.12. Basal plane defects in the 15R-SiC are of crystal B165, observed in a cross polarized optical microscope. Sample was etched in molten KOH at 550°C for 5 minutes.

Growth on (0001) Si-face. A 15R-SiC Si-face on-axis was used as a seed for the growth in both B258 and B272 experiments. The growth temperature was 2200°C and the pressure 13mbar. During growth, nitrogen gas was added in the reactor only for the case of B272 growth. The ratio of the nitrogen flow towards the total flow of gasses was 0.024. The free-carrier concentration using the Raman modes is estimated at $1-2 \times 10^{17} \text{ cm}^{-3}$ $1-2 \times 10^{18} \text{ cm}^{-3}$ for B258 and B272. Crystal B272 was cut perpendicular to the growth direction. Slices were

optically polished and observed under a cross polarized optical microscope. Four slices were made as shown in Figure 4.13a. During growth, 6H-SiC nucleated on the (0001) facet of the 15R-SiC crystal (slice #Nb.2) and expand due to the convex crystal shape (Figure 4.13a). In the volume of the 15R-SiC crystal, the 6H-SiC forms a conical shape inclusion, as shown in the schematic representation of Figure 4.13a.

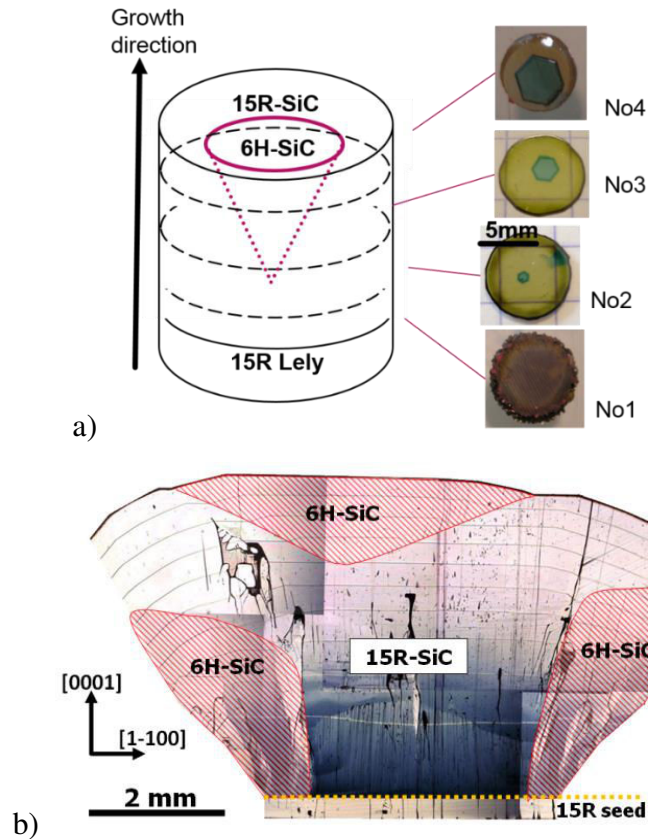


Figure 4.13. a) Schematic illustration and slices cut perpendicular to the growth direction of crystal B272. No1 corresponds to the beginning and No4 to the end of growth. b) Cross section image of crystal B258, under a cross polarized optical microscope.

The nucleation and expansion mechanism of the 6H-SiC inclusion are similar to the polytype transitions observed in B258. Crystal B258 is already presented in chapter 3, but the cross section of the crystal is given again in Figure 4.13b, for better comparison. The top

polytype transition in crystal B258 from 15R-SiC to 6H-SiC, occurs on the (0001) facet at the center of the growth front after 2-3 mm of growth. In both crystals the 15R/6H transition occur in similar spatial position, beside the presence or not of nitrogen.

Nitrogen has proved to affect the stabilization of the 4H-SiC polytype during bulk crystal growth and that was attributed to the reduced step bunching in the {0001} facet [13]. Another effect of nitrogen, is the deformation caused in the unit cell. The smaller size of the substitutional nitrogen donor atoms – in the position of carbon atoms – can change the c/na ratio of the unit cell, where c and a are the lattice constants in the c -axis and a -axis and n the number of Si-C bilayers in the unit cell. The presence of nitrogen is found to decrease the c/na ratio [14]. At the same time, the stabilization of a polytype is reported to be related to the c/na ratio, as a decreased ratio will favor the growth of a smaller in hexagonality SiC polytypes, like 15R-SiC and 6H-SiC (40% and 33% hexagonality respectively) [15]. However, according to the experimental examples presented, it can be concluded that nitrogen doesn't have a primitive or highly contributing role in the stabilization of 15R-SiC, at least in the range of doping that was investigated ($\sim 10^{18} \text{ cm}^{-3}$ for Si-face and $\sim 10^{19} \text{ cm}^{-3}$ for C-face).

4.3.3 Effect of Si/C ratio in the gas phase.

The growth temperature of crystals B264 and B274 was set at 2200°C, the growth pressure at 13mbar and a 15R-SiC Si-face on-axis seed was placed in the growth cavity. A cavity at the back of the seed was created for both experiments, by modifying the geometry of the graphite holder. As discussed in the second chapter, such a modification will increase the Si/C ratio in the gas phase and will change the shape of the grown crystal compared to the “standard geometry” Figure 2.23.

The grown crystal B264 and a cross section of it are shown in Figure 4.14. The presence of a cavity at the back of the seed has a direct effect on the shape of the crystal. The temperature at the center of the growth front was lowered and as a result the growth rate is higher compared to the periphery, as seen by the nitrogen marking. No hexagonal polytype

inclusions were found in the volume of the grown crystal but only 15R-SiC polytype. After 4mm of growth 6H-SiC nucleated at the (0001) facet on the surface of the crystal as found by Raman, Figure 4.14a-b.

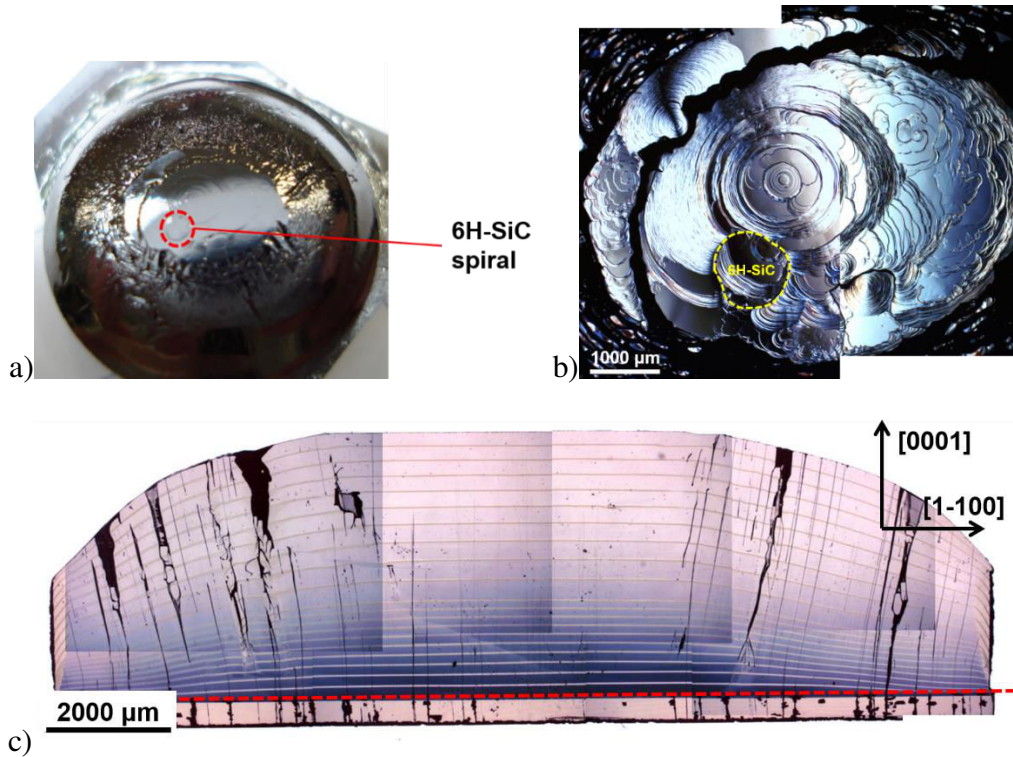


Figure 4.14. a) Photo of a 15R-SiC crystal B264 grown on a 15R-SiC on-axis Si-face seed. At the surface of the crystal a 6H-SiC spiral was found. b) Nomarski image of crystal B264. c) cross section image of a cross polarized microscope (seed separated by red dashed line).

For B274 crystal, similar growth conditions to B264 were applied. However nitrogen was added in the gaseous ambient in order to ensure stable doping conditions and avoid the variation of doping during growth (color variations seen in crystal B264, Figure 4.14c). The free carrier concentration using the LO Raman mode was estimated at around $1 \times 10^{18} \text{ cm}^{-3}$. The grown crystal is of the 6H-SiC polytype and no 15R-SiC inclusions were found. Despite the fact that the same crucible geometry and growth conditions with crystal B264 were applied in the case of crystal B274, no stable 15R-SiC growth was obtained.

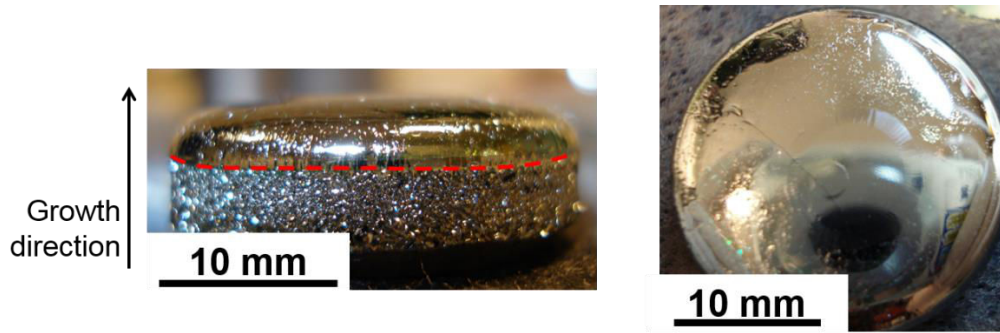


Figure 4.15. Crystal B274, grown on a 15R-SiC Si-face 3° off-axis substrate (separated from the grown crystal by red dashed line). The polytype of the grown crystal is of 6H-SiC and the free carrier concentration $\sim 1 \times 10^{18} \text{ cm}^{-3}$.

The increase of Si/C ratio in the gas phase is reported to enhance the growth of lower in hexagonality polytypes, like 3C-SiC and 6H-SiC [16]. The modification of the crucible (cavity at the back of the seed) increases the Si/C ratio in the gas phase, compared to the “standard case” (Figure 2.23). Thus, the growth of 6H-SiC (hexagonality 33%) is expected compared to 15R-SiC (hexagonality 40%). However, experimentally stable 15R-SiC growth was obtained for crystal B264.

In the case of crystal B274, nitrogen was added in the growth ambient. The role of nitrogen on the variation of Si/C ratio of the gas phase is still not clarified by the existing studies. However, the two following assumptions can be made. First, a reaction of nitrogen with the graphite crucible can provide CN species in the gaseous phase, which act as an extra carbon source. Second, the lattice site competition of nitrogen with carbon will change the amount of carbon absorbed and as a result the carbon concentration in front of the grown surface will increase. By both mechanisms, the presence of nitrogen will lead to the decrease of Si/C ratio. Once the Si/C ratio is lower for crystal B274 compared to B264, the growth of a polytype with higher hexagonality is expected, e.x. 4H-SiC (hexagonality 50%). Yet, the polytype of crystal B274 is 6H-SiC.

Last, for crystal B264, 6H-SiC nucleates at the (0001) facet close to the surface of the crystal (Figure 4.14). Due to the non-congruent growth of SiC, the sublimation rate of the various SiC species (Si, SiC₂ and Si₂C) changes and as a result, the Si/C ratio decreases with

time. The Si/C ratio after 20 hours of growth, when 6H-SiC nucleates, is lower compared to the beginning of growth. Thus, the nucleation of 4H-SiC (higher in hexagonality) is expected.

From all the cases, it is evident that the polytype of the crystal is not in agreement with the expected polytype to nucleate based on the changes of Si/C ratio. The polytype of the crystal is the one defined by the surface polarity of the seed (6H-SiC nucleate on the Si-face and 4H-SiC on the C-face). It appears that the effect of surface polarity is stronger and it is the one to determine which polytype will nucleate.

4.4 Conclusions of Chapter 4.

Bulk growth of 15R-SiC was studied under the basis of different growth parameters. In most of the growth experiments, the grown crystals are a mixture of 15R-SiC with 4H-SiC or 6H-SiC. The occurrence of one of the hexagonal polytypes is related to the polarity of seed's growth surface, as 4H-SiC was systematically obtained on C-face and 6H-SiC on Si-face. Polytype transitions occur on the $\{0001\}$ facet. This implies that 2D nucleation on the 15R-SiC facet occurs. Thus, off-axis growth can favor the stabilization of 15R-SiC, due to the existence of the polytype information in the step edge sites. Statistically it is observed that 15R-SiC was more stable when grown on the (0001) Si-face plane. Despite the optimum growth temperature range given in the literature, stable growth of 15R-SiC was obtained up to 2200°C. However, further studies are needed in order to indicate the preferable temperature for 15R-SiC growth.

The role of Si/C ratio in the gas phase, for 15R-SiC stabilization was highlighted. Due to a modified crucible design, the Si/C in the gas phase was increased and stable 15R-SiC growth was obtained. Once the Si/C ratio was changed due to the presence of nitrogen and due to the non-congruent consumption of the SiC source material, polytype transitions were obtained. However, the polytype nucleated was defined by the surface polarity of the crystal and not the increase or decrease of Si/C ratio. Additional experiments and thermodynamic calculations are needed in this direction, in order to optimize the growth conditions for bulk 15R-SiC growth.

References

1. LILOV, S., T. NISHIGUCHI, and S. NISHINO, STUDY ON THE GROWTH CONDITIONS OF SILICON CARBIDE MONOCRYSTALS FROM VAPOR PHASE.
2. Nishiguchi, T., et al., Crystal Growth of 15R-SiC and Various Polytype Substrates. *Materials Science Forum*, 2001. **353-356**: p. 69-72.
3. Schulze, N., D. Barrett, and G. Pensl, Controlled Growth of 15R-SiC Single Crystals by the Modified Lely Method. *physica status solidi (a)*, 2000. **178(2)**: p. 645-650.
4. Nishiguchi, T., et al., Crystal Growth of 15R-SiC Boules by Sublimation Method. *Materials Science Forum*, 2000. **338-342**: p. 115-118.
5. Yano, H., et al., High Channel Mobility in Inversion Layer of SiC MOSFETs for Power Switching Transistors. *Japanese Journal of Applied Physics*, 2000. **39(Part 1, No. 4B)**: p. 2008-2011.
6. Schulze, N., et al., Near-thermal equilibrium growth of SiC by physical vapor transport. *Materials Science and Engineering: B*, 1999. **61-62**: p. 44-47.
7. Stein, R.A., P. Lanig, and S. Leibenzeder, Influence of surface energy on the growth of 6H- and 4H-SiC polytypes by sublimation. *Materials Science and Engineering: B*, 1992. **11(1-4)**: p. 69-71.
8. Mitani, T., et al., Determination of carrier concentration by Fano interference of Raman scattering in heavily doped n-type 4H-SiC. *Journal of Applied Physics*, 2012. **112(4)**: p. -.
9. Harada, S., et al., Polytype Transformation by Replication of Stacking Faults Formed by Two-Dimensional Nucleation on Spiral Steps during SiC Solution Growth. *Crystal Growth & Design*, 2012. **12(6)**: p. 3209-3214.
10. Zhang, Y., et al., Nucleation Mechanism of 6H-SiC Polytype Inclusions Inside 15R-SiC Crystals. *Journal of Electronic Materials*, 2010. **39(6)**: p. 799-804.
11. Agrosi, G., et al., Near-atomic images of interfaces between twin-related lamellae in a synthetic 6H-SiC sample. *Physics and Chemistry of Minerals*, 2010. **38(2)**: p. 101-109.
12. Seiss, M. 2013, Ph.D Thesis, Universite de Grenoble.
13. Tymicki, E., et al., Effect of Nitrogen Doping on the Growth of 4H Polytype on the 6H-SiC Seed by PVT Method. *Materials Science Forum*, 2012. **717-720**: p. 29-32.
14. Gavrillov, K.I., et al., *Sov. Phys. Crystallogr.*, 1978. **23**: p. 691.
15. Tairov, Y.M. and V.F. Tsvetkov, Progress in controlling the growth of polytypic crystals. *Progress in Crystal Growth and Characterization*, 1983. **7(1-4)**: p. 111-162.
16. Lebedev, A.A. and S.Y. Davydov, A vacancy model of the heteropolytype epitaxy of SiC. *Semiconductors*, 2005. **39(3)**: p. 277-280.

Chapter 5

Nitrogen doping in SiC bulk crystals

In this chapter we study the problem of nitrogen incorporation during bulk crystal growth of 4H-SiC and 6H-SiC by seeded sublimation method. Nitrogen incorporation in bulk SiC crystals with respect to the partial pressure of nitrogen and growth temperature is examined. We will show that the incorporated nitrogen at the (000-1) C-face plane is independent of the polytype of the crystal. Higher desorption rate of nitrogen on Si-face compared to C-face is found, using a Langmuir adsorption equation, which is attributed to the difference in bond density between the two polar faces. The increased nitrogen desorption when growth temperature increases is believed to be the most contributing factor, based on the temperature dependent trends.

5.1 Introduction

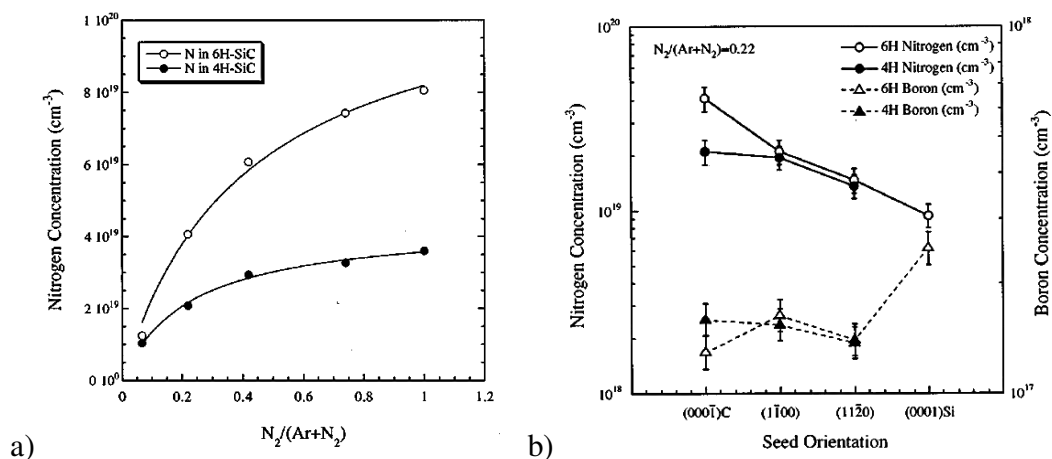
Nitrogen is the most commonly used n-type dopant in SiC and its incorporation via implantation or during crystal growth is an extensively studied topic. In sublimation growth nitrogen is the most abundant dopant, mainly because it is difficult to remove from the building materials of the growth crucible. Even if high purity graphite materials are used, the background level of nitrogen will hardly drop below 10^{17}cm^{-3} . For most of electronic applications highly conductive substrates are needed, so grown crystals are intentionally doped by adding nitrogen to the gaseous phase.

Even if the incorporation of nitrogen with respect to the various growth parameters is described in the chemical vapor deposition system [1-3], no complete description of the phenomena exist for the seeded sublimation method. Many groups have studied the incorporation of nitrogen with dependence of various growth parameters like the orientation of growth, the partial pressure of nitrogen in the gas phase, the growth temperature and the growth rate. The polarity dependent nitrogen incorporation was one of the first phenomena studied. It was shown that (000-1)C plane grown crystals incorporate more nitrogen compared to (0001)Si face 6H-SiC crystals [4]. That work came as a result of the already described idea that nitrogen incorporates into carbon sites by Lely [5] using electrical and X-ray characterization and a few years later by electron spin resonance studies [6]. First, it was shown that any change in the growth rate (in the range of 0.4 – 1.1 mm/h) does not affect the amount of nitrogen to be incorporated [4]. Thus, nitrogen incorporation is not kinetically limited but an equilibrium surface coverage of absorbed nitrogen is always established during growth. Due to that, most of the studies focus on the dependence of incorporated nitrogen with the partial pressure of nitrogen in the gas phase [4, 7, 8]. Incorporated nitrogen increases with increasing nitrogen partial pressure, but a saturation limit arises while approaching 100% of nitrogen in the growth ambient. The obtained trends are best described using a non-dissociative Langmuir adsorption isotherm equation, see Figure 5.1a. Concerning the effect of polytype, during growth on the (1-100) and (11-20) planes, that reveal the stacking sequence of the SiC polytypes, no significant difference was observed between 6H-SiC and 4H-SiC (Figure 5.1b). This implies that the difference in stacking

sequence between the two polytypes does not affect the incorporation of nitrogen. However on the (000-1) C-face growth nitrogen incorporation varies and that was attributed to topological differences between the 6H-SiC and 4H-SiC (000-1) surfaces [7].

The difficulty to differentiate the phenomena in the PVT process, complicates the description of nitrogen incorporation with respect to other growth parameters like growth temperature and Si/C ratio in the gas phase. Also, the role of the surface mechanisms during growth (spiral, step flow growth, 2D nucleation) is not clear. During bulk growth a basal plane facet and a step flow area are formed (see Chapter 3). It is reported that basal plane facet incorporates more nitrogen compared to the step flow area. The difference in incorporated nitrogen takes a maximum value for low doping and saturates for higher values (Figure 5.1c) [9, 10]. The lack of understanding the complete mechanism of nitrogen incorporation in SiC and difficulties that arise from the PVT process itself confine the progress towards a complete model of nitrogen incorporation in the PVT system.

In this chapter, we will demonstrate that the incorporation of nitrogen at the {0001} plane is independent of the polytype of the crystal. Also the temperature dependence is described and the activation energy is reported. We will bring more insight into the nitrogen incorporation mechanism by considering the adsorption/desorption phenomena in the growth surface and different growth mechanisms.



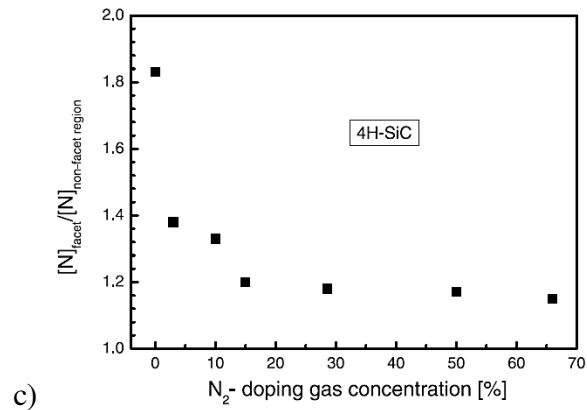


Figure 5.1. **a)** Nitrogen concentration in the crystal as a function of the N₂ partial pressure. A non-dissociative Langmuir adsorption isotherm equation (solid line) is used to best describe the data. **b)** Nitrogen incorporation as a function of the orientation of growth [7]. **c)** Ratio of nitrogen incorporated at the (000-1) facet and the step flow area of a 4H-SiC crystal as a function of nitrogen in the gas phase [9].

5.2 Experimental details

SiC crystals were grown in a top seeded sublimation graphite furnace. Temperature, pressure, argon and nitrogen flows were automatically controlled as already presented in Chapter 2. On-axis and off-axis 4H-SiC, 6H-SiC and 15R-SiC seeds of both silicon and carbon face were used. In a first set of experiments, the partial pressure dependence in nitrogen incorporation was examined. Growth temperature and total pressure were kept constant for all the experiments at 2200°C and at 13 mbar respectively. The ratio of nitrogen flow on the total flow of gases (argon and nitrogen) was in the range of 0.05 – 0.8. In a second set of experiments, the incorporation of nitrogen was examined with respect to the growth temperature. All the growth parameters were constant, pressure was 13 mbar and the partial pressure of nitrogen $N_2/(N_2+Ar)$ was 0.15, while growth temperature was varying in the range of 2130°C to 2350°C. In all of these experiments, the different SiC crystals were

grown in the same growth experiment using a multi seed method, in order to ensure similar growth conditions.

The free carrier concentration of the crystals was estimated using temperature-dependent Hall electrical measurements and room temperature Raman spectroscopy while the nitrogen concentration was measured by Secondary Ion Mass Spectrometry (SIMS). Hall measurements were performed in the temperature range of 30K up to 600 K by the Van de Pauw method. Ohmic contacts were created by alloying nickel onto the sample surface. The magnetic field was constant at 0.66 T during the measurements. A Jobin Yvon T64000 Raman system has been used. A 40 mW mixed Argon/Krypton laser was used as excitation source ($\lambda=660$ nm) and a cooled CCD camera completed the set-up. The measurements were done at room temperature in the range $100-1100$ cm^{-1} . The uncertainties in the Raman frequencies were estimated to be less than 1 cm^{-1} . Since the investigated material is highly nitrogen doped, to determine the carrier concentration we focused on the acoustic part of the spectra. FTA lines are fitted using the Fano interference model. From the extracted asymmetry and broadening parameters (q and Γ , respectively), using the calibration curve from [11] we were able to evaluate the free carrier concentration. Secondary Ion Mass Spectrometry analyses were carried out in a CAMECA SC-Ultra instrument operating with a 5.5 keV energetic Cs^+ beam. N ionization being extremely low, CN^- intensities were recorded. The nitrogen relative sensitivity factor linking N intensity and N concentration was determined from an external standard sample (SiC implanted with ^{14}N , 180 keV, $9.5 \times 10^{12}\text{cm}^{-2}$) allowing to obtain quantitative data.

5.3 Temperature dependence

Four different seeds were placed in the growth chamber (positions I-IV) in order to ensure similar growth conditions and allow the direct comparison of the results. An example of crystals grown at 2280°C is shown in Figure 5.2. The seeds and the growth conditions used are listed in Table 5.1.

Table 5.1. Characteristics of the temperature dependent nitrogen doped SiC crystals.

Growth experiment	Growth temperature [°C]	Pressure [mbar]	Partial pressure of nitrogen
B278	2350	13	0.15
B281	2280		
B280	2200		
B282	2130		
B279	2050		
B283	2200	8	
Seeds			
Position I	Position II	Position III	Position IV
4H-SiC	4H-SiC	4H-SiC	6H-SiC
4° off-axis	on-axis	4° off-axis	on-axis
C-face	C-face	Si-face	C-face
Grown crystals			
4H-SiC	4H-SiC	6H-SiC	6H-SiC

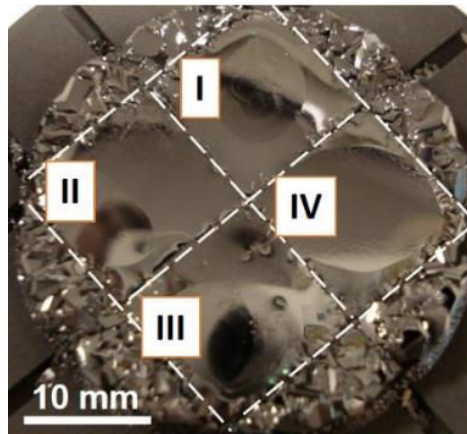


Figure 5.2. Photo of the grown SiC crystals (position I-IV) at 2280°C. Four seeds were placed in the reaction chamber and white dashed lines are used to mark the boundaries of the different crystals.

5.3.1 Hall Electrical measurements.

Crystals were cut perpendicular to the growth direction and polished optically from both sides. Continuously they were cut in square pieces 6x6 mm which is the appropriate size for

Hall measurements. It was not possible to perform Hall measurements in all the grown samples, due to limitations that arise because of small polytype inclusions and defects in the crystals. The samples that were measured are indicated in Table 5.2 with grey color.

Table 5.2. In grey color the samples measured by Hall are indicated.

sample	T _{growth} [°C]	4H C-face	6H C-face	6H Si-face
B278	2350	On-axis		On-axis
B281	2280	On-axis Off-axis	On-axis	On-axis
B280	2200	On-axis		

The free carrier concentration, the Hall mobility and the resistivity of on-axis and off-axis C-face 4H-SiC and on-axis 6H-SiC of silicon and carbon face grown at 2280°C are given in Figure 5.3.

- Free carriers concentration. The free carriers concentration of the on-axis C-face 4H-SiC is higher by $\sim 1 \times 10^{19} \text{cm}^{-3}$ compared to the off-axis crystal (Figure 5.3a). The constant values of free carriers concentration ($1-2 \times 10^{19} \text{cm}^{-3}$) while changing the temperature of 4H-SiC is an indication of a degenerated semiconductor. For the case of 6H-SiC the free carriers decrease when the temperature decreases, because less doping centers are activated. The “tail like” trend at low temperatures (red circle area in Figure 5.3a) is due to the high concentration of doping (hopping effect). Even if the free carrier concentration at room temperature (grey dashed line) of 4H-SiC and 6H-SiC are in the same range, free carriers concentration varies with temperature only for 6H-SiC. This is attributed to the different ionization energies - higher for 6H-SiC - of the two polytypes [12].

- Hall mobility. The carrier mobility is constant in the case of 4H-SiC ($\sim 40 \text{cm}^2/\text{Vs}$) as the material has a semimetal behavior. 6H-SiC exhibits the characteristic temperature dependence of mobility for semiconductors. At high temperatures, mobility decreases due to the increased phonon scattering with a power law of 2-3 ($\mu_{\text{ph}} \sim T^{-3 \dots 2}$). For low temperatures, mobility decreases due to scattering from charged defects, like ionized donors or acceptors ($\mu_{\text{def}} \sim T^{3 \dots 2}$).

○ Hall Resistivity. Resistivity of 4H-SiC is constant at around 0.01 Ωcm , once the free carriers concentration is constant, Figure 5.3c. While the one of 6H-SiC increases as temperature decreases, because the free carrier concentration is decreasing (Figure 5.3c).

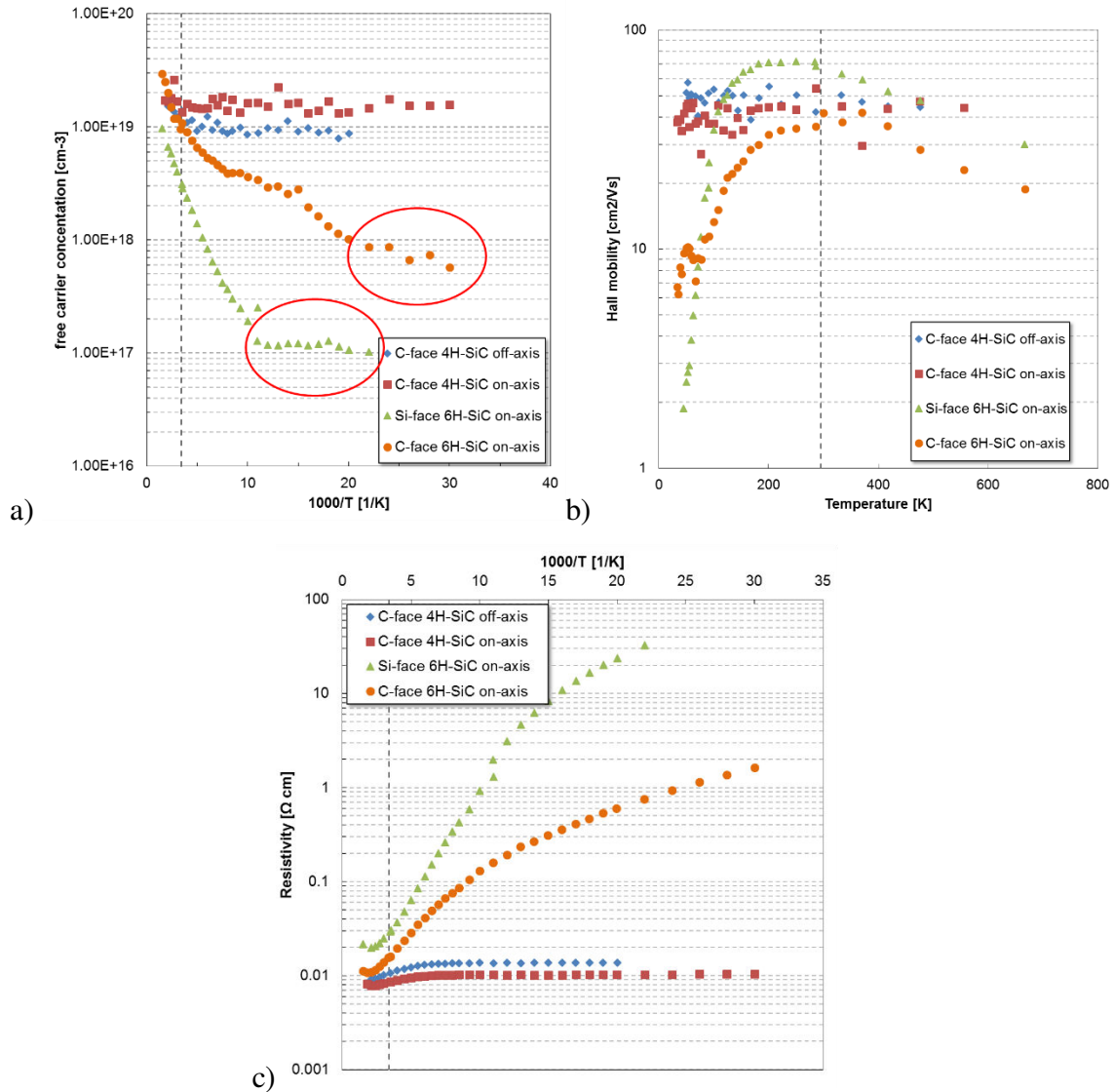


Figure 5.3. a) Free carrier concentration, b) Hall mobility and c) Resistivity of on-axis and 4° off-axis 4H-SiC and on-axis 6H-SiC of silicon and carbon faces grown at 2280°C. Measurements were performed in the temperature range 30K - 600K. The grey dashed line corresponds to the room temperature.

The electrical measurements performed for 4H-SiC crystals grown at different temperatures are shown in Figure 5.4. Free carriers concentration is in the range of $8 \times 10^{18} \text{ cm}^{-3}$ for 2350°C up to $2 \times 10^{19} \text{ cm}^{-3}$ for 2200°C. The trends of resistivity are more clear compared to mobility were no actual comparison can be made. The resistivity at low temperatures is higher for the crystal grown at 2350°C ($0.02 \Omega \text{ cm}$) compared to $0.01 \Omega \text{ cm}$ of 2200°C.

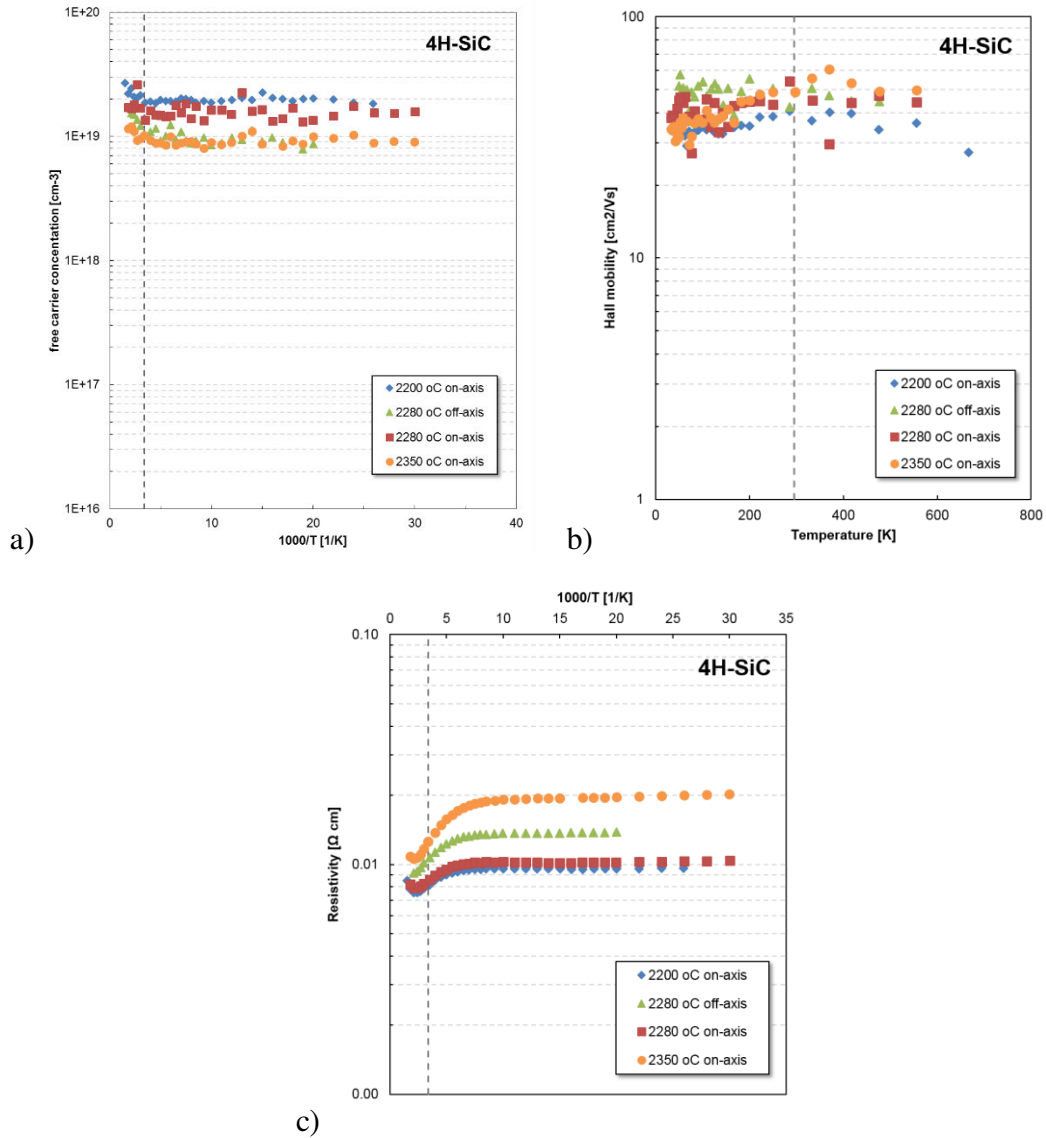


Figure 5.4. a) Free carrier concentration, b) Hall mobility and c) Resistivity of on-axis and 4° off-axis C-face 4H-SiC. Measurements were performed at the temperature range of 30K to 600K. The dashed grey line corresponds to the room temperature.

For the case of Si-face on-axis 6H-SiC there are no significant differences for all the measured crystals grown at different temperatures, as seen in the graphs of Figure 5.5.

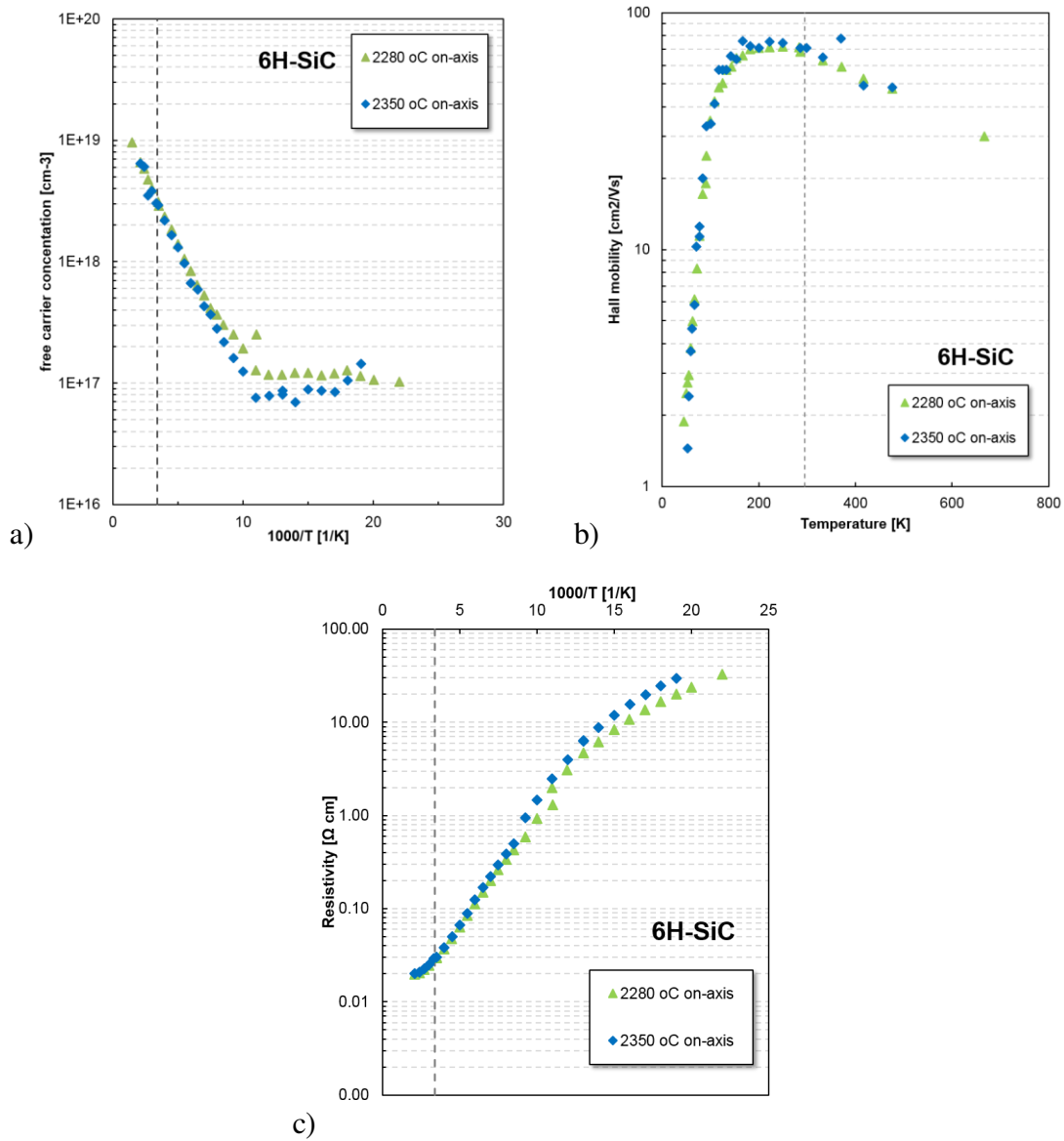


Figure 5.5. a) Free carrier concentration, b) Hall mobility and c) Resistivity of on-axis Si-face 6H-SiC. Measurements were performed at the temperature range of 30K to 600K. The dashed grey line corresponds to the room temperature.

The free carrier concentration data were fitted using a least-squares fit of the neutrality equation presented by Gotz et al. [13] using a homemade program, in order to extract the donor and acceptor concentrations. The fitting parameters are the ionization energy of cubic and hexagonal sites, the free carrier concentration on these sites and the compensating carrier concentration. However, due to the high doping of the crystals it was not possible to obtain a reliable fitting (Figure 5.6), since the fitting equations are best suited for SiC crystals doped in the range of 10^{16} - 10^{18} cm⁻³. The acceptor and donor concentration could not be estimated, thus the values of free carrier concentration, Hall mobility and resistivity at room temperature will only be considered. The values are summarized in Table 5.3 and Figure 5.7. The free carrier concentration of C-face 4H-SiC is higher (difference is less than 1×10^{19} cm⁻³) compared to 6H-SiC (at 2280°C), while the increase of the growth temperature will decrease the free carriers for the case of 4H-SiC. In the case of Si-face 6H-SiC, no significant difference is observed for the measured crystals. The Hall mobility and resistivity increase as growth temperature is increasing for both C-face 4H-SiC and Si-face 6H-SiC, while the values are comparable to other studies [14].

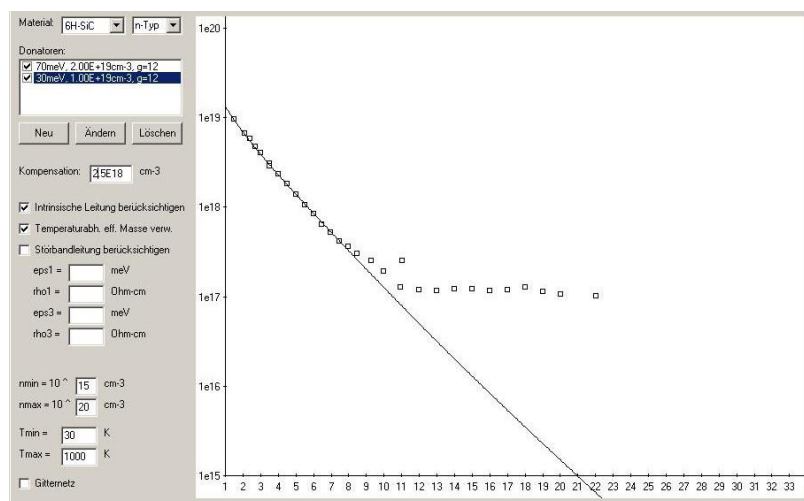


Figure 5.6. Free carrier concentration by Hall measurement as a function of $1000/T$. A least-squares fit of the neutrality equation [13] (solid line) was used to describe the obtained data. On the left the fitting parameters are indicated.

Table 5.3. Electrical characteristics at room temperature of crystals in Table 5.2

T = 295 K	Growth temperature [°C]	SiC crystal		
		4H-SiC C-face	6H-SiC C-face	6H-SiC Si-face
Free carrier concentration [cm ⁻³]	2200	2.02E+19	-	-
	2280	1.52E+19	9.40E+18	2.88E+18
	2350	1.02E+19	-	2.97E+18
Hall mobility [cm ² /Vs]	2200	38.8	-	-
	2280	46.5	38.8	65.6
	2350	48.77	-	70.87
Resistivity [Ωcm]	2200	8.0	-	-
	2280	8.41	15.6	28.13
	2350	12.5	-	28.98

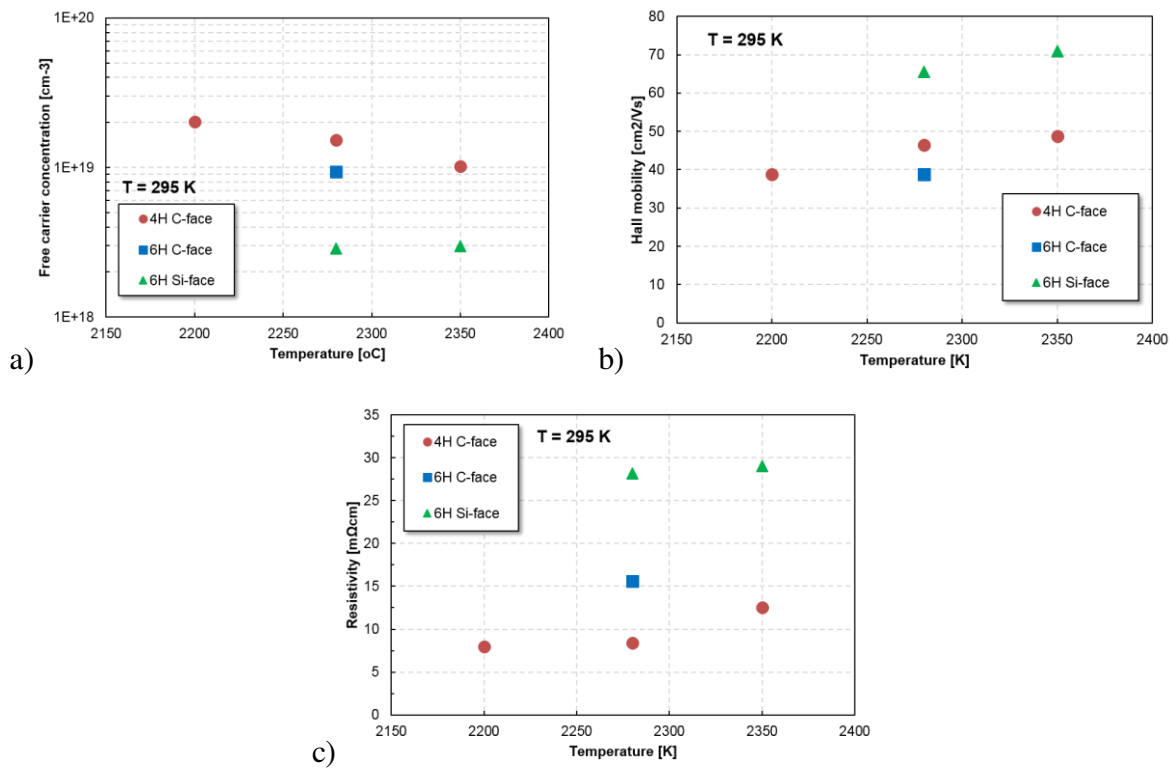


Figure 5.7. a) Free carrier concentration, b) Hall mobility and c) Resistivity of on-axis C-face 4H-SiC and on-axis 6H-SiC of silicon and carbon face as a function of the growth temperature by Hall electrical measurements.

5.3.2 Raman spectroscopy measurements.

The free carrier concentration of the same set of crystals was extracted using Raman spectroscopy. In the graph of Figure 5.8 the free carrier concentration as a function of the growth temperature is plotted, while the differences obtained from the Hall measurements are in the range of $\sim 1 \times 10^{19} \text{cm}^{-3}$. The free carrier concentration for both C-face 4H-SiC and C-face 6H-SiC crystals decreases when the growth temperature increases. Si-face 6H-SiC follows the same trend in contrast to the results from Hall measurements. For the case of C-face 4H-SiC an Arrhenius equation (equation 5.1) is used to fit the data. The activation energy is calculated at 152.4 kJmol^{-1} . The data reported by Ohtani et al. are given for comparison [14]. The Arrhenius equation is given below.

$$k = Ae^{-E_a / RT} \quad \text{Eq. 5.1}$$

k represents the free carrier concentrations, A is a pre-exponential factor, E_a [kJmol^{-1}] the activation energy and T [K] the temperature.

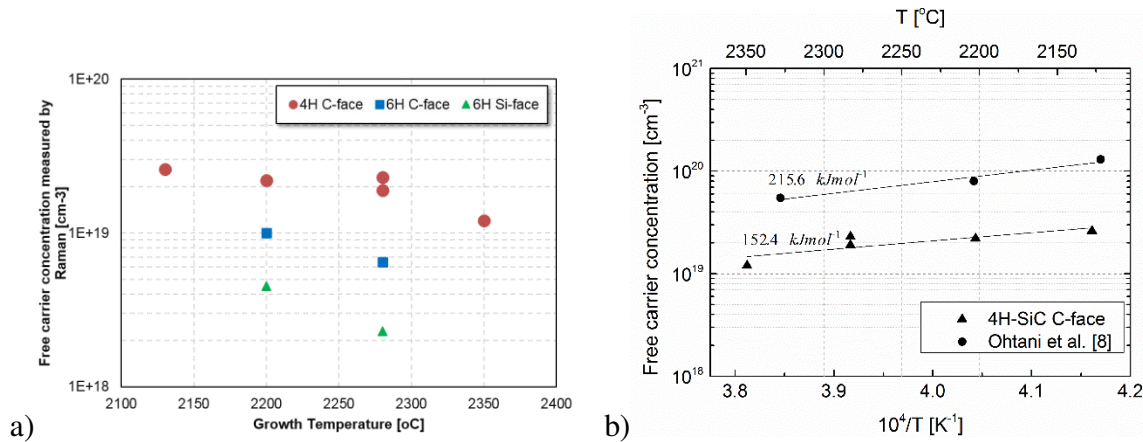


Figure 5.8. a) Free carrier concentration of on-axis C-face 4H-SiC and on-axis 6H-SiC of Si and C-face as a function of the growth temperature, as measured by Raman spectroscopy. b) An Arrhenius equation was used in order to fit the data. The activation energy is found to be 152.4 kJ/mol . Data from Ohtani et al. are used for comparison [14].

5.3.3 Surface morphology.

The surface of C-face 4H-SiC, 6H-SiC and Si-face 6H-SiC grown crystals was observed by a Nomarski optical microscope (Figure 5.10-5.12). Even if it is a qualitative observation, the width of the terraces on the {0001} facet is decreasing, once growth temperature is increasing. The phenomenon is more enhanced in the case of Si-face 6H-SiC (Figure 5.12). When the growth temperature is 2350°C, the growth rate is ~1 mm per hour, which is 3 times higher compared to growth rate at 2200°C. If a growth spiral is schematically illustrated by a triangle (Figure 5.9), the slope or inclination of a spiral will be higher (angle v is bigger than u) when the growth rate is higher ($R_{g2} > R_{g1}$). Thus, the width of the terraces will be smaller ($W_2 < W_1$) for the case of a fast growing spiral.

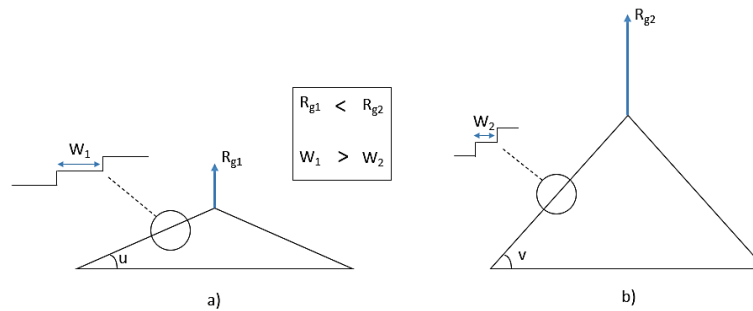
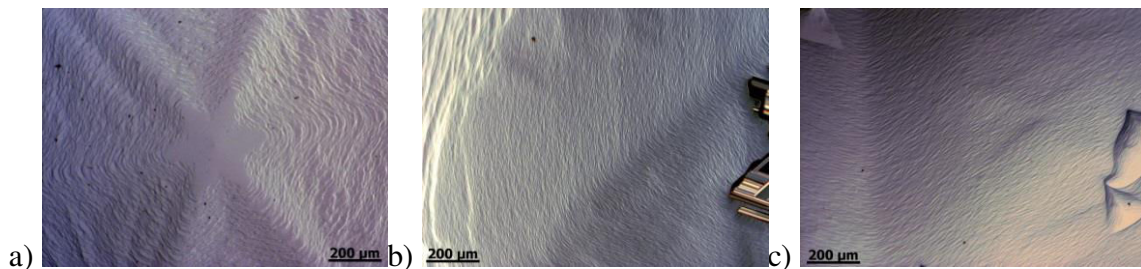


Figure 5.9. Cross sectional schematic illustration of a growth spiral as a triangle shape object. The growth rate R_g , the inclination of the spiral (angle u and v) and the width of the terraces (W) are indicated.



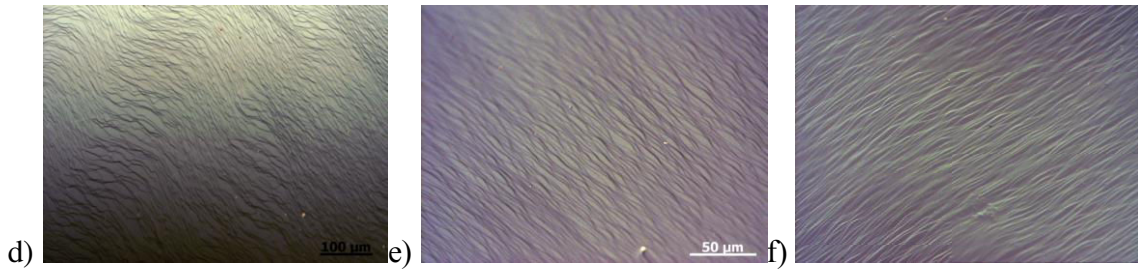


Figure 5.10. Surface morphology of 4H-SiC C-face crystals grown at a) 2130°C, b) 2200 °C, c) 2280°C observed by a Nomarski optical microscope. Figures d, e, and f are higher magnification images of a, b and c respectively.

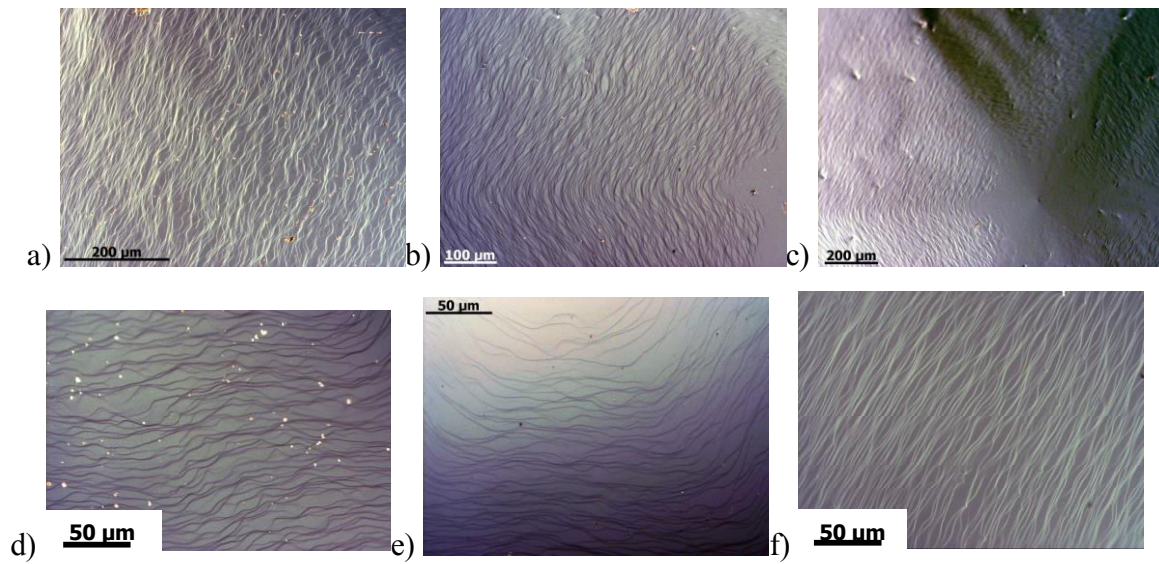


Figure 5.11. Surface morphology of 6H-SiC C-face crystals grown at a) 2130°C, b) 2200 °C, c) 2280°C observed by a Nomarski optical microscope. Figures d, e, and f are higher magnification images of a, b and c respectively.

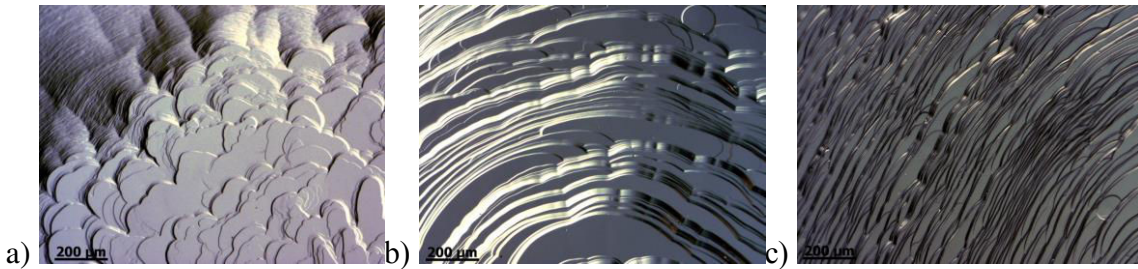


Figure 5.12. Surface morphology of 6H-SiC Si-face crystals grown at a) 2130°C, b) 2200 °C, c) 2280°C observed by a Nomarski optical microscope.

5.4 Nitrogen incorporation as a function of nitrogen partial pressure.

The grown crystals and the growth parameters used are listed in Table 5.4. The nitrogen doping was not constant during all the growth run but altering doped and undoped zones were created by controlling the flow of the input gasses as shown in Figure 5.13. That was made in order to reduce the total number of experiments and ensure similar growth conditions for the different nitrogen flow parameters. Only on-axis seeds were used.

Table 5.4. Characteristics of the partial pressure of nitrogen dependent doped SiC crystals.

Growth experiment	Grown on-axis crystal	Polarity of growth	Partial pressure of nitrogen	Growth Temperature 2200 °C
B275-6	4H-SiC	C-face	0.05 – 0.8	Growth pressure 13 mbar
B284	6H-SiC	C-face	0.05 – 0.8	
B284	6H-SiC	Si-face	0.015 – 0.8	
B273	15R-SiC	Si-face	0.035 – 0.1	

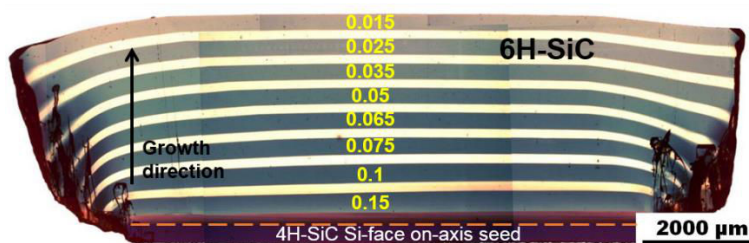


Figure 5.13. Cross section of a 6H-SiC crystals grown on a 4H-SiC Si-face on-axis seed. The dark and bright stripes correspond to doped and undoped zones, created through the control of the input argon and nitrogen gases in the reactor. The partial pressure of nitrogen $N_2/(Ar+N_2)$ is indicated at each stripe.

The nitrogen concentration of the different doped stripes was measured using secondary ion mass spectrometry. The results are plotted in Figure 5.14a as a function of the partial

pressure of nitrogen. The incorporated nitrogen in the grown SiC crystals increases by increasing the partial pressure of nitrogen into the gas phase and reaches a saturation state once the partial pressure of nitrogen is above 0.6. The C-face 4H-SiC and 6H-SiC crystals incorporate more nitrogen compared to the Si-face 6H-SiC and 15R-SiC.

A Langmuir adsorption equation is used to fit the data. The Langmuir adsorption model is used to visualize the adsorption of gaseous molecules at a partial pressure p (at a given temperature) and the available free incorporation sites on a surface. The assumptions of the model are: i) there is a fixed amount of equally distributed incorporation sites on the solid surface where gas molecules can be incorporated. Each of these sites hold maximum of one gaseous molecule and the probability of adsorption on all sites is the same. ii) A dynamic equilibrium between adsorbed gaseous molecules and the free gaseous molecules is established. Molecules from the gas phase can be adsorbed at free sites at the solid (adsorption) and molecules move back to the gas phase from the solid surface (desorption). A two directions system is formed and the equilibrium equation is



where A_g is the gaseous molecules in the gas phase, B_s the empty sites on the solid surface, AB the adsorbed gaseous molecules and K_a , K_D represents the equilibrium constant for the reaction of adsorption and desorption. The equilibrium constant of the reaction (K) is the ratio of K_a and K_D ,

$$K = K_a/K_D \quad \text{Eq. 5.3}$$

and K is dependent on temperature.

The Langmuir adsorption non-dissociative isotherm equation is given by Equation 5.4.

$$\theta = \frac{Kp}{1 + Kp} \quad \text{Eq. 5.4}$$

where “ θ ” is the number of incorporation sites on the surface which are covered by gaseous molecules and is also called “surface coverage”. Therefore, the free incorporation sites will be $(1-\theta)$. The rate of adsorption depends on the free sites available on the surface $(1-\theta)$ and the partial pressure of the gas p , while the rate of desorption depends on the number of occupied incorporation sites (θ) .

In case the gas is a diatomic molecule A_2 , the dissociative Langmuir equation can be used (Equation 5.5),

$$\theta = \frac{(Kp)^{1/2}}{1 + (Kp)^{1/2}} \quad \text{Eq. 5.5}$$

In this case, the A_2 gas dissociates to two molecules of A upon adsorption. The adsorption process is proportional to the square of the available incorporation sites $(1-\theta)^2$ and the desorption rate proportional to the square of the surface coverage (θ^2) .

Equations 5.4 and 5.5 stand out that for a small concentration of gaseous molecules or low partial pressure of gas, the adsorption on the surface is linear to partial pressure of gas, once there are plenty of free incorporation sites. When the partial pressure of the gas is high, the surface coverage is increasing up to a saturation point because no more free sites exist on the surface. The incorporation of nitrogen is not influenced by the growth rate [4], thus nitrogen incorporation is not kinetically limited. At each partial pressure of nitrogen, an equilibrium surface coverage is established. Thus, a Langmuir adsorption isotherm equation without and with dissociation (Equation 5.6 - 5.7 respectively) were used to describe the data [7].

$$C_N = S_T \frac{Kp}{1 + Kp} \quad \text{Eq. 5.6}$$

$$C_N = S_T \frac{(Kp)^2}{1 + (Kp)^2} \quad \text{Eq. 5.7}$$

where C_N is the incorporated nitrogen concentration, p the partial pressure of nitrogen and S_T is the saturation limit for high values of the partial pressure [cm^{-3}]. S_T and K are the fitting parameters.

It was found that the non-dissociative Langmuir equation describes better the experimental data (Figure 5.14b). The difference in the fitting parameter K for the C-face 6H-SiC and 4H-SiC is around 15%, with the one of 6H-SiC being higher. The saturation limit of C-face 4H-SiC appears to be also 15% higher compared to 6H-SiC. For Si-face 6H-SiC both the parameter K and the saturation limit are found to be almost half value of those of C-face grown crystals. The lack of data for 15R-SiC did not allow a reliable fitting.

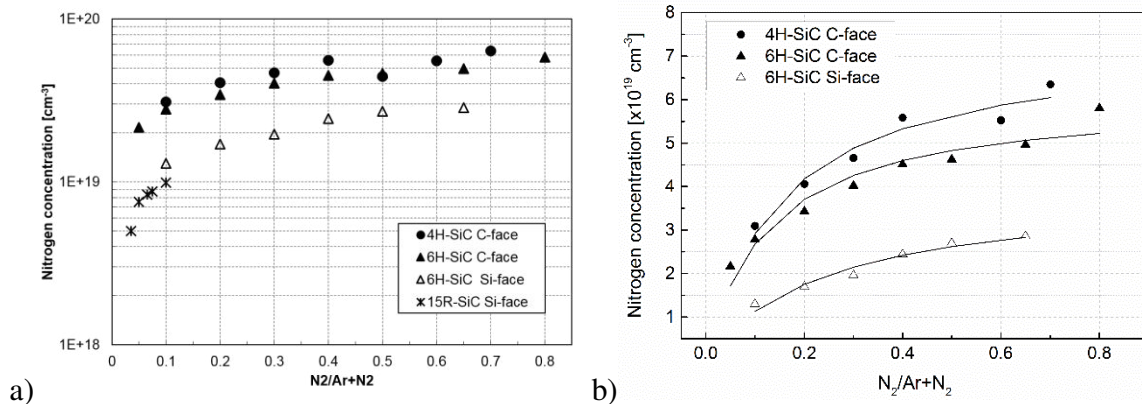


Figure 5.14. a) Nitrogen concentration in SiC grown crystals as a function of the partial pressure of nitrogen during growth. b) A non-dissociative Langmuir isotherm (solid line) was used to best describe the data.

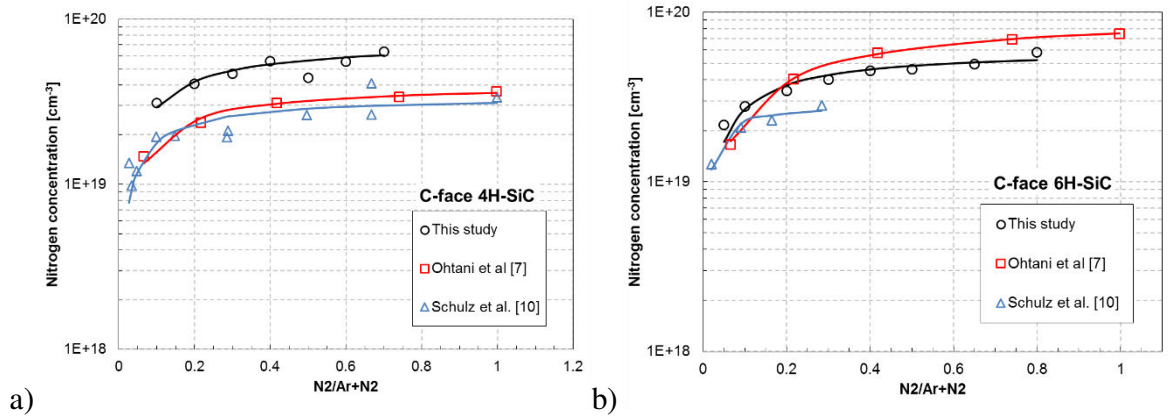
The parameters that best fit our experimental data were compared to those from the bibliography [7, 10] and the values are given in Table 5.5 and in Figure 5.15. Different growth parameters were used by each author and as a result the saturation limit, expressed by fitting parameter S_T , differs. In all cases, nitrogen concentration in the crystals is increasing when partial pressure of nitrogen increases and a saturation limit appears as we approach at 100% nitrogen growth ambient. The small deviation between the different data implies that indeed the partial pressure of nitrogen is the most contributing parameter in nitrogen incorporation of the PVT process.

Bigger variations in the K parameter are obtained when the different experimental data are compared (Table 5.5). Higher K value for the case of C-face 4H-SiC compared to 6H-SiC are reported by Ohtani et al. This implies that higher surface coverage of nitrogen is

established during the growth of 4H-SiC. That was attributed by the author to morphological differences between the two polytypes. Schulz et al. reports that the main difference in K parameter arises between the 4H-SiC and 6H-SiC. For both Si and C-face grown 6H-SiC crystals the K parameter is three times higher compared to C-face 4H-SiC. In order to clarify the difference between the various polytypes and polarity of growth surface, the incorporation mechanism of nitrogen will be considered in the discussion part.

Table 5.5. Best fitting parameters using a non-dissociative Langmuir isotherm

	Fitting parameter		Polytype
	K	S _T [cm ⁻³]	
This study	6.5	7.4x10 ¹⁹	4H-SiC C-face
Ohtani et al. [7]	7.5	4x10 ¹⁹	
Schulz et al. [10]	10.9	3.1x10 ¹⁹	
This study	7.9	6x10 ¹⁹	6H-SiC C-face
Ohtani et al. [7]	3.2	9.8x10 ¹⁹	
Schulz et al. [10]	36.2	-	
This study	4.1	3.2x10 ¹⁹	6H-SiC Si-face
Schulz et al. [10]	46.7	-	



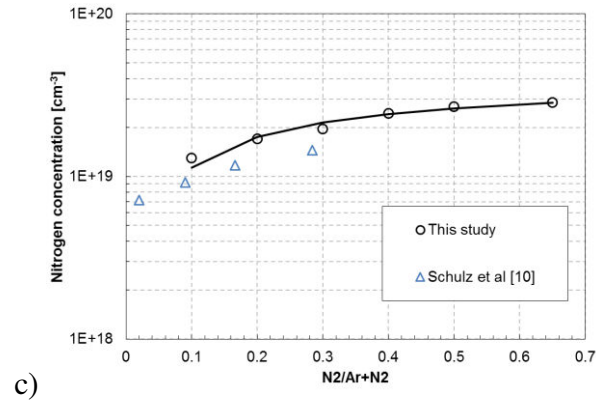


Figure 5.15. Nitrogen concentration as a function of the nitrogen partial pressure for the case of a) C-face 4H-SiC and b) C-face 6H-SiC and c) Si-face 6H-SiC.

5.5 Discussion

In order to explain the experimentally obtained trends, the adsorption/desorption mechanisms at the silicon and carbon {0001} surfaces will be considered (Figure 5.16). The first assumption to be made is that nitrogen substitutes carbon atoms in the SiC lattice due to the comparable size of the two elements. The incorporation of nitrogen at each of the two polar planes will be as follows:

- (000-1) C-face plane: The surface termination of the C-face plane consists of carbon atoms (position A). Adsorption and desorption processes of carbon atoms take place at the surface, thus possible positions for nitrogen atoms to incorporate are created, as nitrogen atoms compete the ones of carbon. In a second phase, silicon atoms will be incorporated, position B. At this point no nitrogen incorporation takes place. At the following step, nitrogen and carbon atoms compete for the available sites, position C.
- (0001) Si-face plane: The surface termination consists of silicon atoms (position A). At this stage no nitrogen incorporation can take place. In the next step, nitrogen and carbon atoms will compete for the available sites, position B. Next, a silicon atomic layer will follow, position C.

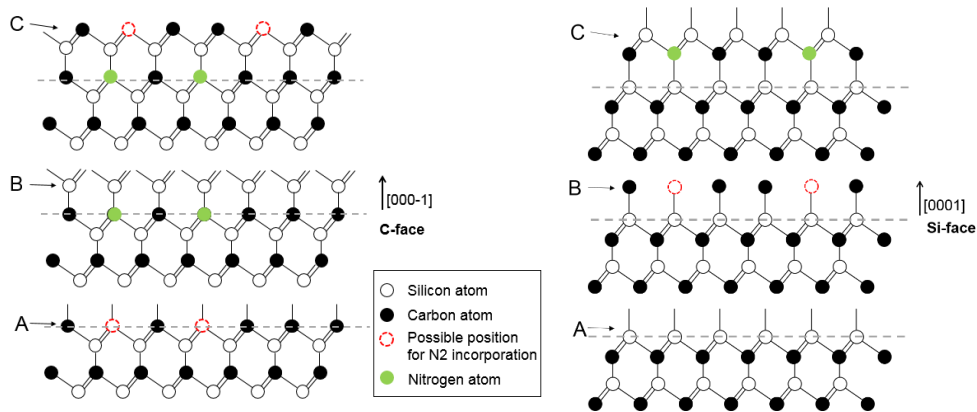


Figure 5.16. Schematic illustration of nitrogen incorporation at the carbon and silicon face plane. Three steps of adatoms' incorporation are considered named as A, B and C.

The incorporation mechanism in the two planes is similar, as nitrogen and carbon atoms are competing when available sites exist on the surface and when silicon is incorporated, no nitrogen incorporation takes place. The difference between the two cases, is related to the dangling bond density of the planes when nitrogen atoms are incorporated. The difference in the bond density between the two planes (higher in the case of C-face) will result in different desorption rates. On (0001)C-face surface, desorption rate is lower compared to the Si-face, or differently said, the surface coverage on (000-1)C-face is higher compared to (0001)Si-face. The parameter that describes adsorption/desorption ratio is the equilibrium constant K , used in the Langmuir adsorption equation. In our study, it was found that the value of the K parameter in the case of Si-face grown 6H-SiC is almost half of the ones of carbon face 4H-SiC and 6H-SiC. This implies that the surface coverage on the C-face is higher compared to the Si-face and that is in agreement with the proposed mechanism above.

Even though the kinetic parameter K and the saturation limit between the Si and C-face surface are different, it is not the case for different polytypes. The similar values of K and S_T fitting parameters, for C-face 4H-SiC and 6H-SiC, indicate that the incorporation of nitrogen on the (000-1) plane is independent on the polytype of the crystal. That result is in

contradiction to previous reports, where a difference in the saturation limit and surface coverage was found at 4H-SiC and 6H-SiC crystals grown on the (000-1) plane [7].

The incorporation of atoms through the surface as described in Figure 5.16 is a simplified idea, because it ignores the incorporation of dopants at steps. Incorporation of atoms on the growth surface will take place on kink sites at the edge of steps and vacancies or free incorporation sites formed on the terraces (Figure 5.17).

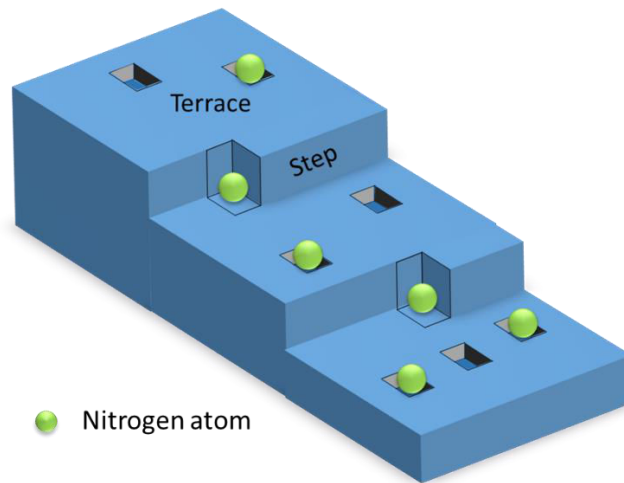


Figure 5.17. Schematic illustration of the growth surface. Incorporation of nitrogen atoms will occur on kink sites on the steps and free incorporation sites or vacancies on the terraces.

Here we will consider that nitrogen incorporation will take place on i) kink sites on the steps and ii) vacancies on the terraces. This statement is enhanced by the fact that nitrogen incorporation in sublimation process is not kinetically limited, but a dynamic equilibrium is established between the adsorbed and desorbed gaseous species. In order to promote growth, SiC species will diffuse on the surface and will be incorporated at kink sites at the step edge. The concentration of SiC species along the width step is described by the BCF and Ehrlich-Schwoebel theory. However, nitrogen is abundant in the gaseous phase compared to the SiC species. No diffusion of nitrogen atoms is needed at the step edge and incorporation of nitrogen can occur at any free incorporation site.

During PVT growth it is systematically reported that nitrogen incorporation is higher at the {0001} facet compared to the step flow area, for a given growth ambient. The ratio of the incorporated nitrogen at the facet and the step flow area as a function of the nitrogen concentration in the gas phase, was plotted by Schulz et al. for C-face 4H-SiC growth [9]. It was shown that the incorporated nitrogen in the facet is 1.5 times higher compared to the step flow area for low partial pressure of nitrogen and saturates at 1.2 for higher values of doping, Figure 5.1c. If nitrogen incorporation takes place only on the kink sites of steps, then nitrogen concentration on the step flow area should have been always higher, once kink sites density is higher there compared to the {0001} facet. However, exactly the opposite is occurring. This indicates that incorporation of nitrogen occurs also in vacancies formed on terraces of the {0001} facet.

Last, possible parameters that reduce the incorporation of nitrogen when the growth temperature increases are the increased desorption of nitrogen, the decrease of Si/C ratio, the increase of the growth rate and the change on the terraces width on the {0001} facet. However, it is reported that the growth rate hardly affects the incorporated nitrogen in the PVT process [4]. Also the change of Si/C ratio is found not to affect the incorporated nitrogen on the C-face but only at the Si-face growth [2, 3].

Thus, the temperature dependent incorporation of nitrogen can be attributed to two factors, i) the equilibrium constant of the Langmuir adsorption equation “K” is dependent on the temperature of the system. Once the temperature of the system is decreasing, the adsorption/desorption ratio is increasing ($K_{T_{low}} > K_{T_{high}}$). The surface coverage “ θ ” will increase as well as the nitrogen concentration in the crystal (Figure 5.18). The increase of surface coverage with temperature, arises due to decrease of the kinetic energy of the atoms. ii) The increase of the growth rate reduces the width of the terraces on the {0001} facet, as presented in Figures 5.10-5.12. Considering that nitrogen incorporation occurs on vacancies on the terraces along with kink sites on steps, nitrogen incorporation is decreased, once the width of the terraces and thus the free incorporation sites is reduced.

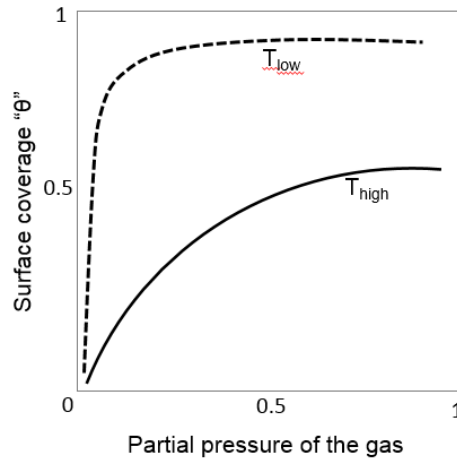


Figure 5.18. *Surface coverage as a function of the partial pressure of the gas, described by a Langmuir adsorption equation. The effect of a lower and higher temperature at saturation limit is shown.*

Even if the nature of the polytype does not introduce any difference in the incorporation of nitrogen, it is not the case for different crystallographic planes. It is already reported that nitrogen concentration is different among (1-100), (11-20) and (0001) planes for both PVT and CVD processes (Figure 5.19). During the growth of bulk crystals, naturally formed facets can be created. A cross section of a C-face 4H-SiC crystal (B257) is shown in Figure 5.20. The color variations of the crystal is due to the presence of nitrogen. The formation of facets (A-D) at the periphery of the crystal are more obvious in the cross section sample due to the differences in color contrast. It is possible to see the “path or footprint” of the facets as they propagate during growth. It was not possible to determine the free carrier concentration of each facet by Raman due to combined effect of orientation and doping in the shift of the Raman modes. At those facets (crystallographic planes), no terraces are formed, but only the step density and bond density at the kink sites is expected to be different. So, the characteristics of the edge step can affect the incorporation of nitrogen. However, further analysis is needed towards this direction.

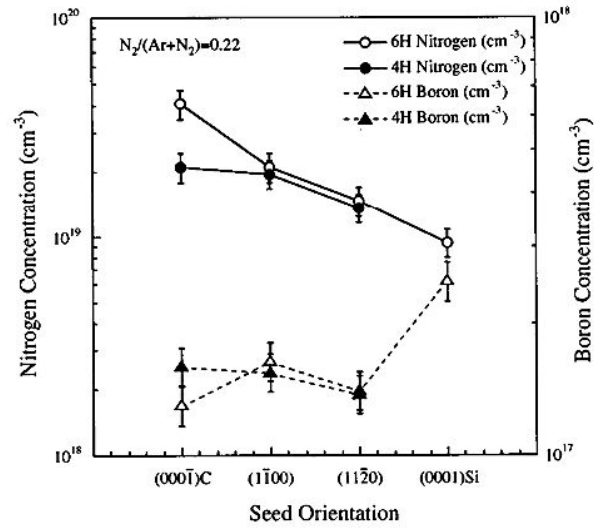


Figure 5.19. Nitrogen concentration of 4H-SiC and 6H-SiC as a function of the orientation of growth [7].

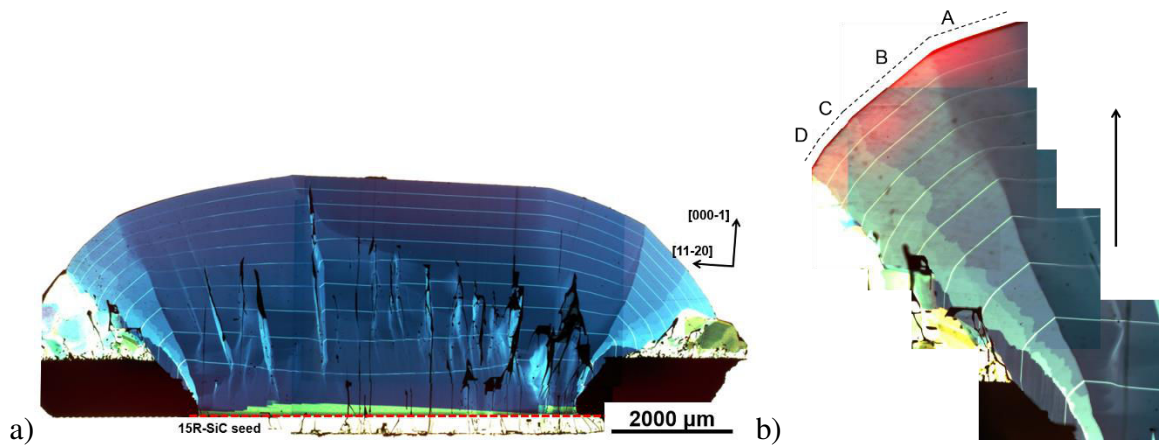


Figure 5.20. a) Cross section image of a 4H-SiC crystal grown on a 3° off-axis 15R-SiC C-face seed. b) Variations of contrast reveal the “footprint” of the various facet during growth, once nitrogen incorporation is different at each plane.

Conclusions of Chapter 5.

The incorporation of nitrogen in 4H-SiC and 6H-SiC was studied as a function of the partial pressure of nitrogen and the growth temperature. The nitrogen concentration of the grown crystals was in the range of 10^{19} - 10^{20} cm⁻³.

The incorporated nitrogen as a function of the nitrogen partial pressure dependence reveals that the concentration of nitrogen in the grown crystals increases once the partial pressure of nitrogen increases and reaches a saturation limit for higher values. A non-dissociative Langmuir adsorption isotherm equation was used to fit the experimental data. The fitting parameter “K” takes a similar value for the C-face 4H-SiC and 6H-SiC crystals, while in the case of Si-face grown crystals it is almost half value. Similar, the saturation limit of the C-face grown crystals is double compared to the Si-face. This indicates i) that the incorporation of nitrogen on the (000-1) surface is independent of the polytype of the crystal and ii) that a higher surface coverage of nitrogen is established on the C-face surface compared to the Si-face.

The difference in dangling bond density for C atoms between the two polar planes, indicate that a higher desorption rate is expected in the silicon (0001) plane. During the PVT process a dynamic equilibrium condition is established between the adsorption and desorption rate of the gaseous species. Thus, it is reasonable to assume that nitrogen incorporation takes place on both kink sites of the steps edges and free incorporation sites on the terraces formed on the {0001} facet. The higher incorporation of nitrogen on the {0001} facet compared to the step flow area, can thus be explained.

The free carrier concentration in C-face 4H-SiC crystals decreases once the growth temperature is increasing. Two plausible mechanisms are proposed for the obtained trend, i) the increase of nitrogen adsorption/desorption ratio due to the increase of temperature. The nitrogen surface coverage is decreased and thus, the nitrogen incorporated in the grown crystal. ii) Due to the increase of the growth rate the width of the terraces on the {0001} facet decreases. So, the number of free incorporation sites is decreasing and less nitrogen is incorporated in the grown crystal. The lack of data does not allow a comparison with the 6H-SiC crystals grown on the Si and C-face.

Additional analysis is needed in order to explain the different incorporation of nitrogen at the various crystallographic planes and propose a complete model for nitrogen incorporation for the PVT process.

References

1. Forsberg, U., et al., *Nitrogen doping of epitaxial silicon carbide*. Journal of Crystal Growth, 2002. **236**(1-3): p. 101-112.
2. Kimoto, T., A. Itoh, and H. Matsunami, *Incorporation mechanism of N, Al, and B impurities in chemical vapor deposition of SiC*. Applied Physics Letters, 1995. **67**(16): p. 2385-2387.
3. Larkin, D.J., *SiC Dopant Incorporation Control Using Site-Competition CVD*. physica status solidi (b), 1997. **202**(1): p. 305-320.
4. Onoue, K., et al., *Nitrogen Incorporation Kinetics during the Sublimation Growth of 6H and 4H SiC*. Japanese Journal of Applied Physics, 1996. **35**(Part 1, No. 4A): p. 2240-2243.
5. Lely, J.A., *Berichte der Deutschen Keramischen Gesellschaft*, 1955. **32**: p. 229.
6. Woodbury, H.H. and G.W. Ludwig, *Electron Spin Resonance Studies in SiC*. Physical Review, 1961. **124**(4): p. 1083-1089.
7. Ohtani, N., et al., *Impurity incorporation kinetics during modified-Lely growth of SiC*. Journal of Applied Physics, 1998. **83**(8): p. 4487-4490.
8. Schulz, D., et al., *Study of Nitrogen Incorporation in 6H-SiC Single Crystals Grown by PVT*. Materials Science Forum, 2000. **338-342**: p. 87-90.
9. Rost, H.J., D. Schulz, and D. Siche, *High Nitrogen Doping During Bulk Growth of SiC*, in *Silicon Carbide*, W.J. Choyke, H. Matsunami, and G. Pensl, Editors. 2004, Springer Berlin Heidelberg. p. 163-178.
10. Schulz, D. 2001, PhD Thesis, Brandenburgische Technische Universität Cottbus.
11. Mitani, T., et al., *Determination of carrier concentration by Fano interference of Raman scattering in heavily doped n-type 4H-SiC*. Journal of Applied Physics, 2012. **112**(4): p. -.
12. Pensl, G. and W.J. Choyke, *Electrical and optical characterization of SiC*. Physica B: Condensed Matter, 1993. **185**(1-4): p. 264-283.
13. Götz, W., et al., *Nitrogen donors in 4H-silicon carbide*. Journal of Applied Physics, 1993. **73**(7): p. 3332-3338.
14. Ohtani, N., et al., *Investigation of heavily nitrogen-doped n+ 4H-SiC crystals grown by physical vapor transport*. Journal of Crystal Growth, 2009. **311**(6): p. 1475-1481.
15. Yamamoto, T., T. Kimoto, and H. Matsunami, *Impurity Incorporation Mechanism in Step-Controlled Epitaxy Growth Temperature and Substrate Off-Angle Dependence*. Materials Science Forum, 1998. **264-268**: p. 111-114.

General Conclusions and future studies

In the present thesis, the growth process was developed in an effort to allow the growth of SiC crystals of sufficient size and shape based on the needs of the experiments. Continuously, the problem of foreign polytype occurrence during bulk growth was addressed, with respect to the evolution of the system with time. The parameters that can affect the stabilization of 15R-SiC were examined. Last, the incorporation of nitrogen as a function of different growth parameters was studied.

In more details, we have shown that contactless growth of SiC in the PVT system can be achieved, while maintaining the control of the growth. The shape of the crystal or the growth rate along the crystal radius and the Si/C ratio of the gas phase can be well governed by the control of temperature distribution and crucible design. A remaining issue is the improvement of the process yield, using the contactless growth configuration. Also, SiC crystals were grown using the “necking technique”. That technique can lead to grown crystals of sufficient size and quality when small diameter seeds are used, however further development is needed.

The occurrence of foreign polytype inclusions is found to be directly related to the presence of the {0001} facet of SiC. The probability to nucleate a foreign polytype is increasing once the presence of the {0001} facet and the minimum of Gibbs free energy for 2D nucleation occur at the same place and time. Thus 2D nucleation appears as a plausible mechanism for polytype transitions in PVT growth. Once a foreign polytype is formed, its propagation is related to the interaction with the global growth interface and the competition between different growth mechanisms. A foreign polytype will propagate at the basal and along the c-axis at the facet to all the directions but not in the one that an advanced growth center is located. In a blocking situation, a thin lamella or an inclusion is formed while in the opposite case, a total polytype conversion will take place. Out of the facet area, the propagating velocity of the foreign polytype inclusion is linked to the curvature of the crystal. If both the propagation of the inclusion at the basal plane and that of the growth front are in the same direction, the inclusion can cross all the crystals length. The evolution of

crystal shape and the competition of the various growth mechanism will define the overlapping or not of a foreign polytype and the shape of the interface between the two polytypes. The last point should be examined in more details in the future.

Continuously the growth of 15R-SiC crystals was addressed and various parameters that can affect its stability were examined. Nucleation of 4H-SiC at the (000-1) C-face and 6H-SiC at the (0001) Si-face 15R-SiC facet is obtained. Grown crystals appear as a mixture of 15R-SiC with only one of the hexagonal polytypes. In contradiction to the case of 4H-SiC growth, nitrogen is found not to directly affect the stabilization of 15R-SiC. Thus, the stabilization of 15R-SiC is found to be dependent on the Si/C ratio in the gas phase. It was shown that a disturbance of the Si/C that favors 15R-SiC, led to the nucleation of hexagonal polytypes. Further development of the thermodynamic calculations is needed in order to specify the range of Si/C ratio values for the growth of 15R-SiC. Also, additional experiments using a multi-seeded method are needed in order to highlight the effect of various growth parameters on both silicon and carbon face grown crystals.

Last, the incorporation of nitrogen during the growth of 4H-SiC and 6H-SiC was studied as a function of the nitrogen partial pressure and growth temperature. The free carrier concentration is found to be decreased when the growth temperature is increasing for the case of C-face 4H-SiC and the activation energy is calculated at 152.4 kJ/mol. The experimentally obtained trend is believed to be due to the increased desorption of nitrogen, when temperature is increasing. Further studies are needed for the case of 6H-SiC of both Si- and C-face, in order to provide additional information. The partial pressure of nitrogen reveals that C-face grown crystals incorporate more nitrogen compared to Si-face, while for both polarities a saturation limit will arise for partial pressure of nitrogen values higher than 0.6-0.7. A non-dissociative Langmuir adsorption isotherm equation was used to fit the experimental trends. Using this equation, it was shown that the surface coverage of nitrogen at the C-face is similar for 4H-SiC and 6H-SiC while the saturation limit for the two polytypes appears to be the same. The difference will arise in the case of Si-face growth, where the saturation limit and the nitrogen surface coverage is found to be almost half value, compared to C-face growth. The adsorption and desorption mechanisms on both kink sites

on steps and incorporation sites on terraces should be considered in order to describe the problem of nitrogen incorporation. Thus, the higher incorporation of nitrogen at the {0001} facet compared to the step flow areas can be explained.

In the present work, crucial issues related to the bulk growth of SiC were tackled. Further advancement of theoretical calculations is needed in order to provide additional information for the problems of polytype nucleation and nitrogen doping. Also, additional experimental data at the nitrogen doped crystals could help to develop a complete model of nitrogen incorporation in SiC in the PVT process.

Résumé de la thèse en français

A. Introduction

L'électronique est l'un des domaines technologiques les plus dynamiques, en raison de son importance croissante dans la vie économique, industrielle et sociale de l'homme. Les matériaux semi-conducteurs tels que le silicium (Si), le germanium (Ge), l'arséniure de gallium (GaAs) et le carbure de silicium (SiC) y jouent un rôle particulier car ils sont à la base des technologies de l'électronique. Le silicium est le semi-conducteur le plus largement utilisé car il peut être obtenu sous forme de cristaux de grande taille et former facilement un oxyde (dioxyde de silicium). Toutefois, en raison des besoins croissant en performances, et notamment dans un contexte d'amélioration de l'efficacité énergétique, la technologie silicium atteint ses limites pour les applications de puissance. Le carbure de silicium est l'un des compétiteurs les plus prometteurs et des dispositifs de SiC ont déjà remplacé le silicium dans certains systèmes électroniques spécifiques.

Un effort considérable a été mené ces dernières décennies, afin d'augmenter la taille et la qualité des cristaux de SiC, d'améliorer les caractéristiques des couches épitaxiées, d'étudier les interfaces de SiC-oxyde ainsi que l'incorporation de divers dopants. L'objectif étant de développer des diodes (e.g. Schottky) et des transistors (e.g.) MOSFET) et de les intégrer dans des circuits électroniques.

A.1 Objet et principale contribution de la thèse.

Cette thèse a pour objectif d'approfondir les connaissances actuelles sur les mécanismes de croissance de cristaux de SiC à partir de la phase vapeur. Pour cela, nous étudierons successivement les quatre points suivants: i) développer le procédé PVT: l'objectif est de proposer et d'évaluer des stratégies afin d'obtenir des cristaux de SiC centimétriques, sans gangue polycristalline. Cela nécessite une étude approfondie des transferts de chaleur et de masse dans le creuset réactionnel, ii) étudier la stabilité des polytypes: le but est de mettre en évidence les paramètres régissant l'apparition et la propagation de polytypes parasites pendant la croissance, iii) étudier la croissance cristalline du polytype 15R-SiC, candidat à fort potentiel pour les applications de type MOSFET, iv) étudier l'incorporation d'azote: l'azote étant le dopant de type n classique dans les technologies SiC. Cependant, son incorporation est mal connue dans le procédé de croissance de cristaux massifs en phase vapeur (PVT).

1. Carbure de silicium: Propriétés et croissance

1.1.1 Polytypisme du SiC.

Le carbure de silicium (SiC) présente naturellement un polytypisme, qui est un cas particulier de polymorphisme à une dimension. La structure est formée de tétraèdres élémentaires SiC_4 ou CSi_4 (Figure 1.1). La structure est construite par l'empilement de plans compacts de tétraèdres. Pour cela, on distingue deux orientations possibles des plans de tétraèdres (Figure 1.2). Ainsi, la séquence d'empilement de ces deux types de plans de tétraèdres va déterminer le polytype (Figure 1.3). Si tous les plans sont de même orientation, la structure cubique appelée 3C-SiC est obtenue. Si les plans sont alternés le long de l'axe c , des structures hexagonales ou rhomboédriques seront obtenues. Dans la notation de Ramsdell, utilisée pour référencer les polytypes, le nombre désigne le nombre de plans de tétraèdres nécessaires pour décrire la séquence unitaire et les lettres correspondent au type de réseau de Bravais (H, C et R pour hexagonal, cubique et rhomboédrique). Près de 200 polytypes ont été référencés [1, 2]. Toutefois, seuls quatre polytypes (3C-SiC, 15R-SiC, 4H-SiC et 6H-SiC) sont essentiellement étudiés, avec un seul d'entre eux (4H-SiC) qui est un produit industriel.

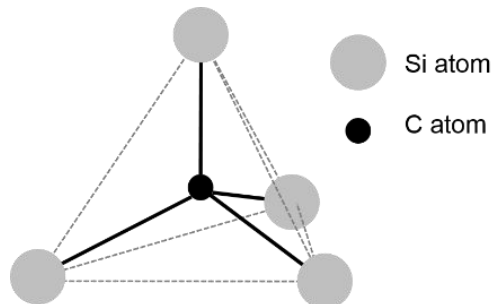


Figure 1.1. Tétraèdre de base de la structure de SiC.

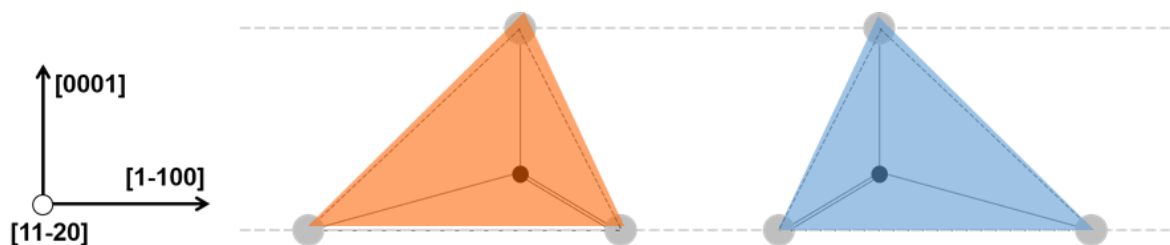


Figure 1.2. Dans les polytypes, les tétraèdres peuvent avoir deux orientations particulières. Projection dans le plan (11-20)

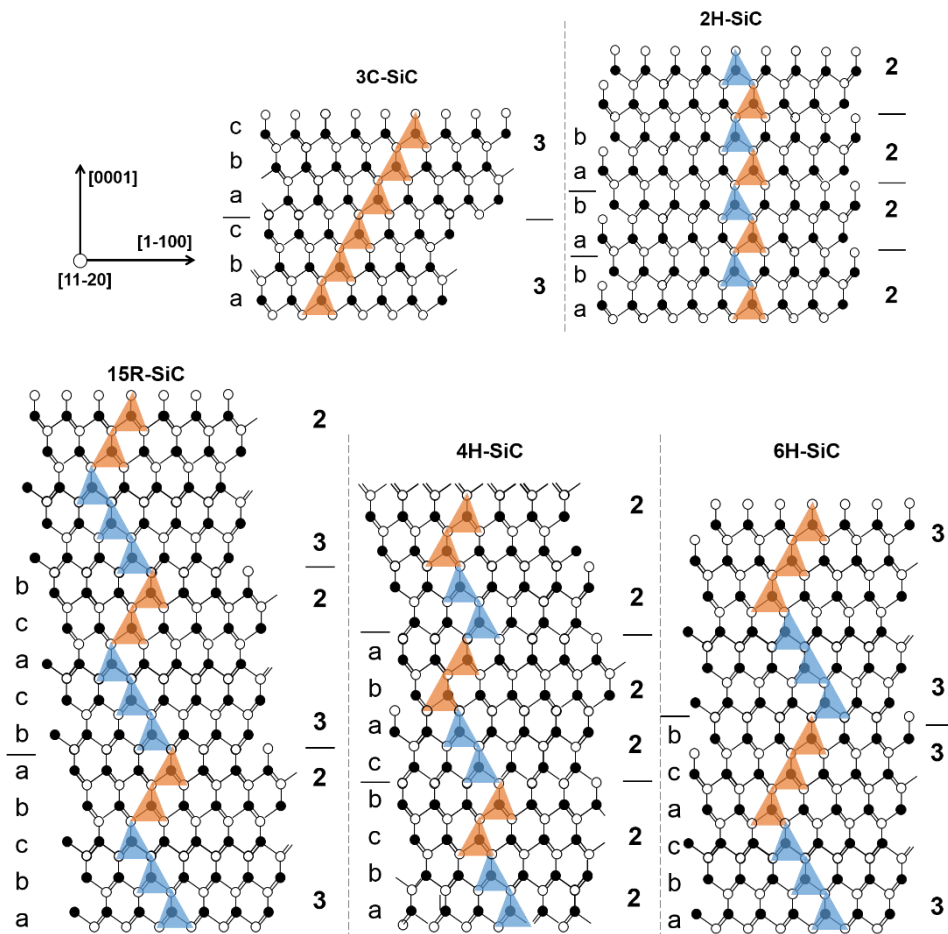


Figure 1.3. Structure cristallographique des principaux polytypes de SiC ; projection dans le plan (11-20).

1.1.2 La polarité du SiC

Lorsque la structure est clivée dans le plan basal, deux surfaces énergétiquement différentes sont créées. Une aura une terminaison Si (0001) et l'autre une terminaison C (000-1). On parlera de polarité Si ou C. Ces deux surfaces ont des propriétés physico-chimiques très différentes, ce qui aura des conséquences sur leur réactivité lors de la croissance, l'incorporation des dopants, l'oxydation etc. Les énergies de surfaces proposées par Pearson sont de 2.2 J/m², et 0.3 J/m² pour les faces Si et C respectivement [3].

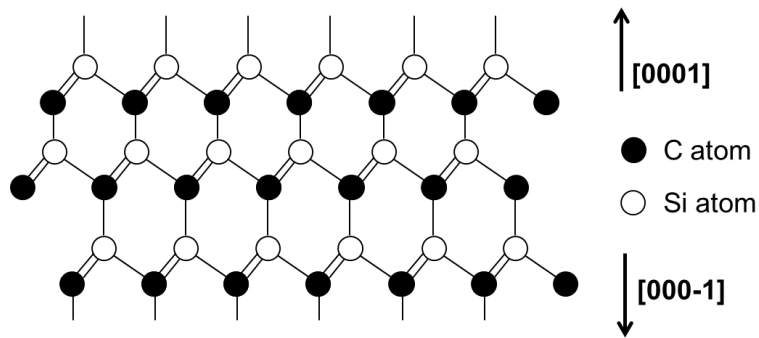


Figure 1.4. Polarités Silicium et Carbone du SiC.

1.1.3 Dopage du SiC

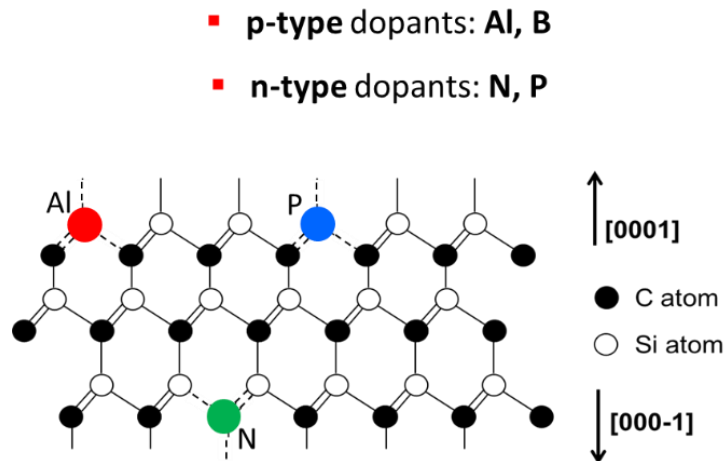


Figure 1.5. Les principaux dopants du SiC

Les propriétés semi-conductrices des matériaux sont généralement ajustées par un dopage fin et contrôlé. Pour le SiC, le dopage de type n ou p est assuré par les éléments du groupe VA ou IIIA du tableau périodique, respectivement. Aluminium et le Bore sont les dopants de type p plus couramment utilisés, tandis que Azote et Phosphore constituent les dopants de type n les plus fréquents. D'une manière générale, Al et P se placent sur les sites Si alors que N se place sur les sites C. B est un peu plus compliqué car il peut s'incorporer sur les deux sites à la fois. Ce point est toujours controversé [4].

1.2. Croissance du SiC

SiC est le seul composé solide du diagramme Si-C (Figure 1.6). Contrairement à la plupart des matériaux semi-conducteurs, la croissance à partir de l'état fondu ne peut pas être appliquée dans des conditions raisonnables de température et de pression car il est à fusion non congruente [5]. Comme le SiC commence à se sublimer à partir de 1800 °C sous basse pression, c'est le procédé de croissance en phase vapeur qui s'est principalement développé.

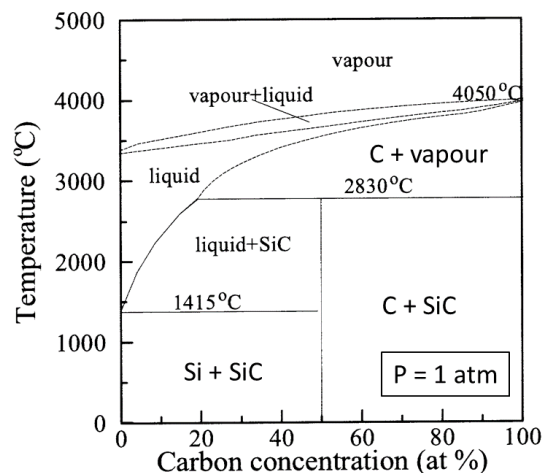


Figure 1.6. Diagramme de phase de Si-C. [6].

Les cristaux issus de la méthode de Lely (sublimation d'une poudre de SiC à très haute température) se forment par nucléation spontanée. Par conséquent, la taille et la forme des cristaux sont aléatoires. Une extension de cette technique Lely sur germe appelée PVT pour Physical Vapor Transport permet la croissance de gros monocristaux de SiC. C'est la technique industrielle actuelle. Le schéma de principe est représenté sur la Figure 1.7. Un creuset en graphite est utilisé pour la croissance, car il est thermiquement et chimiquement compatible avec le système Si-C à plus de 2000°C. Le matériau source est une poudre de SiC, qui est placée au fond du creuset. De l'autre côté de la cavité, un monocristal de SiC sert de germe. Le creuset est isolé thermiquement par du feutre en graphite

Les trois étapes élémentaires du procédé sont :

1. La sublimation dissociative de la source de SiC.
2. Le transfert de matière entre la source et le germe par voie gazeuse.

3. La cristallisation des espèces gazeuses sur le germe de SiC.

Pour une température supérieure à 1800 °C, la source de SiC se sublime en espèces Si, Si₂C, SiC₂. Cette vapeur est riche en Si. La force motrice du procédé est le gradient de température le long de l'axe de symétrie du creuset (typiquement de 5-15K/cm).

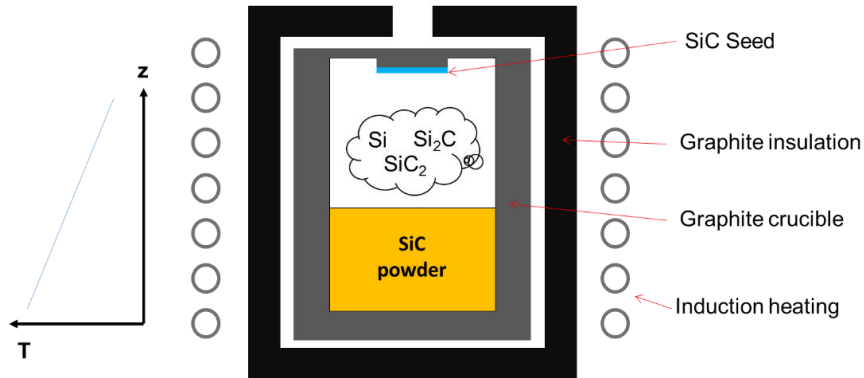


Figure 1.7. Représentation schématique du procédé de sublimation (PVT). Le profil de température est représenté au côté gauche.

2. Développement de procédé

2.1. Dispositif expérimental

L'appareillage expérimental est composé des éléments suivants : le générateur, le boîtier de condensateurs, la baie de contrôle/commande, les organes de sécurité, les dispositifs de mesure de température et de pression, et le réacteur (Figure 2.1).

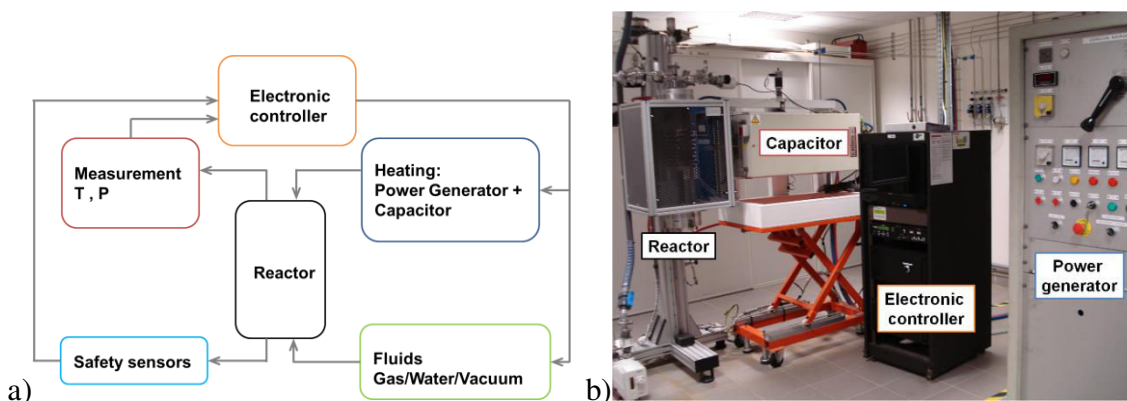


Figure 2.1. (a) Illustration des différents éléments du réacteur de croissance PVT. (b) Photo du réacteur utilisé dans ce travail.

2.2. Croissance sans contact

Sans aucune précaution, une gangue polycristalline de SiC se forme autour du cristal lors de la croissance PVT de SiC. Ceci est à l'origine de nombreux défauts, de joints de grains à faibles angles, d'inclusions de polytypes étrangers [7-8]. Des études ont été faites pour contrôler la formation de ce polycristal parasite, notamment par un meilleur contrôle de la sursaturation [9], l'utilisation d'écrans thermiques [10] ou des modifications de la géométrie du creuset en graphite [11].

Une géométrie qui permet la croissance de cristaux sans contact a été développée. La croissance a été réalisée en formant une cavité latérale dans la partie haute du creuset de graphite (Figure 2.2), dont la température est inférieure à celle du germe. Ceci génère un flux « de fuite » J_P dont le contrôle permet d'éviter la nucléation de polycristal. Des exemples de cristaux élaborés « sans contact » sont donnés dans la Figure 2.3.

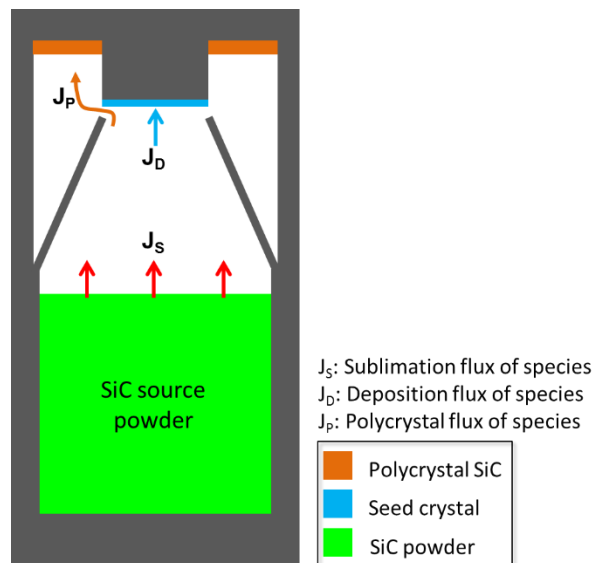


Figure 2.2. Représentation schématique des principaux flux d'espèces de SiC dans le creuset. J_S est le flux qui vient de la sublimation de la poudre SiC, J_D : le flux de dépôt dans la zone de cristallisation et le flux total J_P .

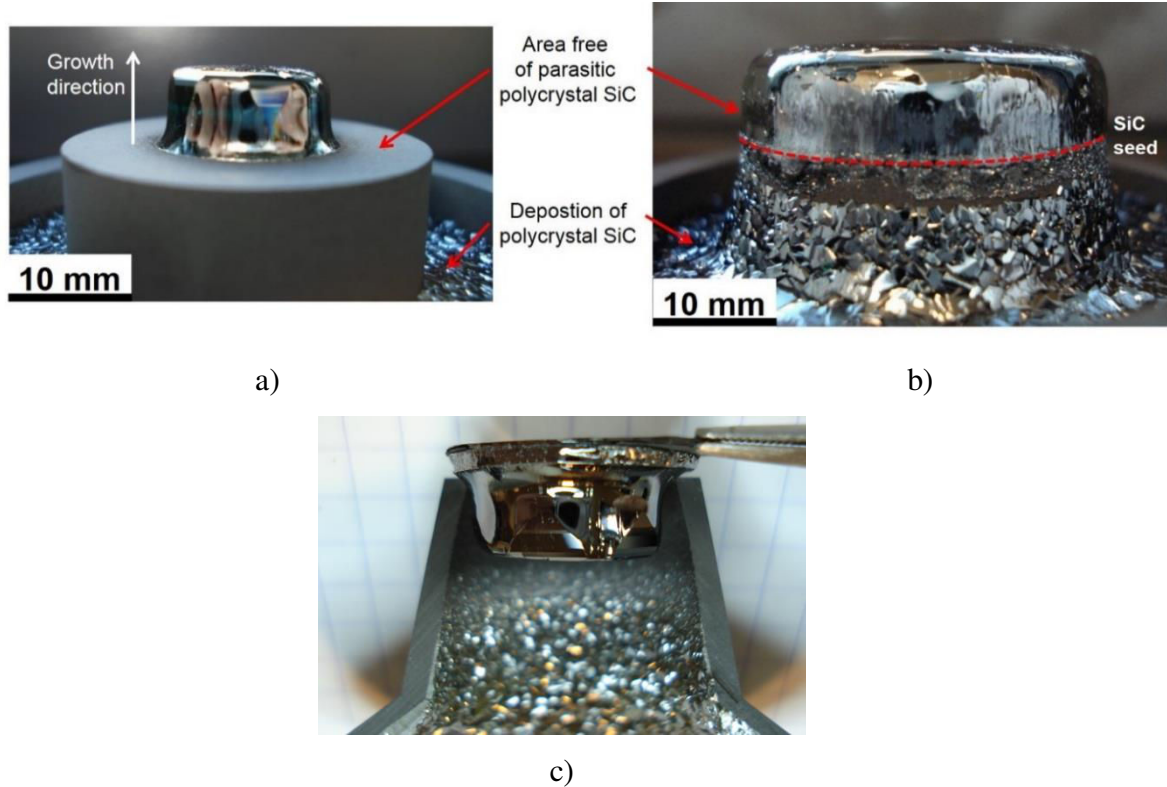


Figure 2.3. SiC monocristallin de (a) 15mm et (b) 30mm de diamètre dans le creuset en graphite. (c) Cristal de SiC dans son écran thermique en graphite.

3. La nucléation et la propagation des inclusions de polytypes.

3.1 Introduction

Pendant la croissance de SiC massif par PVT, les inclusions de polytypes étrangers sont très couramment obtenues et sont généralement accompagnées par un amas de défauts (dislocations) générées aux joints entre les différents polytypes [12-15]. Une avancée dans la compréhension et la stabilisation d'un seul polytype de SiC a été le développement de « la step controlled epitaxy » [16]. L'idée consiste à diminuer la probabilité de nucléation 2D (à l'origine des transitions de polytype) en favorisant la réplique du substrat par un mécanisme d'avancée de marches. Cette approche est systématiquement utilisée pour la croissance épitaxiale de couches minces par CVD [17]. Elle a été aussi tentée pour la croissance massive de SiC par PVT. Cependant, dans ce cas, l'angle de désorientation n'aide à la stabilisation du polytype que pendant les

premiers stades de croissance car la forme de l'interface de croissance évolue considérablement avec l'épaisseur du cristal.

La PVT est par nature un procédé non-stationnaire et la plupart des paramètres de croissance évoluent au cours du temps [18,19]. Les paramètres physiques, tels que le rapport Si/C, la distribution de température et de la sursaturation varient spatialement et temporellement. Dans ces conditions, il est très difficile de comprendre et d'étudier l'apparition et la propagation des inclusions de polytype. Même si au niveau industriel, la croissance de lingots de 4H-SiC de 6 pouces de diamètre est empiriquement maîtrisée, les mécanismes liés à la formation d'inclusions de polytypes restent encore obscures. Une approche intéressante vers la clarification de ce problème a été proposée par l'introduction de la théorie classique de la germination, proposée par Fissel et al. [20] dans la simulation complète du procédé PVT [21].

3.2 Expérimentation et calculs théoriques

Détails expérimentaux : Les paramètres contrôlés pendant les expériences sont la pression (P), la température (T) et la pression partielle d'azote (P_{N_2}). La température de croissance est constante sur l'ensemble de l'étude, fixée à 2200°C. La pression totale varie dans la gamme 6-12 mbar. Les croissances sont réalisées sous atmosphère d'argon ; l'injection périodique d'azote permet le marquage de l'interface, de façon à suivre son évolution. Pour la présente étude, des cristaux d'environ 5 mm de longueur et 15 mm de diamètre ont été produits. Différents substrats ont été utilisés, en faisant varier le polytype (4H-SiC et 15R-SiC), l'orientation (on-axis ou 4° off-axis) et la polarité (face silicium ou face carbone). Les cristaux formés ont ensuite été découpés en sections transverses et observés sous par microscope optique en lumière polarisée, après polissage des deux faces. L'identification des polytypes a été faite par spectroscopie Raman et cathodoluminescence (CL).

Simulation numérique. La simulation du procédé a été effectuée en utilisant la méthode des éléments finis (FEM). Tout d'abord, la simulation complète du procédé a été réalisée en incluant le chauffage par induction, les transferts de chaleur et de matière dans une géométrie axisymétrique [22]. La température et les pressions partielles des espèces

gazeuses Si, Si₂C et SiC₂ sont calculées le long du rayon du cristal, au niveau de la surface de croissance. Les calculs ont été effectués en suivant l'approche proposée par Kakimoto et al. [23]., La sursaturation (équation 3.1) et la différence de potentiel chimique correspondant ($\Delta\mu$, équation 3.2) ont été calculés à partir des pressions partielles des espèces gazeuses et de la température. Enfin, l'énergie libre de nucléation 2D a été calculée à partir de l'équation 3.3.

$$\frac{p}{p_0} = \frac{p_{\text{Si}_2\text{C}} + 2p_{\text{SiC}_2}}{p_{\text{Si}_2\text{C}}^0 + 2p_{\text{SiC}_2}^0} \quad \text{Eq. 3.1}$$

$$\Delta\mu = kT \ln \frac{p}{p_0} \quad \text{Eq. 3.2}$$

$$\Delta G_2 = \frac{b^4 \sigma_1^2}{\Delta\mu - (\sqrt{3}/2)b^2(\sigma_1 + \sigma_i - \sigma_s)} \quad \text{Eq. 3.3}$$

p et p^0 sont respectivement les pressions partielles et à l'équilibre, ΔG_2 est l'énergie libre de nucléation 2D, b est la distance aux premiers voisins (ici, le paramètre de maille dans le plan), $\Delta\mu$ est la différence de potentiel chimique entre le gaz et le solide, σ_1 , σ_i , σ_s sont respectivement l'énergie de surface de la couche épitaxiale, l'énergie interfaciale couche/substrat et l'énergie de surface du substrat.

3.3 Observation de la formation et de la propagation des inclusions

Une coupe transversale d'un cristal obtenu sur un germe de 4H-SiC C-face 4° off-axis observée sous un microscope en polarisation croisée est présentée Figure 3.1a (cristal B254). Pour aider à visualiser, le secteur de croissance (000-1) est indiqué par les lignes pointillées orange. Cette zone correspond à la trajectoire de la facette (000-1) pendant la croissance. Ce secteur de croissance apparaît légèrement plus sombre à l'intérieur des bandes dopées, ce qui est attribué à une plus grande incorporation de l'azote sur la facette de polarité C qu'ailleurs [24.25]. Dans ce cas, de légères modifications de la cavité de croissance ont induit une surface de cristal concave plus prononcée, en particulier au

début de la croissance. Une conséquence est l'apparition de deux facettes (000-1) de chaque côté de la coupe. Sur la facette de droite, trois fines lamelles de 6H-SiC ont germées – signalées par les cercles N°1, 2 et 3 (Figure 3.1a) – et se sont étendus dans la direction [11-20]. Une image à plus fort grossissement des inclusions #1, 2 et 3 dans la zone de la facette et du milieu du cristal est montrée Figure 3.1b-c. Sur la facette de gauche, une épaisse inclusion de 15R-SiC a germée (partie gauche de la Figure 3.1).

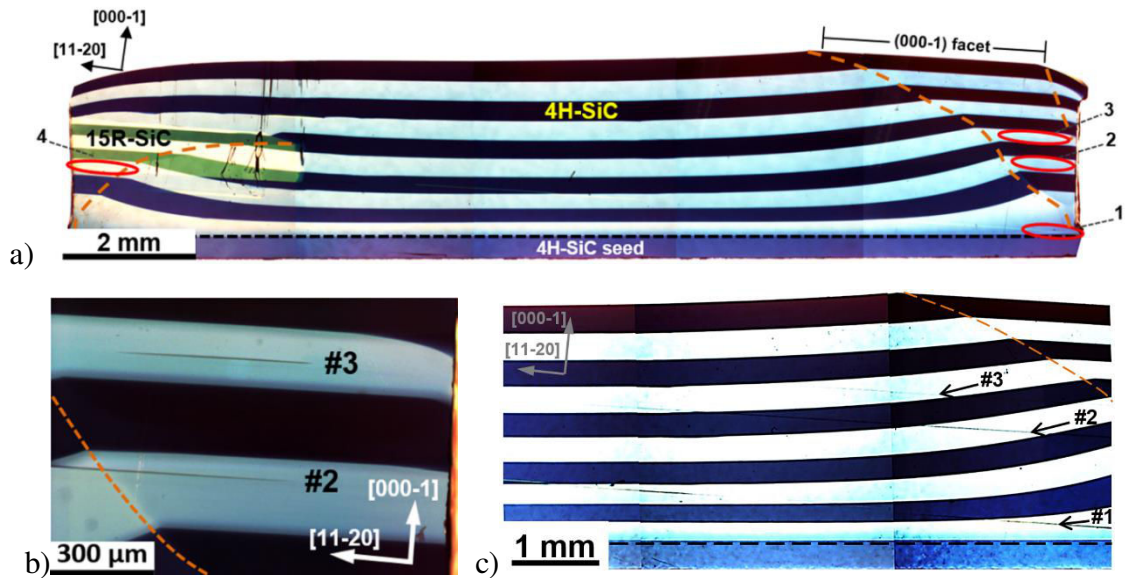
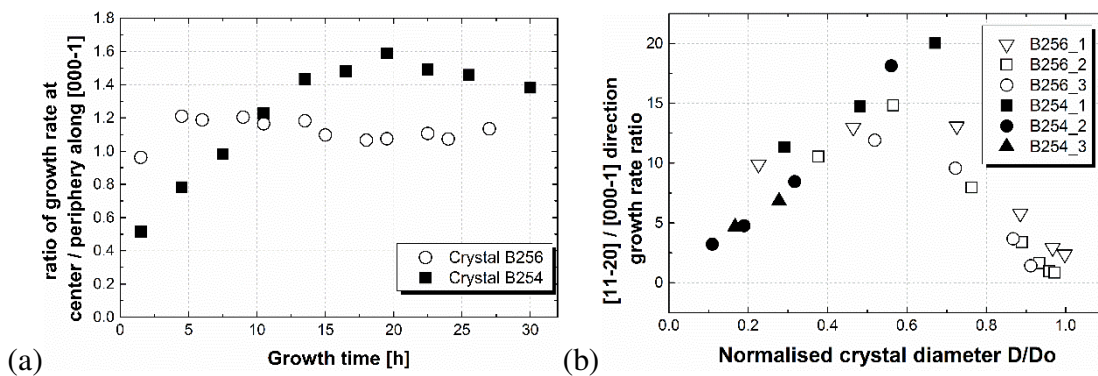
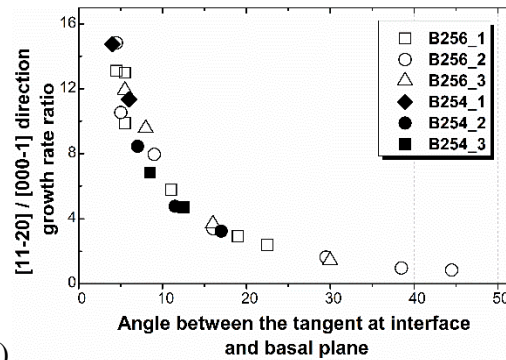


Figure 3.1. a) Coupe transversale d'un cristal de SiC (cristal B254), observée en microscopie à polarisation croisée. Le germe utilisé est du 4H-SiC C-face 4° off-axis séparé du cristal par la ligne pointillée noire. Les bandes sombres et claires correspondent respectivement aux zones dopées à l'azote et non dopées. Les cercles rouges indiquent les points de nucléation des lamelles de 6H-SiC (#1, 2,3) et de l'épaisse inclusion de 15-SiC (#4). b-c) Observation des inclusions #1, 2 et 3 à plus fort grossissement. Chaque bande dopée et non dopée correspond à 3 heures de croissance.

Pour quantifier l'évolution géométrique du cristal, les vitesses de croissance normale (selon la direction [000-1]) et latérale (selon la direction [11-20]) sont mesurées. De plus, la propagation latérale des inclusions de polytypes (A1-A3 et B1-B3 pour les inclusions #1-3 des cristaux B256 et B254, respectivement) a été systématiquement évaluée (pour le cristal B256, voire le Chapitre 3 de la thèse). Pour cela, la vitesse de croissance latérale a été calculée à partir de la longueur des inclusions mesurée selon la direction [11-20]

dans chaque bande dopée et non dopée. Pour les mêmes positions, l'épaisseur de chaque bande dopée et non dopée a été mesurée selon la direction $[000-1]$ afin de déterminer la vitesse de croissance normale. Les mesures obtenues par le marquage à l'azote sont rassemblées en Figure 3.2. Le rapport des vitesses de croissance selon la direction $[000-1]$ prise au centre (axe de symétrie) et au bord (localisation de la facette) est tracé en fonction de la durée de croissance en Figure 3.2a. Pour le cristal B256, le rapport est toujours légèrement supérieur à 1, excepté au tout début. La surface du cristal est par conséquent légèrement convexe. Pour le cristal B254, le rapport des vitesses est proche de 0,5 au début et augmente progressivement pour atteindre 1,4 après 15 heures. L'interface de croissance est par conséquent concave au début, puis s'aplatit progressivement jusqu'à devenir légèrement convexe à la toute fin de la croissance. La vitesse de croissance latérale selon la direction $[11-20]$ est supérieure d'environ un ordre de grandeur à la vitesse de croissance axiale dans la direction $[000-1]$ (Figure 3.2b). De plus, la vitesse de croissance latérale montre des variations beaucoup plus importantes que l'axiale. La vitesse de croissance selon $[11-20]$ augmente au centre du front de croissance et se minimise à la périphérie, bien qu'aucune différence significative ne soit observée pour les différents polytypes. Le fait que le maximum ne soit pas exactement au centre du front de croissance est dû à l'angle de désorientation de 4° . Pour compléter cette série de mesures, le même rapport de vitesse est tracé en fonction de l'angle entre la tangente à la surface du cristal et le plan basal (Figure 3.2c). Alors que la vitesse de croissance normale (selon la direction $[000-1]$) ne montre que de petites variations, la vitesse de croissance latérale (selon $[11-20]$) varie de façon significative. Cette vitesse de croissance latérale présente une décroissance exponentielle par rapport à l'angle entre la surface locale du cristal et le plan de basal.





(c)

Figure 3.2. a) Rapport entre les vitesses de croissance selon la direction [000-1] prises au centre du cristal et sur le côté (facette), en respectant la durée de croissance, pour les cristaux montrés en Figure 3.1 et Figure 3.2 de la thèse. Rapport entre les vitesses de croissance selon [11-20] et [000-1] en fonction de b) le diamètre normalisé (D/Do) et c) l'angle entre la tangente à l'interface du cristal et la plan basal des cristaux B256 et B254

Pour provoquer des inclusions et/ou transitions d'autres polytypes, différents germes ont aussi été utilisés. La Figure 3.3 montre une coupe transversale d'un cristal développé sur un germe de 15R-SiC on-axis Si-face (cristal B258). Par spectroscopie Raman, il a été constaté que le cristal est un mélange de 15R-SiC et 6H-SiC. La mauvaise qualité du germe utilisé est reproduite dans le cristal comme en témoigne le nombre important de micropipes provenant du germe. De plus, de nombreuses micropipes sont formées aux joints entre les différents polytypes. Dans ce cas précis, la courbure de la surface du cristal a été considérablement augmentée, passant rapidement de concave à fortement convexe lors des premières heures de croissance. De même que pour le cristal B254, deux facettes (0001) se sont formées sur les côtés du cristal. Précisément à l'emplacement des facettes, une transition du 15R-SiC au 6H-SiC se produit générant les deux inclusions latérales de 6H-SiC. Tout en devenant convexe, l'interface de croissance a développé une autre facette (0001) au centre du cristal. Au bout de quelques millimètres d'épaisseur, une inclusion de 6H-SiC apparaît au centre du cristal et se propage latéralement.

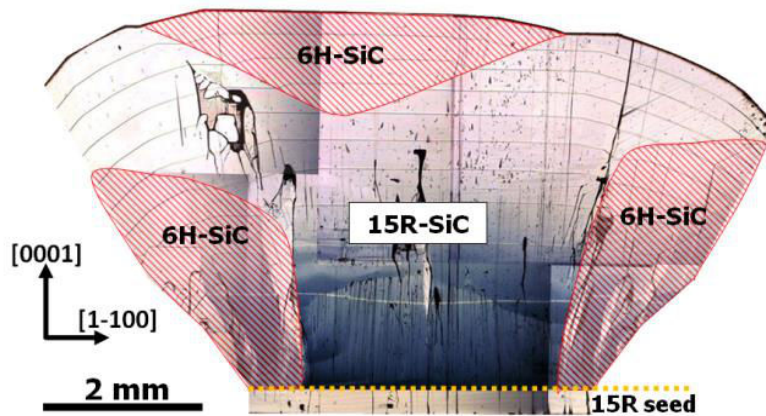


Figure 3.3. Section transversale d'un cristal de SiC (cristal B258), observée sous microscope optique à lumière polarisée. Le germe utilisé (15R-SiC Si-face on-axis) est indiqué par la ligne pointillée jaune. Le marquage périodique à l'azote a été utilisé pour observer l'évolution de la forme du cristal. Le cristal est un mélange de 15R-SiC et 6H-SiC, avec les zones de 6H-SiC indiquées par les régions ombrées en rouge.

3.4 Mécanisme de nucléation d'inclusions

L'enthalpie libre G pour la formation de germes 2D a été calculée pour le 4H-SiC, 6H-SiC et 15R-SiC sur un substrat de 15R-SiC Si-face en fonction du rayon du cristal, à deux épaisseurs différentes sur le cristal B258 (Figure 3.4). Pour toutes les conditions étudiées, l'enthalpie libre de nucléation du 6H-SiC est plus faible comparée aux autres polytypes. Le plus intéressant est la position des minima de l'énergie de nucléation 2D sur le rayon du cristal. Au début de la croissance, le minimum de l'énergie de nucléation 2D est localisé à la périphérie du front de croissance (Figure 3.4a). Après quelques millimètres de croissance (ici 3 mm), la situation change complètement et le minimum de l'énergie de nucléation 2D apparaît sur l'axe de symétrie du creuset, i.e. au centre du cristal (Figure 3.4b).

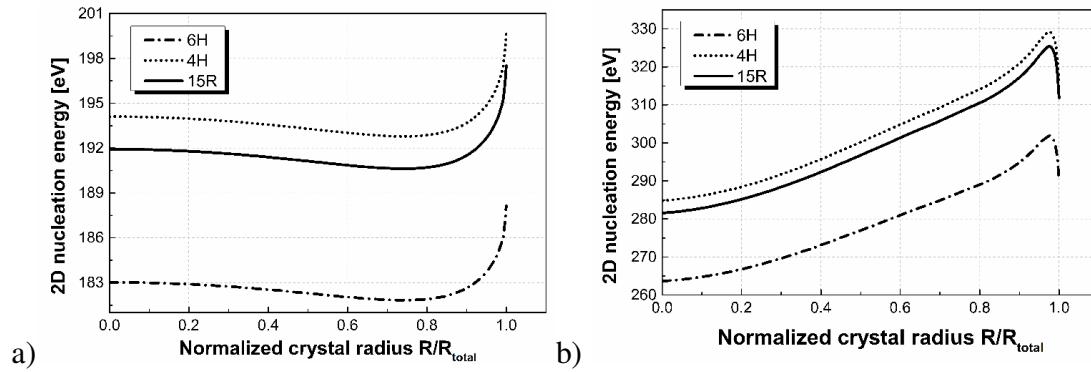


Figure 3.4. a) énergie de nucléation 2D du 4H, 6H et 15R-SiC sur un substrat de 15R-SiC Si-face en début de croissance de B258. Le minimum est localisé près de la périphérie du front de croissance. b) énergie de nucléation 2D du 4H, 6H et 15R-SiC sur un substrat de 15R-SiC Si-face après 3 mm de croissance de B258. Le minimum est localisé au centre du front de croissance.

3.5 Discussion

Les calculs de l'enthalpie libre G de nucléation ont montré que les minima, correspondants à la plus haute probabilité de nucléation 2D, pouvaient être localisés, Figures 3.4, leurs positions étant dépendantes de la forme de l'interface de croissance et du temps de croissance. Par exemple, nous avons montré qu'au début de la croissance, une interface légèrement concave crée un minimum sur la courbe de l'énergie de nucléation au bord du cristal. Après quelques millimètres de croissance, le minimum se déplace au centre du cristal, après que la forme du cristal est devenue légèrement convexe.

En combinant à la fois les observations expérimentales et les calculs numériques, il est possible de définir un modèle macroscopique pour l'apparition de polytype étranger. Les différentes situations sont rassemblées en Figure 3.5.

- Si la facette $\{0001\}$ et le minimum de l'énergie de nucléation 2D sont localisés au même endroit, alors la probabilité de former un polytype étranger est plus élevée sur la facette.

- Si la facette $\{0001\}$ et le minimum de l'énergie de nucléation 2D ne sont pas localisés au même endroit, alors la probabilité de former un polytype étranger sur la facette est beaucoup plus faible.
- En dehors de la facette, la probabilité de nucléation 2D est extrêmement faible étant donné que la densité de crans pour l'incorporation d'adatoms est assez forte, ce qui signifie que la réplique du polytype du substrat est favorable.

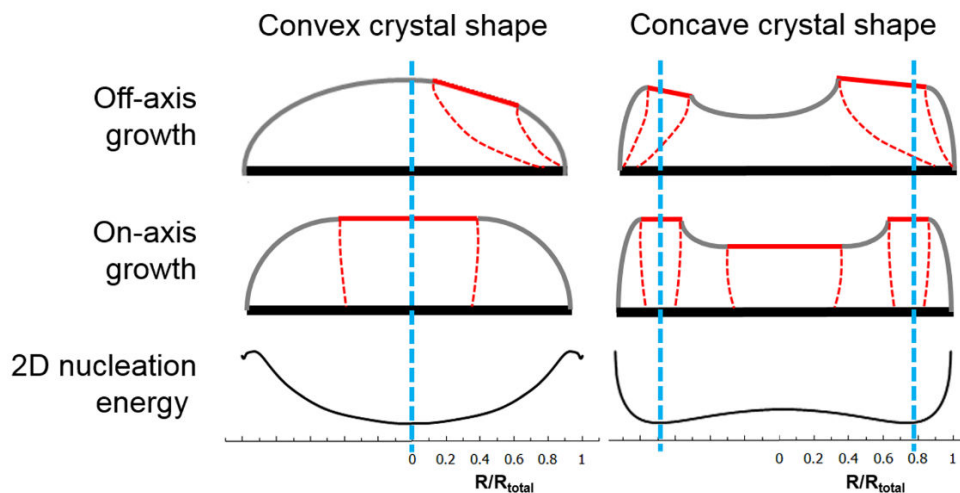


Figure 3.5. Représentation schématique de la corrélation entre la forme du cristal, la formation des facettes et la *position des minima d'énergie de nucléation 2D*. Les lignes pointillées rouges décrivent approximativement l'évolution des facettes pendant la croissance. Les lignes pointillées verticales bleues indiquent la position de l'énergie de nucléation 2D minimale sur les cristaux.

Autrement dit, la présence d'une facette est un prérequis pour l'apparition de polytype étranger mais n'est pas suffisante. L'enthalpie libre de nucléation doit également être à son minimum sur la facette.

4. Dopage azote de cristaux de SiC

4.1 Introduction

L'azote est l'un des dopants de type-n les plus couramment utilisés dans le SiC et son incorporation par implantation ou pendant la croissance des couches épitaxiales a été très

étudiés. Dans la croissance par PVT, l'azote est l'impureté la plus abondante car il est très difficile de l'éliminer du matériau source (poudre de SiC) et du creuset (graphite). Même lorsque du graphite extrêmement pur est utilisé, les niveaux résiduels d'azote ne descendent que rarement en dessous de 10^{17}cm^{-3} . La plupart des applications électroniques ont besoin de substrats fortement conducteurs, c'est pourquoi les cristaux formés sont dopés intentionnellement en rajoutant de l'azote à la phase gazeuse.

Bien que l'incorporation d'azote soit assez bien décrite en CVD [25-27], aucune description détaillée du phénomène n'existe concernant la méthode PVT. Il est connu que les cristaux orientés (000-1) C-face pendant la croissance incorporent plus d'azote que la face (0001)Si [28]. De plus, il semble que l'incorporation d'azote ne soit pas limitée par la cinétique et qu'un équilibre de couverture de la surface par les adatoms d'azote soit atteint. C'est pour cela que la plupart des études se focalisent sur l'effet de la pression partielle d'azote sur son incorporation [28, 29, 30]. Les tendances obtenues sont décrites en utilisant une isotherme de Langmuir pour une adsorption non-dissociative, voir Figure 4.1a. Concernant les effets du polytype, aucune différence significative n'a été observée entre le 6H-SiC et le 4H-SiC (Figure 4.1b) lors de la croissance sur les faces (1-100) and (11-20) qui révèlent la séquence d'empilage du polytype SiC. Ceci implique que la différence de séquence d'empilement entre les deux polytypes n'affecte pas l'incorporation d'azote. Cependant, sur la face (000-1)C, l'incorporation d'azote varie et cela a été attribué aux différences topologiques entre les surfaces 6H-SiC and 4H-SiC (000-1) [29].

La difficulté de séparer les différents paramètres dans le procédé PVT, comme la température et le ratio Si/C dans la phase gazeuse, complique la description de l'incorporation d'azote. De plus, le rôle des mécanismes de surface (spirale, step-flow, nucleation 2D) n'est pas clair. Il a par exemple été rapporté que la facette du plan basal incorpore plus d'azote que les zones de step flow. La différence dans l'incorporation d'azote est maximale pour un faible dopage et sature pour des valeurs plus grandes (Figure 4.1c) [31,32]. Aucune explication n'a été donnée sur ce phénomène.

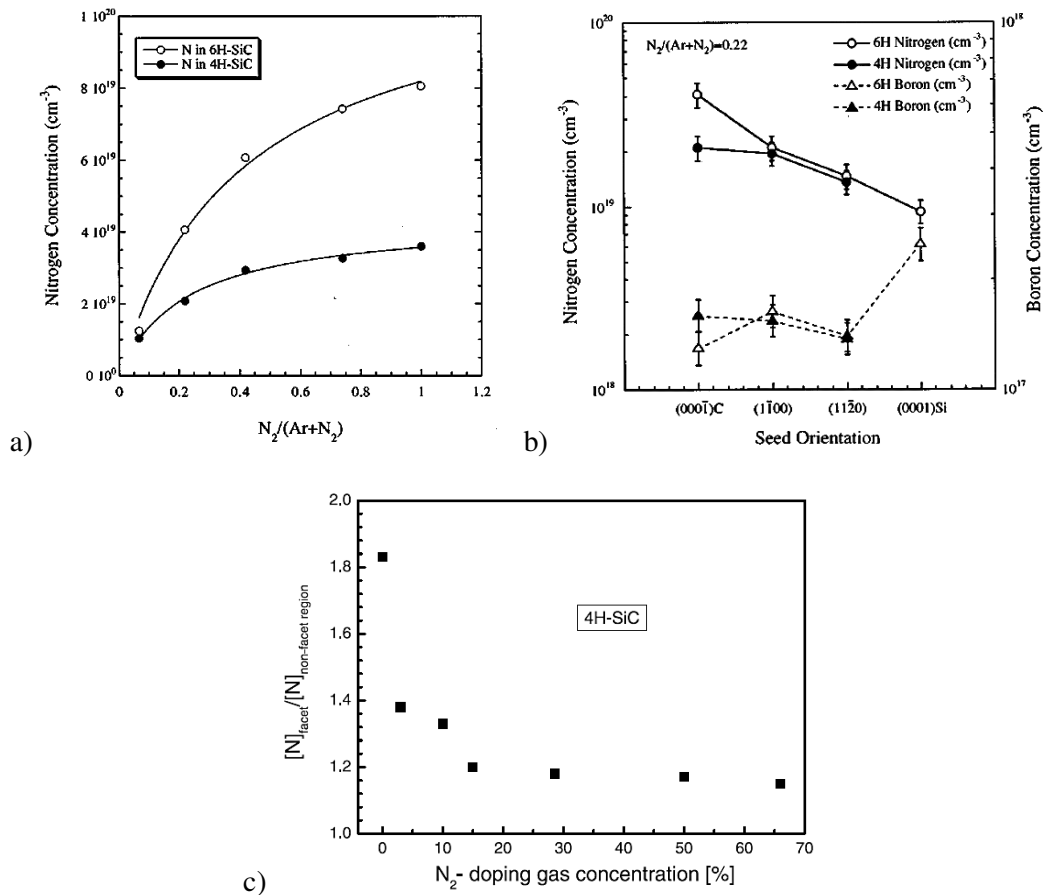


Figure 4.1. a) Concentration d'azote dans le cristal en fonction de la pression partielle de N_2 . Une isotherme de Langmuir est utilisée pour décrire les données. b) Incorporation d'azote en fonction de l'orientation de la croissance [29]. c) Rapport entre l'azote incorporé sur la facette (000-1) et dans la zone de step-fow (hors-facette) d'un cristal 4H-SiC en fonction de l'azote dans la phase gazeuse [31].

4.2 Détails expérimentaux

Des germes de différents polytypes (4H-SiC, 6H-SiC and 15R-SiC) ayant différentes orientations (On-axis, 4° off-axis, polarités C et Si) ont été utilisés. Dans un premier groupe d'expériences, l'effet de la pression partielle d'azote a été étudié en maintenant la température de croissance et la pression totale constantes, soit 2200°C et 13 mbar respectivement. Le ratio du flux d'azote sur le flux total de gaz (argon et azote) varie dans l'intervalle 0.05-0.8. Des bandes de dopages différents ont été créées en modifiant les flux de gaz périodiquement (Figure 4.2).

Dans un second groupe d'expériences, l'incorporation d'azote a été examinée par rapport à la température de croissance dans la gamme 2130°C à 2350°C, tous les autres paramètres étant constants (pression de 13mbar, fraction d'azote $N_2/(N_2+Ar)$ de 0.15). Pour chaque condition expérimentale, les différents germes sont placés dans une et une seule expérience de façon à appliquer exactement les mêmes conditions de croissance. Un exemple de cristal formé à 2280°C est montré en Figure 4.3.

La concentration en « porteurs libres » des cristaux a été étudiée par des mesures d'effet Hall en température et par spectroscopie Raman à température ambiante. La concentration en azote a été mesurée par SIMS (Secondary Ion Mass Spectrometry).

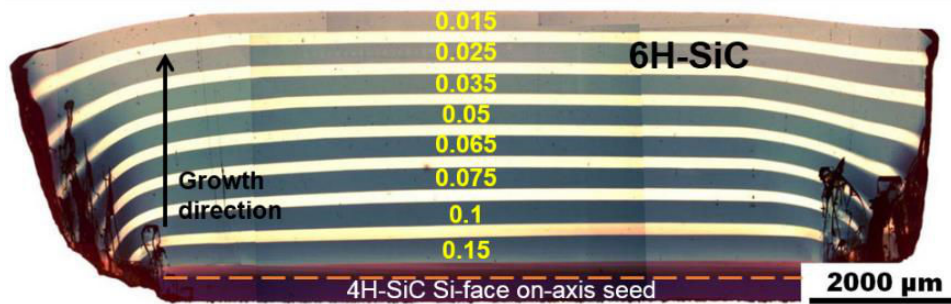


Figure 4.2. Coupe transversale d'un cristal 6H-SiC formé sur un germe 4H-SiC Si-face on-axis. Les bandes noires et blanches correspondent aux zones dopées et non-dopées, créées par le contrôle des gaz d'entrée (argon et azote) du réacteur. La fraction d'azote $N_2/(Ar+N_2)$ est indiquées pour chaque bande.

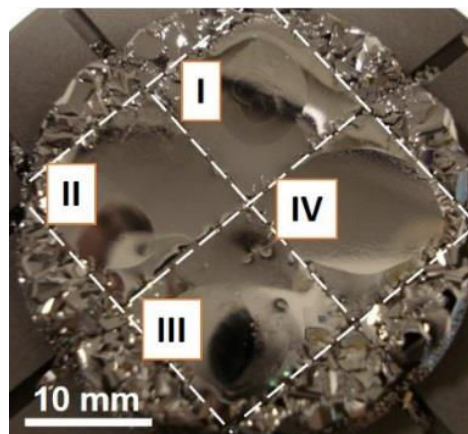


Figure 4.3. Photo d'un cristal SiC (position I-IV) formé à 2280°C. Les lignes pointillées blanches délimitent les 4 germes différents utilisés.

4.3.2 Effet de la température.

Dans le graphe de la Figure 4.4 les concentrations en porteurs libres sont représentées en fonction de la température de croissance. Les concentrations diminuent quand la température de croissance augmente. Pour 4H-SiC face C, une équation d'Arrhenius (Equation 4.1) est utilisée pour représenter les données. L'énergie d'activation est de $152.4 \text{ kJ}\cdot\text{mol}^{-1}$.

$$k = A e^{-E_a / RT} \quad \text{Eq. 4.1}$$

k représente la concentration en porteurs libres, A est un facteur pré-exponentiel, E_a [$\text{kJ}\cdot\text{mol}^{-1}$] l'énergie d'activation et T [K] la température.

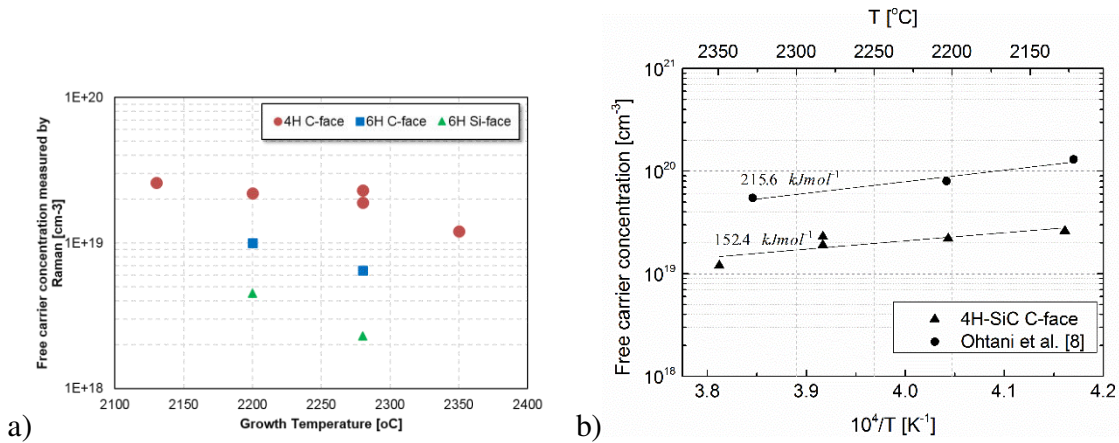


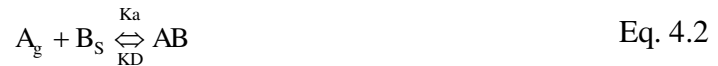
Figure 4.4. a) Concentration de porteurs libres dans les cristaux on-axis C-face 4H-SiC et on-axis 6H-SiC faces Si et C en fonction de la température de croissance, tel que mesurée par une spectroscopie de Raman. b) Une équation d'Arrhenius a été utilisée pour ajuster les données. L'énergie d'activation a été trouvée à $152.4 \text{ kJ}\cdot\text{mol}^{-1}$. Les données de Ohtani et al. sont utilisées pour comparaison [33].

4.3.3 Effet de la pression partielle d'azote.

La concentration d'azote des différentes bandes de dopage en fonction de la pression partielle d'azote a été mesurée par SIMS (Figure 4.5.a). En augmentant la pression partielle d'azote, l'azote incorporée dans le réseau cristallin du SiC augmente. Une fois que la pression partielle d'azote dépasse les 0.6, l'état de saturation est atteint. En comparaison

avec la face silicium du 6H-SiC et du 15R-SiC, plus d'azote a été incorporé dans la face carbone des polytypes 4H-SiC et 6H-SiC

Une isotherme d'absorption de Langmuir a été utilisée pour décrire les données. Une des hypothèses faite sur ce modèle réside sur le fait qu'il s'établit un équilibre dynamique entre les molécules adsorbées en surface et les particules gazeuses libres. Cet équilibre d'adsorption-désorption peut être décrit par :



Avec A_g une molécule de gaz en phase gazeuse, B_s un site libre à la surface du solide, AB les molécules de gaz adsorbées. K_a et K_D sont les constantes d'adsorption et de désorption, respectivement. La constante d'équilibre de la réaction (K) est le rapport entre K_a et K_D :

$$K = K_a/K_D \quad \text{Eq. 4.3}$$

L'isotherme de Langmuir pour une adsorption non-dissociative est donné par :

$$\theta = \frac{Kp}{1 + Kp} \quad \text{Eq. 4.4}$$

Où « θ » est le taux de couverture de la surface. Pour une faible pression partielle de gaz et lorsqu'il y a beaucoup de sites d'incorporation vacants, l'adsorption à la surface est linéaire et fonction de la pression partielle de gaz. Quand la pression partielle de gaz est forte, la couverture de surface augmente jusqu'au point de saturation. L'incorporation d'azote n'est pas influencée par la vitesse de croissance [28], ainsi, l'incorporation d'azote n'est pas cinétiquement limitée. Les données ont été représentées sous la forme suivante :

$$C_N = S_T \frac{Kp}{1 + Kp} \quad \text{Eq. 4.6}$$

Avec C_N la concentration d'azote incorporé dans le cristal, p la pression partielle d'azote et S_T la limite de saturation pour de grande valeur de pression partielle [cm^{-3}]. S_T et K sont des paramètres d'ajustement.

Le modèle non-dissociatif est le plus adapté à la description des données expérimentales de cette étude (Figure 4.5b.). Le paramètre d'ajustement K associé aux faces carbone 6H-SiC et 4H-SiC est 15% plus élevé dans le cas du 4H-SiC. La limite de

saturation de la face carbone 4H-SiC semble également être 15% plus élevée par rapport à celle du 6H-SiC. Pour la face silicium 6H-SiC, K ainsi que S_T s'avèrent être presque moitié moins élevés que pour la face carbone. Le manque de données pour le 15R-SiC ne permet pas un ajustement fiable.

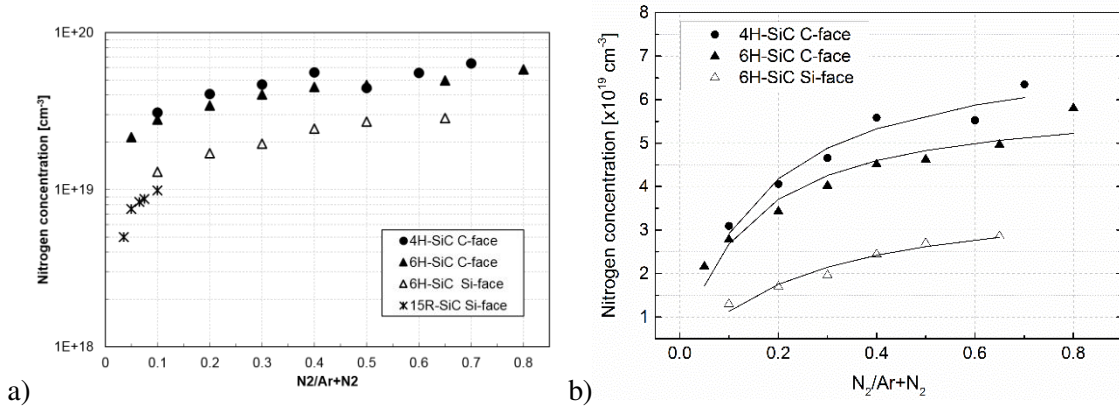


Figure 4.5. a) Concentration d'azote dans les cristaux de SiC représenté en fonction de la pression partielle d'azote durant la croissance. **b)** Ajustement des données par une isotherme de Langmuir (ligne continue).

4.5 Discussion

Dans le but d'expliquer les courbes expérimentales obtenues, les mécanismes d'absorptions/désorption sur des surfaces Si et C {0001} sont considérés (Figure 4.6). Sachant que l'atome d'azote substitue le carbone dans le réseau cristallin, l'incorporation d'azote pour les deux polarités C et Si s'effectue comme décrit ci-dessous :

- Plan (000-1) face carbone : La terminaison de surface est constituée d'atomes de carbone (position A). L'adsorption et la désorption des atomes de carbone a lieu à la surface, ainsi, des positions vacantes sont créées, offrant la possibilité à l'azote de s'y incorporer. Dans un second temps, les atomes de silicium sont incorporés en position B. A ce moment là, aucune incorporation d'azote ne peut avoir lieu. Lors de l'étape suivante, les atomes d'azote et de carbone se répartissent les sites disponibles, c'est la position C.
- Plan (0001) face silicium : La terminaison de surface est constituée d'atome de silicium (position A). A ce stade, l'azote ne peut pas s'incorporer. En position B,

l'azote et le carbone se répartissent les sites disponibles puis sont recouverts par une couche atomique de silicium (position C).

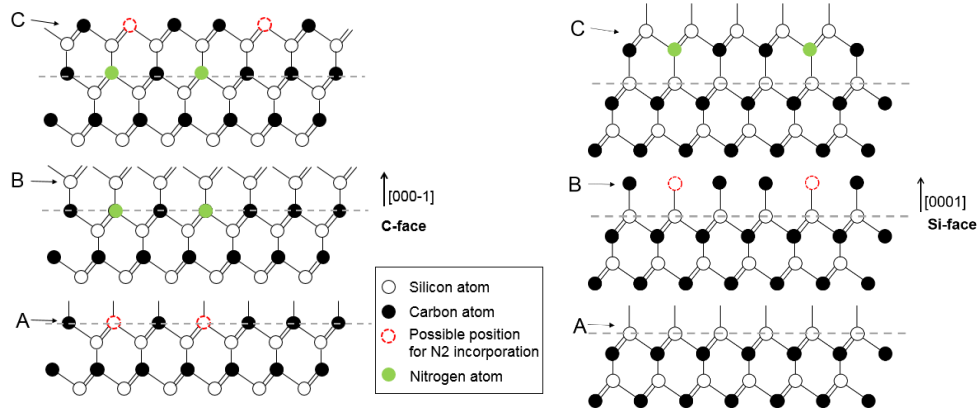


Figure 4.6. Schéma illustrant l'incorporation d'azote sur les différentes faces (carbone et silicium). Trois étapes d'incorporation d'atomes additionnels sont considérées et nommé respectivement A, B et C.

Le mécanisme d'incorporation dans les deux plans est similaire, puisque l'azote et le carbone entre en jeu lorsqu'il y a existence de site disponibles à la surface et que lorsque le silicium est incorporé, l'incorporation d'azote ne peut pas avoir lieu. La différence entre les deux cas est liée à la densité de liaisons pendantes sur les plans lorsque l'azote est introduit. De la différence de densité de liaisons entre les deux plans (plus grande dans le cas de la face carbone) résultera différents taux de désorption. Sur la face C, la désorption est plus faible que sur la face silicium. Autrement dit, la couverture de surface sur la face carbone (000-1) est plus élevée que celle de la face silicium (0001). La constante d'équilibre K utilisée dans l'équation d'adsorption est le paramètre qui décrit de taux d'adsorption/désorption. Dans notre étude, il a été trouvé que la valeur du paramètre K dans le cas de la face Si 6H-SiC est la moitié de celui de la face carbone 4H-SiC et 6H-SiC. Cela implique que la couverture de surface de la face carbone est plus grande que celle de la face silicium, étant ainsi en accord avec le mécanisme proposé ci-dessus.

Bien que le paramètre K et la limite de saturation entre les faces silicium et carbone soient différents, cela n'est pas le cas pour les différents polytypes. Les valeurs similaires des paramètres K et S_T , pour la face carbone 4H-SiC et 6H-SiC, indiquent que

l'incorporation de l'azote dans le plan (000-1) est indépendante du polytype. Ce résultat est en contradiction avec ce qui a été rapporté précédemment où une différence de limite de saturation et de couverture de surface a été trouvée sur le plan (000-1) des cristaux 4H-SiC et 6H-SiC [29].

L'incorporation des atomes décrite en Figure 4.8 est en fait très simplifiée, car elle n'intègre pas l'incorporation des dopants en bord de marche, au niveau des crans (Figure 4.9).

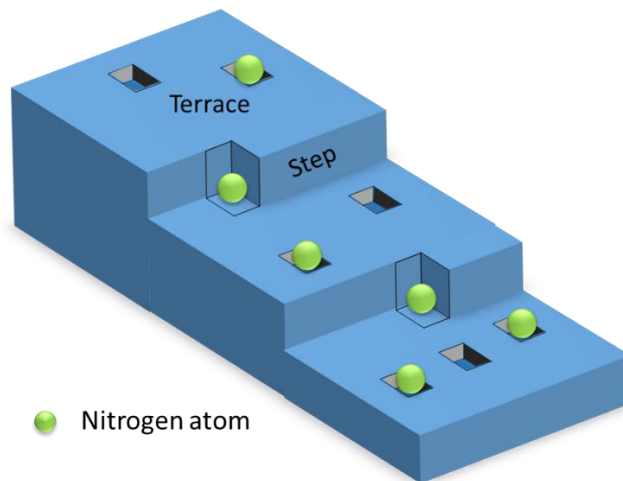


Figure 4.7. Schéma illustrant la surface de croissance. *L'incorporation des atomes d'azote* sur des sites vacants, soit en bord de marche (crans), soit sur les terrasses (lacunes de surface).

Durant la croissance, les atomes de Si et C diffusent sur la surface et sont incorporés au niveau des crans en bord de marche. La concentration des espèces Si et C sur une terrasse est décrite par la théorie BCF. L'azote quant à lui est très abondant dans la phase gazeuse. Il est donc peu probable que son incorporation soit régit par les gradients de concentration de surface et l'incorporation en bord de marche. Si cela était le cas, comment expliquer que la concentration en azote dans le cristal puisse être 1,5 fois plus élevée au niveau de la facette qu'en dehors de la facette (c'est-à-dire, là où la densité de marche est plus élevée) [31]. En fait, l'incorporation d'azote doit également (et peut-être majoritairement) se faire sur les terrasses, par le biais de lacunes de surface {0001} générées par les températures très élevées de la PVT.

Ainsi, la variation de l'incorporation de l'azote en fonction de la température peut être attribuée à deux effets: i) la variation de la constante d'équilibre K avec la température.

Quand celle-ci diminue, le rapport adsorption/désorption augmente ($K_{T_{low}} > K_{T_{high}}$). Le taux de couverture de la surface " θ " augmente ainsi que la concentration en azote dans le cristal (Figure 4.8). L'augmentation du taux de couverture avec la température découle du fait de la diminution de l'énergie cinétique des atomes. ii) L'augmentation de la vitesse de croissance réduit la largeur des « terrasses » sur la facette {0001}. Considérant que l'incorporation d'azote se produit majoritairement sur les lacunes de surface, l'incorporation d'azote diminue quand la largeur des « terrasses » et donc le nombre de sites d'incorporation libres diminue.

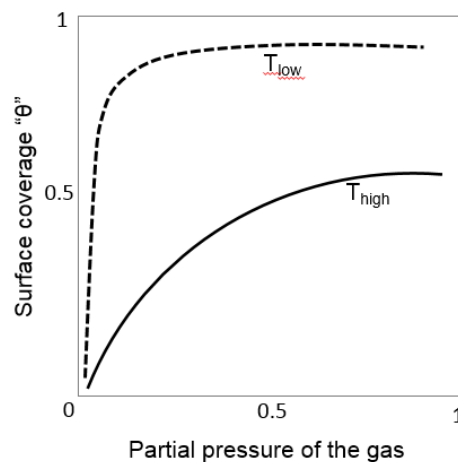


Figure 4.8. Taux de couverture de la surface en fonction de la pression partielle de gaz, décrit par une isotherme d'adsorption de Langmuir. Les effets de températures inférieure et supérieure à la limite de saturation sont indiqués.

Conclusions générales

Le le présent travail visait à apporter des mémoire, une méthode de croissance a été développé dans le but de fabriquer des cristaux de SiC de taille et de forme suffisantes pour les besoins des expériences. Le problème de l'apparition de « polytype » étranger a été continuellement étudié pendant la croissance. Aussi, l'incorporation d'azote en fonction de différents paramètres de croissance a-t-elle été étudiée.

Dans un premier temps, nous avons montré la possibilité d'une croissance de cristaux de SiC sans contact avec le creuset dans un système de PVT. Cette configuration permet la croissance de monocristaux de SiC sans gangue de SiC polycristallin parasite. Ceci a été possible par une compréhension et une optimisation des transferts de matière dans la

cavité de croissance en s'appuyant sur une approche couplée entre expérience et simulation numérique.

Dans un deuxième temps, une étude approfondie de la nucléation et de la propagation d'inclusions de polytypes a été menée. L'apparition d'inclusions est directement liée à la présence de facettes $\{0001\}$. La nucléation de polytypes étrangers est plus probable lorsque l'apparition d'une facette $\{0001\}$ et la minimisation de l'énergie de nucléation 2D se produisent au même endroit et en même temps. En fonction de la direction de croissance (on-axis ou off-axis) et de la forme du cristal (convexe ou concave), on observe des zones où la probabilité de nucléation de polytypes étrangers est plus grande. Une fois formée, le développement ou la disparition d'une inclusion est directement liée à son interaction avec l'interface de croissance.

Enfin, l'incorporation d'azote pendant la croissance de 4H-SiC et de 6H-SiC a été étudiée en fonction de la pression partielle d'azote et de la température de croissance. La concentration de porteurs libres diminue quand la température de croissance augmente dans le cas d'une croissance face C de 4H-SiC et l'énergie d'activation calculée est 152,4 kJ/mol. Ceci est due à la désorption accrue d'azote lorsque la température augmente. De plus, la face C incorpore plus d'azote que la face Si, alors que pour les deux polarités, la limite de saturation se produit à des valeurs de pression partielle d'azote supérieures à 0,6-0,7. Une isotherme d'adsorption de Langmuir (cas non-dissociatif) a été utilisée pour ajuster les tendances expérimentales. Nous avons ainsi pu montrer que la couverture de surface en azote sur C-face est semblable pour le 4H-SiC et le 6H-SiC ainsi que leur limite de saturation. La différence principale provient de la polarité. Dans le cas de la croissance face Si, la limite de saturation et la couverture de surface en azote sont presque deux fois plus faibles que sur la face C. Enfin, nous avons proposé le rôle déterminant de l'incorporation d'azote sur des lacunes de surface de terrasses. Ce mécanisme permet d'expliquer l'incorporation préférentielle au niveau de la facette de croissance.

References

1. Cheung, R., Silicon Carbide Microelectromechanical Systems for Harsh Environments. 2006: Imperial College Press.
2. Mirgorodsky, A.P., et al., Molecular approach to the modeling of elasticity and piezoelectricity of SiC polytypes. *Physical Review B*, 1995. 52(6): p. 3993-4000.
3. Pearson, E., et al., Computer modeling of Si and SiC surfaces and surface processes relevant to crystal growth from the vapor. *Journal of Crystal Growth*, 1984. 70(1-2): p. 33-40.
4. Larkin, D.J., SiC Dopant Incorporation Control Using Site-Competition CVD. *physica status solidi (b)*, 1997. 202(1): p. 305-320.
5. Glass, R.C., et al., SiC-Seeded Crystal Growth. *MRS Bulletin*, 1997. 22(03): p. 30-35.
6. Tairov, Y.M., V.F. Tsvetkov, Handbook on Electrotechnical Materials, in "Semiconductor Compounds AIVBIV", Y.V. Koritskii, V.V. Pasyukov, B.M. Tareev, Editor. 1988.
7. Kitou, Y., et al., Flux-Controlled Sublimation Growth by an Inner Guide-Tube. *Materials Science Forum*, 2002. 389-393: p. 83-86.
8. Kato, T., S.-I. Nishizawa, and K. Arai, Dislocation constraint by etch back process of seed crystal in the SiC sublimation growth. *Journal of Crystal Growth*, 2001. 233(1-2): p. 219-225.
9. Tairov, Y.M., Growth of bulk SiC. *Materials Science and Engineering: B*, 1995. 29(1-3): p. 83-89.
10. Pons, M., et al., State of the art in the modelling of SiC sublimation growth. *Materials Science and Engineering: B*, 1999. 61-62: p. 18-28.
11. Herro, Z.G., et al., Effective increase of single-crystalline yield during PVT growth of SiC by tailoring of temperature gradient. *Journal of Crystal Growth*, 2004. 262(1-4): p. 105-112.
12. Hofmann, D., et al., Analysis on defect generation during the SiC bulk growth process. *Materials Science and Engineering: B*, 1999. 61-62: p. 48-53.
13. Ohtani, N., et al., Dislocation processes during SiC bulk crystal growth. *Microelectronic Engineering*, 2006. 83(1): p. 142-145.
14. Sanchez, E.M., et al., The Nucleation of Polytype Inclusions during the Sublimation Growth of 6H and 4H Silicon Carbide. *Materials Science Forum*, 2002. 389-393: p. 71-74.
15. Siche, D., et al., Evolution of domain walls in 6H- and 4H-SiC single crystals. *Journal of Crystal Growth*, 2002. 237-239: p. 1187-1191.
16. Matsunami, H. and T. Kimoto, Step-controlled epitaxial growth of SiC: High quality homoepitaxy. *Materials Science and Engineering: R: Reports*, 1997. 20(3): p. 125-166.
17. Pelissier, B., et al., Seed Surface Preparation for SiC Sublimation Growth. *Materials Science Forum*, 2000. 338-342: p. 47-50.

18. Bogdanov, M.V., et al., Modeling Analysis of Free-Spreading Sublimation Growth of SiC Crystals. MRS Proceedings, 2011. 742.
19. Madar, R., et al., Numerical Simulation of SiC Boule Growth by Sublimation. Materials Science Forum, 2000. 338-342: p. 25-30.
20. Fissel, A., Thermodynamic considerations of the epitaxial growth of SiC polytypes. Journal of Crystal Growth, 2000. 212(3-4): p. 438-450.
21. Shiramomo, T., et al., Thermodynamical analysis of polytype stability during PVT growth of SiC using 2D nucleation theory. Journal of Crystal Growth, 2012. 352(1): p. 177-180.
22. Thesis, Kanaparin Ariyawong. 2015, Grenoble Institute of Technology
23. Kakimoto, K., et al., Thermodynamic analysis of SiC polytype growth by physical vapor transport method. Journal of Crystal Growth, 2011. 324(1): p. 78-81.
24. Rost, H.J., D. Schulz, and D. Siche, High Nitrogen Doping During Bulk Growth of SiC, in Silicon Carbide, W.J. Choyke, H. Matsunami, and G. Pensl, Editors. 2004, Springer Berlin Heidelberg. p. 163-178.
25. Rost, H.J., et al., Influence of nitrogen doping on the properties of 4H-SiC single crystals grown by physical vapor transport. Journal of Crystal Growth, 2003. 257(1-2): p. 75-83.
25. Forsberg, U., et al., Nitrogen doping of epitaxial silicon carbide. Journal of Crystal Growth, 2002. 236(1-3): p. 101-112.
26. Kimoto, T., A. Itoh, and H. Matsunami, Incorporation mechanism of N, Al, and B impurities in chemical vapor deposition of SiC. Applied Physics Letters, 1995. 67(16): p. 2385-2387.
27. Larkin, D.J., SiC Dopant Incorporation Control Using Site-Competition CVD. *physica status solidi (b)*, 1997. 202(1): p. 305-320.
28. Onoue, K., et al., Nitrogen Incorporation Kinetics during the Sublimation Growth of 6H and 4H SiC. Japanese Journal of Applied Physics, 1996. 35(Part 1, No. 4A): p. 2240-2243.
29. Ohtani, N., et al., Impurity incorporation kinetics during modified-Lely growth of SiC. Journal of Applied Physics, 1998. 83(8): p. 4487-4490.
30. Schulz, D., et al., Study of Nitrogen Incorporation in 6H-SiC Single Crystals Grown by PVT. Materials Science Forum, 2000. 338-342: p. 87-90.
31. Rost, H.J., D. Schulz, and D. Siche, High Nitrogen Doping During Bulk Growth of SiC, in Silicon Carbide, W.J. Choyke, H. Matsunami, and G. Pensl, Editors. 2004, Springer Berlin Heidelberg. p. 163-178.
32. Schulz, D. 2001, PhD Thesis, Brandenburgische Technische Universität Cottbus.
33. Ohtani, N., et al., Investigation of heavily nitrogen-doped n+ 4H-SiC crystals grown by physical vapor transport. Journal of Crystal Growth, 2009. 311(6): p. 1475-1481.

Summary of the thesis

Silicon Carbide is one of the most important and widely used semiconductors for power electronic devices. Due to the increasing demand for high efficiency, low cost and energy saving electronics, further improvement of the properties of single crystal semiconductors is needed. That requires a better understanding of the phenomena involved in the growth process of these materials. This thesis will bring some new insight into two main topics at the field of SiC bulk growth from the vapor phase.

Initially, the growth process used in our laboratory was developed in order to improve the quality and the size of the grown SiC crystal. A geometry that allows the contactless and reproducible growth of SiC single crystals was obtained. Continuously, we investigated the nucleation and propagation of structural instabilities (foreign polytype inclusions) that appear during growth. Two specific criteria must be fulfilled for a foreign polytype to be nucleated. Once the nucleation point is located, the propagation of the foreign polytype in the volume of the grown crystal can be comprehended. Once the stabilization or destabilization of the SiC polytypes was better perceived, an attempt was made to stabilize the growth of the 15R-SiC polytype. As a final objective, the growth parameters that could preferentially enhance the growth of the 15R-SiC are highlighted. Last, nitrogen incorporation during bulk growth from the vapor phase was studied. Indeed as the most commonly used dopant, no full description exists for the incorporation of nitrogen in SiC. We contribute to this effort by exploring the nitrogen concentration in the grown crystals as a function of various growth parameters. Considering the adsorption/desorption mechanisms at the growing surface, effort was given to explain the experimentally obtained trends.

Résumé de la thèse en français

Le carbure de silicium est l'un des semi-conducteurs les plus importants et les plus répandus dans les appareils électroniques de puissance. Du fait de la demande croissante d'électronique à haut rendement, bas coût et économe en énergie, il est nécessaire d'améliorer les propriétés des semi-conducteurs monocristallins. Cela demande une meilleure compréhension des phénomènes impliqués dans le procédé de croissance de ces matériaux. Cette thèse présentera de nouvelles perspectives sur deux sujets majeurs dans le domaine de la croissance en phase gazeuse de monocristaux de SiC.

Dans un premier temps, le procédé de croissance utilisé dans notre laboratoire a été développé dans le but d'améliorer la qualité et la taille des cristaux de SiC obtenus. Une géométrie permettant la croissance sans contact et reproductible de monocristaux de SiC a été obtenue. La nucléation et la propagation des instabilités structurelles (inclusions de polytype étranger) apparaissant lors de la croissance ont été étudiés de façon continue. Deux critères spécifiques doivent être réunis pour qu'un polytype étranger puisse nucléer. Une fois le point de nucléation localisé, la propagation du polytype étranger dans le volume du cristal peut être appréhendée. Lorsque la stabilisation et déstabilisation des polytypes de SiC ont été mieux comprises, une tentative a été faite pour stabiliser la croissance du polytype 15R-SiC. L'objectif final, les paramètres de croissance susceptibles de renforcer la croissance préférentielle de 15R-SiC, a été mis en évidence.

Enfin, l'incorporation d'azote pendant la croissance en phase gazeuse de monocristaux a été étudiée. En effet, aucune description détaillée n'existe pour l'incorporation d'azote dans le SiC, bien que ce soit le dopant le plus couramment utilisé. Notre contribution à cet effort porte sur l'étude de la concentration d'azote dans les cristaux obtenus en fonction de différents paramètres de croissance. Compte tenu des mécanismes d'adsorption/désorption à la surface de croissance, un effort a été fait pour expliquer les tendances obtenues expérimentalement.